Novel routes to $Li_4Ti_5O_{12}$ spinel: Characterization and phase relations

Andreas Laumann

München 2010

Novel routes to $Li_4Ti_5O_{12}$ spinel: Characterization and phase relations

Andreas Laumann

Dissertation
an der Fakultät für Geowissenschaften
der Ludwig–Maximilians–Universität
München

vorgelegt von
Andreas Laumann
aus München

München, den 18. November 2010

Erstgutachter: Prof. Dr. Karl Thomas Fehr
Zweitgutachter: Prof. Dr. Bo Brummerstedt Iversen
Tag der mündlichen Prüfung: 20.06.2011

Contents

List of Figures

List of Tables

Abstract

In the future, renewable energy sources will become more and more important, and thus new possibilities to store this renewable energy will be needed. Lithium-ion batteries are a candidate to replace and improve upon lead-acid batteries in stationary applications like wind and solar power plants. Therefore, $Li_4Ti_5O_{12}$ spinel is of high interest to the energy industry as it shows an excellent long term stability at high rates and it could also play an important role for energy storage in (hybrid)-battery electric vehicles.

During this dissertation, two new methods to synthesize $Li_4Ti_5O_{12}$ were developed. The first approach (patent pending, Süd Chemie AG) is a two-step synthesis which combines a hydrothermal step with a subsequent solid-state reaction. The key was the formation of a previously poorly described α-Li_2TiO_3. α-Li_2TiO_3 was synthesized by hydrothermal reactions at 180 $^\circ C$ for 18 hours, using titania powder and lithium hydroxide in de-ionized water. The samples are unstable under atmospheric conditions, and lithium loss could be systematically determined due to leaching experiments with de-ionized water, which helped to explain existing ambiguities concerning the composition of α-Li_2TiO_3.

An *in-situ* neutron experiment upon heating of α-Li_2TiO_3 proved expected phase transitions from α-Li_2TiO_3 to the monoclinic Li_2TiO_3 and then again to a cubic Li_2TiO_3, which is isostructural with α-Li_2TiO_3. Moreover, for the first time, the crystal structure of α-Li_2TiO_3 was determined and its formation under hydrothermal conditions was recorded *in-situ* by synchrotron powder X-ray diffraction.

The commercialized $Li_4Ti_5O_{12}$ sample (Süd-Chemie AG) shows excellent cycling stability and good capacity at high rates. The same commercial sample was studied at high temperatures, once with impedance spectroscopy and again with *in-situ* neutron powder diffraction. Both measurements support the theory of enhanced lithium mobility at T > 500 $^\circ C$. Notably, at 900 $^\circ C$, the neutron diffraction demonstrates lithium migration from tetrahedral $8a$ positions to positions close to the center of $16c$ octahedrons, which might be the reason for the variable behavior in ionic conductivity of $Li_4Ti_5O_{12}$ at high temperatures. Finally, $Li_4Ti_5O_{12}$ was for the first time crystallized directly by a hydrothermal method using a reactant comprising lithium ethoxide and titanium (IV) isopropoxide (TTIP). After $\approx$ 30 seconds, nano particles with a specific surface of 230 m^2/g were obtained by treating the reactant with supercritical water in a continuous flow reactor. However, non-annealed particles show fading in capacity when electrochemically tested, and the exact reasons for this fading are still under discussion.

Zusammenfassung

In unserer Zeit der Wende zu erneuerbaren Energien und der damit verbundenen notwendigen Erforschung neuer Speichermedien, stehen Lithium-Ionen Akkumulatoren in aktueller Diskussion. Bei der Suche nach Ersatz für Bleibatterien in stationären Anlagen, wie Wind- und Solarkraftwerken, ist $Li_4Ti_5O_{12}$ ein vielversprechendes Anodenmaterial, da es eine ausgezeichnete Zyklenbeständigkeit, Belastbarkeit und Betriebssicherheit aufweist. Zudem kommt es auch für den Einsatz in Elektrofahrzeugen in Frage.

Im Laufe dieser Dissertation wurden zwei neue Methoden entwickelt um $Li_4Ti_5O_{12}$ herzustellen. Der erste Ansatz (Patentanmeldung, Süd-Chemie AG) ist ein zweistufiger Prozess, bestehend aus einer Hydrothermal- und einer Festkörpersynthese. Grundlage für diesen Prozess war die Forschung an der zuvor nahezu unbekannten Phase α-Li_2TiO_3, welche auf hydrothermalem Wege mittels einer Titan-Komponente in Lithiumhydroxid Lösung umgesetzt werden kann. Die instabilen α-Li_2TiO_3 Proben zeigten beim Waschen mit Wasser Lithiumverlust und die Ergebnisse systematischer Analysen halfen die in der Literatur bestehenden Unklarheiten bezüglich dieser Phase zu klären. Zuvor angenommene Phasenumwandlungen von α-Li_2TiO_3 beim Erhitzen derselben konnten mittels *in-situ* Neutronen-Diffraktometrie nachgewiesen werden. Darüber hinaus wurde seine Kristallstruktur zum ersten Mal bestimmt und mit Hilfe von *in-situ* Synchrotron-Diffraktometrie die Kinetik seiner hydrothermalen Herstellung.

Das schon kommerziell produzierte $Li_4Ti_5O_{12}$ (Süd-Chemie AG) zeigt eine ausgezeichnete Zyklenstabilität und Belastbarkeit und wurde mittels Impedanz Spektroskopie und Neutronen-Diffraktometrie beim Erhitzen bis zu 1100 $°C$ untersucht. Hierbei konnten bestehende Vermutungen bezüglich Li-Wanderung bei erhöhten Temperaturen bestätigt werden, jedoch mit einer von der allgemeinen Annahme abweichenden Deutung der Resultate. Schliesslich wurde eine Möglichkeit gefunden, $Li_4Ti_5O_{12}$ auf direktem Wege hydrothermal herzustellen. Mit Lithiumethoxid und Titan (IV) Isopropoxid als Reaktanden bildete sich innerhalb von $\approx$ 30 Sekunden ein nanopartikuläres $Li_4Ti_5O_{12}$ mit einer spezifischen Oberfläche von 230 m^2/g. Das Produkt zeigt jedoch erst nach Wärmebehandlung ($<$ 500 $°C$) eine stabile Zyklenbeständigkeit. Die konkrete Ursache für die abfallende Kapazität des unbehandelten Produkts ist Gegenstand aktueller Untersuchungen und möglicher weiterer Forschung.

Chapter 1

Introduction

Nowadays, incessant growth of the world's energy consumption is leading to a faster depletion of fossil fuels like coal, petrol and gas. This tendency has driven up the price of these fuels in the market and has created a strong dependence on the countries producing these materials (Scrosati and Garche, 2010). Furthermore, burning fossil fuels causes CO_2 emissions, which are ascribed to accelerate the global warming (Xu et al., 2010). In order to reduce CO_2 emissions, renewable energy sources are becoming increasingly important. However, for an efficient exploitation of these sources new ways to store this sustainable energy require development (Liu et al., 2010).

$Li_4Ti_5O_{12}$ spinel is, due to its excellent cyclability and inherent safety, currently used as anode material in lithium-ion batteries, which are ubiquitous to most new technologies. Their application in terms of electric vehicles (EV) and hybrid-electric vehicles (HEV) is booming (Liu et al., 2010), while large-scale applications to store energy, e.g. produced in wind or solar power plants, are under discussion. Lithium-ion batteries could help the society to benefit from sustainable energies, through saving the environment and redeeming the economy.

1.1 Rechargeable lithium-ion batteries

As previously mentioned, lithium-ion batteries can be used to store the energy produced in solar and wind power plants and to supply power to EVs among many other applications. However, fundamental research is required to improve the characteristics of these batteries to endow them with longer life times, faster charging rates and higher power densities. With regard to the energy density, lithium-ion batteries offer a much better performance when compared to other rechargeable batteries (see Figure 1.1, Scrosati and Garche (2010)).

Lithium is, at room temperature, the lightest solid element in the periodic table. It possesses the highest reducing potential (-3.04 V), as well as a very high specific capacity (3862 mAh/g). The specific capacity of any active lithium-ion material can be calculated in relation to the weight percentage ($wt\%$) of lithium in the compound or the amount of lithium that can be intercalated in these compounds. For example, the 4.4 $wt\%$ of lithium

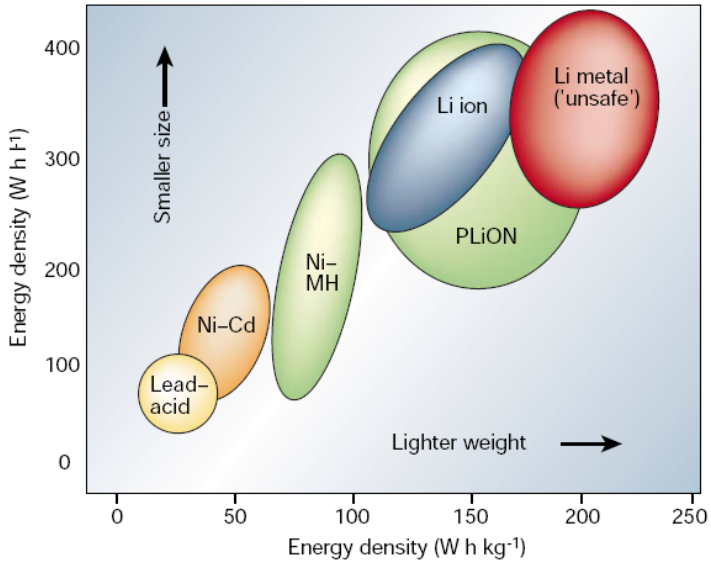

Figure 1.1: Energy densities of different types of rechargeable batteries (Scrosati and Garche, 2010).

in $LiFePO_4$ leads to a theoretical capacity of 170 mAh/g, while the possible intercalation of $3\,Li^+$ in $Li_4Ti_5O_{12}$ to $Li_7Ti_5O_{12}$ results in the theoretical capacity of 175 mAh/g.

The high specific capacity in combination with the low molar mass of lithium makes it at the moment, the best electrochemical active element for rechargeable batteries. In a rechargeable lithium battery, lithium is shuttled between a positive and a negative electrode. The electrodes must be held apart from each other by a separator, which allows the passage of lithium ions, and an electrolyte is used to improve the ionic conductivity upon charging and discharging (see Figure 1.2).

Especially for EVs and HEVs or large-scale applications, fast charging and discharging rates are essential, highlighting the importance of the rate capability of a rechargeable battery. To define the charging/discharging rate, let us consider a battery with a theoretical capacity of 160 mAh/g. Charging/discharging of this battery with a current of 160 mA gives a charging/discharging rate of 1C/1D. Charging this battery with 10C would then require a current of 1600 mA. In general, the capacity decreases with higher rates, i.e. the lithium ions have less time to find an empty spot in the other electrode. Diffusion paths in large compounds are long, which results in a decrease of the rate performance, and therefore the particle size of an active material is a decisive factor in terms of the rate performance.

The cyclability is another crucial factor which describes the quality of a rechargeable battery, defined as the possibility to charge and discharge a battery for a certain number of times. It is important to point out that every battery loses capacity with time. This is mainly ascribed to mechanical processes during charging and discharging (Wagemaker et al., 2006), which might change the properties of the active material and thus lithium

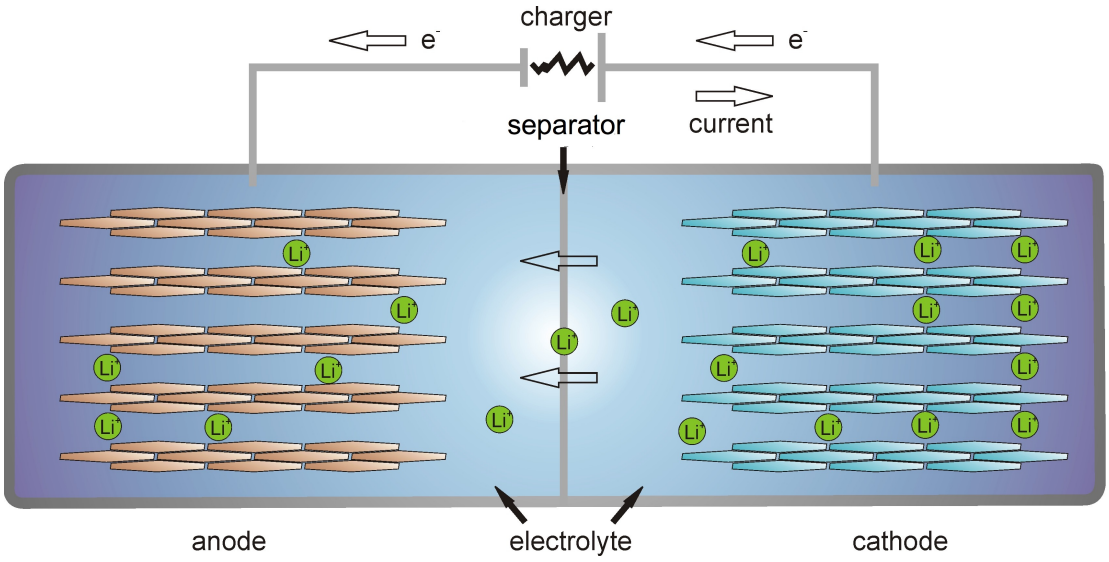

Figure 1.2: Outline of a lithium-ion battery.

can no longer be fully intercalated.

1.1.1 Cathode materials

Large amounts of effort is put into the development of new and better cathode materials, and a tremendous variety of cathode materials are used in lithium-ion batteries. The present study concentrates on $Li_4Ti_5O_{12}$, which is due to its potential of ca. 1.55 V versus Li/Li^+ theoretically applicable as a cathode in rechargeable lithium-ion batteries. However, current applications consider $Li_4Ti_5O_{12}$ exclusively as anode material, and thus here only a brief introduction in cathode materials will be given.

Todays most discussed cathode material is the lithium iron phosphate $LiFePO_4$ (Padhi et al., 1997). Interestingly enough, it is, up to now, the only known battery material that exists in nature in a similar composition: the mineral triphylite. In triphylite, iron is partly substituted by manganese, but a natural manganese-free end-member of triphylite has not been found so far. However, in theory, triphylite could be used as cathode material in rechargeable batteries.

The production of the electrode material $LiFePO_4$ is cheap, as iron is a very low-cost resource compared with other battery materials, which often comprise, e.g., cobalt or nickel. The electrical conductivity of $LiFePO_4$ is weak and therefore the material must be enhanced via carbon-coating (Doeff et al., 2006). In comparison with cobalt-containing battery materials, $LiFePO_4$ is environmentally friendly and, due to its low working voltage of 3.45 V, considerably safer (Goddenough and Kim, 2010; Padhi et al., 1997), and has a good cyclability (Shukla and Kumar, 2008). When cycling, delithiation of $LiFePO_4$ leads to $FePO_4$, in which all ferrous iron is oxidated to ferric iron. Once again, there exists a manganese containing analogue in nature, the mineral heterosite (Fehr et al., 2010a).

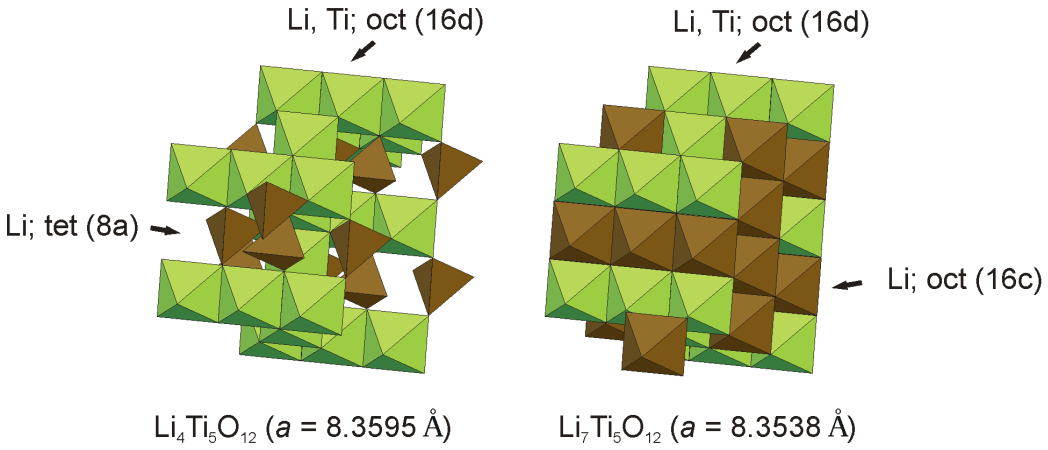

Figure 1.3: Crystal structure of $Li_4Ti_5O_{12}$ and $Li_7Ti_5O_{12}$.

1.1.2 Anode materials

Graphite is the anode material which is currently used in the majority of lithium-ion batteries. Production costs for graphite as an anode are unbeatably low, and it has a very high specific capacity of 372 mAh/g at a low potential of $\approx 0.05\ V$. Lithium can be inserted in the graphite structure, up to a 1 : 6 lithium-carbon ratio of atoms. Its drawbacks are a weak cyclability and the possibility of the formation of dendrites, which may cause short-circuits when breaking through the separator (Huggins, 2009).

$Li_4Ti_5O_{12}$ is a comparably new anode material, and it is one of the most promising alternative active materials to replace graphite as the anode in rechargeable lithium-ion batteries. In comparison with graphite, it is known as an inherently safe anode material with excellent lithium-ion mobility (Belharouak et al., 2007; Zaghib et al., 1998, 1999). Thinking of EVs equiped with lithium-ion battery packs of several kilos, the safety of these batteries is of the highest priority and it is unimaginable if these batteries would overheat and catch fire as, e.g., has already happened to portable computers (Balakrishnan et al., 2006).

At a flat potential of ca. 1.55 V (versus Li^+/Li), 3 Li^+ ions can be electrochemically intercalated in $Li_4Ti_5O_{12}$ to its lithiated form $Li_7Ti_5O_{12}$. Its potential is significantly higher than that of graphite, which has a striking disadvantage regarding the overall cell voltage. During the intercalation process, $Li_4Ti_5O_{12}$ undergoes only minor structural changes ("zero strain material"), and thus the variations in the cubic lattice dimension between $Li_4Ti_5O_{12}$ and $Li_7Ti_5O_{12}$ remain negligible. The only structural change is the migration of lithium ions from tetrahedral 8a sites to octahedral 16c sites and the occupation of the 16c with 3 Li^+ (Figure 1.3). As a consequence, it has a good Li^+ insertion and de-insertion reversibility, i.e. an excellent cyclability (Aldon et al., 2004; Borghols et al., 2010; Colin et al., 2010; Scharner et al., 1999).

The volume change between $LiFePO_4$ and its de-lithiated form $FePO_4$ is approximately

6.5% (Padhi et al., 1997), which is also a reasonably low value, but higher than in $Li_4Ti_5O_{12}$, and therefore the cyclability of $LiFePO_4$ is weaker. Particularly for large-scale applications, like EVs or stationary power plants, active materials with a very good cyclability are desirable, and thus, the $Li_4Ti_5O_{12}$ spinel is probably the best choice. Although its high potential of 1.55 V versus Li^+/Li is a drawback, the combination of $Li_4Ti_5O_{12}$ as the anode and, $LiFePO_4$ as the cathode leads to a battery with a potential difference of approximately 2 V (Morales et al., 2010). When connecting 6 such batteries in series, the resulting voltage is 12 V, within the range of conventional lead-acid batteries, and therefore, they could replace lead-acid batteries in stationary applications like wind and solar power plants, or starter batteries in conventional cars.

Although $Li_4Ti_5O_{12}$ is established as anode material for lithium-ion batteries, better knowledge of its structural properties and of its phase relations can contribute to develop new techniques to produce $Li_4Ti_5O_{12}$ with a better electrochemical performance. Therefore, in the present work, not only the compound $Li_4Ti_5O_{12}$ itself was studied, but as well its phase relations.

1.2 The family of compounds in the Li-Ti-O-H system

The present study deals with lithium titanium compounds of the system Li-Ti-O, but as hydrogen and water have a strong influence at low temperatures, the system is expanded for hydrogen to Li-Ti-O-H. The phase relations in the system Li-Ti-O at temperatures above 600 °C are well known, and most recent publications concerning these are based on the study of Kleykamp (2002) (see Figure 1.4).

Phase diagrams at lower temperatures or in the system Li-Ti-O-H have not been presented so far, and data published about lithium titanium phases produced at low temperatures under hydrothermal conditions differ remarkably, especially data of the cubic α-Li_2TiO_3 (see below and a detailed discussion in Chapter 2).

It is known that four stable lithium titanate compounds, which are mainly produced by solid-state reactions, exist in the system Li-Ti-O (Kleykamp, 2002). $Li_2Ti_3O_7$ is, as $Li_4Ti_5O_{12}$, being discussed as an active material for lithium-ion batteries. In addition, the two phases with the highest Li/Ti ratio of the system, β-Li_2TiO_3 and Li_4TiO_4, are both considered as solid tritium breeder materials for fusion reactors. Nuclear fusion is a process in which atomic nuclei join together to form a new and heavier nucleus, usually with the release of high quantities of energy, as occurs in the sun. However, applications of the Li-Ti-O system for nuclear fusion is not part of the present study. Here, only analyses of β-Li_2TiO_3 concerning its structural properties will be given. Moreover, the lithium diffusion of β-Li_2TiO_3 (Vijayakumar et al., 2009) and its cyclability (Shu, 2009) are weak and, therefore, it cannot be considered as an active material for lithium-ion batteries. With respect to the phase diagram presented by Kleykamp (2002), the data obtained during this study via neutron *in-situ* measurements of Li_2TiO_3 (Chapter 2) and $Li_4Ti_5O_{12}$ (Chapter 4) are in good agreement with the reported temperatures. As such, the phase transition of β-Li_2TiO_3 to γ-Li_2TiO_3, as well as the temperature of the decomposition of $Li_4Ti_5O_{12}$

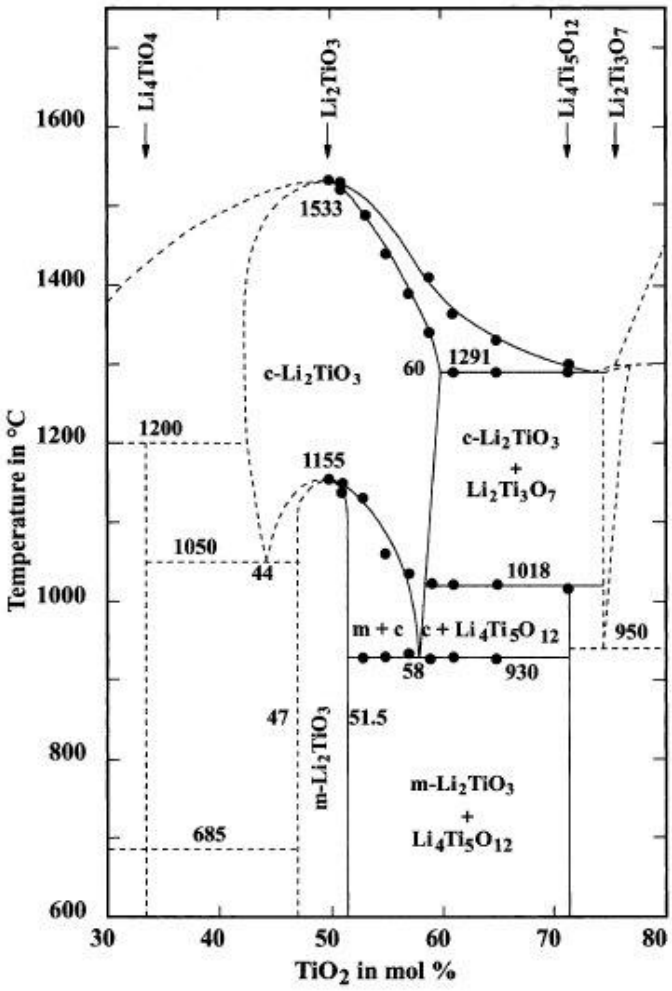

Figure 1.4: Phase diagram of the Li-Ti-O system at temperatures above 600 $°C$ by Kleykamp (2002).

to γ-Li_2TiO_3 and $Li_2Ti_3O_7$, match well with the expected values (see Figure 1.4).

1.2.1 Li_2TiO_3 – its three modifications

The compound Li_2TiO_3 and its three different modifications, α, β and γ, are the main topics of the Chapters 2 and 3, with emphasis placed on the poorly described, metastable cubic α-Li_2TiO_3. The well known monoclinic β-Li_2TiO_3 is the stable Li_2TiO_3 modification at room temperature. At ≈ 1155 $°C$, it transforms to the disordered cubic γ-Li_2TiO_3 (Kleykamp, 2002). Cubic α-Li_2TiO_3 is described as the metastable low-temperature Li_2TiO_3 modification, which can only be produced via hydrothermal reactions. No study on lithium titanate compounds synthesized in aqueous solutions presented structural analyses and, moreover, ambiguities concerning the stoichiometry of α-Li_2TiO_3 and

phases which can be obtained after annealing of intermediate lithium titanium compounds have been presented. The ambiguities surrounding cubic α-Li_2TiO_3 and other hydrothermally produced lithium titanate phases are described in Chapter 2, and an explanation thereof was obtained by testing the stability of α-Li_2TiO_3 when exposed to water. The first structural analyses of α-Li_2TiO_3 are displayed in Chapter 2, as well as its behavior upon heating to 1200 $°C$. Finally, kinetic studies for the formation of α-Li_2TiO_3 under hydrothermal conditions are shown in Chapter 3, recorded by *in-situ* synchrotron powder diffraction.

1.2.2 $Li_4Ti_5O_{12}$ – its structure and production

The anode material $Li_4Ti_5O_{12}$ is the topic in the Chapters 4 and 5. Its spinel-type structure in the space group $Fd\bar{3}m$ has been determined by Deschanvres et al. (1971) and recently a single crystal study revealed a detailed structural characterization (Kataoka et al., 2008) (Figure 1.3). When using the second choice of the space group $Fd\bar{3}m$ in the *International Tables of Crystallography* (Hahn, 1983) with the symmetry centre at the origin, lithium fully occupies tetrahedral 8*a* sites and 1/6 of the octahedral 16*d* sites in the inverse spinel structure (Julien and Zaghib, 2004; Kataoka et al., 2008; Vijayakumar et al., 2010). The other 5/6 of the 16*d* sites are filled by titanium-ions, while oxygen occupies the 32*e* tetrahedral sites ($(Li)^{8a}[Li_{1/3}Ti_{5/3}]^{16d}O_4^{32e}$) (Ohzuko et al., 1995; Kataoka et al., 2008). Recent spectroscopic studies (Leonidov et al., 2003, 2004; Vijayakumar et al., 2009, 2010) show the possible lithium occupancy as well on other crystallographic sites in the spinel structure, e.g. on 16*c*, which will be discussed in Chapter 4 and Chapter 5.

Research on nanoparticulate $Li_4Ti_5O_{12}$ powders displayed the possible intercalation of more than 3 Li^+ in the $Li_4Ti_5O_{12}$ structure (Borghols et al., 2010). Similar observations have been found in the present study by the investigation of a nano-scale $Li_4Ti_5O_{12}$ which has been produced by a new hydrothermal syntheses (Chapter 5). The hydrothermally produced $Li_4Ti_5O_{12}$ shows structural properties which vary from another $Li_4Ti_5O_{12}$ compound, for which a patent pending method has been developed during the present study (Chapter 4). The later was produced in two steps, first by the hydrothermal treatment of titania in LiOH solution, and second, due to annealing of the obtained hydrothermal composite. The inconsistent characteristics of both $Li_4Ti_5O_{12}$ allows the assumption that the synthesis method has a great influence on the structural or microstructural properties and thus the electrochemical performance. A brief introduction into the most relevant production methods for the applied techniques of this study is given in the following section.

Solid-state reactions are frequently applied to produce $Li_4Ti_5O_{12}$ spinel. It is the reaction of titania powder (anatase or rutile) with a lithium salt, e.g. Li_2CO_3, or LiOH at high temperatures (Colbow et al., 1989; Ohzuko et al., 1995; Scharner et al., 1999; Zaghib et al., 1998). The high temperatures cause particle growth and the resulting longer diffusion paths lower the rate capability. The usage of smaller titania reactants may lower the reaction temperature to obtain the pure phase $Li_4Ti_5O_{12}$. Therefore, ball-milling techniques are applied to reduce the particle size of the reactants, as grinding is often cheaper

than buying nano-sized titanium particles. The lower melting point of LiOH compared with Li_2CO_3 enables lower synthesis temperatures when using LiOH. But LiOH is more corrosive than Li_2CO_3, and special vessels for the heat treatment have to be chosen. In summary, trials to lower the synthesis temperature are always accompanied with higher costs, either for buying small titania particles, grinding titania or investing in resistant materials for the furnaces and vessels. Subsequent ball-milling of annealed particles $Li_4Ti_5O_{12}$ is implemented as well, but here again, the production costs rise. Moreover, high-energy ball milling may lead to highly defective material and often impurities due to abrasion are found (Iwaniak et al., 2009).

Sol gel methods can be used to synthesize $Li_4Ti_5O_{12}$ as well. These methods have the advantage that $Li_4Ti_5O_{12}$ can be produced in small particle sizes due to the low temperatures of the heat treatment. This often leads to $Li_4Ti_5O_{12}$ compounds with excellent electrochemical properties, but the relevance for commercial applications is unclear, due to the high cost of the reactants, problems for large-scale production and long syntheses times of up to a few days.

Hydrothermal syntheses in general have a low energy demand and are therefore also called green energy methods (Yoshimura and Byrappa, 2008) and thus are becoming more and more popular. Besides their low energy demand, hydrothermal syntheses have a broad spectrum of advantages compared to solid-state reactions. Whereas for solid-state reactions the syntheses temperature, the time and the choice of reactants influence the production, in hydrothermal syntheses, e.g., the pH, the concentration of reactants, the pressure and the solvent can also be varied. Therefore, it is not surprising that hydrothermal methods are already applied to supply the active material $LiFePO_4$ (Dokko et al., 2007). But ideas like the "hydrothermal and solvothermal vending machine" (Byrappa and Adschiri, 2007), where desired characteristics like particle size and shape of any product can be easily adjusted and forecasted, remain a dream.

In this study, cubic α-Li_2TiO_3 was synthesized by a hydrothermal technique, and it was shown that this technique enables the production of cubic Li_2TiO_3 at low temperatures. The low-temperature modification was found to be isostructural with γ-Li_2TiO_3, the high temperature modification of Li_2TiO_3. The α-Li_2TiO_3 produced by low temperatures might be stabilized by protons due to the synthesis procedure (Chapter 2).

When working with supercritical fluids, nanoparticles can be synthesized in a very short time span (Lester et al., 2006), and by varying the temperature and synthesis time, nanoparticles of a narrow size distribution can be obtained (Bremholm et al., 2008). For syntheses using supercritical fluids, the choice of reactants is often similar with sol-gel methods. The big advantage of supercritical syntheses when compared with sol-gel methods is the highly reduced reaction time and moreover, supercritical syntheses produce crystalline materials which often do not demand subsequent annealing.

Chapter 5 shows the first attempt to synthesize $Li_4Ti_5O_{12}$ in a continuous flow synthesis with supercritical water as the solvent. This method enables the production of $Li_4Ti_5O_{12}$

in less than one minute. However, although crystalline, the electrochemical performance fades which may be ascribed to high strain in the particles which only relaxes when heating above 500 $°C$. Heat treated materials show a stable cyclability and when annealed at only 600 $°C$, they remain nanoparticulate, which was shown by *in-situ* synchrotron powder diffraction.

1.3 Characterization methods

The techniques to study the lithium titanate phases applied in this dissertation are mentioned in their corresponding methods sections. Here, *in-situ* synchrotron and neutron powder diffraction are introduced to specifically outline their key characteristics and advantages over other methods.

1.3.1 *In-situ* synchrotron powder diffraction

Synchrotron diffraction enables enhanced crystallographic investigations using X-ray beams of high brilliance, which can be employed to measure particles of small size and in small amounts, but with short exposure times, which makes it feasible to study the kinetics of rapid reactions (Cerenius et al., 2000). The experiments presented in Chapter 3 were performed at the crystallography beam-line I711 at the synchrotron MAX-lab II in Lund, Sweden. A photo of the setup is shown in Figure C.1 in the supplementary material 2 of Appendix C. In this setup, the synchrotron beam has to pass through a sapphire capillary, the hydrothermal solution and still has enough energy to extract the crystallographic information of the crystalline powder. This is only enabled by a very high flux, which at beam-line I711 is approximately 1011 photons s^{-1} at a wavelength of 0.997 Å. With a time-resolution of 10.5 s per exposure, single exposures could be recorded. Firstly, thorough masking (e.g. of the beam-stop and noise in form of spikes (See Figure C.2 in the supplementary material 2 of Appendix C) of the obtained two-dimensional frames was done with the program FIT 2D (Hammersley et al., 1996) before the data was converted to ASCI files, which can be read with a wide range of analysis programs. The structural Rietveld refinements were performed with the program FullProf.

To exemplify the fast kinetics of the formation of α-Li_2TiO_3 under hydrothermal conditions, a plot of the reaction progress vs. time is shown in Figure 1.5 (at a temperature of 230 $°C$). The progression plots of all performed experiments can be seen in the supplementary material 1 of Appendix C .

1.3.2 *In-situ* neutron powder diffraction

Neutron powder measurements (Chapters 2 and 4) were performed at the instrument SPODI at FRM II in Garching, Germany (Hoelzel et al., 2007). In neutron diffraction, the neutron beam interacts with the nucleus of an atom, whereas in X-ray diffraction, the electron beam interacts with the electron cloud. For structural determinations of

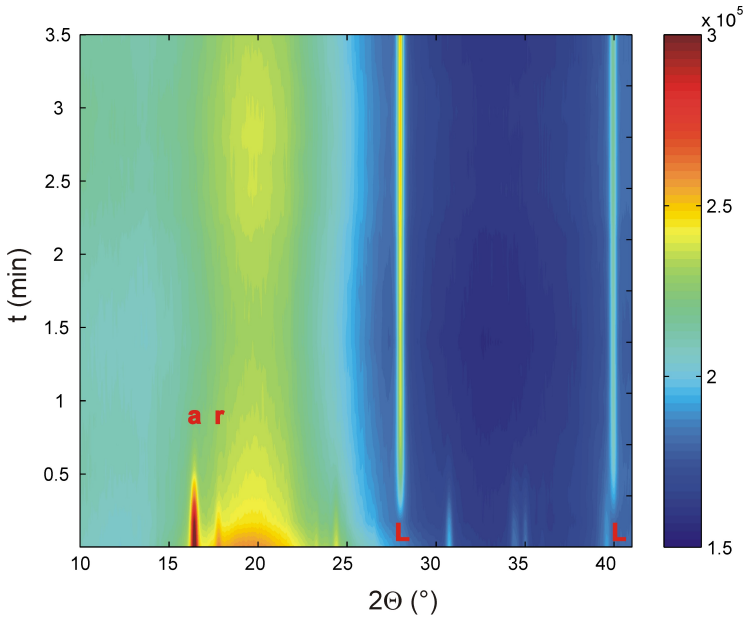

Figure 1.5: Decreasing reflections of anatase (a) and rutile (r) with ongoing formation of α-Li_2TiO_3 (L) versus time at a temperature of 230 $°C$. ($\lambda = 0.997$ Å).

compounds containing light elements with a low electron density (e.g. lithium), neutron powder diffraction is the most appropriate method. For neutron powder diffraction, lithium has a high negative scattering length, and thus its position in the crystal structure is easy to detect. In comparison, lithium is nearly invisible to X-rays due to its low scattering factor.

The experiments were performed for structure determinations and to observe structural changes upon heating. High time-resolution is not required, as it was expected that the structural transformations would be temperature-dependent but not time-dependent. Therefore, the setup and the wavelength were chosen for an optimized resolution rather than for a high flux.

1.4 Outline of this study

The system Li-Ti-O contains important intermediate lithium titanate phases which are discussed as solid tritium breeder compounds used in fusion reactors, or are currently produced as anode materials for rechargeable batteries. The phase relations of intermediate lithium titanates are well known above 600 $°C$, but fairly unknown and inconsistent at temperatures below. The present dissertation helps to unravel existing ambiguities concerning the phase relations in the system Li-Ti-O, especially at low temperatures and when water is involved during synthesis. Moreover, two novel processes to produce the anode material $Li_4Ti_5O_{12}$ for rechargeable lithium-ion batteries were developed, of which one is patent pending by Süd-Chemie AG, Moosburg.

Chapter 2 deals with the synthesis of the formerly poorly described cubic α-Li_2TiO_3. In tests of the stability of α-Li_2TiO_3, it was found to be unstable when exposed to humidity, water or atmospheric moist. Due to washing of α-Li_2TiO_3 samples, lithium-ion exchange with protons occurred, and depending on the amount of lithium leached, such intermediate lithium titanium phases transform to the anode material $Li_4Ti_5O_{12}$ when annealed (Laumann et al. (2010) in Appendix A). As the structure of α-Li_2TiO_3 has not been described so far, structural investigations were performed upon heating of the metastable cubic α-Li_2TiO_3 by neutron powder diffraction. Therewith two major phase transformations were observed, first to the stable monoclinic β-Li_2TiO_3 modification, and at high temperatures to the cubic γ-Li_2TiO_3. The α and the γ-phase where found to be isostructural, proposing that by hydrothermal reactions cubic Li_2TiO_3 can be produced in a metastable form, in which protons might stabilize the α-structure (Laumann et al. (2011b) in Appendix B).

In order to understand the reaction mechanisms of the formation of $Li_4Ti_5O_{12}$, a kinetic *in-situ* synchrotron radiation study was performed, presented in Chapter 3. Therewith the activation energy of the formation of α-Li_2TiO_3 by hydrothermal reaction could be determined and it was shown that, by hydrothermal synthesis, lithium is directly intercalated into the titania structure, without prior dissolving of the titania (Laumann et al. (2011c) in Appendix C).

Surprisingly, α-Li_2TiO_3 was found to be the key to developing a new synthesis route to produce the anode material $Li_4Ti_5O_{12}$, as shown in Chapter 4. The patent pending idea (Appendix D) is the synthesis of $Li_4Ti_5O_{12}$ using a combination of a hydrothermal and a solid-state process. In electrochemical tests, the produced $Li_4Ti_5O_{12}$ shows an excellent cycling performance and a good performance at high rates. On one of these samples, produced by Süd-Chemie AG Moosburg, an impedance spectroscopy study (Fehr et al. (2010b) in Appendix E), and a multi-temperature *in-situ* neutron diffraction study has been performed (Laumann et al. (2011a) in Appendix F). Here, higher lithium mobility could be demonstrated from around 700 $°C$, leading to a non-linear thermal expansion and an observed kink in the activation energy at similar temperatures, measured by impedance spectroscopy. Previously, neutron measurements on $Li_4Ti_5O_{12}$ have been performed by other groups, but the measurement during this thesis was the first high temperature study up to the decomposition temperature of $Li_4Ti_5O_{12}$.

The synthesis of $Li_4Ti_5O_{12}$ was the key focus of this study and therefore various different approaches to produce it were performed. For the syntheses under hydrothermal conditions, the choice of precursors proved to be crucial for the successful hydrothermal syntheses of $Li_4Ti_5O_{12}$. When using crystalline titania powder in lithium hydroxide solution, the resulting lithium titanate was exclusively Li_2TiO_3, and for a Li/Ti ratio < 2 mixed with unreacted titania. Therefore, working with crystalline titania, the compound $Li_4Ti_5O_{12}$ could never be synthesized directly by hydrothermal syntheses up to a temperature of 400 $°C$ and a pressure of 250 bar. The hydrothermal conversion of an amorphous titanium precursor (obtained e.g. via hydrolyzation of titanium (IV) isopropoxide (TTIP)) in a lithium hydroxide solution results in the compound $(Li_{1.81}H_{0.19})Ti_2O_5{\cdot}2H_2O$. Upon annealing by solid-state reaction, $(Li_{1.81}H_{0.19})Ti_2O_5{\cdot}2H_2O$ transforms into $Li_4Ti_5O_{12}$ (Sugita et al., 1990; Qiu et al., 2010), which also could be proven during this study.

Chapter 5 describes the first successful synthesis of $Li_4Ti_5O_{12}$ in one hydrothermal step without subsequent annealing (Appendix G). Here, the reactant is a solution of lithium metal in absolute ethanol mixed with TTIP, which is hydrothermally treated in a continuous flow reactor with water heated to $> 350\ ^\circ C$. After dissolution of lithium in absolute ethanol, a milky solution was typically obtained, which cleared up by adding TTIP. It can be proposed that the formation of a lithium titanium complex clears up the solution and functions like a template for the reaction to $Li_4Ti_5O_{12}$, in contrast to what occurs when using crystalline titania as reactant. Thus it seems that the nature of the bonding of the formed lithium titanium precursor influences the structure of the hydrothermal product.

However, the short reaction time and the low synthesis temperature of about $350\ ^\circ C$ produced $Li_4Ti_5O_{12}$ with a fading capacity when electrochemical tested. Annealing of the hydrothermally synthesized $Li_4Ti_5O_{12}$ at $600\ ^\circ C$ caused only minor particle growth which was demonstrated by *in-situ* synchrotron powder diffraction and $Li_4Ti_5O_{12}$ nanoparticles with a very good cyclability and rate performance were produced. But the reasons for the fading of the capacity of the non-annealed samples are not fully resolved. Probably the relative low crystallinity is the main reason, but a differing lithium distribution than the commonly reported one ($(Li)^{8a}[Li_{1/3}Ti_{5/3}]^{16d}O_4^{32e}$), due to a possible Li occupancy on octahedral 16*c* sites, might also affect the electrochemical performance, as presented and discussed in Chapter 5. In a brief outline in the end of Chapter 5, ideas will be given for future work and possible methods to finally solve unanswered questions about differing crystal structures of $Li_4Ti_5O_{12}$ compounds, and particularly of the hydrothermally produced $Li_4Ti_5O_{12}$, will be proposed.

Chapter 2

Synthesis of α-Li_2TiO_3 – Its stability and structural transformations upon heating

This chapter shows the results of the manuscripts in Appendices A and B. It presents the hydrothermal synthesis of α-Li_2TiO_3 under P_{sat} at 180 $^\circ C$. Water-flushing and bathing experiments were performed to test the stability of the prepared samples in the presence of water at room temperature. Here it was shown that lithium ions in α-Li_2TiO_3 are bond weakly and can be easily leached with de-ionized water. Then, the structural changes of an un-washed α-Li_2TiO_3 sample were studied *in-situ* by neutron powder diffraction, initially upon heating up to 1200 $^\circ C$, and then upon cooling down back to room temperature. The unit cell dimensions obtained by the neutron diffraction study were compared with the ones measured by *in-situ* synchrotron diffraction of a sample showing a Li-deficit of about 40% due to washing.

2.1 Introduction

Cubic α-Li_2TiO_3 has been introduced as the low-temperature modification of Li_2TiO_3, which can only be produced via hydrothermal reaction. However, ambiguous data have been published concerning its composition and structural properties. These ambiguities, especially large, concern the lithium content (Pei et al., 2007; Zhang et al., 2007; Sikhwivhilu et al., 2009) and the phases obtained after annealing (Fattakhova and Krtil, 2002b,a). The displayed powder X-ray (PXRD) patterns of the synthesized α-Li_2TiO_3 look alike, but the Li/Ti ratios vary from 2 : 1 (calculated from the given atomic %) (Song et al., 2007) over 1.69 : 1 (Tabuchi et al., 2003) to 0.34 : 1 (Tomiha et al., 2002). The PXRD patterns were compared with the high-temperature form γ-Li_2TiO_3 (Song et al., 2007; Tabuchi et al., 2003), which was first described by Kordes (1933, 1935). Furthermore, various PXRD patterns of intermediate lithium titanates, similar to the pattern of the α-Li_2TiO_3 have been published (Fattakhova and Krtil, 2002a,b; Fattakhova et al., 2005; Pei et al., 2007;

Zhang et al., 2007; Jiang et al., 2008). The phases were described as $Li_{0.665}Ti_{0.82}O_2{\cdot}H_2O$ (Fattakhova and Krtil, 2002a), $Li_{1+x}Ti_{2-x}O_{4+\delta}$ (x between 0 and 0.1, δ between 0.3 and 0.5) (Fattakhova et al., 2005; Jiang et al., 2008), or $LiTiO_2$ (Fattakhova and Krtil, 2002b; Pei et al., 2007; Zhang et al., 2007; Sikhwivhilu et al., 2009). It must be noted, that the hydrothermally produced compounds, described above, were all washed after synthesis. Then, annealing of some of these water treated intermediate lithium titanium phases led to compounds similar to $Li_4Ti_5O_{12}$ (Fattakhova and Krtil, 2002a; Fattakhova et al., 2005; Jiang et al., 2008).

Diverse results were also published on the cubic γ-Li_2TiO_3. It was asserted that it can be quenched to room temperature without transformation to the stable β-modification at low temperatures (Kordes, 1935; Barblan et al., 1958). Others negated the possibility of quenching γ-Li_2TiO_3 (Castellanos and West, 1979; Baños et al., 1990), but showed that solid solutions of cubic Li_2TiO_3-MgO (Castellanos and West, 1979) or Li_2TiO_3-Li_3NbO_4 (Baños et al., 1990) keep their cubic structure when quenched to room temperature. Annealing of these cubic solid solutions leads to a slow phase transition between 550 and 750 $°C$ to an ordered monoclinic solid solution which is isostructural with β-Li_2TiO_3 (Baños et al., 1990).

2.2 Experimental

2.2.1 Preparation of cubic Li_2TiO_3 powders

Cubic α-Li_2TiO_3 powders were synthesized at 180 $°C$ for 18 hours in polytetrafluorethylene (PTFE) containers. The reactants were TiO_2 powder, comprising anatase and rutile (Evonik, formerly Degussa, AEROXIDE TiO_2 P25), and lithium hydroxide (SQM, Chile). For the reaction, 0.025 mol of P25 were stirred in a solution of 0.05 mol lithium hydroxide dissolved in 15 ml of de-ionized water. The product was filtered with a vacuum filter and left unwashed. It was dried at 60 $°C$, de-agglomerated in an agate mortar, and kept in an argon atmosphere.

2.2.2 Water-flushing and bathing experiments

For a series of water-flushing experiments, 100 mg of α-Li_2TiO_3 were flushed with a flow rate of approximately 100 ml/h in a paper filter with various amounts of de-ionized water (Table 2.1). For bathing experiments, 100 mg of α-Li_2TiO_3 were stirred for 5 hours in 10, 25, 50, 100, 300 and 500 ml of de-ionized water and then left to precipitate over a period of 4 days in a glass beaker (Table 2.1).

2.2.3 Characterization

The lithium content of washed and unwashed samples was measured by atomic absorption spectroscopy (AAS), using a Perkin-Elmer 3300 in an air-acetylene flame at a

Table 2.1: Sample list of the water-flushing (F) and bathing (B) experiments, the resulting Li-loss and the Li/Ti ratio, respectively, as well as the hypothetical formulas. Sample U remained un-washed.

Sample	Volume H_2O (ml)	Li-loss (%)	Li/Ti ratio	Hypothetical formula[a]
U	0	0	2:1	$(Li_1H_0)_2TiO_3$
F1	50	25	1.50:1	$(Li_{0.75}H_{0.25})_2TiO_3$
F2	100	13	1.74:1	$(Li_{0.8}7H_{0.13})_2TiO_3$
F3	200	24	1.52:1	$(Li_{0.76}H_{0.24})_2TiO_3$
F4	300	26	1.48:1	$(Li_{0.74}H_{0.26})_2TiO_3$
F5	500	43	1.16:1	$(Li_{0.57}H_{0.43})_2TiO_3$
F6	750	37	1.26:1	$(Li_{0.63}H_{0.37})_2TiO_3$
B1	10	44	1.12:1	$(Li_{0.56}H_{0.44})_2TiO_3$
B2	25	57	0.86:1	$(Li_{0.43}H_{0.57})_2TiO_3$
B3	50	62	0.76:1	$(Li_{0.38}H_{0.62})_2TiO_3$
B4	100	66	0.68:1	$(Li_{0.34}H_{0.66})_2TiO_3$
B5	200	68	0.64:1	$(Li_{0.32}H_{0.58})_2TiO_3$
B6	300	73	0.54:1	$(Li_{0.27}H_{0.73})_2TiO_3$
B7	500	75	0.50:1	$(Li_{0.25}H_{0.75})_2TiO_3$

[a] Hydrogen calculated by charge balance (see Section 2.4.2).

wavelength of 670.8 nm. Samples were dried at 275 $°C$, i.e. below the temperature of the transition to the monoclinic phase, and dissolved in hot H_2SO_4. Powder X-ray diffraction (PXRD) was performed in transmission geometry on a Stoe STADI P diffractometer (CuKα1-radiation λ = 1.544056 Å, curved Ge(111) monochromator). Synchrotron data were recorded in temperature increments of 100 $°C$ in a temperature range of 100 K (-173 $°C$) to 600 K (327 $°C$) at SPring8, Japan. PXRD patterns were recorded. To ascertain the particle size, the instrumental broadening was determined with a CeO_2 standard.

Neutron powder diffraction measurements were carried out on the instrument SPODI (Hoelzel et al., 2007) at FRM II (Garching, Germany). Two grams of the α-Li_2TiO_3 powder were filled into a niobium container and placed in a high vacuum furnace. The reflections of niobium were included in all refinements as a second phase. The sample was heated at 5 $°C/min$ in a stepwise manner from room temperature to a maximum temperature of 1200 $°C$ and then cooled similarly to room temperature (see Table 2). Before the measurements (4 hours), a holding time of 15 minutes was given for temperature equilibration. The neutron patterns were recorded from 0.95° to 160° 2θ with a step width of 0.05°. The wavelength λ was determined from a previous measurement of silicon standard SRM 640c to be 1.5483 Å.

Rietveld refinement was performed by using the program FullProf (Rodríguez-Carvajal, 1993). To model the considerable line broadening, the pseudo Voigt function in the formulation of Thompson-Cox-Hastings (Thompson et al., 1987) was used, restricting it to

the refinement of Gaussian strain and Lorentzian size parameters. The full width at half maximum is calculated from

$$FWHM_G^2 = (U + e^2)\tan^2\Theta + V\tan\Theta + W \quad (2.1)$$

$$FWHM_L = \frac{Y + \lambda/L}{\cos\Theta} \quad (2.2)$$

where U, V, W and Y are the instrumental resolution parameters (obtained from a standard Y_2O_3 sample), λ is the wavelength and $e = \Delta d/d$ and L are the "apparent" strain and size parameters, respectively. The background was linearly interpolated between a set of background points with refinable heights.

2.3 Results

2.3.1 Interaction of α-Li_2TiO_3 with water

Li analyses of unwashed samples revealed the stoichiometric amount of lithium, with an error up to 3% below the theoretical value. Particularly in the bathing experiments, a decrease of the lithium contents when increasing the amount of water was observed (Table 2.1). The bathing experiments showed in general a higher Li-loss than the water-flushing tests, and a maximum loss of 75% was attained after a sample was bathed for 4 days in 500 *ml* of de-ionized water (Table 2.1). Samples left under atmospheric conditions started to react with CO_2 and thus the first traces of Li_2CO_3 were detected by PXRD after leaving samples for 3 days in air and the reflections of Li_2CO_3 became more pronounced after a longer latency.

2.3.2 PXRD at room temperature

At first glance, all samples with Li/Ti ratios in the range from 2 : 1 to 0.50 : 1 showed similar PXRD patterns to the one presented in Figure 2.2a. The unit cell parameter a of water-flushed samples only varied between 4.141 and 4.150 Å. Samples with high Li-loss showed a clear shift of the reflections to higher 2θ-angles and the lowest unit cell parameter was revealed for sample B6 with $a = 4.121(3)$ Å.

2.3.3 PXRD after annealing at 800 $^\circ C$

Interestingly, after the annealing of water treated samples at high temperatures (800 $^\circ C$) striking structural variations were noted, linked to the Li-loss of the samples (Figures 2.2b–d). Unwashed samples transformed to the monoclinic β-Li_2TiO_3 (Figure 2.2b); samples with a moderate Li-deficit, e.g. sample F6, resulted in a mixture of β-Li_2TiO_3 and $Li_4Ti_5O_{12}$ (Figure 2.2c), whereas samples with a high Li-deficit, like sample B5, showed the presence of $Li_4Ti_5O_{12}$ and TiO_2 (rutile) after the heat treatment (Figure 2.2d).

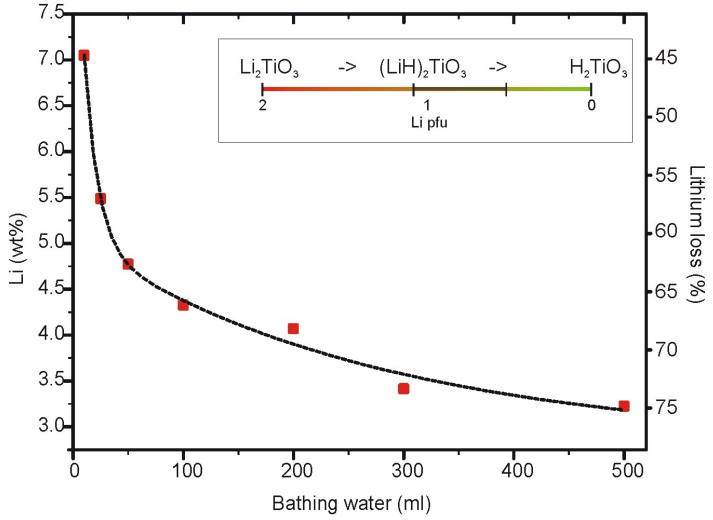

Figure 2.1: Bathing experiments on α-Li_2TiO_3. When interacting with water, lithium is leached from α-Li_2TiO_3 and products of the solid solution Li_2TiO_3-H_2TiO_3 are produced (see Section 2.4).

2.3.4 Neutron powder diffraction

Phase transformation upon heating An unwashed α-Li_2TiO_3 sample was used for the *in-situ* neutron experiment. At room temperature it could be clearly refined in the cubic space group $Fm\bar{3}m$ with a unit cell parameter of $a = 4.14276(1)$ Å. Minor impurities of 2.2(2) $wt\%$ of Li_2CO_3 (without regarding niobium) were detected (Figure 2.3a). Traces of LiOH may be expected from the synthesis procedure, but could not be discerned in the patterns.

The atomic array of the cubic phase is of the NaCl structure type, with a statistical distribution of lithium and titanium on one site and oxygen on the other site. Taking into account the strong bonding within the TiO_6 octahedra, the occupancies of titanium and oxygen were fixed to 0.333 and 1, respectively, and the occupancy of lithium was refined (0.667 occupancy for lithium is stoichiometric). Although the AAS measurement showed a lithium content close to the theoretical value, by neutron diffraction a clear Li-deficit of 7.5% ± 1% was observed at room temperature, corresponding to $Li_{1.85(2)}TiO_3$.

Upon heating, the reflections of Li_2CO_3 decreased between 300 and 400 $°C$ and vanished at 500 $°C$. For α-Li_2TiO_3 no structural changes were observed up to 250 $°C$. At 300 $°C$ small broad reflections of β-Li_2TiO_3 started to appear, but they were too broad to be included in the refinement. Upon further heating, the ratio of cubic to monoclinic Li_2TiO_3 decreased and the reflections of the monoclinic phase sharpened. Between 600 and 1000 $°C$ only the monoclinic phase could be refined. At 1100 $°C$, the cubic modification in space group $Fm\bar{3}m$ reappeared and, at the final temperature of 1200 $°C$, solely cubic (γ)-Li_2TiO_3 was present (Figure 2.3c).

The lithium occupancy of α-Li_2TiO_3 could only be refined at temperatures showing

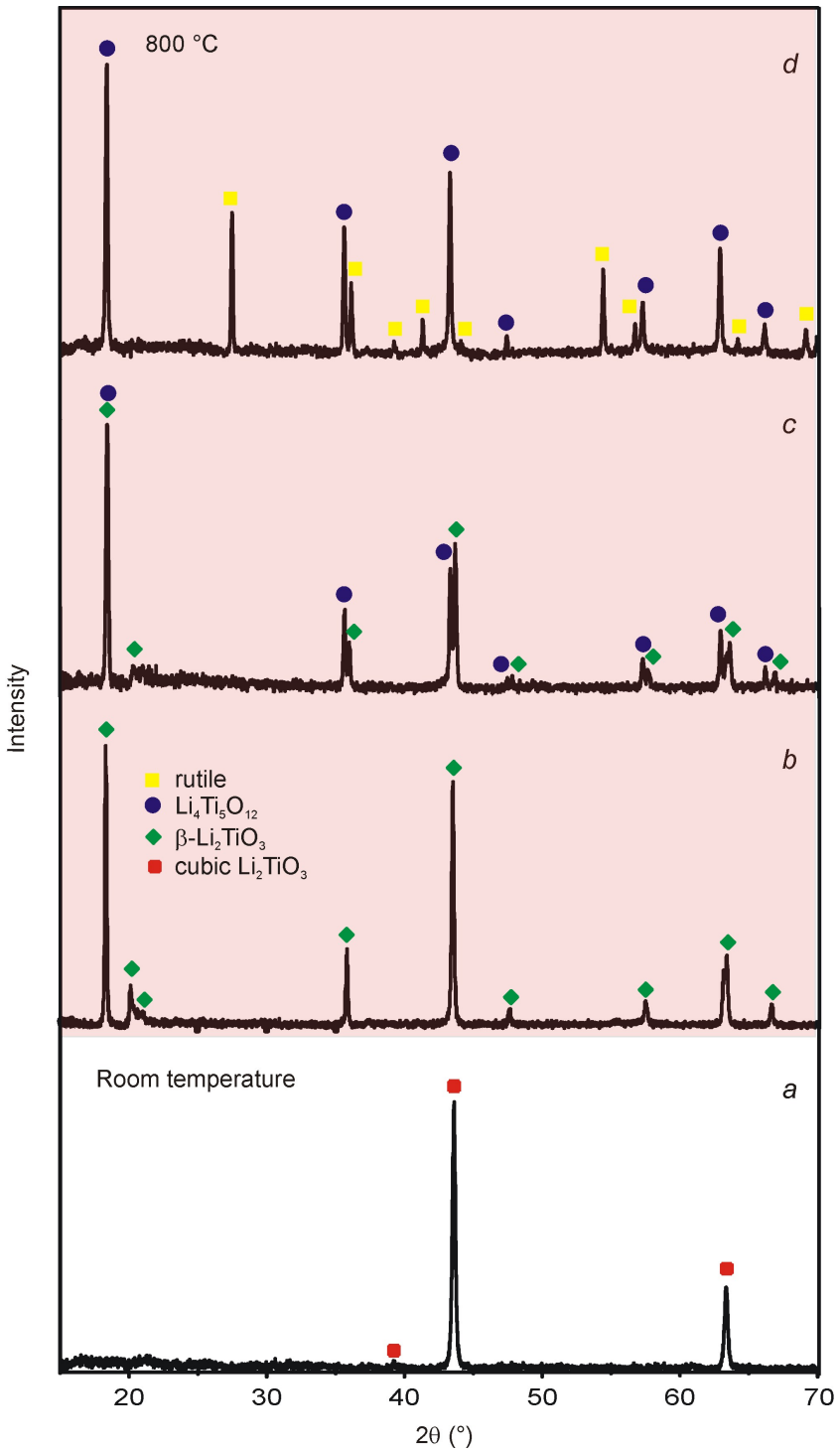

Figure 2.2: XRPD patterns of (a) sample U1 after the hydrothermal synthesis and of samples (b) U1, (c) F6 and (d) B5 annealed at 800 °C.

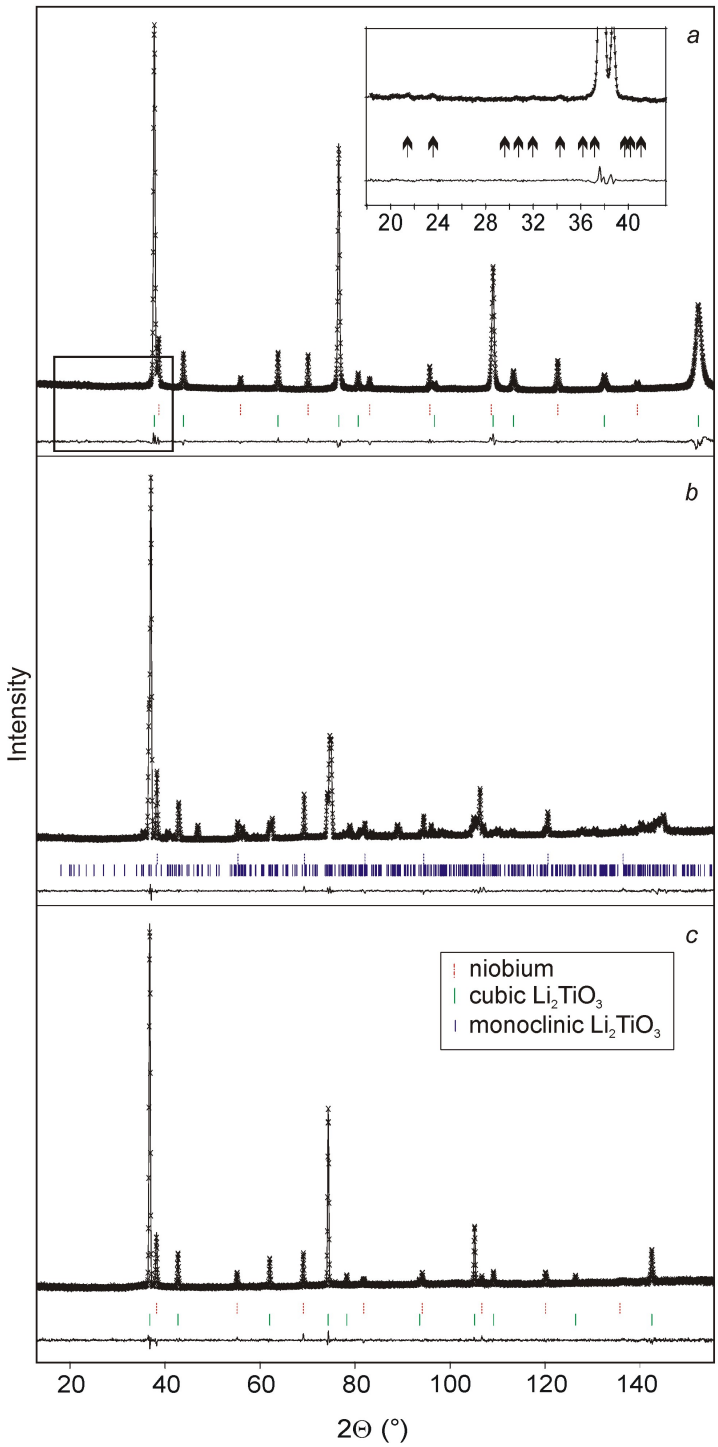

Figure 2.3: Rietveld fits at (a) room temperature, (b) 1000 °C, and (c) 1200 °C. At room temperature and at 1200 °C, the structure of Li_2TiO_3 was refined in the cubic space group, and at 1000 °C it was refined in the monoclinic space group C2/c. Observed (stars) and calculated pattern (solid line). The traces of Li_2CO_3 (arrows) at room temperature are shown in the inset.

a high fraction of the cubic Li_2TiO_3. This fraction increased with temperature, and at 350 $°C$ a deficit of 2.5% ± 1% was determined. At 1200 $°C$, the Li/Ti ratio was close to stoichiometry within the higher error margin, ca. 2.5% ± 2% ($Li_{1.95(4)}TiO_3$), and this value was maintained upon cooling. Lithium, originating from LiOH and Li_2CO_3, most likely intercalated into the Li_2TiO_3 structure, such that it became stoichiometric within error margins at 1200 $°C$.

In particular between 400 and 500 $°C$, the refinement of the cubic structure was found to be difficult due to superposition of the cubic and monoclinic reflections, and the cubic unit cell parameters at 400 and 500 $°C$ deviated from the linear trend observed from room temperature up to 1200 $°C$ (Figure 2.4). The slightly lower value at room temperature in Figure 2.4 may be due to the non-stoichiometry of the sample at low temperatures (see above).

The monoclinic structure was highly disordered at low temperatures and ordered while increasing the temperature. The final ordered monoclinic structure in space group C2/m was reached above 1000 $°C$. The full mechanism of the complex ordering of the monoclinic structure could not yet be determined, but a detailed analysis of the investigations are presented in Appendix B.

Phase transformation upon cooling Upon cooling, the monoclinic Li_2TiO_3 started to form below 1160 $°C$, which is in good agreement with the proposed transformation temperature of 1155 $°C$ (Kleykamp, 2001). At 1100 $°C$, 12.2(5) % of the cubic phase was left, comparable to the amount of the cubic structure at the same temperature upon heating. Below 1100 $°C$, only the monoclinic Li_2TiO_3 modification was found.

Size and strain The refined particle size at room temperature was approximately 68 nm and it did not change remarkably up to 300 $°C$. In the range from 300 to 500 $°C$ the refinement was not possible without restrictions, as the reflections of the cubic phase overlap with the reflections of the monoclinic superstructure, thus the parameters of the atomic positions had to be fixed. In particular, below 400 $°C$ the reflections of the ordered monoclinic structure are very broad and its particle size was only $\approx$ 5 nm at 350 $°C$, which should be taken as a rough estimate. At 400 $°C$, reflections of the monoclinic phase are still broad, but the particle size increased to 43 nm. For this temperature range, the refined values will represent the size of monoclinic domains within the cubic structure which slowly grow when increasing the temperature. A similar observation was made upon heating of cubic solid solution of Li_2TiO_3-Li_3NbO_4 (Baños et al., 1990). Here as well, over a temperature range of about 200 $°C$, small monoclinic domains start to grow in the cubic structure until the transformation is completed. At 500 $°C$, when only ca. 12% of the cubic phase was left, the particle size of the ordered structure increased to more than 61 nm and reached almost the value for the cubic particles determined at lower temperatures. Refinements of FWHM parameters of the cubic phase between 350 and 500 $°C$ were not reliable. At 600 $°C$, the size of the monoclinic particles increased to over 86 nm, at 700 $°C$ to 129 nm, and at 800 $°C$ the refined particle size was higher than 400 nm, therewith

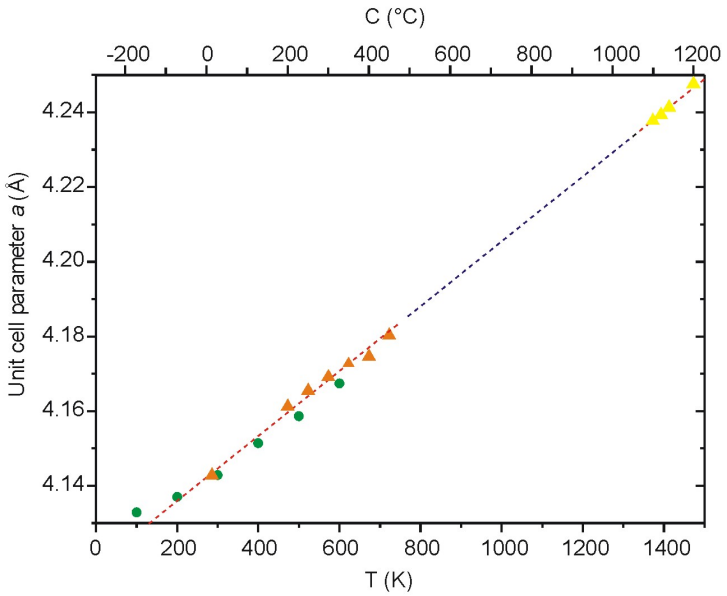

Figure 2.4: Lattice constants of cubic Li_2TiO_3 measured by neutron diffraction (triangles) and synchrotron diffraction (circles). The dashed line illustrates the connectivity between the low and high temperature values upon heating (squares) and cooling (circles). Upon cooling to a temperature of 100 K, the decrease of the unit cell is initially linear, but at lower temperatures the decline slows as expected due to decreasing inharmonic motion (Ashcroft and Mermin, 1976). Due to the lower Li-content, a slightly lower unit cell was recorded in the synchrotron experiment.

reaching the limit of the instrumental resolution. Due to that, the "size" parameter was fixed to "zero" above 800 $°C$ and also for all data obtained upon cooling.

A general decreasing trend of the strain at higher temperatures is observed, both for increasing and decreasing temperatures. However, the temperature range of the cubic to monoclinic transformation during the first heating is exceptional, as here the strain is much larger in both phases. This may be related to the intimate inter growth of both co-existing phases in this temperature range (see Appendix B).

2.3.5 Synchrotron measurements

Synchrotron measurements were performed on sample F5, a sample with approximately 43% lithium deficit. The lithium occupancy was refined for all temperatures and its occupancy was 0.40(3), corresponding to a Li-deficit of 40% ± 3.5%, which is within the error of the AAS measurement. At room temperature, the unit cell parameter was $a = 4.14528(5)$ Å, slightly below the value of the neutron measurement. Below 227 $°C$, the particle size was 63 nm, within an error margin of 1%. It started to increase slightly at 227 $°C$, and at 327 $°C$ the broad reflections represent the first indication of the transformation to the monoclinic structure, as observed by neutron diffraction.

2.4 Discussion

2.4.1 Stability and formation of cubic Li_2TiO_3 particles

The lithium titanates synthesized under hydrothermal conditions showed Li/Ti ratios close to 2 : 1, corresponding to 12.65 $wt\%$ of lithium, as long the samples remained dry after the syntheses. Generally, bathing experiments led to higher Li-loss than the water-flushing experiments, probably due to the longer time span of the interaction between the water and the α-Li_2TiO_3 powders. With a higher water content, the flushing experiments tended towards a higher Li-loss, but the decline in the lithium content was not constant, which is most likely caused by inhomogeneous washing in the filter. In contrast, the samples treated in the bathing experiments were exponentially de-lithiated with a higher water volume (Figure 2.1). When treating with water, α-Li_2TiO_3 seems to have a maximum Li-loss of ca. 75%. In the water-flushing experiments, Li-losses of ca. 25% occurred frequently, which fortifies the assumption that lithium occupancies of 1/4 and 3/4 are more stable than intermediate values. In the master thesis of Linda Irbe (2010) it was shown that lithium can be totally leached from α-Li_2TiO_3 in low concentrated acid media like citric acid or hyperclodic acid. The same study demonstrated that from monoclinic β-Li_2TiO_3 only 25 - 30% of lithium could be leached in strong inorganic acid solutions, which has already been observed (Zainullina et al., 2003). To maintain stoichiometry, the Li-loss requires the substitution of other cations to balance the charge. Diminishing unit cell parameters with decreasing lithium content allows the assumption that ions smaller than Li^+ ions are inserted into the structure. The Li^+ exchange with H^+ in the system Li-Ti-O-H might be similar to the well-known exchange of D^+ with H^+ under atmospheric conditions. In a study on $Li_4Ti_5O_{12}$ it was shown that Li can be leached with HCl and thereafter the presence of hydrogen was determined by neutron diffraction (Simon, 2007). Following the assumption that Li^+ ions are exchanged by H^+, products of the solid solution Li_2TiO_3-H_2TiO_3 are obtained. For instance the 13% Li-loss of sample $F2$ can be written as $(Li_{1-0.13}H_{0.13})_2TiO_3$. The hypothetical formulas of all samples are listed in Table 2.1.

Discrepancies of the Li/Ti ratios in previous studies on cubic α-Li_2TiO_3 can be explained by the water-flushing and bathing experiments in the present study. That Li-loss may be caused by washing had already been speculated by Tabuchi et al. (2003), but in another study the very low Li/Ti ratio of 0.34 : 1 of cubic Li_2TiO_3 was ascribed to a mixture of cubic Li_2TiO_3 and amorphous TiO_2 (Tomiha et al., 2002). In the latter study, after using 7 nm diameter anatase as a reactant, the resulting cubic Li_2TiO_3 had a similar primary particle size, which presumably eased the de-lithiation.

2.4.2 Li_2TiO_3-H_2TiO_3 solid solution

The XRPD patterns of unwashed and of water-flushed cubic Li_2TiO_3 showed a unit cell parameter a between 4.141(1) and 4.150(1) Å. This is in good agreement with the results of the neutron and the synchrotron study, where at room temperatures, the unit cell parameter of the sample F6 (ca. 40% Li-deficit) is not significantly smaller than the

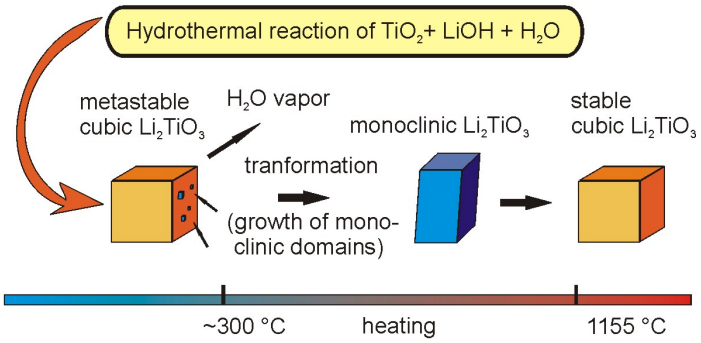

Figure 2.5: Illustration of the structural transformations of α-Li_2TiO_3 upon heating. The high-temperature modification (γ-Li_2TiO_3) can be produced in a metastable form via hydrothermal syntheses and might be stabilized by protons.

unit cell of the stoichiometric sample 2.4. The low unit cell parameters of samples with high Li-loss (e.g. sample B6) can be ascribed to the intercalation of smaller hydrogen ions in the structure.

Heat treated samples with varying Li-content reacted to different products after annealing at 800 $°C$. Only samples showing Li/Ti ratios close to 2 : 1 transformed to pure monoclinic β-Li_2TiO_3 (Figure 2.2b). Samples with Li-loss resulted in the intermediate compound $Li_4Ti_5O_{12}$, either mixed with β-Li_2TiO_3 (sample F6, Figure 2.2c), or with rutile (TiO_2) if the lithium content was low (sample B5, Figure 2.2d). The intermediate spinel $Li_4Ti_5O_{12}$ contains 52% less lithium than Li_2TiO_3, which corresponds to the theoretical calculated formula of $(Li_{0.48}H_{0.52})_2TiO_3$ – this value is in between sample F6 and sample B5. Similarly Li_2TiO_3 and $Li_4Ti_5O_{12}$ compositions can be produced by annealing a mixture of 5 - 30 $wt\%$ TiO_2 with monoclinic Li_2TiO_3 (Tsuchiya et al., 2003). By the heat treatment of an intermediate Li-Ti-O compound, produced via hydrothermal synthesis, $Li_4Ti_5O_{12}$ was formed with minor impurities (Jiang et al., 2008) and a lithium titanate of cubic spinel structure was produced after annealing a ternary Li-Ti-O compound, which was previously synthesized by hydrothermal reaction (Fattakhova and Krtil, 2002b,a). These studies, as well as the results of the present work, show that $Li_4Ti_5O_{12}$ can be obtained after annealing ca. 50% de-lithiated α-Li_2TiO_3 and that α-Li_2TiO_3 without Li-loss can not transform to $Li_4Ti_5O_{12}$ upon heating.

2.4.3 Cubic structure

The cubic structure of α-Li_2TiO_3 obtained by hydrothermal reaction is isostructural with that of γ-Li_2TiO_3 at high temperatures. The interlinked data points of the cubic unit cell volume at low temperatures and above 1100 $°C$ indicate a constant thermal expansion (Figure 2.4), thus showing that α- and γ-Li_2TiO_3 belong to the same phase. Accordingly, by hydrothermal reactions, disordered cubic Li_2TiO_3 can be produced at temperatures far below its stability field (Figure 2.5).

In general, structures disorder when rising the temperature, but similar to metastable cubic Li_2TiO_3, α-Li_2SnO_3 fully orders at T > 1000 $°C$ and below it shows disorder related to stacking faults. Two different explanations are conceivable for this behavior. First, the low temperature cubic structure may be stabilized by protons or water entering the structure during the synthesis, in allusion to quenchable cubic Li_2TiO_3-MgO solid solutions (Castellanos and West, 1979), i.e. protons could stabilize the cubic structure in the hydrothermal process, like MgO enables quenching of cubic Li_2TiO_3. Second, the cubic structure may be the preferred modification for syntheses at low temperature, due difficulties in forming the complex layered monoclinic structure, and the monoclinic Li_2TiO_3 can be formed under hydrothermal conditions (Laumann et al., 2011c), which will be presented in Chapter 3.

The deviations from the linear trend at 400 and 500 $°C$ (Figure 2.4) may be explained by a preferred exsolution of the more mobile lithium into the initial monoclinic phase. Test refinements at these temperatures revealed a higher (negative) scattering density at the Li/Ti site. This can only be explained by a higher titanium content, thus supporting this assumption.

2.5 Conclusions

Cubic α-Li_2TiO_3 was synthesized via the hydrothermal reaction of titania powder in lithium hydroxide solution at 180 $°C$ for 18 hours. The resulting products were unstable under ambient conditions, and reacted with atmospheric H_2O and CO_2. Flushing and bathing experiments showed that lithium is easily washed out of the cubic Li_2TiO_3 structure when in contact with de-ionized water. The de-lithiation leads to compositions along the solid solution Li_2TiO_3-H_2TiO_3. Differences between various compounds of this solid solution are difficult to detect by PXRD, but the effect of the Li-loss clearly can be analyzed by PXRD after annealing samples at high temperatures (800 $°C$) due to transformations into different phases. Annealed samples with Li/Ti ratios close to 2 resulted in the monoclinic β-Li_2TiO_3. Annealed samples having lost less than 52% of lithium transformed into mixtures of β-Li_2TiO_3 and $Li_4Ti_5O_{12}$. Samples with a Li-loss greater than 52% resulted in rutile and $Li_4Ti_5O_{12}$.

By *in-situ* neutron diffraction, it was shown, that α-Li_2TiO_3, which has never been characterized structurally before, is of the NaCl-type and its structure is identical with the one of the γ-phase. Metastable cubic Li_2TiO_3, which is produced by hydrothermal syntheses, transforms between 300 and 600 $°C$ to a disordered monoclinic form. Above 1160 $°C$, the cubic phase reappears again and upon cooling it turns into an ordered monoclinic phase. It was shown that the high-temperature stable phase of Li_2TiO_3 is isostructural with the metastable low temperature form. They have the same structure (space group $Fm\bar{3}m$) and their thermal expansion is linear from room temperature to 1200 $°C$. The metastable phase is probably stabilized by protons or water entering the structure during the hydrothermal syntheses.

Chapter 3

In-situ synchrotron X-ray diffraction study of the formation of cubic Li_2TiO_3 under hydrothermal conditions

Time-resolved *in-situ* synchrotron powder X-ray diffraction was used to study the hydrothermal reaction of lithium hydroxide with titania powder. The kinetics of the formation of crystalline titania to α-Li_2TiO_3 were modeled for temperatures between 155 and 230 $^\circ C$ to determine the reaction mechanism.

3.1 Introduction

The compound α-Li_2TiO_3 can be produced by the hydrothermal reaction of anatase or rutile with lithium hydroxide for $LiOH/TiO_2 \geq 2$, and syntheses have been reported from a 2 : 1 ratio (Laumann et al., 2010) ratio up to a 50 : 1 ratio (Tomiha et al., 2002). So far, no lithium titanium compounds other than α-Li_2TiO_3 have been observed as product from the hydrothermal reaction of anatase or rutile in lithium hydroxide solution. Even when using a highly over-stoichiometric amount of lithium (Tomiha et al., 2002), the surplus of lithium hydroxide remains unreacted and dissolved. Kinetic experiments of the hydrothermal formation of α-Li_2TiO_3 have not been reported so far, whereas kinetic studies with divalent cations instead of lithium were performed in the system $MTiO_3$, where M = Ba, Ca or Pb (Moon et al., 2003; Jr. et al., 1996; Testino et al., 2005; Walton et al., 2001; Croker et al., 2009; Jr. et al., 1992).

3.2 Experimental

3.2.1 *In-situ* experiments on α-Li_2TiO_3

All experiments were performed using an aqueous suspension of titania powder (Evonik, formerly Degussa, AEROXIDE TiO_2 P25) and dissolved lithium hydroxide (SQM, Chile). P25 comprises anatase and rutile in a ratio of about 4 : 1. Before the synchrotron experiments were started, 0.4 g of P25 and 0.58 g of $LiOH{\cdot}H_2O$ were stirred in 25 ml of de-ionized water for 1 hour in air. In total, 7 kinetic experiments, denoted EXP1 to EXP7 with increasing number for higher syntheses temperatures, were conducted. The adjusted temperatures were 133, 155, 168, 169, 195, 215 and 230 $°C$ at a pressure of 230 bar. In addition EXP3, was subsequently heated to the maximum possible temperature of 420 $°C$ after a holding time of 22.5 minutes at 168 $°C$.

3.2.2 Setup at the synchrotron in Lund

The *in-situ* synchrotron data was recorded at beamline I711 at MAX-lab in Lund, Sweden (Cerenius et al., 2000). The syntheses were performed in a custom build reactor (Bremholm et al., 2008; Becker et al., 2010; Tyrsted et al., 2010) using a sapphire capillary with an inner diameter of 0.7 mm. For all experiments, the suspension was injected into the capillary with a syringe. The capillary was aligned in the X-ray beam, pressurized to 230 bar, and then heated to the desired temperature in a hot air flow. The temperature in the capillary was measured with a thermocouple right next to the beam. The reactor design has been described in detail elsewhere (Bremholm et al., 2008), and a photo of the stage at the synchrotron can be seen in Figure C.1 in Appendix C.

3.2.3 Synchrotron X-ray data analysis

The wavelength was adjusted to 0.997 Å and the detector had a time resolution of 10.5 s per frame. The 2D diffraction data were integrated in the program Fit2D (Hammersley et al., 1996) and subsequently, the time resolved PXRD data sets were analyzed by sequential Rietveld refinement using the program FullProf (Rodríguez-Carvajal, 1993). Peak fitting and treatment of the background was performed as already described in Chapter 2.2.3.

The atomic coordinates of anatase (Djerdj and Tonejc, 2006), rutile (Bokhimi et al., 2002) and the cubic Li_2TiO_3 (Laumann et al., 2011b) were fixed at the values from the literature. The isotropic thermal parameters (B_{iso}) were fixed to 1. In the supplementary material 1 in Appendix C, specific examples of Rietveld fits are shown together with relevant crystallographic details.

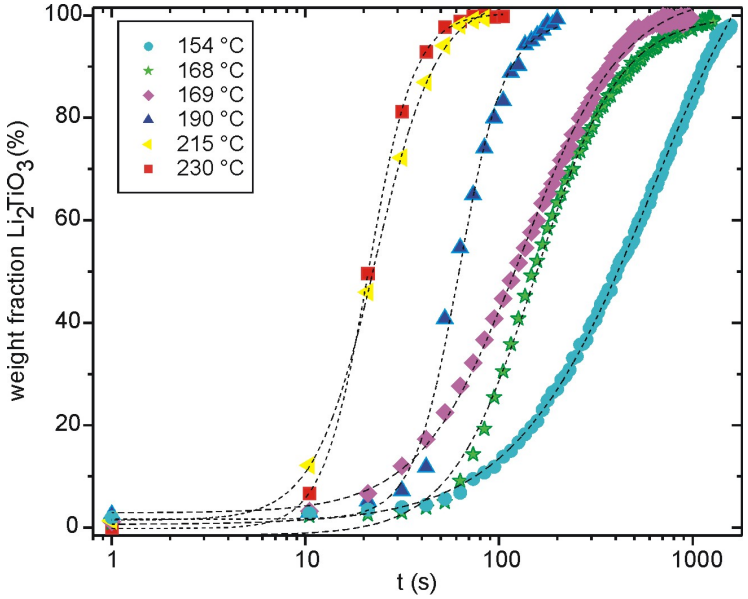

Figure 3.1: Data points and sigmoidal fits for the fractional progressions of EXP2 - EXP7 versus time.

3.3 Results

In all performed *in-situ* experiments, the hydrothermal reaction of titania in a lithium hydroxide solution to α-Li_2TiO_3 was recorded. The reaction can be expressed as $TiO_2(s) + 2\ LiOH(aq) = Li_2TiO_3(s) + H_2O(l)$. At 133 $°C$, the lowest temperature of all performed experiments (EXP1), partial formation of Li_2TiO_3 was observed, but the kinetics were too slow for the complete formation of α-Li_2TiO_3 in a suitable time due to the restricted beam-time. The experiment was aborted after 26 *min* as the α-Li_2TiO_3 fraction was only ca. 20% and a high proportion of anatase and a minor proportion of rutile were still present. Higher temperatures lead to the complete formation of α-Li_2TiO_3 in less than 30 minutes (Table 3.1 and Figure 3.1).

The progress of all reactions could be fitted with a sigmoidal shape. The fractional progress of α-Li_2TiO_3 and titania versus time of EXP6 is plotted in detail in Figure 3.2, which shows an increasing fraction of the lithium titanate with a corresponding simultaneous decrease in the titania fraction. The temperature dependence of the half-fractions ($\alpha = 0.5$) of Li_2TiO_3 displays an exponential decay, Figure 3.3.

For EXP3, which was heated to 420 $°C$ after 22.5 minutes, the progression of the reaction is shown in a three-dimensional plot versus time in Figure 3.4. First, the formation of Li_2TiO_3 was observed as an increasing intensity of the lithium titanate reflections and the diminishing reflections of titania, so that after about 18 minutes only reflections of lithium titanate were detected. The broad hump around $2\theta = 20°$ is caused by the aqueous lithium hydroxide solution in the sapphire capillary. Then, after 22.5 minutes, the temperature was set to 420 $°C$ and the critical temperature of water ($T_C = 374\ °C$) was crossed within

Table 3.1: Temperature for each experiment T, the times for the half-fraction $t_{1/2}$ and the calculated values for the rate constant k.

Run	T ($°C$)	$t_{1/2}$ (s)	k (s^{-1})[c]
EXP1[a]	133	—	—
EXP2	154	328.7	$2.1{\cdot}10^{-3}$
EXP3[b]	168	156.1	$4.4{\cdot}10^{-3}$
EXP4	169	121.5	$5.7{\cdot}10^{-3}$
EXP5	195	38.9	$1.8{\cdot}10^{-2}$
EXP6	215	22.7	$3.1{\cdot}10^{-2}$
EXP7	230	21.1	$3.3{\cdot}10^{-2}$

[a] Half-fraction was not reached within 30 minutes
[b] Experiment was heated to 420 $°C$ after 22.5 min holding time at 168 $°C$
[c] See Section 3.3.2

a single detector exposure. The broad feature observed at a temperature of 168 $°C$ flattens as the fluid turns supercritical (Figure 3.4). At 420 $°C$, the reflections of the α-Li_2TiO_3 shift to slightly smaller 2θ angles due to the thermal expansion of α-Li_2TiO_3. Moreover, new and broad reflections appear, whereas the reflection of the highest intensity at 2θ 11.8° can clearly be ascribed to the (002) reflection of the monoclinic β-Li_2TiO_3 phase. Especially at the beginning of the cubic-monoclinic transformation, the monoclinic Li_2TiO_3 is disordered due to stacking faults and it was not possible to refine the FWHM parameters (see discussion of Appendix B).

3.3.1 Modelling of anatase and α-Li_2TiO_3 particles

The refined particle size of P25 yielded a value of approximately 20 nm, which is in good agreement with the specification of Evonik (21 nm). P25 comprises anatase and rutile in a ratio of 4 : 1, thus a reasonable refinement of the particle size of rutile was only possible at the very beginning of each experiment. Therefore, sequential refinement of the size of the anatase particles produced better results, especially for reactions at lower temperatures, where anatase was detectable over a longer period.

Anatase can be described in the tetragonal space group $I4_1/amd$ with unit cell parameters of $a = 3.785(1)$ Å and $c = 9.482(3)$ Å (Djerdj and Tonejc, 2006). The structure has various empty octahedral sites, where lithium can possibly be accommodated (Koudriachova and de Leeuw, 2004; Tielens et al., 2005; Wagemaker et al., 2003, 2004). The unit cell parameters of anatase at the onset of all experiments show some minor variations compared with the theoretical values. These small changes are probably caused by a minor displacement of the capillary due to heating. With ongoing reaction time, the unit cell parameters changed and the values of the unit cell parameter a increased slightly and the values of the unit cell parameter c decreased, more pronounced with longer reaction time

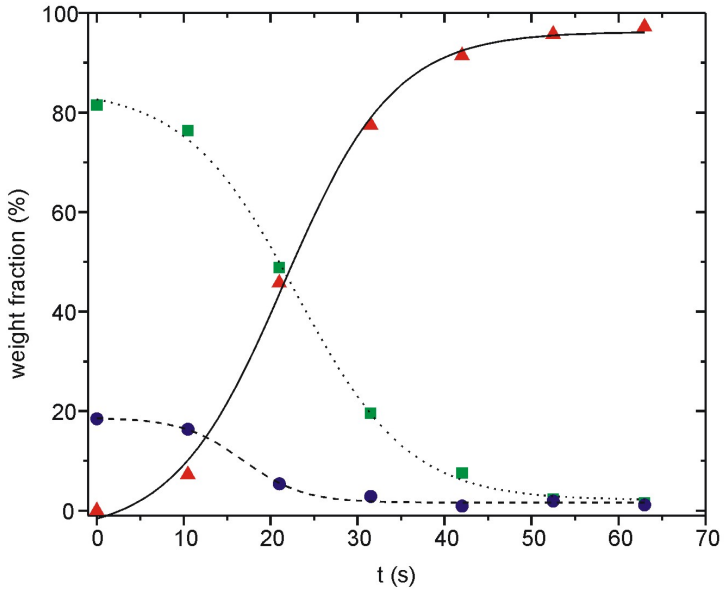

Figure 3.2: Fractional progression of anatase (squares) and rutile (circles) to α-Li_2TiO_3 (triangles) versus time at 215 $°C$ (EXP6) and sigmoidal fits of the formation of α-Li_2TiO_3 (solid) with the decay of anatase (dotted) and rutile (dashed).

and particularly before the full cell formation of α-Li_2TiO_3 was accomplished (Figure 3.5). The particle size of anatase remained fairly constant until the lithium intercalation was completed (Figure 3.6).

The unit cell parameter of the α-Li_2TiO_3 particles seems to increase slightly at the very beginning of each experiment, which could be caused by errors in the refinement due to the low fraction of the titanate. Then, during the formation to α-Li_2TiO_3 and until the experiments were aborted, the unit cell parameter stayed constant around $a = 4.14$ Å (Figure 3.5). The first detectable α-Li_2TiO_3 particles showed about the same size as the crystalline titania reactant P25 (Figure 3.6). With ongoing reaction time, the lithium titanate particles grew, slightly faster at higher temperatures. The two experiments with the highest synthesis temperature showed a similar fast particle growth, and in EXP6 the particle growth is about ca. 8 nm within 1000 s (Figure 3.6).

3.3.2 Kinetics of the formation of α-Li_2TiO_3

As mentioned before, the increase of the fractions of the lithium titanate, as well as the decrease of the fractions of the titania powders, show a sigmoidal reaction progress, suggesting that nucleation and crystal growth control the reaction (Testino et al., 2005). In solid state chemistry, the Avrami-Erofe'ef equation (Avrami, 1939, 1940, 1941; Erofeev, 1946) is broadly applied to model phase transformations, nucleation and crystal growth.

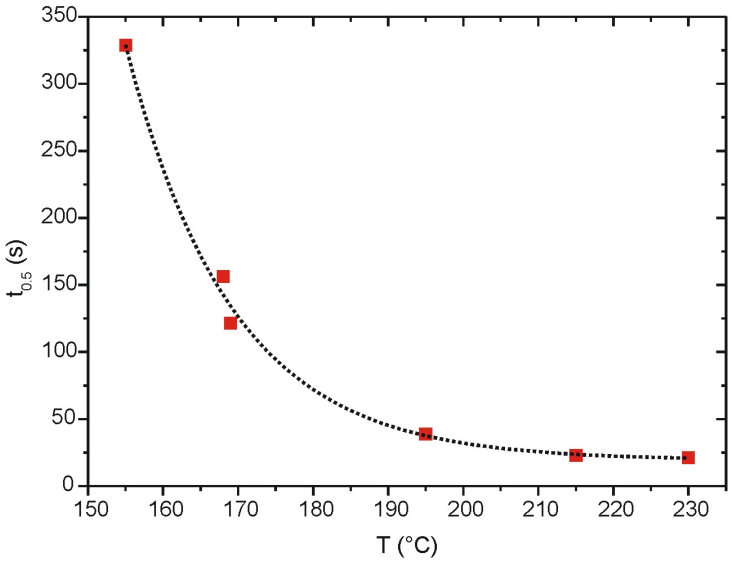

Figure 3.3: Half-fraction time $t_{1/2}$ of the transformation to α-Li_2TiO_3 at different temperatures.

It relates the fraction of a reaction α at each temperature by using the relationship

$$\alpha = 1 - \exp[-k(t - t_0)^n] \tag{3.1}$$

where n is the Avrami exponent, t_0 the induction time and k the rate constant. The exponent n gives details about the rate of nucleation and the mechanism of nuclei growth. The expression is most valid in the fractional range from $0.15 < \alpha < 0.5$. Reactions in the present study were fast, so that for EXP5, EXP6 and EXP7 only one or two data points could be found in the $0.15 < \alpha < 0.5$ range, and therefore these experiments are not included in the following considerations. The value of n can be determined by applying a Sharp-Hancock plot (Hancock and Sharp, 1972), which is a plot of $ln(-ln(1-\alpha))$ versus $ln(t)$. This gives a straight line with a slope of n. Changes in the reaction mechanism can be identified as a change in slope. At low fractions, the experiments EXP2, EXP3 and EXP4 show a slope of nearly 2. The reaction mechanism seems to change at about $\alpha = 0.35$, especially evident for EXP2. Thus, the range of $0.15 < \alpha < 0.85$ was applied for EXP2, EXP3 and EXP4 (Figure 3.7). At fractions of $\alpha \approx 0.45$, the slope is less steep in all of the three experiments and an average value of $n \approx 1.2$ is obtained.

In order to calculate the activation energy for the crystallization of α-Li_2TiO_3, $ln(n)$ against $1000/T$ (in Kelvin) is plotted, displaying the logarithmic form of the Arrhenius equation

$$k = A \exp\left(-\frac{E_A}{RT}\right) \tag{3.2}$$

here, A is the pre-exponential factor, E_A the effective activation energy, R the gas constant and T the absolute temperature. The calculated values are listed in Table 3.1 and the

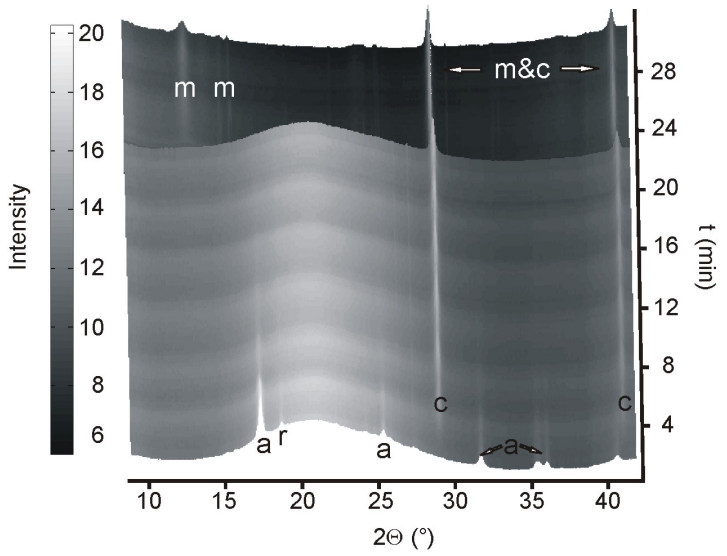

Figure 3.4: Three dimensional plot of diffraction data showing the transformation from anatase (a) and rutile (r) to the cubic α-Li_2TiO_3 (c) at 168 $°C$ (EXP3). Heating to 420 $°C$ after 23 minutes results in the beginning of the transformation from α-Li_2TiO_3 to the monoclinic β-Li_2TiO_3 (m). The broad hump around $2\theta = 20°$ is caused by the lithium hydroxide solution.

Arrhenius plot in Figure 3.8 displays $ln(k)$ versus $1000/T$. E_A can be calculated from the slope of the plot, which gives a value of 66 kJ/mol.

3.4 Discussion

3.4.1 Lithium intercalation in titania powder

The unit cell parameters of anatase change during the formation of α-Li_2TiO_3, as shown in Figure 3.5. This observation might be explained by lithium ions beeing inserted into the anatase structure, yet without transforming to α-Li_2TiO_3. The simultaneous decrease of the titania fraction and the growth of the lithium titanate (Figure 3.2) proves that lithium intercalates the titania particles, i.e. a direct reaction to α-Li_2TiO_3 takes place without a prior formation of, a e.g. $Ti(OH)_4$ phase. This has been proposed for the hydrothermal synthesis of $BaTiO_3$ (Testino et al., 2005). The comparable particle sizes of the reactant and the first formed products (Figure 3.6) also suggests that lithium ions are intercalated into the titania structure without the dissolution of the titania particles. Hypothesizing that the reaction mechanism is controlled by dissolution and recrystallization, one would expect a decrease in the average particle size of the titanium oxide precursors prior to and during the crystallization of the Li_2TiO_3. The constant size of the anatase indicates that a dissolution-recrystallization mechanism can be excluded and suggests a topotactic

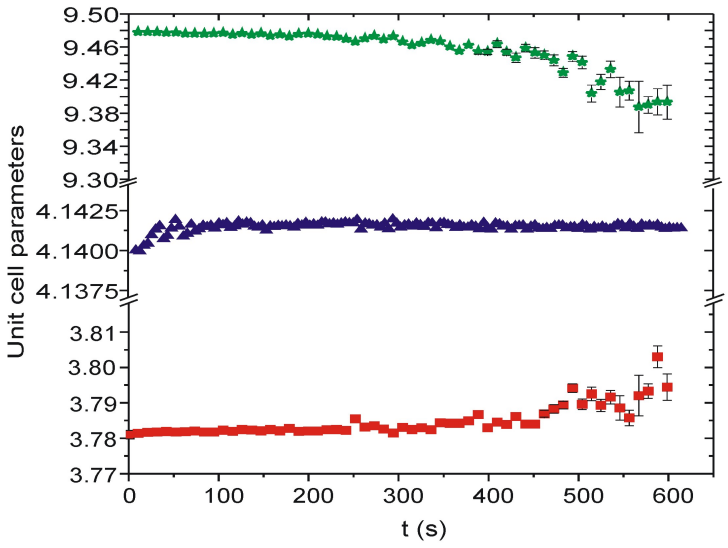

Figure 3.5: Progression of unit cell a (circles) and unit cell c (squares) of anatase and the constant unit cell of α-Li_2TiO_3 (triangles) with time and ongoing formation of α-Li_2TiO_3 (EXP2).

transformation mechanism.

Most studies on the intercalation of lithium ions in titania were performed by electrochemical intercalation of lithium in anatase (Koudriachova and de Leeuw, 2004; Tielens et al., 2005; Wagemaker et al., 2003, 2004). By electrochemical intercalation, Ti^{4+} is partially reduced to Ti^{3+}, and compositions of $Li_x(Ti_x^{3+}Ti_{1-x}^{4+})O_2$ are obtained. For $x < 0.25$ the tetragonal anatase structure is maintained. The unit cell parameter a increases with lithium insertion, while c decreases (Tielens et al., 2005; Wagemaker et al., 2003), as also observed in the present study (Figure 3.5). However, the reaction taking place in the present study is hardly comparable with the electrochemical intercalation of lithium in anatase, as titanium is unlikely to be reduced under the present conditions. Nevertheless, before the anatase phase finally transforms to α-Li_2TiO_3, lithium ions might fill empty sites of the anatase structure and cause the minor variation in the unit cell parameters. This will occur at the end of each reaction, when most of the anatase is already transformed to α-Li_2TiO_3 and in the remaining anatase some lithium ions will already have intercalated.

3.4.2 Cubic-monoclinic transformation of Li_2TiO_3

The transformation of the metastable α-Li_2TiO_3 to the monoclinic Li_2TiO_3 above 300 $°C$ was so far only described in air or vacuum (Laumann et al., 2011b, 2010; Gicquel et al., 1972; Kleykamp, 2001, 2002; Mikkelsen, 1980). The complete transformation to the β-phase occurs above 500 $°C$ (Laumann et al., 2011b) and at 420 $°C$ a two-phase system comprising the cubic and the monoclinic structure is expected. Lithium has low X-ray scattering power and all reflections of the cubic phase are superimposed on the reflections

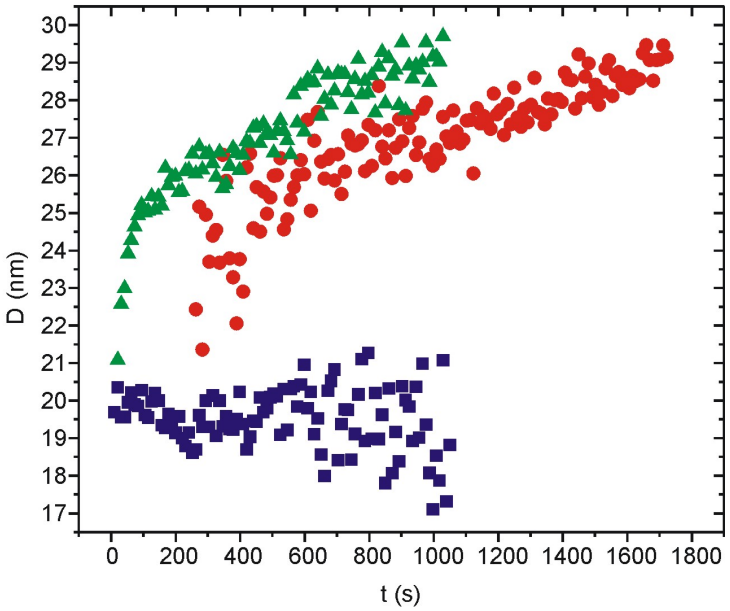

Figure 3.6: Particle growth of α-Li_2TiO_3 in EXP2 (circles) and in EXP6 (triangles), and the size of the anatase particles in EXP2 (squares) versus reaction time (error $\approx 1\ nm$). Due to the low fraction of α-Li_2TiO_3 in EXP2 before 250 s the FWHM parameters could not be refined. The same problem occurred for anatase particles after 1000 s. Both are indicated by the wide scattering of the data points of α-Li_2TiO_3 at the beginning of its formation and for anatase when only a low fraction is left.

of the monoclinic phase. Thus, the FWHM parameters had to be fixed, and the refined fraction of 47(1) % of the cubic phase at 420 $°C$ must be considered as a first estimate only. This number, however compares well with fractions of the cubic phase (60(2) %) at 400 $°C$ and at 500 $°C$ (11.5(7) %) (Laumann et al., 2011b) (see appendix B). This leads to the assumption, that the cubic-monoclinic transformation takes part at a similar temperature, irrespective of whether a dry powder is heated in high vacuum or in aqueous lithium hydroxide solution above the critical point of water.

3.4.3 Reaction mechanisms

The slope n which is obtained from Equation 3.1 can give information about the mechanisms of the reactions. According to Hancock and Sharp (1972), for n = 0.54 - 0.62 a diffusion-limited rate is inferred, where the rate of diffusion of the reactive species to the nucleation sites is the rate-determining step. For n = 1.0 - 1.24, a zero-order, first-order, or a phase boundary mechanism between the product and the reagent mixture is rate determining, and for n = 2.0 - 3.0, the formation of nucleation sites is the process that controls the rate. In the present study, the slope $n = 2$ in the beginning of the reactions (Figure 3.7) suggests that the nucleation of Li_2TiO_3 sites is the rate-determining step. Then, the slope becomes less steep at higher fractions and $n \approx 1.2$ suggests that once enough Li_2TiO_3 nuclei

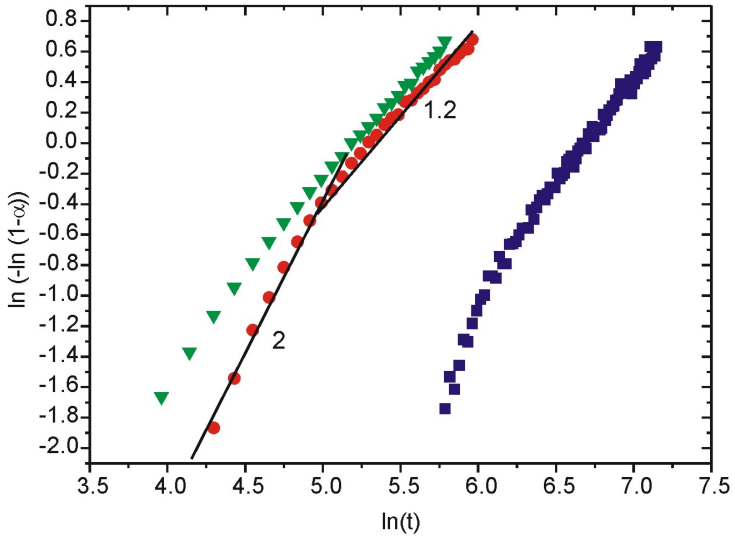

Figure 3.7: Sharp-Hancock plot for the transformation of P25 titania powder in lithium hydroxide solution to α-Li_2TiO_3 at 155 $°C$ (squares), 168 $°C$ (circles) and 169 $°C$ (triangles).

are formed, the reaction mechanism changes, and then the reaction at the phase boundary is the rate determining mechanism at higher fractions. The rather high activation energy of 66 kJ/mol also suggests a phase boundary or nucleation controlled mechanism. $E_A <$ 32 kJ/mol would be an indicator for diffusion controlled processes (Lasaga, 1998).

The present study focused on the reaction of the titania powder P25 with a 0.5 M lithium hydroxide solution. It is expected that by using other titania reactants, or a higher or less concentrated lithium hydroxide solution, the kinetics, and even the reaction mechanisms, might vary. For the formation e.g. of $BaTiO_3$, the activation energies were found to depend mainly on the titania reactant (Walton et al., 2001), thus for $BaTiO_3$ various activation energies between 21 kJ/mol (Ovramenko et al., 1978) and 105.5 kJ/mol have been reported (Hertl, 1988). For the hydrothermal formation of the lithium titanate it was reported that coarser particles ($\approx$ 100 nm) cause problems to obtain a complete reaction at 160 $°C$ (Laumann et al., 2010), whereas by using a 5 nm anatase, lithium intercalation can be performed in a 2.5 M lithium hydroxide solution at 60 $°C$ (Jiang et al., 2008). Obviously, a faster reaction at the same temperature can be expected for a higher concentration of the lithium hydroxide solution. Here, especially at low temperatures e.g. in EXP2, the reactions slowed down before getting to the end of the complete formation of α-Li_2TiO_3, indicating that low concentrations of remaining lithium ions in the solution decelerate the kinetics (see Figure 3.1).

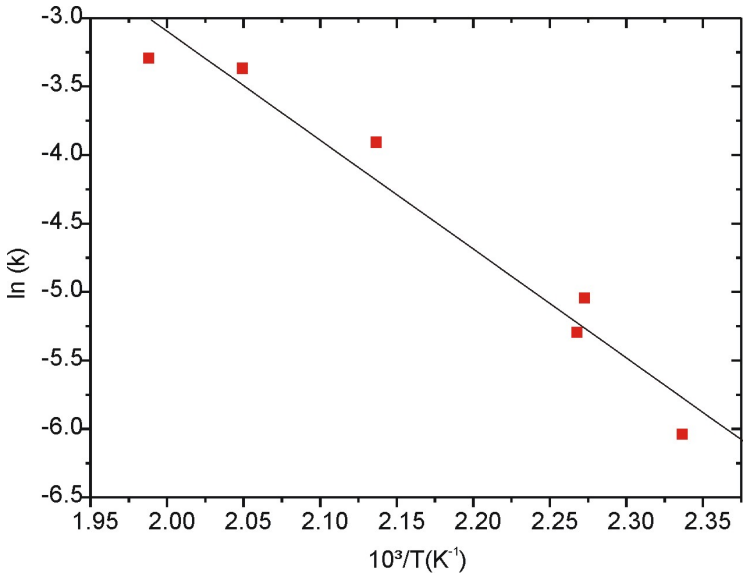

Figure 3.8: Arrhenius plot used to determine the activation energy of the intercalation of lithium in titania.

3.5 Conclusions

For the first time, *in-situ* synchrotron radiation has been used to study the interaction of titania powder in a lithium hydroxide solution under hydrothermal conditions. Lithium ions were found to intercalate in the titania structure without a prior dissolution of the titania compounds and the particle growth of the formed metastable cubic α-Li_2TiO_3 was recorded. Upon heating of the suspension of α-Li_2TiO_3 particles in a lithium hydroxide solution above the critical point of water, α-Li_2TiO_3 was found to transform to the monoclinic β-Li_2TiO_3 in a similar way as observed for dry α-Li_2TiO_3 powder heated in air or in high vacuum. By applying the Avrami-Erofe'ef equation the rate controlling mechanism could be determined for the reactions at lower temperatures. The process was found to be non-isokinetic due to a change from a nucleation controlled to a phase boundary controlled reaction, which might depend on the used titania reactant and the concentration of the lithium hydroxide solution. The calculated activation energy of 66 kJ/mol also will be sensitive to variations of the reaction conditions.

Chapter 4

Two-step synthesis of $Li_4Ti_5O_{12}$

This chapter describes a new process to synthesize $Li_4Ti_5O_{12}$ spinel in a two-step manner, patent pending, Süd-Chemie (Appendix D). This novel method is a combination of a hydrothermal step with a subsequent solid-state reaction. The synthesized products are electrochemically tested and its structural properties are investigated upon heating by impedance spectroscopy (Appendix E) and neutron powder diffraction (Appendix F).

4.1 Introduction

An introduction in synthesis methods for $Li_4Ti_5O_{12}$ is given in Chapter 1. Standard solid-state syntheses require, in general, 800 $°C$ or higher temperatures to obtain a pure product. These high temperatures cause particle growth and thus lower the rate capability of active materials. As already introduced, $Li_4Ti_5O_{12}$ is of spinel-type with a unit cell containing eight formula units of $(Li)^{8a}[Li_{1/3}Ti_{5/3}]^{16d}O_4^{32e}$, in which lithium (Li1) fully occupies the tetrahedral $8a$ sites. The octahedral $16d$ sites are occupied randomly in a ratio of 1 : 5 by lithium atoms (Li2) and titanium atoms (Kataoka et al., 2008; Julien and Zaghib, 2004), the tetrahedral $32e$ sites are occupied by oxygen atoms (Ohzuko et al., 1995; Kataoka et al., 2008).

Upon heat treatment of $Li_4Ti_5O_{12}$ samples, variations in its activation energy were determined by impedance spectroscopy, which are inferred to relate to structural changes of the order-disorder type (Leonidov et al., 2003, 2004; Vītņiš et al., 2002). Similar conclusions were reported based on data obtained by infrared spectroscopy (Pecharroman and Amarilla, 2000), Raman spectroscopy (Leonidov et al., 2004), and NMR spectroscopy (Vijayakumar et al., 2009). Based upon impedance data, $Li_4Ti_5O_{12}$ is presumed to undergo two order-disorder phase transitions upon heating. First, due to migration of lithium from $8a$ to $16c$ sites, a transition to an ordered $Fd\bar{3}m$ structure ($Li^{16c}[Li_{1/3}Ti_{5/3}]^{16d}O_4^{32e}$), and second, due to the migration of lithium from $16d$ to $16c$ sites, a transformation into a disordered NaCl structure $Fm\bar{3}m$ ($Li_{4/3}^{16c}Ti_{5/3}^{16d}O_4^{32e}$) (Leonidov et al., 2003, 2004). All proposed structural transformations are well below 1000 $°C$, the temperature at which the decomposition of $Li_4Ti_5O_{12}$ into the ramsdellite-type $Li_2Ti_3O_7$ and the cubic γ-Li_2TiO_3 is expected

(Gicquel et al., 1972; Izquierdo and West, 1980; Kleykamp, 2002).

4.2 Synthesis of $Li_4Ti_5O_{12}$ and its characterization

4.2.1 Synthesis of $Li_4Ti_5O_{12}$

Hydrothermal syntheses were performed using anatase powder (Sachtleben) in lithium hydroxide solutions at 180 $°C$ under P_{sat}. The Li/Ti ratio was $4+x/5$. The obtained composite of anatase and α-Li_2TiO_3 was annealed at T > 675 $°C$. Electrochemical tests were performed on a sample annealed at 750 $°C$. The calzined particles were de-agglomerated in a jet-mill. In the following sections, the final product is referred to its working term "LiAn".

4.2.2 Preparation of electrodes and electrochemistry

LiAn was electrochemically tested in half-cells with lithium metal as the counter electrode. Electrodes were prepared of 85% active material (loading 2.3 mg/cm^2), 10% carbon black and 5% poly(vinylidene difluoride) PVdF binder on Al foil. The electrolyte was a mixture of ethylene carbonate (EC) and dimethyl carbonate (DMC) (1:1 molar ratio), 1 M LiPF6. Glass fibre was used as the separator. The cells were dried at 105 $°C$ under vacuum, assembled in an argon-filled glove box, cycled between 1.0 - 2.0 V versus Li/Li^+ and held at 1.0 V until the current reached C/50, D/50 for the discharge at 2.0 V.

4.2.3 Charaterization

The neutron diffraction measurement were performed using the instrument SPODI of FRM II, as described in Section 2.2.3. Here, approximately 2 g of LiAn were heated in a niobium cuvette up to 1100 $°C$ in a stepwise manner and then cooled again to room temperature. The electronic conductivity of LiAn and a second $Li_4Ti_5O_{12}$ sample, prepared by solid-state reaction, were measured by impedance spectroscopy by Mr. Elmar Schmidbauer. The methodology part and the detailed information is to be seen in Appendix E.

4.3 Results

Surprisingly, temperatures of approximately 675 $°C$ were sufficient for the calzination of LiAn. Minor traces of Li_2TiO_3 can not be completely ruled out, as their X-ray patterns are very similar and minor fractions of Li_2TiO_3 might only cause small shoulders on peaks of the major $Li_4Ti_5O_{12}$ phase (see also Section 4.3.3). At lower temperatures, higher fractions of non-reacted titania and Li_2TiO_3 can be detected. Higher temperatures cause strong particle growth, which can be seen in Figure 4.1, and heavy sintering of the particles occurs above $\approx$ 800 $°C$.

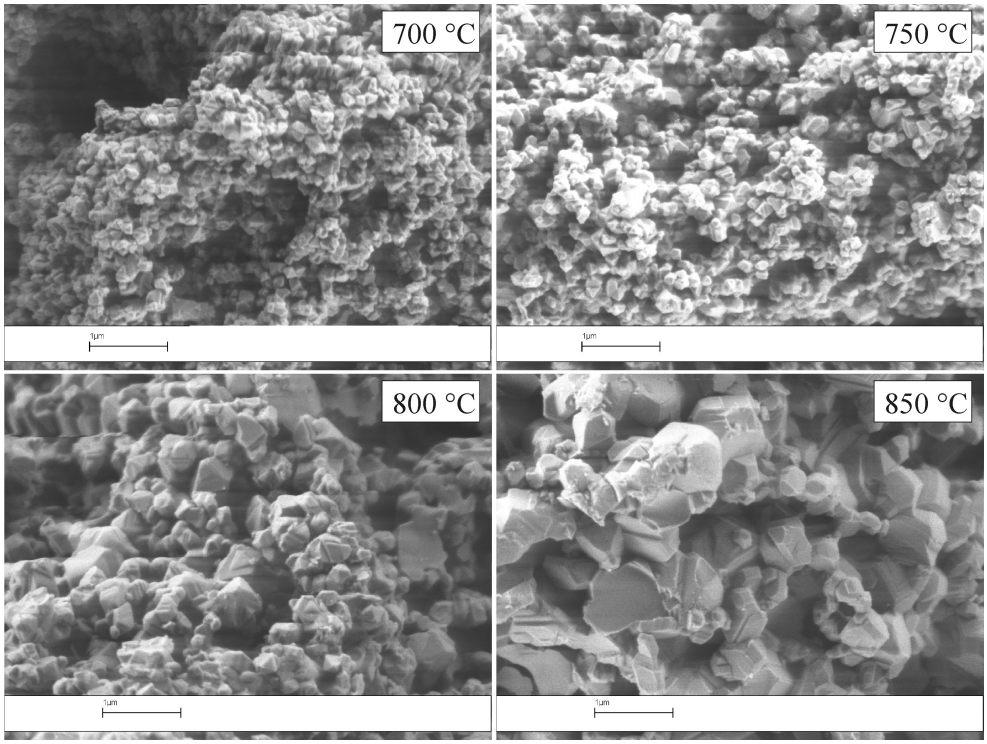

Figure 4.1: Growth of LiAn ($Li_4Ti_5O_{12}$) with higher temperatures (annealing time was 12 hours each).

4.3.1 Electrochemistry

The electrochemical tests revealed an excellent cyclability and rate capability for LiAn samples. When charging at 20C, the capacity dropped only to 120 mAh/g, and the discharge capacity at 20D was still close to the theoretical value (Figure 4.2). Especially at low rates, the plateau of $Li_4Ti_5O_{12}$ was typically at approximately 1.55 V. After 400 cycles at 1C, the material still showed a capacity of 152 mAh/g, which is 87% of the theoretical capacity (Figure 4.3). The discharge capacity did not show a remarkable fading. The results presented here are of non-coated material. When testing carbon-coated LiAn, the charging capacity was 140 mAh/g at a charge rate of 20C.

4.3.2 Impedance spectroscopy

In the impedance study of Fehr et al. (2010b), LiAn was compared to a $Li_4Ti_5O_{12}$ sample synthesized by standard solid-state reaction at 800 $°C$. Comparing the results of these two samples, variations in the ionic conductivity are mainly caused by the differences in the microstructure of grains and by grain boundary effects. This study obtained results similar to the works of Leonidov et al. (2003, 2004), which suggested two major order-disorder phase transitions upon heating of the $Li_4Ti_5O_{12}$. However, impedance spectroscopy cannot directly determine the Li-occupacion and for a precise interpretation of the electrochemical

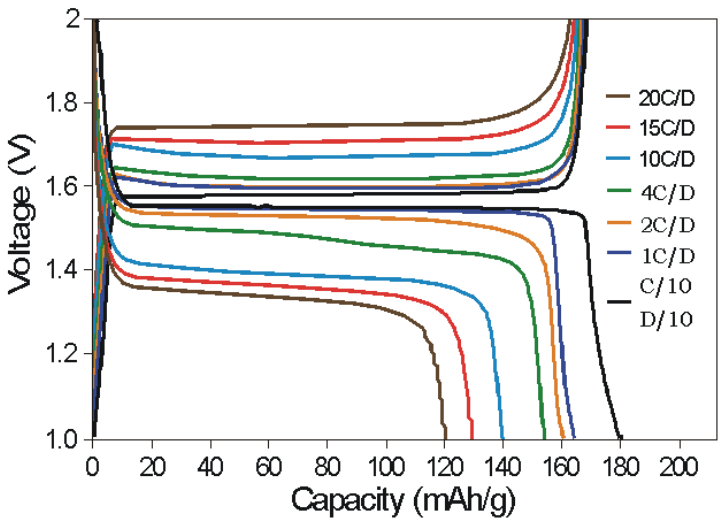

Figure 4.2: Rate capability up to 20C and 20D, respectively.

processes a detailed microstructural analysis of the compounds was performed. Therefore, a subsequent neutron study of LiAn was carried out to verify the possible order-disorder phase transitions of $Li_4Ti_5O_{12}$ upon heating.

4.3.3 Results from neutron powder diffraction

The spinel $Li_4Ti_5O_{12}$ was refined in space group $Fd\bar{3}m$ with a unit cell parameter of a = 8.35952(4) Å at 15 $°C$, showing good agreement with reported values, e.g. a = 8.352(4) Å (Kataoka et al., 2008) and a = 8.35950 Å (Scharner et al., 1999). A minor impurity phase of monoclinic Li_2TiO_3 was found to be present (< 3 $wt\%$), which could not be detected by PXRD. The impurity of Li_2TiO_3 was within uncertainties constant up to 700 $°C$. At 900 $°C$, a clear reflection of Li_2TiO_3 could no longer be detected.

Up to 700 $°C$, the unit cell parameter, the u parameter of the oxygen position and all isotropic thermal displacement parameters B_{iso} increased in a near-linear manner. At higher temperatures, and clearly seen at 900 $°C$, the unit cell volume, the u parameter and the isotropic thermal displacement parameter B_{iso} especially of Li1 on 8a, show deviations from linearity (see Figure 4.4), which will be discussed in detail below. At 1000 $°C$, $Li_4Ti_5O_{12}$ started to decompose into the ramsdellite-type phase $Li_2Ti_3O_7$ and the cubic Li_2TiO_3 and at 1100 $°C$ $Li_4Ti_5O_{12}$ was fully decomposed. The detailed decomposition and the subsequent cooling can be seen in Appendix F.

As mentioned above, the unit cell volume, the oxygen position (u parameter) and the isotropic thermal displacement parameter B_{iso} of Li1 on 8a deviated significantly from linearity. Therefore, test refinements following the proposal of Leonidov et al. (2003, 2004) were performed, with lithium either partially or fully on 16c instead of 8a, or with all lithium on 16c ($Li^{16c}_{4/3}Ti^{16d}_{5/3}O^{32e}_4$) either in space group $Fd\bar{3}m$ or in space group $Fm\bar{3}m$. All

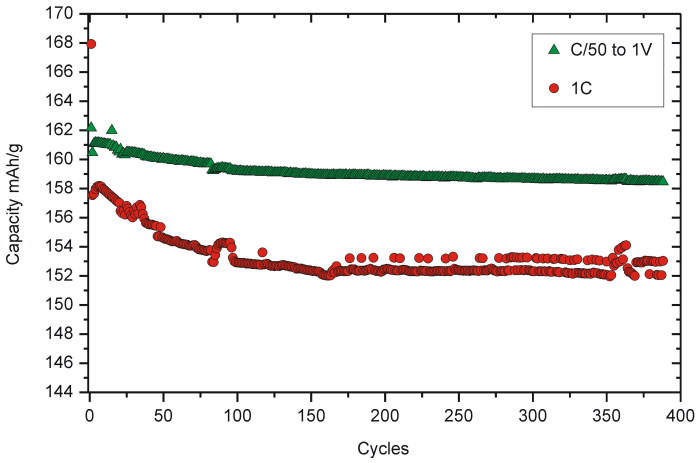

Figure 4.3: Cyclability at 1C (circles). The sample was held at 1.0 V until current reached C/50, D/50 for the discharge at 2.0 V (triangles)

these attempts were unsuccessful and, especially, 4/3 lithium on 16c can be completely ruled out.

On the contrary, remaining in space group $Fd\bar{3}m$, refinements of the Li occupancy on 8a at higher temperatures enabled stable fits and showed increasing Li-deficits with heating. Confirming full occupancy at low temperatures (700 °C), the refinement revealed a deficit slightly lower than the error margin (0.966(22)) suggesting almost full occupancy, but at 900 °C, a striking decrease of ca. 10% towards 0.88(2) was revealed. This apparent Li-deficit is not due to evaporation of lithium (see later discussion), but can be assigned to anharmonic motions and/or migration to other sites in the structure. This could be shown by additional refinements using the program JANA (Petricek and Dusek, 2000) which allows the inclusion of anharmonic terms in the Debye-Waller factor. Note that the local symmetry of $4\bar{3}m$ only allows isotropic anharmonic displacement parameters (ADPs). There is a third-order term c123 and two fourth-order terms d1111 and d1122. While c123 turned out to be highly significant, the other two were less reliable and produced some artifacts, and thus only c123 was used in the following refinements. During these refinements, the Li occupancy on 16d was kept constant. A subsequent difference Fourier analysis revealed weak but significant negative residual densities within the 16c octahedron (note that the scattering length of Li is negative). This was found as two peaks along the xxx-direction displaced from the central 16c position. Therefore, a new atom Li* was introduced on 32e sites. A free refinement of both the occupancy and an isotropic ADP (U_{iso} of Li*) was unsuccessful due to the usual strong correlation between these two parameters, in particular for the very low occupancy. Therefore, U_{iso} was constrained to that of Li1. Free refinement of the occupancies of Li1 and Li* gave values such that the overall sum was conserved within the rather large standard uncertainties, and so, in the final refinement the overall occupancy was fixed. It should be added that similar refinements at lower temperatures were unsuccessful due to the lower occupancy of the Li*

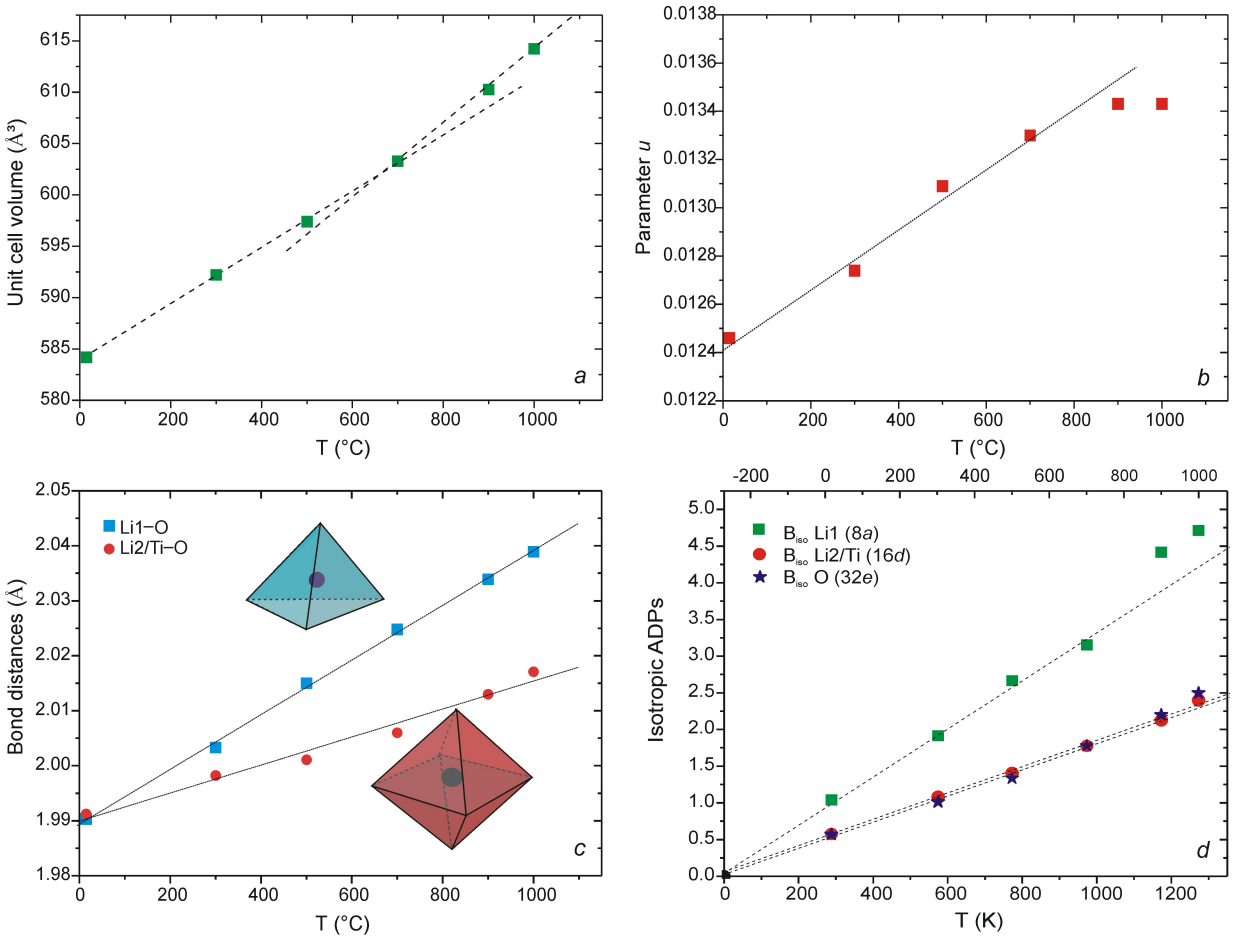

Figure 4.4: Structural evolution of LiAn upon heating with respect to (a) the unit cell volume, (b) the parameter u, (c) selected bond distances and (d) the isotropic ADPs.

site and, at higher temperatures, the results might be influenced by the gradual onset of $Li_4Ti_5O_{12}$ decomposition (see above).

Although these results should not be taken too literally because of the necessary constraints, the general distribution of Li can be deduced with confidence. The corresponding probability density function (PDF) as derived from the ADPs is shown in Figure 4.5. Moreover, a plausible new Li-diffusion path along 8*a*-Li*-Li*-8*a* can be proposed for which the activation energy could be determined. Both are presented in detail in Appendix F.

4.4 Discussion

4.4.1 Electrochemical performance of $Li_4Ti_5O_{12}$

The hydrothermal step for the synthesis of LiAn appears to activate the titania, and thus comparable low annealing temperatures can be adjusted to avoid particle growth at

high temperatures (see Figure 4.1). The small particle size demonstrates possible charging and discharging at very high rates without a serious capacity loss. The discharge rates are especially outstanding, showing nearly no decrease of the capacity after 400 cycles or when discharging with rates up to 20D. As expected, carbon coating improves the electrochemical performance as has frequently been described, e.g. (Doeff et al., 2006).

4.4.2 Structure evolution of $Li_4Ti_5O_{12}$ with temperature

As seen from the behavior of the u parameter (Figure 4.4b) the $8a$ tetrahedral volume (Figure 4.4c) increases strongly with temperature. At about 100 $°C$ the Li1-O distance is already becoming larger than the Li2/Ti-O distance ($u > 0.0125$). Extrapolation of the isotropic ADPs to 0 K shows that all pass through $B_{iso} = 0$ at 0 K (see Figure 4.4d). This means that no appreciable disorder is present in this compound. Only B_{iso} of Li starts to deviate above 700 $°C$ indicating the onset of anharmonic motion. For this reason anharmonic refinements have been performed at 900 $°C$.

4.4.3 Lithium migration at high temperatures

The PDF of Li1 on $8a$ shows bulges in the directions of the tetrahedral faces, typical for anharmonic vibrations in tetrahedral symmetry. The negative areas in Figure 4.5 are artifacts due to series termination effects which usually appear for very large gradients of the PDF. Here, they simply demonstrate the repulsion towards the nearest oxygen atom. About 14(2) % of these Li have migrated from the tetrahedra to the split site around $16c$. It has to be noted that the distance between this position and the nearest O is almost identical to that between Li1 and O, meaning that a transient bond between Li* and O is established (see the connecting lines in Figure 4.5). Note that Li* exactly on $16c$ would lead to an unacceptable long bond distance of about 2.24 Å.

The results of the present study partly match with former studies, but disagree with some theoretical aspects especially about the order-disorder phase transformations. The fractional migration of lithium depends on many factors, e.g. different syntheses techniques used to produce the spinel-type $Li_4Ti_5O_{12}$ and different treatments during the analyses. These are important factors which may influence the crystal structure, the thermal conductivity and the lithium migration. For example, the crystallinity of $Li_4Ti_5O_{12}$ strongly depends on the annealing temperature (Qiu et al., 2010), and even the possibility of electrochemical intercalation of more than 3 Li^+ in nano particulate $Li_4Ti_5O_{12}$ samples has been reported (Borghols et al., 2010). In addition, variable measuring conditions are used for the different analytic types. The measured samples can be, e.g., pressed pellets for impedance analyses or loose powders such as in the present study. The atmosphere, either argon, air or vacuum, and the selected heating rates are not consistent as well. Moreover, theories are based on changes of the conductivity as observed by impedance spectroscopy (Leonidov et al., 2003, 2004) where no direct structure determination can be performed.

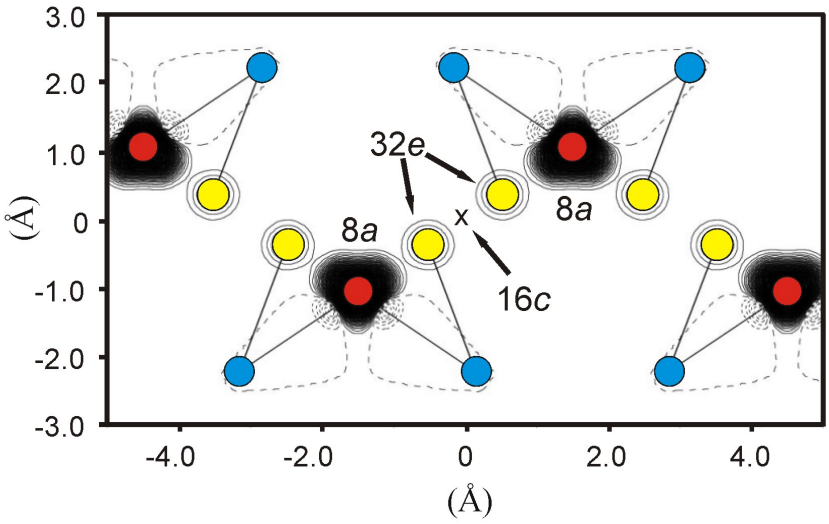

Figure 4.5: Probability density function (PDF) of Li at 900 $°C$ in the xxz-plane through $8a$ and $16c$ sites. The shortest bond distances between Li on $8a$ (red), Li* (yellow) and O (blue) are indicated. Long dashed lines represent zero density, short dashed lines negative densities.

4.5 Conclusions

During this study, a new two-step route to synthesize the anode material $Li_4Ti_5O_{12}$ was developed. Due to its excellent electrochemical performance it is currently produced by Süd-Chemie AG in batches of 200 kg. Studies by impedance spectroscopy and neutron powder diffraction performed on $Li_4Ti_5O_{12}$ showed enhanced lithium mobility at high temperatures. By neutron powder diffraction, the inferred lithium migration from $8a$ to $16c$ sites can be partly confirmed. However, in contrast to all previous suppositions, neutron powder diffraction (capable to derive actual positions of Li) showed that Li does not reside exactly on the $16c$ sites but is displaced from it into metastable positions determined by a potential minimum imposed by the surrounding oxygen geometry.

Chapter 5

Continuous flow synthesis of $Li_4Ti_5O_{12}$

This chapter describes a second pioneering method which was developed during this dissertation to produce the $Li_4Ti_5O_{12}$ spinel. Here, a solution comprising lithium ethoxide and titanium (IV) isopropoxide (TTIP) was treated in super-heated water at T > 350 $°C$ and a pressure of 250 bar. In reaction times of less than one minute, the lithium titanium spinel was produced with a very high specific surface area of approximately 230 m^2/g and a primary particle size of about 5 nm. It is not fully solved yet whether, upon annealing of the hydrothermal product, an amorphous lithium titanate phase starts to crystallize, or if the structure is disordered due to empty sites on 8a and part Li occupancy on 16c or 32e sites. The electrochemical results, and the general results of the *in-situ* synchrotron measurements, can be taken with confidence.

5.1 Introduction

The $Li_4Ti_5O_{12}$ spinel has already been well introduced, and as mentioned previously, its theoretical capacity is 175 mAh/g. This value is achieved when 3 Li^+ are intercalated in the spinel structure. But specific capacities of > 200 mAh/g have also been measured, which in general decrease rapidly after the first cycles. These enhanced capacities were recently ascribed to nanoparticulate $Li_4Ti_5O_{12}$ powders (Borghols et al., 2010). However, besides to common opinion that Li1 fully occupies the tetrahedral 8a sites and Li2 1/6 of the octahedral 16d sites (Kataoka et al., 2008; Julien and Zaghib, 2004), inconsistencies about the lithium distribution in $Li_4Ti_5O_{12}$ have been reported at room temperature. On the contrary, partial lithium occupation of 16c octahedral positions at room temperature due to migration of tetrahedrally bound lithium to interstitial sites has been proposed (Leonidov et al., 2003, 2004), and shown by NMR spectroscopy (Vijayakumar et al., 2009, 2010) and infrared spectroscopy (Pecharroman and Amarilla, 2000).

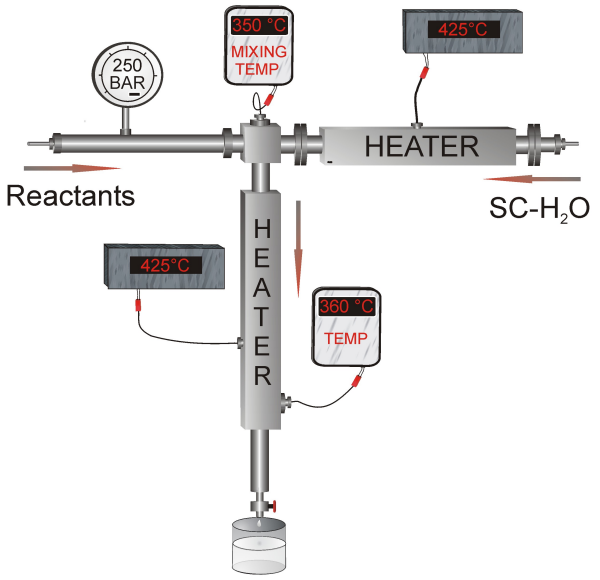

Figure 5.1: Outline of the continuous hydrothermal flow reactor used to synthesize $Li_4Ti_5O_{12}$ nanoparticles.

5.2 Experimental

5.2.1 Setup of the experiments

The syntheses were performed in a continuous flow hydrothermal reactor, which is designed for high pressures and temperatures, at the university of Aarhus, Denmark. An outline of the reactor design is shown in Figure 5.1. When the desired temperature and pressure are maintained, a prepared solution or suspension of reactants, and a solvent to react with, are pumped separately in the reactor. Water was used as the solvent, and it was heated close to, or above, its critical point in the first heating block, so that the cold reactants hit the hot solvent and start to react immediately. The product remains, depending on the flow rate of reactant and solvent, for up to 1 minute in the hot zone of the second heating block before it exits the outlet valve. Experiments were performed for set temperatures of the heaters between 350 and 425 $°C$ at a constant pressure of 250 bar. For the product which was studied the most (referred to as LTO in the following), the reaction conditions were: both heaters were set to 425 $°C$, the pressure was 250 bar and the flow rates were 3 ml/min and 6 ml/min for the reactants and the preheated water, respectively. For the current configuration of the flow reactor, these conditions correspond very closely to the maximum heat input. The injection of the cold reactants into the reactor results in a temperature at the mixing point of 350 $°C$ and a maximum of 360 $°C$ in the final section. The residence time in the heated part of the reactor can be estimated from the reactor volume, the overall flow rate and average fluid density to ≈ 30 s.

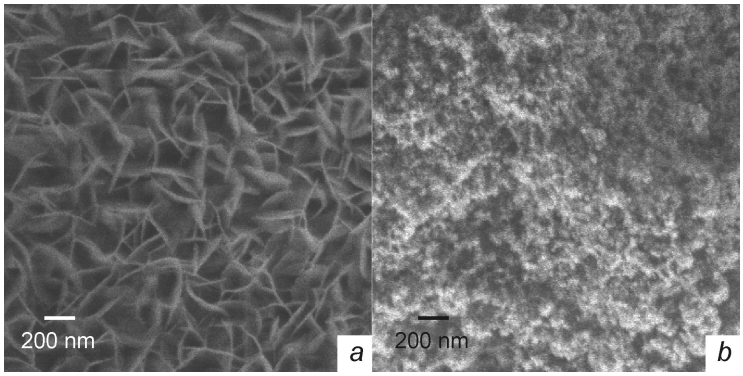

Figure 5.2: SEM pictures of (a) flake-like $Li_4Ti_5O_{12}$ particles after hydrothermal synthesis and (b) $Li_4Ti_5O_{12}$ particles after annealing at 600 $°C$.

5.2.2 Preparation of the reactants

The reactants were prepared using lithium and titanium reactants in a ratio of 4 : 5 with 5% lithium in excess. The lithium component was lithium metal dissolved in absolute ethanol, and TTIP (Sigma-Aldrich, 97%) was used as the titanium precursor. For sample LTO, 0.745 g of lithium metal was dissolved in 100 ml of absolute ethanol, and then 300 ml of isopropyl alcohol (IPA) and 37 ml of TTIP were added while stirring. After dissolving higher amounts of lithium metal in absolute ethanol, the solution appeared saturated, i.e. the mixture did not totally turn clear. After adding TTIP (50 ml) the mixture turned clear. To prevent clogging of the continuous flow reactor, IPA was used to dilute the solutions. After synthesis, the products were separated from the solvent using a centrifuge and washing with IPA. For the syntheses in the flow reactor, deionized water was used as the preheated solvent.

5.2.3 Electrochemistry

$Li_4Ti_5O_{12}$ samples, produced from reactant solutions of different concentrations and synthesized at varying temperatures, were used as active materials for half-cells to test the electrochemical performance of the material. Electrochemical measurements were performed as shown in Section 4.2.2. The electrochemical performance of LTO and sample LTO heated to 600 $°C$ for 12 hours (LTO-HT) can be seen in the Figures 5.5a-d.

5.2.4 Characterization

Synchrotron powder X-ray (PXRD) measurements were performed on LTO at beamline Bl02B2, SPring8, Japan. PXRD patterns were recorded (λ = 0.4332 Å) in temperature increments of 100 $°C$ in a temperature range from 27 $°C$ to 727 $°C$. Measuring time for each temperature step was 2.5 minutes. Data refinement was performed as shown in Chapter 2.2.3.

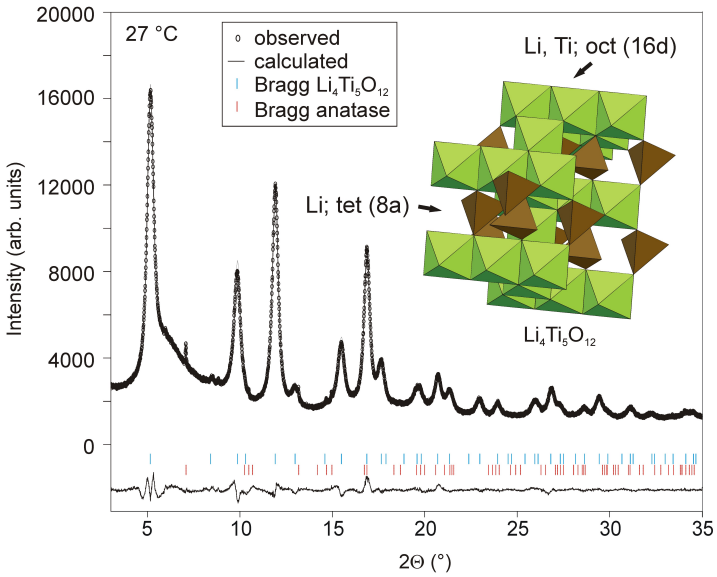

Figure 5.3: Structure and Rietveld fit of $Li_4Ti_5O_{12}$ at 27 $°C$. The insert shows the unit cell of $Li_4Ti_5O_{12}$.

5.3 Results

Products were in general white in color, and only when a slow flow rate of the solvent was used the products had a blue tint. Thus, partial reduction of tetravalent to trivalent titanium can be expected when the reaction conditions are slightly reducing. The $Li_4Ti_5O_{12}$ particles form flake-like aggregates (Figure 5.2a) with a very high specific surface area (BET), e.g. LTO of $\approx$ 230 m^2/g, indicating a open structure of the aggregates. After heating to 600 $°C$ (LTO-HT), the flake-like aggregates had transformed to a isotropic shape (Figure 5.2b).

5.3.1 *In-situ* synchrotron PXRD

Preliminary PXRD measurements with standard X-ray powder diffraction revealed that syntheses in the continuous flow reactor brought out $Li_4Ti_5O_{12}$ samples of which some showed minor impurities of anatase. LTO was found to be a pure phase, and it was studied in detail by synchrotron PXRD upon heating from room temperature to 727 $°C$. It could clearly be identified as $Li_4Ti_5O_{12}$ and was refined in space group $Fd\bar{3}m$. Due to the low X-ray scattering factor for light elements, such as Li, the atomic occupancies of $Li_4Ti_5O_{12}$ were fixed to the stoichiometric values. The unit cell parameter of $a = 8.3526(5)$ Å of LTO at room temperature is slightly lower than values reported previously (Kataoka et al. (2008) $a = 8.352(4)$ Å, Laumann et al. (2011b) $a = 8.35952(4)$ Å). The increase of the unit cell upon heating is depicted in Figure 5.4a. At room temperature, an impurity of $\approx$ 0.5 $wt\%$ anatase was found (Figure 5.3), which could not be detected by standard

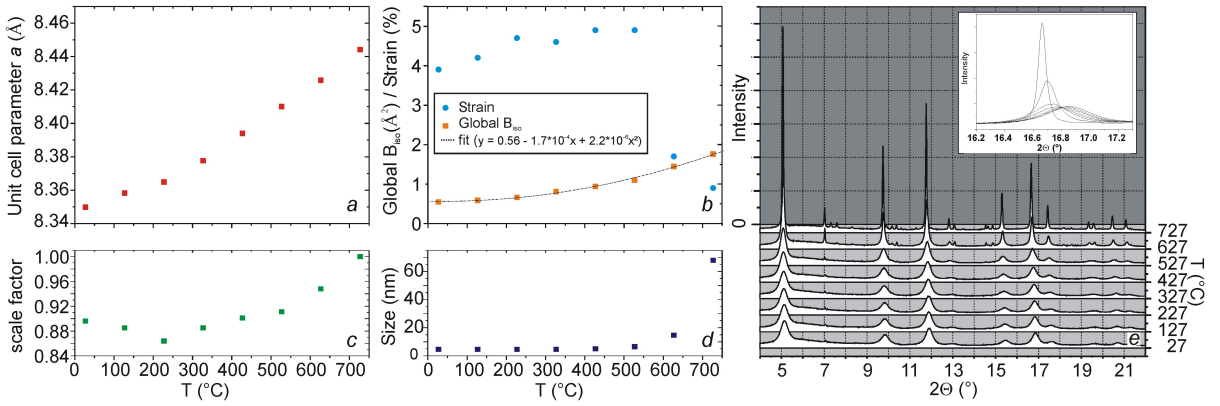

Figure 5.4: Graphs showing, (a) unit cell parameters, (b) strain and Global B_{iso}, (c) crystallinity, (d) particles size, and (e) multi-temperature plot upon annealing of LTO to 727 $°C$, with detailed view of the (440) reflection given in the insert.

PXRD. Upon heating of LTO to 527 $°C$, this impurity was constant at about 0.5 $wt\%$. At 627 $°C$, higher impurities of anatase were found and at 727 $°C$ an impurity of $\approx$ 5 $wt\%$ comprising anatase and rutile was present. It was observed that lithium from LTO started to react with the quartz capillary at 627 $°C$, and at 727 $°C$ distinct reflections of high-quartz (PDF No.: 870703) were detected. The reaction of lithium with the quartz capillary is likely the cause for the increase in anatase and rutile impurities.

Strain and size From room temperature up to 527 $°C$, LTO showed extremly high strain. Strong correlations of the strain parameter U with B_{iso} were found, resulting in unphysical B_{iso} values. By constraining the B_{iso}'s of all atoms to a global B_{iso}, refinement was enabled with reliable values. At 627 $°C$, the strain decreased remarkably (Figure 5.4b). But in order to present data which was refined uniformly, data at 627 and 727 $°C$ was treated the same way, although B_{iso} returned to reliable values when the sample was comparatively strain-free. The particle size of $Li_4Ti_5O_{12}$ at room temperature was refined to be 4.6(3) nm (Figure 5.4d). Upon heating to 427 $°C$, the particle sizes were constant within acceptable error. Then, after having a size of 6.4(3) nm at 527 $°C$, at 627 $°C$ the particle size reached 14.56(4) nm, and the measurement at 727 $°C$ depicted particles of 62(1) nm in size. The sharpening of the $Li_4Ti_5O_{12}$ peaks with increasing particle size is shown in Figure 5.4e.

Crystallinity The refined scale factor of LTO could be regarded as a measure of the crystallinity of the sample. Considering LTO to be fully crystalline at 727 $°C$, the observed scale factor for the synthesized LTO corresponds to a crystallinity of 88.9(5) %. Similar to the particle size and the strain, the scale factor shows no significant change between room temperature and 527 $°C$. Striking changes were observed at 627 $°C$ and especially at 727 $°C$ (shown in Figure 5.4c).

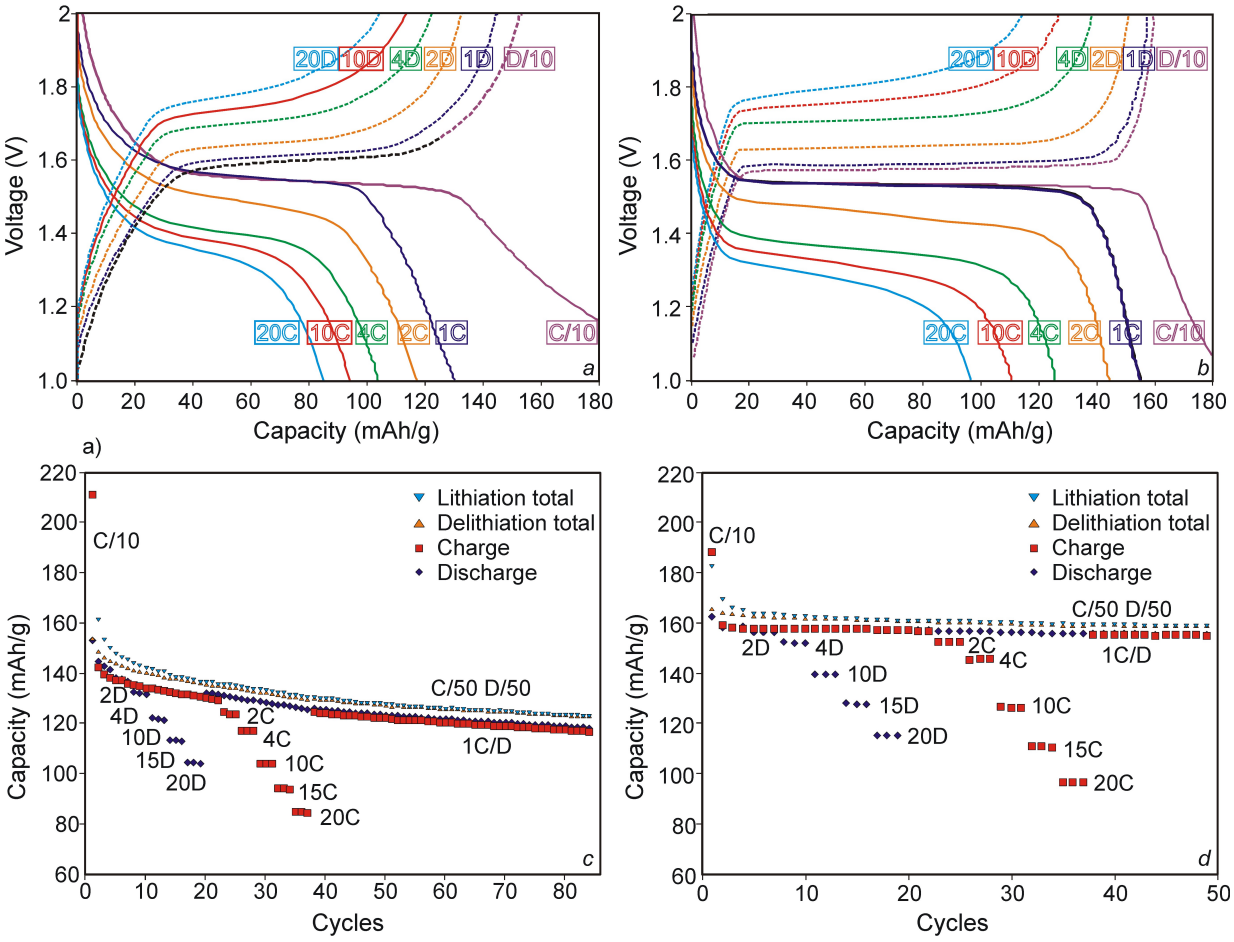

Figure 5.5: (a) Charge-discharge plateaus of LTO for currents from C/10 to 20C, D/10 to 20D, respectively; (b) charge-discharge plateaus of LTO-HT for currents from C/10 to 20C, D/10 to 20D, respectively; (c) cyclability of LTO and (d) cyclability of the LTO-HT.

Li occupancy For refinements of the lithium occupancy on sites other than 8*a* and 16*d*, the overall ltihium occupancy was fixed to its stoichiometric value. Refinements with lithium on 16*c* revealed surprising results. Contrary to most previous studies (Ohzuko et al., 1995; Julien and Zaghib, 2004; Kataoka et al., 2008), about 25% of total lithium seems to occupy 16*c* sites at room temperature. Upon heating, the Li occupancy increased first to a maximum value of over 35% at 227 °*C* and then, the occupancy on 16*c* dropped finally to 0 at 627 °*C*. Notably, the Li occupancy follows the scale factor (crystallinity) (Figure 5.6), such that the scale factor has its apparent maximum for full Li occupancy on 8*a*. But taking the low scattering power of lithium into account, it is doubtful if the migration of lithium causes more than 10% increase of the scale factor. However, B_{iso}, the particle size and the strain were relatively unaffected when refining parts of lithium on 16*c*, showing the certainty of these results. The partial occupation of lithium on 16*c* was

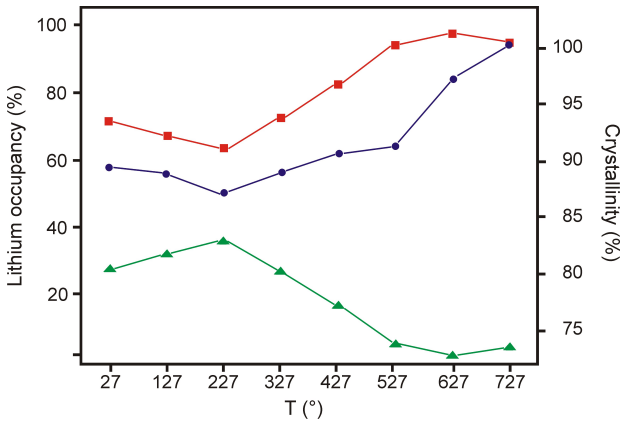

Figure 5.6: Lithium occupancies on 8*a* (red) and 16*c* (green) sites (Li on 16*d* not taken into account, as it was fixed to its stoichiometric value) of the hydrothermally produced $Li_4Ti_5O_{12}$ upon heating. The crystallinity is also shown in blue.

reported before and the percentage of lithium on 16*c* at room temperature and up to 227 $°C$ is in very good agreement with the results of the NMR study of Vijayakumar et al. (2010). But at temperatures above 227 $°C$, in the study of Vijayakumar et al. (2010), the lithium occupancy on 8*a* further decreases with an increase of lithium on 16*c*, which is the opposite to the observations of this study (Figure 5.6).

5.3.2 Electrochemistry

Electrochemical tests were performed on various samples without heat treatment and in particular on LTO (Figure 5.5a and Figure 5.5c), and the annealed sample LTO-HT (Figure 5.5b and Figure 5.5d). Although the synthesis conditions varied, electrochemical measurements of $Li_4Ti_5O_{12}$ samples without heat treatment showed only minor aberrations from each other. The first charging cycle at C/10 shows a very high specific capacity ($>$ 200 mAh/g). By charging and discharging at higher rates (up to 20C/20D), the specific capacity degreases to about 80 mAh/g for charging and to 100 mAh/g for discharging, respectively (Figure 5.5a). In the following cycles, the specific capacity at 1C/1D drops to $\approx$ 140 mAh/g and degreases to a value of about 100 mAh/g after 85 cycles (Figure 5.5c).

LTO-HT showed a much better electrochemical performance than LTO, in terms of the specific capacity, the capacity at high rates (Figure 5.5b), and the long term cyclability (Figure 5.5d). The characteristic plateau at 1.55 V of LTO-HT is flatter and longer than the one of LTO, which indicates the particle growth due to annealing. In the first cycle the specific capacity is $\approx$ 160 mAh/g and decreases only by $\approx$ 5 mAh/g after 50 cycles (Figure 5.5d).

5.4 Discussion

The hydrothermally produced $Li_4Ti_5O_{12}$ samples were crystalline ($\approx 89\%$) but show a high degree of crystal strain, which might be due to the short reaction time of ca. 30 s and the low reaction temperature, especially when compared to solid-state reactions. Above 527 $°C$, the crystalline fraction is observed to increase to 100% concurrent with relaxation of the crystal strain and growth of the nanoparticles. The general lower capacity of LTO (Figure 5.5a) compared with LTO-HT (Figure 5.5b) matches well with the 89% crystallinity of LTO, thus the increase of the crystalline fraction due to annealing might result in the higher overall capacity. The high specific capacity in the first cycles can be ascribed to the particle size (Borghols et al., 2010) (for details see Appendix G).

The relatively fast capacity decrease of samples without heat treatment, and of LTO (5.5c), could also be due to low crystallinity. Low crystallinity in battery materials (Qi et al., 2008) and also in $Li_4Ti_5O_{12}$ (Qiu et al., 2010) was attributed to cause poor cycling performance, and heat treatment improved the cyclability of the active materials corresponding with the observations of this study. Whether the discussed lithium occupancy on 16c (see 5.3.1) affects the electrochemical performance, or if it is even the main reason for the lower overall capacity and its more rapid drop, still has to be solved. It can be proposed that a higher hydrothermal synthesis temperature, longer synthesis time and a higher concentration of the reactants could be implemented to obtain products of higher crystallinity and of less strain, leading to an improved electrochemical performance. When comparing the electrochemical performance of LTO-HT with other presented and commercial $Li_4Ti_5O_{12}$ samples, its cyclability and its capacity at high rates are competitive.

5.5 Conclusions

The present study is the first method so far describing the synthesis of $Li_4Ti_5O_{12}$ in a direct way via sub- or supercritical syntheses (T $>$ 350 $°C$) by using a lithium ethoxide solution and TTIP as reactants. However, the short reaction time and the relative low reaction temperature of about 350 $°C$ resulted in only partly crystalline samples. Annealing at 600 $°C$ only causes minor particle growth as demonstrated by synchrotron PXRD and thus $Li_4Ti_5O_{12}$ nanoparticles with an excellent cyclability and rate performance can be produced, which are competitive with other $Li_4Ti_5O_{12}$ active materials produced at higher temperatures.

Regarding the Li occupancy on 16c at room temperature, the results seem to be reliable, but are, however, not in agreement with the ones presented on the $Li_4Ti_5O_{12}$ synthesized by the two-step method in Chapter 4. Apparently, via different syntheses methods, $Li_4Ti_5O_{12}$ samples of varying crystal chemistry can be produced and it can be proposed that the annealing temperature and the particle size are highly influential, the cooling rate may also be. As seen in Chapter 4, lithium migration to split sites close to 16c starts at high temperatures, whereas analyzes of the hydrothermally synthesized $Li_4Ti_5O_{12}$ reveal Li-occupacion partly on 16c at room temperature.

Outlook For future work, the crystal structure of $Li_4Ti_5O_{12}$, synthesized via the two different processes (two-step and hydrothermal), should be analyzed by neutron diffraction upon heating to 900 $°C$ and then upon cooling to room temperature. These studies would show the importance of the annealing temperature on the crystal structure and whether the cooling rate has an influence on the sample when cooled again to room temperature. Of further interest will be whether the two $Li_4Ti_5O_{12}$ samples have the same crytallographic properties at higher temperatures and if they either retain that structure upon cooling or if lithium migrates back to its positions at room temperature before heating. As such, the crystallite size might be crucial for the starting temperature of the lithium migration.

Appendix A

First publication

Metastable formation of low temperature cubic Li_2TiO_3 under hydrothermal conditions — Its stability and structural properties

Solid State Ionics **181** 1525–1529 (2010)

Andreas Laumann,[a] **Karl Thomas Fehr,**[a] **Martin Wachsmann,**[a] **Michael Holzapfel,**[b] **Bo Brummerstedt Iversen**[c]

[a] Ludwig-Maximilians-Universität München, Department of Earth and Environmental Sciences, Section for Mineralogy, Petrology and Geochemistry, Munich, Germany
[b] Süd-Chemie AG, Battery Materials, Moosburg, Germany
[c] Aarhus University, Department of Chemistry and iNANO, Aarhus C, Denmark

Solid State Ionics 181 (2010) 1525–1529

Contents lists available at ScienceDirect

Solid State Ionics

journal homepage: www.elsevier.com/locate/ssi

Metastable formation of low temperature cubic Li_2TiO_3 under hydrothermal conditions — Its stability and structural properties

Andreas Laumann [a,*], Karl Thomas Fehr [a], Martin Wachsmann [a], Michael Holzapfel [b], Bo Brummerstedt Iversen [c]

[a] Ludwig-Maximilians-Universität München, Department of Earth and Environmental Sciences, Section for Mineralogy, Petrology and Geochemistry, Munich, Germany
[b] Süd-Chemie AG, Battery Material, Moosburg, Germany
[c] Aarhus University, Department of Chemistry and iNANO, Aarhus C, Denmark

ARTICLE INFO

Article history:
Received 31 May 2010
Received in revised form 22 August 2010
Accepted 22 August 2010

Keywords:
Hydrothermal synthesis
Cubic Li_2TiO_3
Phase stability
Synchrotron diffraction

ABSTRACT

Cubic Li_2TiO_3 samples (space group Fm-3m) were synthesized by hydrothermal reactions at 180 °C for 18 h, using titania powder and lithium hydroxide in de-ionized water. The samples were found to be unstable under atmospheric conditions as Li_2CO_3 could be detected by X-ray powder diffraction (XRPD) on their surface. Therefore, the stability of cubic Li_2TiO_3 when exposed to water was investigated. In water-flushing and bathing experiments the interaction of water with the samples could be demonstrated. The observed lithium loss was analyzed by atomic absorption spectroscopy and its influence on the structural properties of cubic Li_2TiO_3 was determined by conventional XRPD and *multi-temperature* synchrotron XRPD.

1. Introduction

Hydrothermal syntheses have gained importance due to their low energy demand and thus, they are considered "green chemistry" methods [1]. Syntheses of lithium titanium compounds in general require high temperatures and solid state syntheses are the most common [2–6]. Recently it has been shown that the cubic modification of Li_2TiO_3 (γ-Li_2TiO_3), which is stable above 1155 °C, can be synthesized by a hydrothermal technique in a metastable form (α-Li_2TiO_3) at low temperatures [7]. Compared with γ-Li_2TiO_3, the stable phase at high temperatures, the metastable α-form is supposedly stabilized by protons during the hydrothermal synthesis [7].

The compound Li_2TiO_3 has been described in three structural modifications, α, β and γ [3,8]. The cubic α-Li_2TiO_3 (space group Fm-3m) is synthesized hydrothermally at low temperature. Above 300 °C it transforms irreversibly to the monoclinic β-Li_2TiO_3 (space group C2/c) [6,7]. Below 1000 °C, during the first heating, the β-phase is disordered due to stacking faults, which is indicated in the powder X-ray diffraction (XRPD) patterns by sharp reflections of higher intensity, and missing, or very broad, low intensity reflections [7]. β-Li_2TiO_3 remains stable up to 1155 °C [3], above it transforms to the cubic γ-Li_2TiO_3 (space group Fm-3m).

In general, the metastable α-Li_2TiO_3 is synthesized by a hydrothermal technique using titania powder and lithium hydroxide with de-ionized water as the solvent, but ambiguous data has been published concerning its composition and structural properties [9–20]. The ambiguities especially concern the lithium content [13–15], and the phases obtained after annealing [9–11]. The displayed XRPD patterns of the hydrothermally synthesized α-Li_2TiO_3 look alike, but Li/Ti ratios vary from 2:1 (calculated from the given atomic %) [16] over 1.69:1 [18] to 0.34:1 [17]. The XRPD patterns were compared with the high-temperature form γ-Li_2TiO_3 [16,18] which was first described by Kordes [21,22]. Furthermore, various XRPD patterns of intermediate lithium titanates, similar to the pattern of the metastable cubic Li_2TiO_3, were published [10–15,20]. The phases were described as $Li_{0.665}Ti_{0.82}O_2 * H_2O$ [11], $Li_{1+x}Ti_{2-x}O_{4+\delta}$ (x between 0 and 0.1, δ between 0.3 and 0.5) [12,20], or $LiTiO_2$ [10,13–15]. In all studies, the obtained products were washed after synthesizing. Annealing of some of these intermediate lithium titanium phases led to compounds similar to $Li_4Ti_5O_{12}$ [11,12,20].

In the present study, cubic α-Li_2TiO_3 was synthesized via hydrothermal reaction. Water-flushing and bathing experiments on the samples were performed to test their stability in the presence of water at room temperature. An *in-situ* synchrotron measurement upon heating of a sample with a lithium deficit of about 40% was performed and the results were compared with data recently obtained using neutron powder diffractometry of a sample with a Li/Ti ratio close to 2:1 [7].

* Corresponding author. Department of Earth and Environmental Sciences, Section for Mineralogy, Petrology and Geochemistry, Theresienstr. 41, 80333 Munich, Germany. Tel.: +49 8921804276; fax: +49 8921804176.
E-mail address: laumann@min.uni-muenchen.de (A. Laumann).

0167-2738/$ – see front matter
doi:10.1016/j.ssi.2010.08.017

2. Experimental

2.1. Preparation of cubic Li_2TiO_3 powders

Cubic α-Li_2TiO_3 powders were synthesized at 180 °C for 18 h in polytetrafluorethylene (PTFE) containers. The reactants were TiO_2 powder, comprising anatase and rutile (Evonik, formerly Degussa, AEROXIDE TiO_2 P25), and lithium hydroxide (SQM, Chile). For the reactions, 0.025 mol of P25 were stirred in a solution of 0.05 mol lithium hydroxide dissolved in 15 ml of de-ionized water. The product was filtered with a vacuum filter and left unwashed. It was dried at 60 °C, de-agglomerated in an agate mortar, and kept under argon atmosphere.

2.2. Water-flushing and bathing experiments

For a series of water-flushing experiments, 100 mg of α-Li_2TiO_3 were flushed with a flow rate of approximately 100 ml/h in a paper filter with various amounts of de-ionized water (Table 1). For bathing experiments, 100 mg of α-Li_2TiO_3 were stirred for 5 h in 10, 25, 50, 100, 300, and 500 ml of de-ionized water and then left to precipitate over a period of 4 days in a glass beaker (Table 1).

2.3. Characterization

The elements Li, Ti, Fe, Cr, Ni, Mn, P, S, Al, Ca, Na, K, Mg and Sb of sample U1 (Table 1), which was dried for 2 h in vacuum at 105 °C, were analysed by ICP-OES with an error <0.3% (ICP-OES Varian Vista Pro 720-ES). The lithium content of washed and unwashed samples was measured by atomic absorption spectroscopy (AAS), using a Perkin-Elmer 3300 in an air-acetylene flame at a wavelength of 670.8 nm. Samples were dried at 275 °C, i.e. below the temperature of the transition to the monoclinic phase, and dissolved in hot H_2SO_4.

In order to measure the amount and the type of volatiles, thermogravimetric analysis (TGA) and Fourier transform spectroscopy (FTIR) analyses were performed. TGA measurements were carried out in an Argon (5.0) atmosphere on a Jupiter STA 449C from Netzsch in a temperature range from 25 up to 900 °C and at a heating rate of 3 °C/min. FTIR measurements were performed with a Bruker Equinox 55 in the mid infrared region (4000 to 400 cm^{-1}). For sample preparation, approximately 2 mg of each sample were dispersed in 300 mg of KBr powder and compressed. X-ray powder diffraction (XRPD) was measured in transmission geometry on a Stoe Kristalloflex diffractometer (CuKα1-radiation $\lambda = 1.544056$ Å, curved Ge(111) monochromator). Synchrotron data was recorded on sample F5 (Table 1) at Spring 8, Japan. XRPD patterns were recorded in temperature increments of 100 °C in a temperature range of 100 K (−173 °C) to 600 K (327 °C). Structural Rietveld refinement was performed by using the program FullProf [23] and the peaks were fitted with Thompson–Cox–Hastings pseudo-Voigt Axial divergence asymmetry peak shape [24]. To ascertain the particle size, the instrumental broadening was determined with a CeO_2 standard.

Table 1
Sample list of the water-flushing and bathing experiments, the resulting lithium loss and the Li/Ti ratio, respectively, as well as the hypothetical formulas.

Sample	Flushing (ml)	Lithium loss (%)	Li/Ti ratio	Hypothetical formula[a]
U1	0	0	2:1	$(Li_1H_0)_2TiO$
F1	50	25	1.50:1	$(Li_{0.75}H_{0.25})_2TiO_3$
F2	100	13	1.74:1	$(Li_{0.87}H_{0.13})_2TiO_3$
F3	200	24	1.52:1	$(Li_{0.76}H_{0.24})_2TiO_3$
F4	300	26	1.48:1	$(Li_{0.74}H_{0.26})_2TiO_3$
F5[b]	500	43	1.16:1	$(Li_{0.57}H_{0.43})_2TiO_3$
F6	750	37	1.26:1	$(Li_{0.63}H_{0.37})_2TiO_3$
Bathing experiments				
B1	10	44	1.12:1	$(Li_{0.56}H_{0.44})_2TiO_3$
B2	25	57	0.86:1	$(Li_{0.43}H_{0.57})_2TiO_3$
B3	50	62	0.76:1	$(Li_{0.38}H_{0.62})_2TiO_3$
B4	100	66	0.68:1	$(Li_{0.34}H_{0.66})_2TiO_3$
B5	200	68	0.64:1	$(Li_{0.32}H_{0.58})_2TiO_3$
B6	300	73	0.54:1	$(Li_{0.27}H_{0.73})_2TiO_3$
B7	500	75	0.50:1	$(Li_{0.25}H_{0.75})_2TiO_3$

[a] Hydrogen calculated by charge balance (see the Discussion section).
[b] Sample used for synchrotron measurements.

3. Results

The lithium titanate powders synthesized by hydrothermal reactions for 18 h at 180 °C were polycrystalline and of white colour. The primary particles showed a size in the range of 50–80 nm and a cubic shape (Fig. 1).

3.1. Element analysis

The ICP-OES measurements on sample U1 yielded a lithium content of 12.6 wt.% and a titanium content 43.8 wt.%, which is in good agreement with the calculated theoretical values of 12.65 wt.% and 43.62 wt.%, respectively. The contents of all other elements were negligible. For unwashed samples, AAS measurements gave the same lithium value ±3%. The samples treated with water showed lower lithium content and especially in the bathing experiments a decrease of the lithium content with increasing amount of water was observed (Table 1). When comparing the bathing and flushing experiments done with the same amount of water, a higher lithium loss is observed in the bathing experiments, and the highest loss of 75% was obtained after bathing a sample for 4 days in 500 ml of de-ionized water (Table 1).

3.2. Volatiles

Samples kept at 275 °C showed a weight loss between 5 and 8% compared with the sample weights before starting the heat treatment. If the de-vaporized samples are left for 30 min in air, ~60% of the initial weight was regained after 30 min, and after 1 day the sample weights were approximate the same as initially. In addition, TGA experiments were performed. Upon heating of sample U1 to 900 °C, a total weight loss of 6.34% was recorded (Fig. 2). The TGA curve of sample F1 was in good agreement with these results.

FTIR spectra were recorded on the samples U1 (Fig. 3a), B1 (Fig. 3b), and B6 (Fig. 3a). These samples were dried at 275 °C, the same temperature at which samples were dried for AAS analyses. The strongest variation in these spectra is noted at low wavenumbers, where infrared bands of the bulk composition of lithium titanates are expected [25,26]. The peaks in this range broaden and become less distinct with higher lithium loss. The two bands at 1456 cm^{-1} and 1506 cm^{-1} (Fig. 3a) can be attributed to carbonates associated with Li^+ anions [25]. With increasing amounts of bathing water, these peaks diminish, which is most likely caused by the removal of the Li_2CO_3 from the surface of the

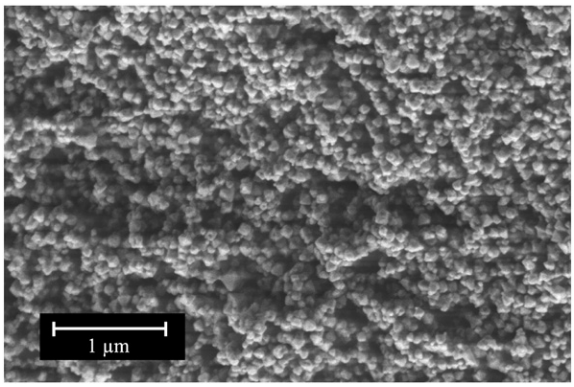

Fig. 1. SEM picture of α-Li_2TiO_3 particles displaying cubic shape.

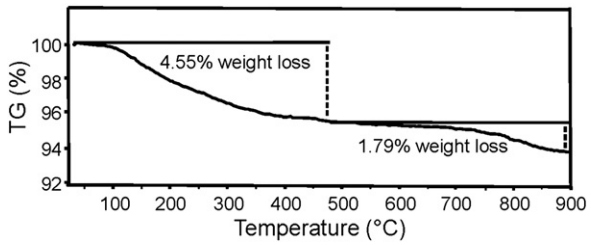

Fig. 2. Weight loss of sample S1 measured by TGA.

samples. Samples left under atmospheric conditions showed increasing amounts of Li_2CO_3 with time, detected by XRPD. The first traces of Li_2CO_3 were observed after leaving samples for 3 days in air and the reflections of Li_2CO_3 became more pronounced after a longer latency. The band at 1635 cm^{-1} is formed by the H_2O bending vibration of atmospheric water vapour [25]. The broad band around 3420 cm^{-1} can be attributed to the stretching vibration on the hydroxyl bond [26,27], which Jones and Hockey [28] ascribed to the hydroxylation and hydration of particle surfaces. No sharp –OH bond at wavenumbers ~3500 cm^{-1} is visible, or increasing in intensity with higher lithium deficits. This leads to the assumption, that hydrogen is not bonded in distinct –OH bonds in the structure. The samples dried at only 105 °C showed stronger bands around 3400 cm^{-1} and at 1635 cm^{-1}. Detailed FTIR analyzes of the bulk compositions of water-treated and non-treated lithium titanium compounds in mid- and far-infrared will be given in a forthcoming paper.

3.3. Structural analysis

At first glance, all samples with Li/Ti ratios in the range from 2:1 to 0.50:1 showed similar XRPD patterns to the one presented in Fig. 5a. The unit cell parameter of water-flushed samples only varied between 4.141 Å and 4.150 Å. Samples with high lithium loss showed a clear shift of the reflections to higher 2θ-angles and the lowest unit cell parameter was revealed for sample B6 with $a = 4.121(3)$ Å.

Synchrotron measurements were performed on sample F5. The refined room temperature pattern is presented in Fig. 4 and the reflections list is given in Table 2. The atomic array of the cubic Li_2TiO_3 structure is a NaCl close packed unit cell, with a statistic distribution of 2/3 lithium and 1/3 titanium on one site and oxygen on the other site. The occupancies of titanium and oxygen were fixed to 0.3333 and 1, respectively. The lithium occupancy was refined for all temperatures and its occupancy was 0.40(3) (Table 3), corresponding to a lithium deficit of 40% ± 3.5%, which is within the error of the AAS measurement. At room temperature, the unit cell parameter was $a = 4.14528(5)$ Å,

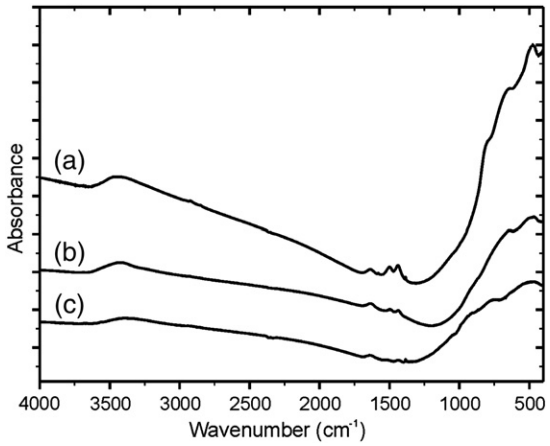

Fig. 3. FTIR spectra of (a) sample U1, (b) sample B1 and (c) sample B6.

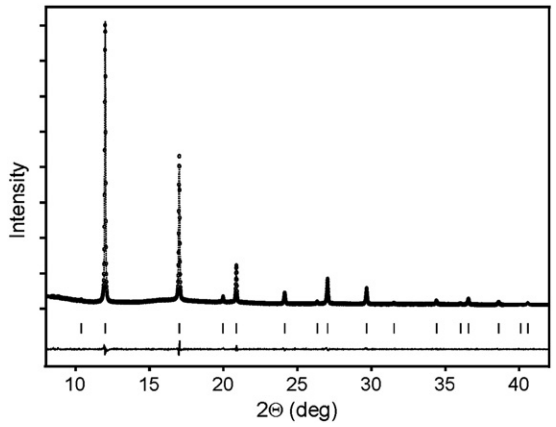

Fig. 4. Structural Rietveld refinement of sample F5 at room temperature. Observed (circles) and calculated (dashed line). The background was linearly interpolated between set background points with refinable heights.

similar to the values obtained with standard X-ray diffraction. Below 500 K (227 °C), the particle size was 63 nm within an error margin of 1% (Table 1). It started to increase slightly at 500 K, and at 600 K (327 °C) broad reflections occurred, representing the first indication of the transformation to the monoclinic structure, which has been previously described [7].

By XRPD, non-annealed samples with variations in the Li/Ti ratios could not be differentiated in diverse compounds. The contrary is true for heat-treated samples, which displayed the decrease in the Li/Ti ratio, and differing products occurred after annealing samples at e.g. 800 °C for 12 h (Fig. 5b–d). Unwashed samples transformed to the monoclinic β-Li_2TiO_3 (Fig. 5b). Samples with a moderate Li-deficit, e.g. sample F6, resulted in a mixture of β-Li_2TiO_3 and $Li_4Ti_5O_{12}$ (Fig. 5c). Samples with a high Li-deficit, like sample B5, showed the presence of $Li_4Ti_5O_{12}$ and TiO_2 (rutile) after the heat treatment (Fig. 5d).

4. Discussion

4.1. Stability and formation of cubic Li_2TiO_3 particles

The lithium titanates synthesized under hydrothermal conditions in the present study showed Li/Ti ratios close to 2:1, corresponding to 12.65 wt.% of lithium, as long the samples remained dry after syntheses. Flushing and bathing of cubic Li_2TiO_3 with de-ionized water led to lithium loss. The flushing experiments showed a general

Table 2
Parameters of the structure refinement of sample F5 at 300 K (27 °C).

HKl	d-spacing (Å)	I (cal)	I (obs)
111	2.3933	35	38.9
200	2.0726	6148.4	6077.1
220	1.4656	3241.1	3297.6
311	1.2498	113.6	124.9
222	1.1966	874.8	849.2
400	1.0363	327.9	324.2
331	0.9510	53.9	48.7
420	0.9269	745.7	744
422	0.8462	462.4	471.2
333/511	0.7978	9.2/27.7	9.3/28
440	0.7328	104.8	107.6
531	0.7007	31.1	29
442/600	0.6909	148.9/37.2	150.2/37.5
620	0.6554	108.3	107.8
533	0.6321	9.3	8
622	0.6249	80.3	81.8

λ = 0.433207 Å, step size = 0.01 °2θ, M (Li_2TiO_3) = 109.75, Vol = 71.230(2) $Å^3$, space group: Fm-3m, number of fitted parameter: 61, number of reflections = 16, Rp: 9.41, Rwp: 7.84, Rexp: 4.63, χ^2: 2.87, Bragg R-factor: 1.58, Rf-factor: 1.08.

Table 3
Refined unit cell parameters, lithium occupancies and particle sizes of sample F6 for the temperatures from 100 K (−173 °C) to 600 K (327 °C).

T (K)	a (Å)	Li occupancy	Particle size (nm)
100	4.13290(7)	0.41(3)	62(1)
200	4.13702(6)	0.40(3)	63(1)
300	4.14281(5)	0.38(3)	64(1)
400	4.15143(5)	0.38(3)	63(1)
500	4.15867(5)	0.42(3)	67(1)
600	4.16742(5)	0.41(3)	71(1)

trend of higher lithium loss with higher water content, but the decline in the lithium content was not constant, which is most likely caused by inhomogeneous washing in the filter. In contrast, the samples treated in the bathing experiments were increasingly de-lithiated with a higher water volume. By plotting the lithium loss of the bathing experiments vs. the volume of water, an exponential decay is seen (Fig. 6). The methods used to remove lithium prove that α-Li_2TiO_3 seems to have a maximum Li-loss of around 75%. In the water-flushing experiments, lithium loss of ~25% occurred frequently, which fortifies the assumption that lithium occupancies of 1/4 and 3/4 are more stable than intermediate values.

Lithium loss from Li_2TiO_3 requires the substitution of other cations to balance the charge. Diminishing unit cell parameters with decreasing lithium content support the assumption that ions smaller than Li^+ ions are inserted into the structure. In the FTIR spectra (Fig. 3), no distinct –OH bond could be detected, which show that OH-groups are not getting

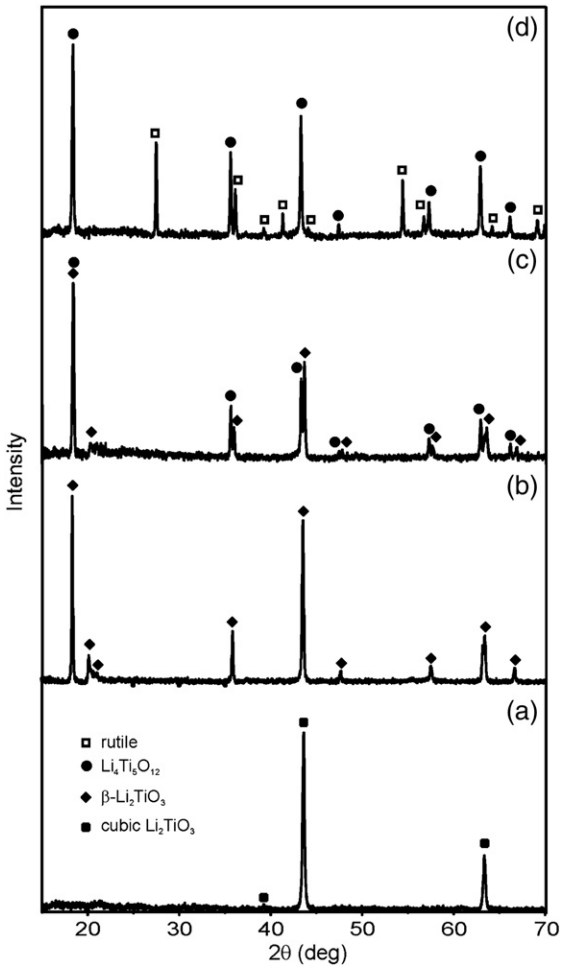

Fig. 5. XRPD patterns of (a) sample U1 after the hydrothermal synthesis, and of samples annealed at 800 °C (b) sample U1, (c) sample F6 and (d) sample B5.

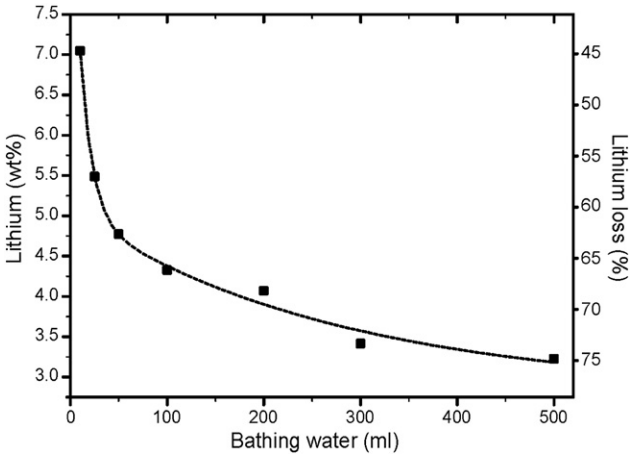

Fig. 6. Plot of decreasing lithium content of α-Li_2TiO_3 with increasing amount of water used for the bathing experiments.

into the structure. Another point is that OH-groups would not balance the charge of a lithium loss. However, the spectra of the bathed samples between wavenumber 3600 cm^{-1} and 1000 cm^{-1} seem to be increased. Hydrogen would not occupy octahedral sites, but rather bind to oxygen at different sites in the octahedron similar to the multi-site substitution of OH^- in silicate garnets [29]. Presumably the increased spectra in the mentioned range is caused by hydrogen ions that bind randomly distributed to lattice oxygen. The Li^+ exchange with H^+ in the system Li–Ti–O–H, then might be similar to the well-known exchange of D^+ with H^+ under atmospheric conditions. In natural petalite ($LiAlSi_4O_{10}$), a correlation between a decreasing lithium content and an increasing hydrogen content has been reported [30]. Following the assumption that Li^+ ions are exchanged by H^+, products of the solid solution Li_2TiO_3–H_2TiO_3 may be obtained. For instance the 13% lithium loss of sample F2 can be written as $(Li_{1-0.13}H_{0.13})_2TiO_3$. The hypothetical formulas of all samples are listed in Table 1.

The reaction of cubic α-Li_2TiO_3 with water and CO_2 in ambient air was indirectly observed in another study and the presence of protons in the structure is mentioned as 'realistic' [12]. The authors combined TGA measurements with ICP-MS on a Li–Ti–O compound synthesized in a similar manner to the material in the present study. Their obtained peak maxima were around 150 °C and 300 °C for de-vaporized water and

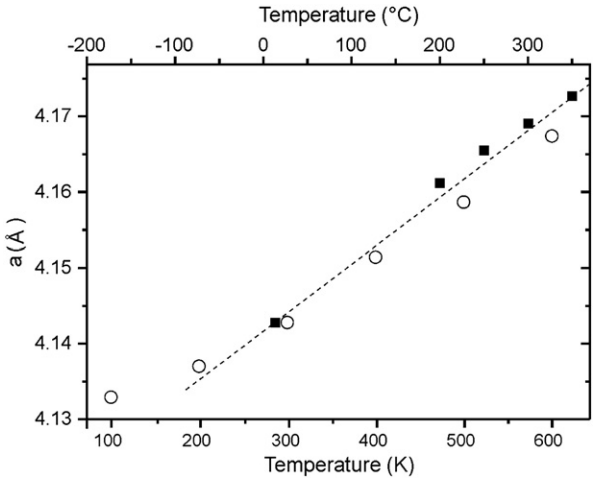

Fig. 7. Temperature-dependent change of the unit cell parameter of cubic Li_2TiO_3. Data of the present study (circles) is compared with data from an *in-situ* neutron measurement study (squares) [7].

CO_2, respectively. The reaction of cubic Li_2TiO_3 with atmospheric water and CO_2 can be described as:

$$Li_2TiO_3 + xH_2O + xCO_2 \rightarrow (Li_{1-x}H_x)_2TiO_3 + xLi_2CO_3$$

The discrepancies of the Li/Ti ratios in previously published studies on cubic α-Li_2TiO_3 can be explained by the water-flushing and bathing experiments of the present study. That lithium loss may be caused by washing had already been speculated by Tabuchi et al. [18], but in another study the very low Li/Ti ratio of 0.34:1 of cubic Li_2TiO_3 was ascribed to a mixture of cubic Li_2TiO_3 and amorphous TiO_2 [17]. In the latter study, after using 7 nm diameter anatase as a reactant, the resulting cubic Li_2TiO_3 had a similar primary particle size, which presumably eased the de-lithiation.

In a recent study, the intercalation of lithium into titania under hydrothermal conditions was recorded using *in-situ* synchrotron XRPD [31], and the temperature dependence on the reaction time could be shown. By using titania powder of small particle size (7 nm), the lithium intercalation can be performed at very low temperatures; 100 °C [17], or 60 °C [20], respectively. Presumably lithium would not be bound strongly in the structure, which could explain why lithium can be washed out easily, even by atmospheric water. In another study it was demonstrated that lithium in cubic Li_2TiO_3 can be totally substituted for the phase H_2TiO_3 in low acid media [32], whereas in the monoclinic Li_2TiO_3 only 25–30% of lithium could be substituted in strong inorganic acid solutions. In aqueous media, the lowest Li/Ti ratio so far reported was 0.34:1 [17]. In the present study a minimum of 0.50:1 was reached. Whether cubic Li_2TiO_3 can be completely de-lithiatiated with de-ionized water and whether the crystal structure can endure the full de-lithiation remains to be determined.

4.2. Crystal structure

The XRPD patterns of unwashed and of water-flushed cubic Li_2TiO_3 showed a unit cell parameter of between 4.150(1) Å and 4.141(1) Å which is in good accordance with reported lattice constants for cubic Li_2TiO_3 of 4.1405 Å [18] and 4.15 Å [19]. The low unit cell parameters of samples with high lithium loss (sample B6) can be ascribed to the intercalation of smaller hydrogen ions in the structure. The synchrotron measurement on a sample with ~40% lithium deficit shows a lower unit cell parameter than a sample with ~5% lithium deficit [7]. In Fig. 7 the changes of the unit cell parameter with temperature is shown. Upon cooling to a temperature of 100 K, the decrease of the unit cell is initially linear, but at lower temperatures the decline slows as expected due to decreasing inharmonic motion [33].

Heat-treated samples of the present study reacted to different products after annealing at 800 °C. Only samples showing Li/Ti ratios close to 2:1 transformed to pure monoclinic β-Li_2TiO_3 (Fig. 5b). Samples with lithium loss resulted in the intermediate compound $Li_4Ti_5O_{12}$, either mixed with β-Li_2TiO_3 (sample F6, Fig. 5c), or with (TiO_2) rutile if the lithium content was low (sample B5, Fig. 5d). The intermediate spinel $Li_4Ti_5O_{12}$ contains 52% less lithium than Li_2TiO_3, which corresponds to the theoretical calculated formula of $(Li_{0.48}H_{0.52})_2TiO_3$ — this value is in between sample F6 and sample B5. Similarly Li_2TiO_3 and $Li_4Ti_5O_{12}$ compositions can be produced by annealing a mixture of 5–30 wt.% TiO_2 with monoclinic Li_2TiO_3 [34]. By heat treatment of an intermediate Li–Ti–O compound produced via hydrothermal synthesis, $Li_4Ti_5O_{12}$ was formed with minor impurities [20] and a lithium titanate of cubic spinel structure (Fd-3m) was determined after annealing a ternary Li–Ti–O compound which was prior produced by hydrothermal reaction as well [10,11]. These studies as well as the results of the present work show that $Li_4Ti_5O_{12}$ can be obtained after annealing ~50% de-lithiated Li_2TiO_3. α-Li_2TiO_3 without lithium loss cannot transform to $Li_4Ti_5O_{12}$ upon heating.

5. Conclusions

Cubic α-Li_2TiO_3 was synthesized via the hydrothermal reaction of titania powder in lithium hydroxide solution at 160 °C for 18 h. The resulting products were unstable under ambient conditions, and reacted with atmospheric H_2O and CO_2. Flushing and bathing experiments showed that lithium is easily washed out of the cubic Li_2TiO_3 structure when in contact with de-ionized water. The de-lithiation leads to compositions along the solid solution Li_2TiO_3–H_2TiO_3. Differences between various compounds of this solid solution are difficult to detect by XRPD, but the effect of the lithium loss clearly can be analyzed by XRPD after annealing samples at high temperatures (800 °C) due to transformations to different phases. Annealed samples with Li/Ti ratios close to 2 resulted in the monoclinic β-Li_2TiO_3. Annealed samples having lost less than 52% of lithium transformed to mixtures of β-Li_2TiO_3 and $Li_4Ti_5O_{12}$. Samples with a lithium loss greater than 52% resulted in (TiO_2) rutile and $Li_4Ti_5O_{12}$.

Acknowledgements

We want to thank Yan Lavallée, Jonathan Bruce Hanson, and Hans Boysen for the fruitful discussions. The funding for this project was provided by Süd-Chemie AG in Moosburg, Germany.

References

[1] M. Yoshimura, K. Byrappa, J. Mater. Sci. 43 (2008) 2085.
[2] H. Kleykamp, J. Nucl. Mater. 295 (2001) 244.
[3] H. Kleykamp, Fusion Eng. Des. 61–62 (2002) 361.
[4] J.C. Mikkelsen, J. Am. Ceram. Soc. 63 (1980) 331.
[5] T. Hoshino, M. Dokiya, T. Terai, Y. Takahashi, M. Yamawaki, Fusion Eng. Des. 61–62 (2002) 353.
[6] N. Roux, J. Avon, A. Floreancing, J. Mougin, B. Rasneur, S. Ravel, J. Nucl. Mater. 233–237 (1996) 1431.
[7] A. Laumann, K.T. Fehr, H. Boysen, M. Hölzel, M. Holzapfel, Z. Kristallogr. (in press).
[8] C. Gicquel, M.M. Michel Mayer, R. Bouaziz, C.R. Acad. Sci. Paris C 275 (1972) 1427.
[9] K. Kataoka, Y. Takahashi, N. Kijima, H. Nagai, J. Akimoto, Y. Idemoto, K. Ohshima, Mater. Res. Bull. 44 (2009) 168.
[10] D. Fattakhova, P. Krtil, Mater. Res. Soc. Symp. Proc. 703 (2002) 165.
[11] D. Fattakhova, P. Krtil, J. Electrochem. Soc. 149 (2002) A1224.
[12] D. Fattakhova, V. Petrykin, J. Brus, T. Kostlánová, J. Dědeček, P. Krtil, Solid State Ionics 176 (2005) 1877.
[13] X.R. Pei, S.L. Zhang, J.W. Zhang, J.J. Yang, Z.S. Jin, Chin. J. Inorg. Chem. 22 (2007) 84.
[14] D.R. Zhang, H.L. Liu, R.H. Jiun, N.Z. Zhang, Y.X. Liu, Y.S. Kang, J. Ind. Eng. Chem. 13 (2007) 92.
[15] L.M. Sikhwivhilu, S.R. Suprakas, N.J. Coville, Appl. Phys. A 94 (2009) 963.
[16] H. Song, H. Jiang, T. Liu, X. Liu, G. Meng, Mater. Res. Bull. 42 (2007) 334.
[17] M. Tomiha, N. Masaki, S. Uchida, T. Sato, J. Mater. Sci. 37 (2002) 2341.
[18] M. Tabuchi, A. Nakashima, H. Shigemura, K. Ado, H. Kobayashi, H. Sakaebe, K. Tasumi, J. Mater. Chem. 13 (2003) 1747.
[19] J. Morales, J. Santos-Peña, R. Trócoli, S. Franger, J. Nanopart. Res. 10 (2008) 217.
[20] C. Jiang, E. Hosono, M. Ichihara, I. Honma, H. Zhou, J. Electrochem. Soc. 155 (2008) A553.
[21] E. Kordes, Fortschr. Miner. Krist. 17–18 (1933) 27.
[22] E. Kordes, Z. Kristallogr. 92 (1935) 139.
[23] J. Rodriguez-Carvajal, Abstract of the Satellite Meeting on Powder Diffraction of the Congress of the International Union of Crystallography, Toulouse, France, 1990, p. 127.
[24] P. Thompson, D.E. Cox, J.B. Hastings, J. Appl. Crystallogr. 2 (1987) 79.
[25] M.Q. Snyder, W.J. DeSisto, C.P. Tripp, Appl. Surf. Sci. 253 (2007) 9336.
[26] M.R. Mohammadi, D.J. Fray, J. Sol–Gel Sci. Technol. Published online (10. April 2010) http://www.springerlink.com/content/J0NNG86422538V25.
[27] R. Wang, K. Hashimoto, A. Fujishima, M. Chikuni, E. Kojima, A. Kitamura, M. Shimohigoshi, T. Watanabe, Adv. Mater. 10 (1998) 135.
[28] P. Jones, J.A. Hockey, Trans. Faraday Soc. 67 (1971) 2669.
[29] G. Amthauer, G.R. Rossman, Am. Mineral. 83 (1998) 835.
[30] P. Černý, D. London, Tschermaks Min. Petr. Mitt. 31 (1983) 81.
[31] A. Laumann, K.M. Ørnsbjerg Jensen, C. Tyrsted, M. Bremholm, K.T. Fehr, M. Holzapfel, B.B. Iversen, Phys. Chem. Chem. Phys. (submitted for publication).
[32] V.M. Zainullina, V.P. Zhukov, T.A. Denisova, L.G. Maksimova, J. Struct. Chem. 44 (2003) 180.
[33] N.W. Ashcroft, N.D. Mermin, Solid State Physic, Holt, Rinehart, and Winston, New York, 1976.
[34] K. Tsuchiya, C. Alvani, H. Kawamura, H. Yamada, S. Casadio, V. Contini, Fusion Eng. Des. 69 (2003) 443.

Appendix B

Second publication

Temperature-dependent structural transformations of hydrothermally synthesized cubic Li_2TiO_3 studied by in-situ neutron diffraction

Zeitschrift für Kristallographie **226** 53–61 (2011)

Andreas Laumann,[a] **Karl Thomas Fehr,**[a] **Hans Boysen,**[b] **Markus Hoelzel,**[c,d] **Michael Holzapfel**[e]

[a] Ludwig-Maximilians-Universität München, Department of Earth and Environmental Sciences, Section for Mineralogy, Petrology and Geochemistry, Munich, Germany
[b] LMU München, Department für Geo- und Umweltwissenschaften, Sektion Mineralogie
[c] Fachbereich Material- und Geowissenschaften, Fachgebiet Strukturforschung, Technische Universität Darmstadt, 63762 Darmstadt, Germany
[d] Forschungsneutronenquelle FRM II, 85747 Garching, Germany
[e] Süd-Chemie AG, Battery Materials, Moosburg, Germany

Z. Kristallogr. **226** (2011) 53–61 / **DOI** 10.1524/zkri.2011.1286

Temperature-dependent structural transformations of hydrothermally synthesized cubic Li_2TiO_3 studied by *in-situ* neutron diffraction

Andreas Laumann*, [I], Karl Thomas Fehr[I], Hans Boysen[II], Markus Hoelzel[III, 1] and Michael Holzapfel[IV]

[I] Department für Geo- und Umweltwissenschaften, Sektion für Mineralogie, Petrologie und Geochemie, Theresienstr. 41, 80333 München, Germany
[II] Department für Geo- und Umweltwissenschaften, Sektion Kristallographie, LMU München, Am Coulombwall 1, 85748 Garching, Germany
[III] Fachbereich Material- und Geowissenschaften, Fachgebiet Strukturforschung, Technische Universität Darmstadt, 63762 Darmstadt, Germany
[IV] Battery Materials, Süd-Chemie AG, Ostenriederstr. 15, 85368 Moosburg, Germany

Received May 26, 2010; accepted September 16, 2010

Hydrothermal synthesis / Neutron diffraction / Phase transformations

Abstract. The structural changes of hydrothermally synthesized cubic Li_2TiO_3 were studied *in-situ* during heating and cooling at the neutron powder diffractometer SPODI at FRM II, Garching. The initially cubic ($Fm\bar{3}m$) phase shows a slight Li deficit, but becomes stoichiometric with increasing temperature. It transforms to a monoclinic ($C2/c$) structure above 300 °C and back to the same cubic ($Fm\bar{3}m$) structure at 1155 °C. A two-phase region is observed between 300 and 500 °C, indicating a first order character of the transformation. Below 1000 °C, during the first heating, the monoclinic Li_2TiO_3 phase is disordered due to stacking faults. Between 1160 and 1140 °C, the cubic phase becomes monoclinic again upon cooling and stays well ordered down to room temperature. Anomalies in the thermal expansion of the monoclinic modification occur at around 600 °C for both, heating and cooling. These are assigned to strains building up during the first phase transformation upon heating and the confinement in the compacted ceramic sample during cooling, respectively.

Introduction

In the last decades, lithium titanium compounds have gained high attention, especially due to their usage in lithium ion batteries [1–4]. For instance, $Li_2Ti_3O_7$ is a good candidate as electrode material in rechargeable lithium-ion batteries [1] and $Li_4Ti_5O_{12}$ is an anode material currently commercially produced as it shows long-term stability at high capacity [1–3]. Li_2TiO_3 is another intermediate compound of the system Li−Ti−O. It has been described in three structural modifications, α, β and γ [4, 5]. The cubic α-Li_2TiO_3 is synthesized hydrothermally at low temperature [4, 5]. Above 300 °C it transforms irreversibly to a monoclinic structure, known as β-Li_2TiO_3. Lithium diffusion [6] in this compound and its cyclability [1] are weak, but β-Li_2TiO_3 is discussed as solid tritium breeder material for fusion reactors [7, 8]. The β-phase remains stable up to 1155 °C [4], at which temperature it transforms to the cubic γ-Li_2TiO_3.

The β-structure is the most studied Li_2TiO_3 modification. It is a derivate of sodium chloride type structure and isostructural with the high temperature modification of Li_2SnO_3 [9]. In comparison, Li_2SnO_3 exists in two different monoclinic modifications, a low temperature α-type modification below 800 °C and the high temperature β-form, which is stable above 1000 °C [10, 11]. The low-temperature modification is often less ordered due to stacking faults [12] which either causes a peak broadening of certain reflections, or their absence [9]. A β-Li_2TiO_3 modification which is isostructural with α-Li_2SnO_3 has been assumed in [10]. Due to the observation of anomalies between 400 and 600 °C, a possible second monoclinic Li_2TiO_3 modification was inferred in studies of impedance spectroscopy [13, 14] and high temperature X-ray diffraction studies [15, 16]. There are striking inconsistencies of the published values of the β angle of monoclinic Li_2TiO_3. In a single crystal study [17] it was given as 100.21(1)°, and a similar value was already presented before [18]. Other authors reported smaller angles; 100° [9], 100.08(5)° [14], 100.01° [19], 99.9° [20], 100.07° [15], and ∼99.5° [21].

Diverse results were published on the cubic γ-Li_2TiO_3. It was asserted that it can be quenched to room temperature without transformation to the monoclinic structure [22, 23], the stable modification at low temperatures. Others negated the possibility of quenching of γ-Li_2TiO_3 [18, 24], but showed that solid solutions of cubic Li_2TiO_3−MgO [18] or Li_2TiO_3−Li_3NbO_4 [24] keep their cubic structure when quenched to room temperature. Annealing of these cubic solid solutions leads to a slow phase transition between 550 and 750 °C to an ordered monoclinic solid solution which is isostructural with β-Li_2TiO_3 [24].

* Correspondence author (e-mail: laumann@min.uni-muenchen.de)
[1] Further address: Forschungsneutronenquelle FRM II, Lichtenbergstraße 1, 85747 Garching, Germany

Cubic α-Li_2TiO_3 has been introduced as the low-temperature modification of Li_2TiO_3, which can only be produced via hydrothermal reaction [5] and syntheses for cubic Li_2TiO_3 compounds via hydrothermal reactions were reported [25–28]. Due to their similar X-ray powder diffraction (XRPD) patterns hydrothermally synthesized cubic Li_2TiO_3 has been compared to or confused with the compound $LiTiO_2$ [29–32].

Recently, the stability of hydrothermally produced cubic Li_2TiO_3 when exposed to water was tested [33]. Lithium is bound weakly in the structure and can easily be leached from the structure with de-ionized water, and the de-lithiation was attributed to a stoichiometric exchange of lithium for protons. On non-treated cubic Li_2TiO_3 a weight loss of up to 7% upon heating to 700 °C was determined by TG-measurements and the weight loss was ascribed to the vaporization of water and CO_2 [33].

In the present study, the structural changes of hydrothermally produced cubic Li_2TiO_3 were studied *in-situ*, initially upon heating up to 1200 °C, and then upon cooling down to room temperature again. The structures of the two cubic modifications could be refined in space group $Fm\bar{3}m$. The monoclinic phase in space group $C2/c$ showed stacking disorder upon the first heating below 1000 °C. In this paper the general phase transformation behaviour is discussed with emphasis on lattice constants and occupancies. Full structural details of the monoclinic Li_2TiO_3 are presented only for well ordered phases at selected temperatures, while those influenced by stacking fault disorder require a more careful analysis to be presented in a forthcoming paper.

Experimental

Preparation of metastable cubic Li_2TiO_3

The synthesis of metastable cubic Li_2TiO_3 is described in [25–28, 33]. In the present study, first 2.04 g of $LiOH \cdot H_2O$ (SQM, Chile) was dissolved in de-ionized water. Then, 2g of TiO_2 powder (Evonik, formerly Degussa, AEROXIDE TiO_2 P 25) was stirred in the lithium hydroxide solution to obtain a Li/Ti molar ratio of 2. The suspension was hydrothermal treated for 16 h at 180 °C in a polytetraflourethylene (PTFE) container. The obtained product was vacuum-filtered, and remained un-washed. It was dried at 60 °C and de-agglomerated in an agate mortar and kept in argon atmosphere to avoid reaction with atmosphere.

Neutron diffraction experiments

Neutron powder diffraction measurements were carried out on the instrument SPODI [34] at FRM II (Garching, Germany). 2 g of the hydrothermally synthesized Li_2TiO_3 powder was filled in a niobium container and placed in a high vacuum furnace. The reflections of niobium were included in all refinements as a second phase. The sample was heated at 5 °C/min in a stepwise manner from room temperature to a maximum temperature of 1200 °C and then cooled similarly to room temperature (see Table 2). Before the measurements (4 h), a holding time of 15 min was given for temperature equilibration. After the experiment the sample was found to be compacted, *i.e.* converted from a loose powder into a sintered ceramic at an unspecified temperature. This means that the overall density was considerably increased.

The neutron patterns were recorded from 0° to 160° 2θ with step width 0.05°. The wavelength was determined from a previous measurement of silicon standard SRM 640c to be 1.5483 Å. Rietveld refinement was performed by using the program FullProf [35]. To model the considerable line broadening, the pseudo Voigt function in the formulation of Thompson-Cox-Hastings [36] was used, restricting it to the refinement of Gaussian strain and Lorentzian size parameters. The full width at half maximum is calculated from

$$fwhm_G^2 = (U + e^2)\tan^2\Theta + V\tan\Theta + W\,, \quad (1)$$

$$fwhm_L = (Y + \lambda/L)/\cos\Theta\,, \quad (2)$$

where U, V, W and Y are the instrumental resolution parameters (obtained from a standard Y_2O_3 sample), λ is the wavelength and $e = \Delta d/d$ and L are the "apparent" strain and size parameters, respectively. This formulation assumes isotropic size and strain which is certainly not appropriate in view of the expected stacking disorder and is only used here to derive some approximate general trends. The background was linearly interpolated between a set background points with refinable heights.

Additional XRPD measurements at room temperature were accomplished in transmission geometry on a Stoe Kristalloflex STOE STADI P diffractometer ($CuK_{\alpha 1}$-radiation $\lambda = 1.544056$ Å, curved Ge(111) monochromator).

Results

Phase transformations upon heating

At room temperature, the metastable Li_2TiO_3 could clearly be refined in the cubic space group $Fm\bar{3}m$. Minor impurities of Li_2CO_3 (2.2(2) wt%, without regarding niobium) were indicated by small extra reflections (Fig. 1a). Traces of LiOH may be expected from the synthesis procedure, but could not be discerned in the patterns. The reflections of Li_2CO_3 decreased between 300 and 400 °C and vanished at 500 °C. Especially the room temperature pattern shows an elevated incoherent background caused by hydrogen (Fig. 2). Upon heating, it decreases reaching a constant value at about 500 °C, probably due to the evaporation of water [33].

No structural changes were observed up to 250 °C. At 300 °C small broad reflections of monoclinic Li_2TiO_3 started to appear (Fig. 2), but they were too broad to be included in the refinement. Upon further heating, the ratio of cubic to monoclinic Li_2TiO_3 decreases and the reflections of the monoclinic phase sharpen. Between 600 and 1000 °C only the monoclinic phase could be refined. At 1100 °C the cubic modification with space group $Fm\bar{3}m$ appeared again and at the final temperature of 1200 °C solely cubic (γ)-Li_2TiO_3 was present (Figs. 1, 2, Tables 1 and 2).

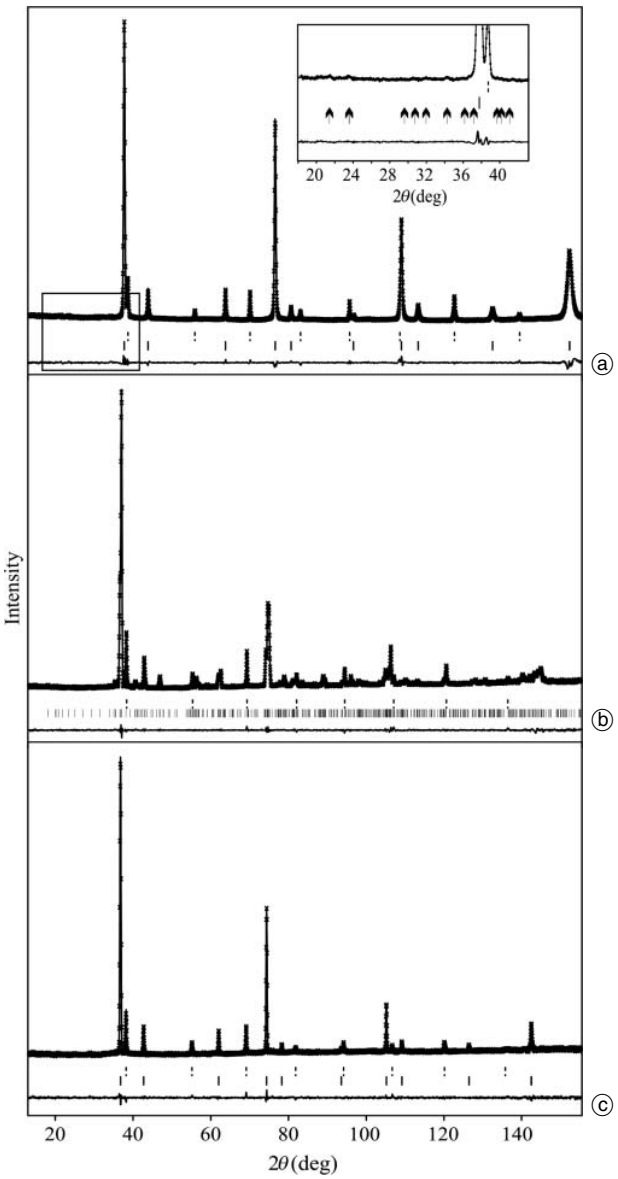

Fig. 1. Rietveld fits (**a**) at room temperature, (**b**) at 1000 °C, and (**c**) at 1200 °C. At room temperature and at 1200 °C, the structure of Li_2TiO_3 was refined in the cubic space group $Fm\bar{3}m$, and at 1000 °C it was refined in the monoclinic space group $C2/c$. Observed (stars) and calculated pattern (solid line), Bragg reflections of niobium (dashed), Li_2TiO_3 (solid) and the difference curve (below) are shown, as well as the traces of Li_2CO_3 (arrows) at room temperature in the insert of Fig. 1a.

Phase transformation upon cooling

Upon cooling, the monoclinic Li_2TiO_3 started to form below 1160 °C, which is in good agreement with the proposed transformation temperature of 1155 °C [8]. At 1100 °C, 12.2(5)% of the cubic phase was left, comparable to the amount of the cubic structure at the same temperature upon heating. Below 1100 °C, only the monoclinic Li_2TiO_3 modification was found (Table 2). The temperature-dependent transformation upon heating and cooling between 85 and 125° 2Θ are shown in Fig. 2 and structural parameters of selected temperature steps are listed in Table 1.

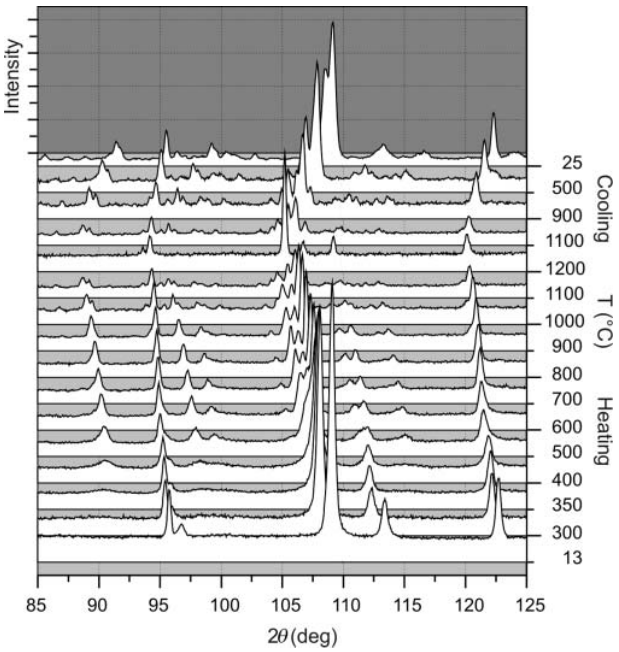

Fig. 2. Temperature-dependent transformations of Li_2TiO_3 upon heating to 1200 °C and the subsequent cooling to room temperature.

Cubic structure

The atomic array of the cubic phase is of the NaCl structure type, with a statistical distribution of lithium and titanium on one site and oxygen on the other site. Taking into account the strong bonding within the TiO_6 octahedra, the occupancies of titanium and oxygen were fixed to 0.3333 and 1, respectively, and the occupancy of lithium was refined. At room temperature, a clear Li-deficit of 7.5% ± 1% was observed, corresponding to $Li_{1.85(2)}TiO_3$. The atomic absorption spectroscopy (AAS) analysis [33], which was performed prior to the neutron-experiment, indicated a lithium content close to the calculated theoretical value of 12.65 wt%. The lithium occupancy could be refined only at temperatures showing a high fraction of the cubic Li_2TiO_3 (Table 2). It increased with temperature, and at 350 °C a deficit of 2.5% ± 1% was determined. At 1200 °C, the Li/Ti ratio was close to 2 within the higher error margin, ∼2.5% ± 2% ($Li_{1.95(4)}TiO_3$), and this value was maintained upon cooling.

At room temperature, the unit cell parameter of cubic Li_2TiO_3 is 4.14276(1) Å, at 1200 °C it is 4.24811(4) Å (Table 2). Especially between 400 and 500 °C, the refinement of the cubic structure was found to be difficult due to the superposition of the cubic and monoclinic reflections. The refined unit cell parameters of the cubic phase at 400 and 500 °C deviate from the observed linear trend (Fig. 3). A possible explanation will be given below. The good linear connectivity between the high and low temperature data clearly shows that α- and γ-Li_2TiO_3 belong to the same phase. The slightly lower value at room temperature in Fig. 3 may be due to the non-stoichiometry of the sample at low temperatures (see above).

Table 1. Atomic coordinates, temperature factors, and the reliability factors of Li_2TiO_3 at 13 and 1000 °C upon heating, at 1200 °C, and at 900 and 25 °C upon cooling.

13 °C before heating, cubic Li_2TiO_3

Atom	Site	x	y	z	B (Å)
Li	4*a*	0	0	0	1.09(3)
Ti	4*a*	0	0	0	1.09(3)
O	4*b*	0.5	0.5	0.5	1.19(1)
R_p, R_{wp}, R_{exp}, χ^2		2.87	3.44	2.14	2.58

1000 C upon heating, monoclinic Li_2TiO_3

Atom	Site	x	y	z	B (Å)
Li1	8*f*	0.233(3)	0.083(2)	−0.003(1)	3.7(2)
Li2	4*d*	0.25	0.25	0.5	6.6(7)
Li3	4*e*	0	0.082(3)	0.25	3.8(4)
Ti1	4*e*	0	0.419(1)	0.25	2.2(1)
Ti2	4*e*	0	0.751(1)	0.25	2.6(2)
O1	8*f*	0.1419(7)	0.2652(4)	0.1414(5)	2.06(7)
O2	8*f*	0.1008(5)	0.5863(5)	0.1388(3)	2.25(6)
O3	8*f*	0.1395(6)	0.9076(5)	0.1352(4)	2.17(5)
R_p, R_{wp}, R_{exp}, χ^2		3.03	3.78	2.84	1.76

1200 °C, cubic Li_2TiO_3

Atom	Site	x	y	z	B (Å)
Li	4*a*	0	0	0	4.04(8)
Ti	4*a*	0	0	0	4.04(8)
O	4*b*	0.5	0.5	0.5	3.75(3)
R_p, R_{wp}, R_{exp}, χ^2		5.17	6.46	5.66	1.31

900 °C upon cooling, monoclinic Li_2TiO_3

Atom	Site	x	y	z	B (Å)
Li1	8*f*	0.239(3)	0.083(2)	−0.004(1)	2.6(2)
Li2	4*d*	0.25	0.25	0.5	6.4(8)
Li3	4*e*	0	0.083(5)	0.25	5.2(6)
Ti1	4*e*	0	0.421(2)	0.25	1.3(2)
Ti2	4*e*	0	0.754(1)	0.25	1.4(2)
O1	8*f*	0.1411(8)	0.2655(5)	0.1406(5)	1.38(8)
O2	8*f*	0.1001(6)	0.5854(6)	0.1393(3)	1.38(6)
O3	8*f*	0.1431(7)	0.9066(6)	0.1347(4)	1.63(6)
R_p, R_{wp}, R_{exp}, χ^2		4.05	5.20	4.04	1.66

25 °C after cooling, monoclinic Li_2TiO_3

Atom	Site	x	y	z	B (Å)
Li1	8*f*	0.246(3)	0.098(2)	−0.001(2)	1.8(2)
Li2	4*d*	0.25	0.25	0.5	0.7(4)
Li3	4*e*	0	0.087(3)	0.25	0.7(3)
Ti1	4*e*	0	0.425(1)	0.25	0.1(1)
Ti2	4*e*	0	0.756(1)	0.25	0.1(1)
O1	8*f*	0.1383(9)	0.2649(5)	0.1361(6)	0.59(8)
O2	8*f*	0.1048(7)	0.5839(6)	0.1381(3)	0.66(6)
O3	8*f*	0.1402(7)	0.9064(6)	0.1337(4)	0.12(5)
R_p, R_{wp}, R_{exp}, χ^2		6.25	8.14	5.70	2.04

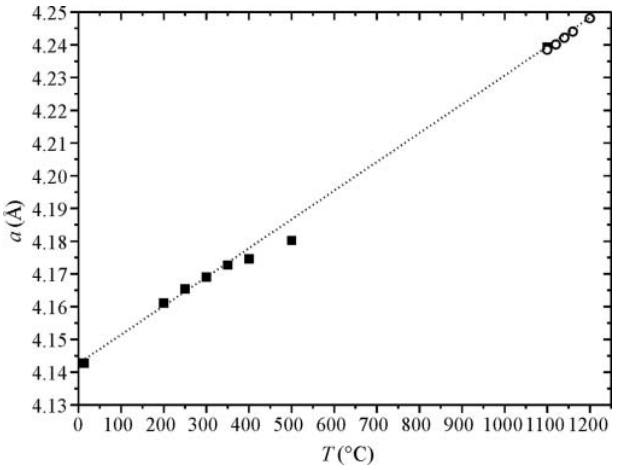

Fig. 3. Lattice constants of cubic Li_2TiO_3. The dashed line illustrates the connectivity between the low and high temperature values upon heating (squares) and cooling (circles).

Monoclinic Li_2TiO_3

The monoclinic structure in space group *C*2/*c* can be derived from the parent cubic NaCl structure by the transformation

$$\begin{pmatrix} 1/2 & 1 & 1/2 \\ 3/2 & 0 & -3/2 \\ -3/2 & 1 & -3/2 \end{pmatrix}$$

from which ideal monoclinic lattice constants $a_m = \sqrt{3/2}a_c$, $b_m = \sqrt{9/2}a_c$, $c_m = \sqrt{11/2}a_c$, and $\cos\beta_m = -1/\sqrt{33} \rightarrow \beta_m = 100.025°$ can be calculated. The cationic ordering leads to a layered structure, comprising three layers. The first layer consists of lithium ions in Li1 and Li2 positions only, while the second layer is occupied by oxygen and the third layer is an alternation of titanium and lithium on Ti1, Ti2 and Li3 positions. While the stacking of the O- and Li-layers is imposed by the rigidity of the oxygen framework, the Ti−Li-layers, which are separated by two O- and one Li-layer, may exhibit different stacking due to weaker interaction forces between them. This might lead to an alternative stacking order with trigonal $R\bar{3}m$ symmetry and disorder (stacking faults) [11].

Fits of the patterns collected during heating from 300 °C up to 900 °C were not perfect using *C*2/*c* only. Test refinements with $R\bar{3}m$, or other ordering schemes as realized in Li_2ZrO_3 (*C*2/*c* with half the *c* constant) [37] and Li_2MnO_3 (*C*2/*m*) [38] were unsuccessful. Therefore, *C*2/*c* is the dominant ordering, although very small contributions from the others cannot be completely ruled out. Especially at low temperatures (300–400 °C), the peak broadening of the reflections is not isotropic and is typical for stacking disorder. Unfortunately, for neutrons, the low-order reflections are of very low intensity (see Fig. 1b) making it more difficult to include this stacking disorder in the fits. Therefore, additional X-ray measurements were carried out on samples hydrothermally synthesized the same way as the one used for the neutron experiments. Two samples were annealed at 700 and 1000 °C, respectively. As clearly seen in Fig. 4, the former sample exhibits typical asymmetric line shapes characteristic of stacking faults, while the latter sample shows sharp reflections of the well ordered *C*2/*c* structure only.

Table 2. Unit cell parameters of cubic and monoclinic (mon.) Li_2TiO_3, lithium occupancies in cubic Li_2TiO_3, volume (V) of the monoclinic unit cell, and weight fraction of cubic to monoclinic Li_2TiO_3 in the order of data collection. Two lines per temperature (T) are given for both choices of β where ambiguous; (β1) refinement with starting parameters from low β angles; (β2) refinement with starting parameters from large β angles (see text).

T (°C)	a (Å) (cubic)	Lithium occupancy	a (Å) (mon.)	b (Å) (mon.)	c (Å) (mon.)	β (°)	V (Å) (mon.)	Cubic fraction (%)[a]
13	4.14276(1)	0.616(8)	–	–	–	–	–	100
200	4.16118(5)	0.618(12)	–	–	–	–	–	100
250	4.16547(6)	0.619(15)	–	–	–	–	–	100
300	4.16910(4)	0.637(9)	–	–	–	–	–	1[b]
350	4.17271(1)	0.643(7)	–	–	–	–	–	80.3(4)
400 (β1)	4.17455(4)	–	5.1068(4)	8.8574(12)	9.8228(10)	99.616(10)	438.07(9)	60(2)
400 (β2)	4.17455(4)	–	5.0873(5)	8.8954(12)	9.8414(10)	100.003(8)	438.59(9)	60(2)
500 (β2)	4.18022(14)	–	5.1157(2)	8.8524(3)	9.8570(3)	99.751(2)	439.93(2)	11.5(7)
500 (β2)	4.18022(14)	–	5.1117(2)	8.8609(4)	9.8673(2)	100.117(3)	439.98(3)	11.5(7)
600 (β1)	–	–	5.1234(1)	8.8657(2)	9.8852(2)	99.783(2)	442.49(2)	0
600 (β2)	–	–	5.1194(1)	8.8720(2)	9.8941(2)	100.086(2)	442.44(2)	0
700 (β1)	–	–	5.1312(2)	8.8830(2)	9.9104(2)	99.804(2)	445.13(2)	0
700 (β2)	–	–	5.1290(1)	8.8868(2)	9.9182(2)	100.054(2)	445.13(2)	0
800 (β1)	–	–	5.1422(1)	8.9051(2)	9.9385(2)	99.811(1)	448.45(2)	0
800 (β2)	–	–	5.1414(1)	8.9068(2)	9.9461(2)	100.046(1)	448.49(2)	0
900 (β1)	–	–	5.1537(1)	8.9226(2)	9.9655(2)	99.791(1)	451.58(2)	0
900 (β2)	–	–	5.15161(9)	8.9275(1)	9.9755(1)	100.0823(9)	451.70(1)	0
1000	–	–	5.15905(7)	8.9520(1)	10.0101(1)	100.2187(7)	454.97(1)	0
1100	4.23929(10)	–	5.16690(5)	8.9704(1)	10.0399(1)	100.2402(8)	457.93(1)	7.6(5)
1200	4.24811(4)	0.644(14)	–	–	–	–	–	100
1160	4.24404(9)	0.630(28)	–	–	–	–	–	100
1140	4.24214(5)	0.655(22)	5.1690(2)	8.9753(5)	10.0491(4)	100.246(4)	458.77(3)	54.8(8)
1120	4.24012(4)	0.632(34)	5.1661(1)	8.9721(2)	10.0444(2)	100.247(2)	458.22(2)	31.2(7)
1100	4.23851(6)	–	5.16579(6)	8.9687(1)	10.0379(1)	100.2446(9)	457.64(1)	12.2(5)
900	–	–	5.14644(7)	8.9343(1)	9.9808(1)	100.2474(7)	451.60(1)	0
500	–	–	5.10646(8)	8.8644(1)	9.8787(2)	100.239(1)	440.05(1)	0
25	–	–	5.06473(8)	8.7907(1)	9.7669(2)	100.2218(1)	427.95(1)	0

a: Depicted values are fractions of the cubic vs. the monoclinic Li_2TiO_3. Li_2CO_3 at low temperatures and niobium are not considered.
b: At 300 °C, the monoclinic Li_2TiO_3 could not be refined without fixing all structural parameter (see text).

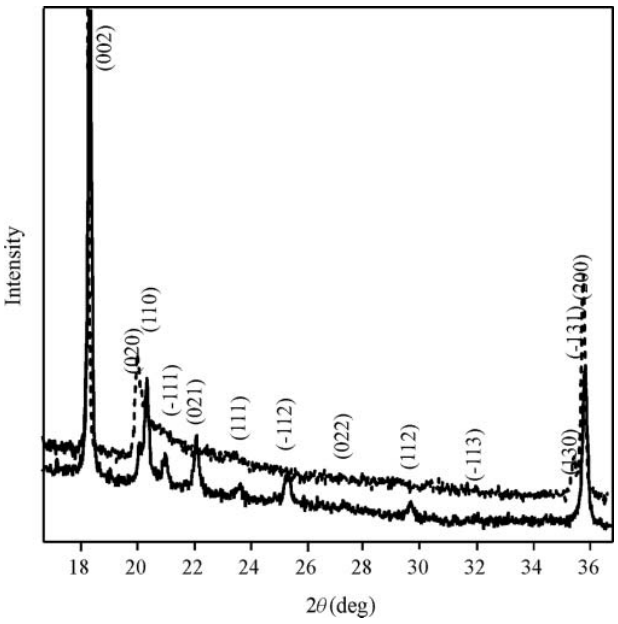

Fig. 4. X-ray powder patterns of cubic hydrothermally produced samples heated to 700 (dotted line) and 1000 °C (solid line), respectively.

In spite of rather good fits (χ^2 values below 2), full structural results (atom positions and displacement parameters) have to be regarded with care as long as this stacking disorder is not properly taken into account. Therefore, only selected temperature steps are shown in Table 1, but the lattice constants of all temperatures are included in Table 2.

Test refinements of possible incomplete ordering by placing Ti on Li-sites and vice versa did not lead to improved fits. Moreover, errors were rather large due to strong correlations with the displacement parameters. Therefore, complete order was assumed for all monoclinic structures.

As already mentioned, different experimental values of the monoclinic angle β can be found in the literature as either around 100° or above 100.2°; the ideal value is 100.025° (see above). For $\geq T = 1000$ °C, the β angle was unambiguously above 100.2° and remained so upon cooling, diminishing only slightly at low temperatures (Fig. 5). However, during heating from 300 to 900 °C, no clear answer could be given, since refinements starting with β angles of 100.2° or 99.8° gave almost equally good fits resulting in two different angles: β1 between 99.62 and 99.82°, and β2 between 100 and 100.12° (Table 2 and

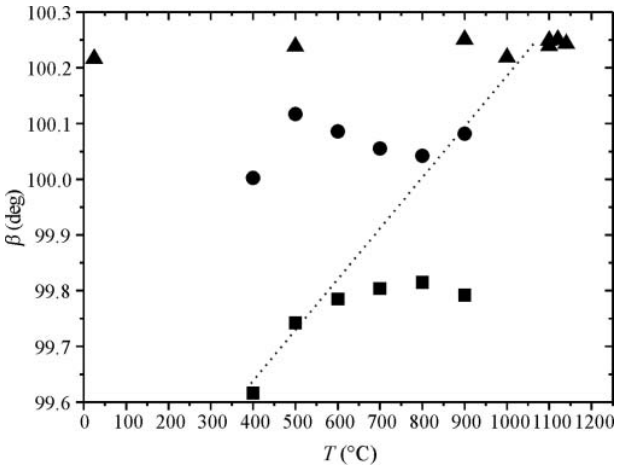

Fig. 5. Monoclinic angles β of Li_2TiO_3 upon heating for $\beta 1$ (squares) and $\beta 2$ (circles), and cooling (triangles).

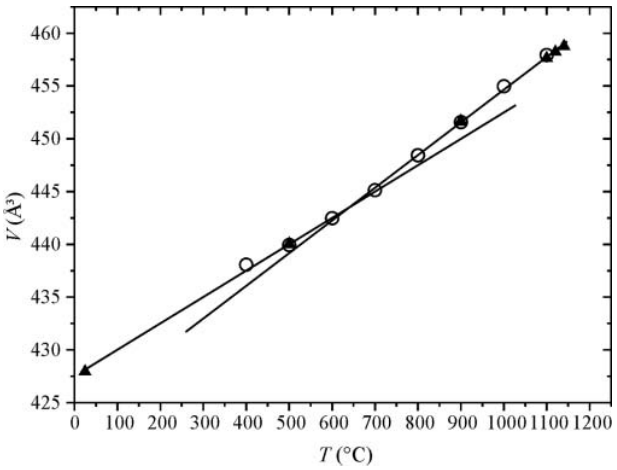

Fig. 7. Volume of the monoclinic unit cell upon heating (circles) and cooling (triangles).

Fig. 5). Closer inspection of individual peaks and comparing the (only slightly differing) *R*-factors indicate that $\beta 2$, the larger angle, is realised at 900 °C (although the angle is clearly lower than 100.2°), while $\beta 1$ seems to be realized at lower temperatures. This changeover (tentatively suggested by the dotted line in Fig. 5) should be regarded with some care in view of the problems mentioned above. It might be connected with the changeover from the disordered to the ordered structure. We emphasize this problem as it might explain the different values reported in the literature, which may thus be due to either different states of order in the samples or to ambiguities during the determination.

To illustrate the distortion of the monoclinic structure from the cubic one, pseudo cubic lattice constants are displayed in Fig. 6. These are obtained from the monoclinic ones by inversion of the relations given above leading to the following equations

$$a_c^2 = c_c^2 = \tfrac{1}{16} a_m^2 + \tfrac{1}{9} b_m^2 + \tfrac{1}{16} c_m^2 - \tfrac{1}{8} a_m c_m \cos\beta_m , \qquad (3)$$

$$b_c^2 = \tfrac{9}{16}\, a_m^2 + \tfrac{1}{16}\, c_m^2 + \tfrac{3}{8}\, a_m c_m \cos\beta_m . \qquad (4)$$

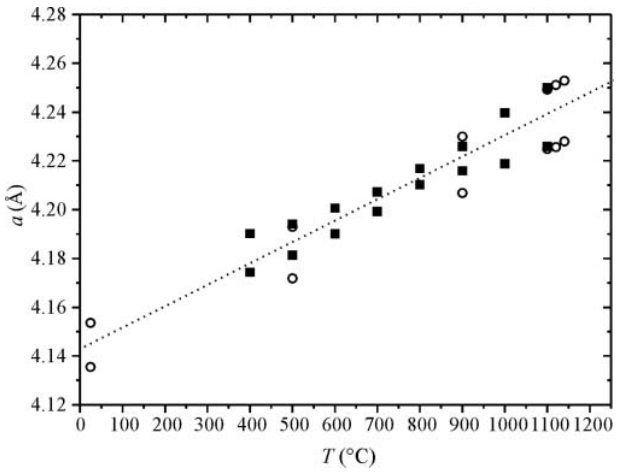

Fig. 6. Pseudo cubic lattice constants of monoclinic Li_2TiO_3 upon heating (squares) and cooling (circles). The dashed line indicates the variation in the cubic phase (cf. Fig. 3).

The resulting two different values a_c ($= c_c$) and b_c lie slightly above and below the line representing the variation of the lattice constant of the cubic phase (Fig. 6). In the initial disordered state the difference between a_c ($= c_c$) and b_c diminishes with temperature, becoming almost zero around 800 °C, and increases again with further heating. Moreover, at about 800 °C the pseudo cubic lattice constants almost coincide with that of the (extrapolated) cubic phase. This behaviour is opposite to what could have been expected, namely an approach close to the phase transition, and demonstrates a strongly first order character. On the other hand, in the ordered state during cooling the difference stays almost constant independent of temperature. It is notable that the volume per formula unit of the cubic and the monoclinic phases are nearly identical at all temperatures, *i.e.* there is no volume anomaly involved in the phase transformation.

Although the β angle and the other unit cell parameters differ appreciably at the same temperatures during heating and cooling, the unit cell volumes are nearly equal (Fig. 7). Due to limited beam time and the slow cooling of the furnace at low temperatures, the last data point was recorded at about 25 °C, slightly above the first data point before heating (13 °C). As seen in Fig. 7, the thermal expansion is not linear. Around 600 °C a kink, emphasised by two lines with different slopes in Fig. 7, suggests a slightly higher thermal expansion at higher temperatures.

Size and strain

In most patterns both size and strain broadening was observed. At room temperature the particle size was about 68 nm, and did not change remarkably up to 300 °C. In the range from 300 to 500 °C the refinement was not possible without restrictions as all the reflections of the cubic phase are overlapped by the reflections of the monoclinic superstructure, thus the parameters of the atomic positions had to be fixed. In particular, below 400 °C the reflections of the ordered monoclinic structure are very broad and the refined particle size of only ~5 nm at 350 °C should be taken as a rough estimate only. At 400 °C, reflections of the monoclinic phase are still broad, but the particle or

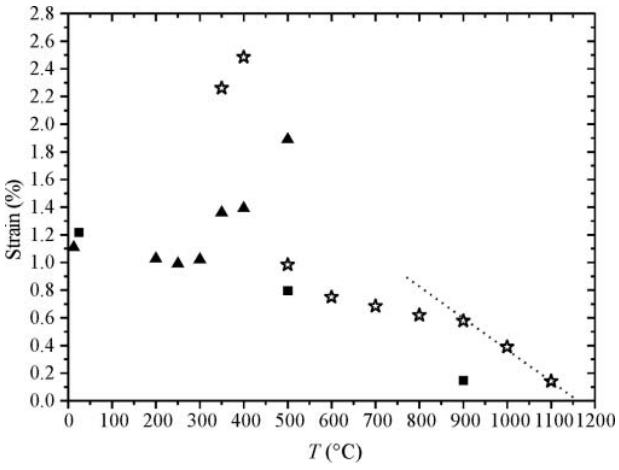

Fig. 8. Strain values of the cubic Li_2TiO_3 (triangles), the monoclinic Li_2TiO_3 (stars), and upon cooling (squares).

domain size increased to 43 nm. For this temperature range, the refined values represent the size of monoclinic domains within the cubic structure which slowly grow with increasing temperature. A similar observation was made upon heating of cubic solid-solution of Li_2TiO_3–Li_3NbO_4 [24]. Here as well, over a temperature range of about 200 °C, small monoclinic domains start to grow in the cubic structure until the transformation is completed. At 500 °C, when only ~12% of the cubic phase was left, the particle size of the ordered structure increased to more than 61 nm and reached almost the value of the cubic particles determined at lower temperatures. Refinement of FWHM parameters of the cubic phase between 350 and 500 °C were not reliable. At 600 °C, the size of the monoclinic particles increased to over 86 nm, at 700 °C to 129 nm, and at 800 °C the refined particle size was higher than 400 nm, therewith reaching the limit of the instrumental resolution. Due to that, the "size" parameter was fixed to "zero" above 800 °C and also for all data obtained upon cooling.

A general decreasing trend of the strain with higher temperatures is observed (Fig. 8), both for increasing and decreasing temperatures. An exception is the temperature range of the cubic to monoclinic transformation during the first heating, where it is much larger in both phases. This may be related to the intimate intergrowth of both phases co-existing in this temperature range.

Discussion

Lithium deficit

The lithium deficit of ~7.5% at room temperature seems to be inconsistent with the AAS analysis which yielded a lithium content close to the calculated theoretical value of Li_2TiO_3. By AAS measurements, bulk compositions are recorded – here, a mixture of Li_2TiO_3 and impurities of non-reacted LiOH used for the hydrothermal reaction. Due to carbonisation, LiOH reacts to Li_2CO_3, found to be present in the neutron patterns. The lithium content increased with temperature. Lithium, originating from LiOH and Li_2CO_3, most likely intercalated into the Li_2TiO_3 structure, such that it became stoichiometric within error margins at 1200 °C.

To keep the stoichiometry, the lithium deficit at low temperatures is probably compensated by protons. It can be ruled out that these are located at the same octahedral sites as lithium ions, since H has a larger negative scattering length than Li and would therefore lead to an apparent over occupancy at this site. Due to the small amount and probable large disorder of H it was not possible to locate them within the structure. Additional Fourier transform infrared measurements at room temperature did not reveal distinct OH^- bonds [33]. Only a broad band around 3420 cm^{-1} was found, which has been attributed to stretching vibrations of hydroxyl bonds, caused by hydroxylation and hydration of the particle surfaces [39]. The loss of H (and concomitant increase of Li occupancy) with increasing temperature is confirmed by the decrease of the incoherent background mentioned above.

Cubic structure

The cubic structure obtained by hydrothermal reaction is isostructural with that at high temperatures. The interlinked data points of the cubic unit cell volume at low temperatures and above 1100 °C indicate a constant thermal expansion (Fig. 3). Accordingly, by hydrothermal reactions, disordered cubic Li_2TiO_3 can be produced at temperatures far below its stability field. In general, structures disorder with rising temperature, but in analogy to metastable cubic Li_2TiO_3, α-Li_2SnO_3 fully orders at $T >$ 1000 °C and below it shows disorder due to stacking faults. Two different explanations are conceivable for this behaviour. First, the low temperature cubic structure may be stabilized by protons or water entering the structure during the synthesis, in allusion to quenchable cubic Li_2TiO_3–MgO solid solutions [18], *i.e.* protons could stabilize the cubic structure in the hydrothermal process, like MgO enables quenching of cubic Li_2TiO_3. Second, the cubic structure may be the preferred modification for syntheses at low temperature, due difficulties to form the complex layered monoclinic structure. The monoclinic structure can be synthesized hydrothermally as well when heating to higher temperatures. In an *in-situ* synchrotron experiment under hydrothermal conditions, first cubic Li_2TiO_3 was formed at temperatures between 155 and 230 °C and then, after heating above 300 °C, the prior synthesized cubic phase started to transform to the monoclinic modification of Li_2TiO_3 [40].

The deviations from the linear trend at 400 and 500 °C (Fig. 3) may be explained by a preferred exsolution of the more mobile Li into the initial monoclinic phase. Test refinements at these temperatures revealed a higher (negative) scattering density at the Li/Ti site. This can only be explained by a higher Ti content, therewith supporting this assumption. Unfortunately, as mentioned, occupancies in the monoclinic phase could not be refined reliably to confirm this assumption unambiguously.

Monoclinic structure

Observations of the monoclinic Li_2TiO_3 are in a good agreement with observations that have been made on α- and β-Li_2SnO_3 [11]. Between 300 and 900 °C, not all reflections have the theoretical intensity expected for space group *C*2/*c*. Some reflections are missing, or are too broad, or too sharp, similar to the situation in α-Li_2SnO_3, when compared with β-Li_2SnO_3 [11].

Most authors report monoclinic $\sim\beta1$ or $\beta2$ [9, 14, 15, 19–21], but only three of those mentioned annealing temperatures: 800 °C [21], 860 °C [14] and 1000 °C [19]. Monoclinic single crystals with a β angle of 100.21(1)°, $a = 5.0623(5)$ Å, $b = 8.7876(9)$ Å, and $c = 9.7533(15)$ Å were synthesized at 1050 °C [17]. These parameters are in very good agreement with those of the last data point taken at 25 °C ($\beta = 100.2218(1)°$, $a = 5.06473(8)$ Å, $b = 8.7907(1)$ Å, and $c = 9.766(2)$ Å). The β angle reaches its final value above 1000 °C. Below, during the first heating, *i.e.* in the disordered state, it is considerably smaller in any case, irrespective of using $\beta1$ or $\beta2$ (Table 2, Fig. 5), and also after holding for 4 h at 1000 °C the ordering process was not completed. It was mentioned that the annealing of a Li_2TiO_3 sample for a longer time (12 h) at 1000 °C might result in the full transformation to the monoclinic Li_2TiO_3 structure [13]. Presumably, the annealing temperatures used in [9, 14, 15, 19–21] were too low or too short to result in the fully ordered monoclinic Li_2TiO_3. Detailed studies on the variation of the thermal expansion and the β angle were performed using high temperature X-ray diffraction [15, 16]. The samples were prepared by annealing of a pressed pellet comprising Li_2CO_3 and TiO_2 at 1000 °C for 8 h. The XRPD pattern presented in [15] is similar to our high-temperature sample shown in Fig. 4, *i.e.* it is a well ordered sample. However, upon heating from room temperature to 900 °C, the β angle decreased in both studies [15, 16], from 100.07 to around 99.6° [15] and less pronounced in the synchrotron radiation study [16]. In the present study the opposite trend was observed (Fig. 5). The results of [15, 16] suggest a kink of the monoclinic unit cell parameters at 450 °C, resulting in a faster increase of the monoclinic unit cell volume at higher temperatures. The slight change of the monoclinic unit cell volume (Fig. 7) displays a comparable kink, but at higher temperatures. By impedance spectroscopy, a change of the activation energy of monoclinic Li_2TiO_3 was detected between 500 and 700 °C [13, 14] and was ascribed to an order-disorder transformation [14]. In another study [41], the thermal expansion of monoclinic Li_2TiO_3 samples with different densities was investigated. These authors showed that a sample of higher density has a smaller thermal expansion than two samples of lower density, which was attributed to internal cracks and microstructural changes of the high density sample.

In conclusion, these data suggest that the annealing time and its temperature, as well as the reactants used and their particle size may be critical to obtain the desired solid tritium breeder material Li_2TiO_3 with an ordered *C*2/*c* structure. The strain analysis (Fig. 8) shows that the approach of the ordered monoclinic structure above 1000 °C is accompanied by a strong decrease in strain (illustrated by the dashed line in Fig. 8). The final monoclinic β angle (greater than 100.2°) was reached at 1100 °C and stayed so upon cooling. However, the strain, staying small at 900 °C, increased again upon cooling to and below 500 °C. This might be understood as being due to the intimate intergrowth of the monoclinic grains within the now dense ceramic-like sample, causing strains via anisotropic contraction. This means that structural and also microstructural effects are essential to understand the behaviour of sintered Li_2TiO_3. As no structural changes were observed upon cooling below 900 °C, it can be proposed that microstructural effects cause the change in the thermal expansion.

Conclusion

It has been shown for the first time, by *in-situ* neutron diffraction, that the α-phase of Li_2TiO_3, which has never been characterised structurally, is of the NaCl-type and identical with the γ-phase. Metastable cubic Li_2TiO_3, which is produced by hydrothermal syntheses, transforms between 300 and 600 °C to a disordered monoclinic form. Above 1160 °C, the cubic phase reappears again and upon cooling it turns into an ordered monoclinic phase. It was shown that the high-temperature stable phase of Li_2TiO_3 is isostructural with the metastable low temperature form. They have the same structure (space group $Fm\bar{3}m$) and their thermal expansion is linear from room temperature to 1200 °C. The metastable phase is probably stabilized by protons or water entering the structure during the hydrothermal syntheses.

Fully ordered monoclinic Li_2TiO_3 can be produced only by heating to high temperatures (>1000 °C). Even the ordered monoclinic structure, being strain-free at high temperatures, shows anomalies due to high strains building up within compacted samples upon cooling to low temperatures. Although the lattice constants differ appreciably below 1000 °C, the unit cell volume is nearly identical upon heating and cooling, and a change in the thermal expansion around 600 °C is notable for both.

Acknowledgments. We want to thank Yan Lavallée, María Eckholt and Jonathan Bruce Hanson for fruitful discussions. Funding for the project was provided by Süd-Chemie AG in Moosburg, Germany.

References

[1] Shu, J.: Li–Ti–O compounds and carbon-coated Li–Ti–O compounds as anode materials for lithium ion batteries. Electrochim. Acta **54** (2009) 2869–2876.
[2] Colbow, K.M.; Dahn, J.R.; Haering, R.R.: Structure and electrochemistry of the spinel oxides $LiTi_2O_4$ and $Li_{4/3}Ti_{5/3}O_4$. J. Power Sources **26** (1989) 397–402.
[3] Zaghib, K.; Simoneau, M.; Armand, M.; Gauthier, M.: Electrochemical study of $Li_4Ti_5O_{12}$ as negative electrode for Li-ion polymer rechargeable batteries. J. Power Sources **81–82** (1999) 300–305.
[4] Kleykamp, H.: Phase equilibria in the Li–Ti–O system and physical properties of Li_2TiO_3. Fusion Eng. Des. **61–62** (2002) 361–366.
[5] Gicquel, C.; Michel Mayer, M.M.; Bouaziz, R.C.: Sur quelques composés oxygénés du titane et des alcalins (Li, Na); étude des

binaries M_2O-TiO_2 dans les zones riches en oxide alcalin. R. Acad. Sc. Paris Série C **275** (1972) 1427–1430.

[6] Vijayakumar, M.; Kerisit, S.; Yang, Z.; Graff, G.L.; Liu, J.; Sears, J.A.; Burton, S.D.; Rosso, K.M.; Hu, J.: Combined ^{6,7}Li NMR and molecular dynamics study of Li diffusion in Li_2TiO_3. J. Phys. Chem. C **113** (2009) 20108–20116.

[7] Roux, N.; Avon, J.; Floreancig, A.; Mougin, J.; Rasneur, B.; Ravel, S.J.: Low-temperature tritium releasing ceramics as potential meterials for the ITER breeding blanket. J. Nucl. Mater. **233–237** (1996) 1431–1435.

[8] Kleykamp, H.: Enthalpy, heat capacity and enthalpy of transformation of Li_2TiO_3. J. Nucl. Mater. **295** (2001) 244–248.

[9] Lang, G.: Die Kristallstruktur einiger Vertreter der Verbindungsklasse $Me^I_2Me^{IV}O_3$ als Beitrag zur Aufklärung der Ordnungsphase von Li_2TiO_3. Z. anorg. Allg. Chem. **276** (1954) 77–94.

[10] Lang, G.: Strukturvergleiche an ternären und quarternären Oxiden. Z. anorg. Allg. Chem. **348** (1966) 246–256.

[11] Trömel, M.; Hauck, J.: Über Fehlordnung in Gittern vom Li_2SnO_3-Typ und die Tieftemperaturform dieser Verbindung. Z. anorg. Allg. Chem. **373** (1970) 8–14.

[12] Tarakina, N.V.; Denisova, T.A.; Maksimova, L.G.; Baklanova, Y.V.; Tyutyunnik, A.P.; Berger, I.F.; Zubkov, V.G.; Tendeloo, G.: Investigation of stacking disorder in Li_2SnO_3. Z. Kristallog. Suppl. **20** (2009) 375–380.

[13] Fehr, K.T.; Schmidbauer, E.: Electrical conductivity of Li_2TiO_3 ceramics. Solid State Ionics **178** (2007) 35–41.

[14] Vītņiš, G.; Ķizāne, G.; Lūsis, A.; Tīliks, J.: Electrical conductivity studies in the system Li_2TiO_3–$Li_{1.33}Ti_{1.67}O_4$. J. Solid State Elechtrochem. **6** (2002) 311–319.

[15] Hoshino, T.; Tanaka, K.; Makita, J. Hashimoto, T.: Investigation of phase transition in Li_2TiO_3 by high temperature X-ray diffraction. J. Nucl. Mat. **367–370** (2007) 1052–1056.

[16] Omoto, K.; Takuya, H.; Sasaki, K.; Terai, T.; Hoshino, T.; Yashima, M.: Analysis of crystal structure and thermal expansion property of Li_2TiO_3 by high temperature X-ray diffraction using synchrotron radiation. Photon Factory Activity Report (Materials Science) v.26 (2009) 126.

[17] Kataoka, K.; Takahashi, Y.; Kijima, N.; Nagai, H.; Akimoto, J.; Idemoto Y.; Ohshima, K.: Crystal growth and structure refinement of monoclinic Li_2TiO_3. Mater. Res. Bull. **44** (2009) 168–173.

[18] Castellanos, M.; West, A.R.: Order-disorder phenomena in oxides with rock salt structures: the system Li_2TiO_3–MgO. J. Mater. Sci. **14** (1979) 450–454.

[19] Dorrian, J.F.; Newnham, R.E.: Refinement of the structure of Li_2TiO_3. Mat. Res. Bull. **4** (1969) 179–184.

[20] Yang, L.H.; Dong, C.; Guo, J.: Hybrid microwave synthesis and characterization of the compounds in the Li–Ti–O system. J. Power Sources **175** (2008) 575–580.

[21] Hoshino, T.; Sasaki, K. Tsuchiya, K.; Hayashi, K.; Suzuki, A.; Hashimoto, T.; Terai, T.: Crystal structure of advanced lithium titanate with lithium oxide additives. J. Nucl. Mat. **386–388** (2009) 1098–1101.

[22] Kordes, E.: Die Steinsalzstruktur der Verbindung Li_2TiO_3 und ihre Mischbarkeit mit MgO und $Li_2Fe_2O_4$. Z. Kristallogr. **92** (1935) 139–153.

[23] Barblan, F.; Brandenberger, E.; Niggli, P.: Geregelte und ungeregelte Strukturen von Titanaten und Ferriten und geregelte Umwandlungen der TiO_2 Modifikationen. Helv. Chim. Acta **27** (1958) 88–96.

[24] Baños, L.; Villafuerte-Castrejon, M.E.; Valenzuela, R.; West, A.R.: Kinetics and mechanism of the cation-ordering transformation in Li_2TiO_3–Li_3NbO_4 solid solutions. J. Chem. Soc. Farady. Trans. **86** (1990) 2979–2983.

[25] Song, H.; Jiang, H.; Liu, T.; Liu, X.; Meng, G.: Preparation and photocatalytic activity of alkali titanate nano materials $A_2Ti_nO_{2n+1}$ (A = Li, Na and K). Mater. Res. Bull. **42** (2007) 334–344.

[26] Tabuchi, M.; Nakashima, A.; Shigemura, H.; Ado, K.; Kobayashi, H.; Sakaebe, H. Tatsumi, K.; Kageyama, H.; Nakamura, T.; Kanno, R.: Fine $Li_{(4-x)/3}Ti_{(2-2x)/3}Fe_xO_2$ ($0.18 = x = 0.67$) powder with cubic rock-salt structure as a positive electrode material for rechargeable lithium batteries. Mater. Chem. **13** (2003) 1747–1757.

[27] Tomiha, M.; Masaki, N.; Uchida, S.; Sato, T.: Hydrothermal synthesis of alkali titanates from nano size titania powder. J. Mater. Sci. **37** (2002) 2341–2344.

[28] Morales, J.; Santos-Peña, J.; Trócoli, R.; Franger, S.: Electrochemical activity of rock-salt-structured $LiFeO_2$/$Li_{4/3}Ti_{2/3}O_2$ nanocomposites in lithium cells. J. Nanopart. Res. **10** (2008) 217–226.

[29] Fattakhova, D.; Krtil, P.: Solvothermal synthesis of electrochemically active nanocrystalline Li–Ti–O spinel. Mat. Res. Soc. Symp. Proc. **703** (2002) 165–169.

[30] Pei, X.R.; Zhang, S.L.; Zhang, J.W. Yang, J.J.; Jin, Z.S.: Preparation and characterization of rock salt-type $LiTiO_2$. Chinese J. Inorg. Chem. **22** (2007) 84–88.

[31] Zhang, D.R.; Liu, H.L.; Jin, R.H.; Zhang, N.Z.; Liu, Y.X.; Kang, Y.S.: Synthesis and characterization of nanocrystalline $LiTiO_2$ using a one-step hydrothermal method. J. Ind. Eng. Chem. **13** (2007) 92–96.

[32] Sikhwivhilu, L.M.; Suprakas, S.R.; Coville, N.J.: Influence of bases on hydrothermal synthesis of titanate nanostructures. Appl. Phys. A **94** (2009) 963–973.

[33] Laumann, A.; Fehr, K.T. Holzapfel, M.; Wachsmann, M.; Iversen, B.B.: Metastable formation of low temperature cubic Li_2TiO_3 under hydrothermal conditions – its stability and structural properties. Solid State Ionics **181** (2010) 1525–1529.

[34] Hoelzel, M.; Senyshyn, A.; Gilles, R.; Boysen, H.; Fuess, H.: Scientific Review: The Structure Powder Diffractometer SPODI. Neutron News **18** (2007) 23–26.

[35] Rodriguez-Carvajal, J.: FULLPROF: A program for Rietveld refinement and pattern matching analysis. Abstracts of the satellite meeting on powder diffraction of the XV congress of the International Union of Crystallography, Toulouse, France (1990) 127.

[36] Thompson, P.; Cox, D.E.; Hastings, J.B.: Rietveld refinement of Debye-Scherrer synchrotron X-ray data from Al_2O_3. J. Appl. Crystallogr. **20** (1987) 79–83.

[37] Hodeau, J.L.; Marezio, M.: Neutron profile refinement of the structures of Li_2SnO_3 and Li_2ZrO_3. J. Solid State Chem. **45** (1982) 170–179.

[38] Strobel, P.; Lambert-Andron, B.: Crystallographic and magnetic structure of Li_2MnO_3. J. Solid State Chem. **75** (1988) 90–98.

[39] Jones, P.; Hockey, J.A.: Infra-red studies of rutile surfaces. Part 1. Trans. Faraday Soc. **67** (1971) 2669.

[40] Laumann, A.; Ørnsbjerg Jensen, K.M.; Tyrsted, C.; Bremholm, M.; Fehr, K.T.; Holzapfel, M.; Iversen, B.B.: In-situ synchrotron radiation study of the formation of cubic Li_2TiO_3 under hydrothermal conditions. Submitted to Eur. J. Inorg. Chem.

[41] Saito, S.; Tsuchiya, K.; Kawamura, H. Terai, T.; Tanaka, S.: Density dependence on thermal properties of Li_2TiO_3 pellets. J. Nuc. Mat. **253** (1998) 213–218.

FRM II
Forschungs-Neutronenquelle
Heinz Maier-Leibnitz

User Office
Lichtenbergstr. 1, 85748 Garching/ Germany
Tel.: +49.(0)89.10703/ 10794
Fax: +49.(0)89.10799
Email: userinfo@frm2.tum.de **Web: user.frm2.tum.de**

EXPERIMENTAL REPORT

Experiment Title

Structure determination of low-temperature α-Li_2TiO_3 and its structural changes during heating

Proposal number	3570
Instrument	SPODI
Date of Experiment	25.01. – 28-01.2010
Local Contact	Dr. Markus Hölzel

Experimental Team

Andreas Laumann[1] Karl Thomas Fehr[1] Michael Holzapfel[2] Hans Boysen[3]

Affiliations

[1]LMU München, Department für Geo- und Umweltwissenschaften, Sektion Mineralogie, Petrologie und Geochemie, [2]Süd-Chemie AG Moosburg, [3]LMU München, Department für Geo- und Umweltwissenschaften, Sektion Mineralogie

The compound Li_2TiO_3 has been described in three structural modifications, α, β and γ. The metastable cubic α-Li_2TiO_3 is synthesized hydrothermally at low temperature. Above 300 °C it transforms irreversibly to a monoclinic structure, known as β-Li_2TiO_3, which is a promising compound as a solid tritium breeder material for fusion reactors. The β-phase remains stable up to 1155 °C, at which temperature it transforms to the cubic γ-Li_2TiO_3.

For the experiment, 2 g of a hydrothermally synthesized Li_2TiO_3 powder was filled in a niobium container and placed in a high vacuum furnace. The reflections of niobium were included in all refinements as a second phase.

At room temperature, Li_2TiO_3 was refined in the cubic in space group Fm-3m (Fig. 1a). At 300 °C, broad reflections of the monoclinic modification started to appear. Upon further heating, the ratio of the cubic to the monoclinic phase decreases and the reflections of the monoclinic Li_2TiO_3 sharpen. Between 600 °C and 1000 °C (Fig 1b) only the monoclinic phase could be refined. At 1100 °C the cubic modification with space group Fm-3m reappeared and at 1200 °C (Fig. 2a) solely the cubic (γ)-Li_2TiO_3 was present.

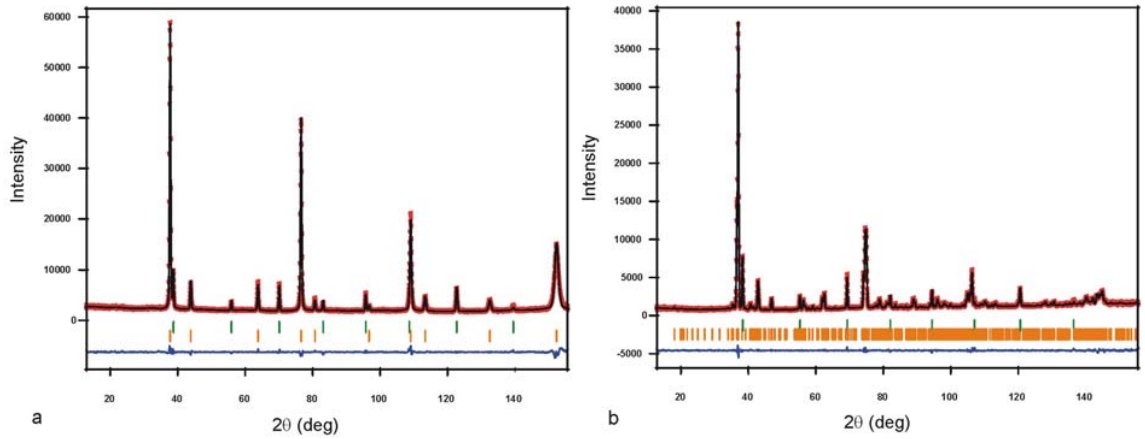

Fig. 1: Rietveld fits of Li_2TiO_3 a) at room temperature and b) at 1000 °C. Observed (red), calculated (solid black line), Bragg reflections of Li_2TiO_3 (orange) and of niobium (green).

FRM II
Forschungs-Neutronenquelle
Heinz Maier-Leibnitz

User Office
Lichtenbergstr. 1, 85748 Garching/ Germany
Tel.: +49.(0)89.10703/ 10794
Fax: +49.(0)89.10799
Email: userinfo@frm2.tum.de **Web: user.frm2.tum.de**

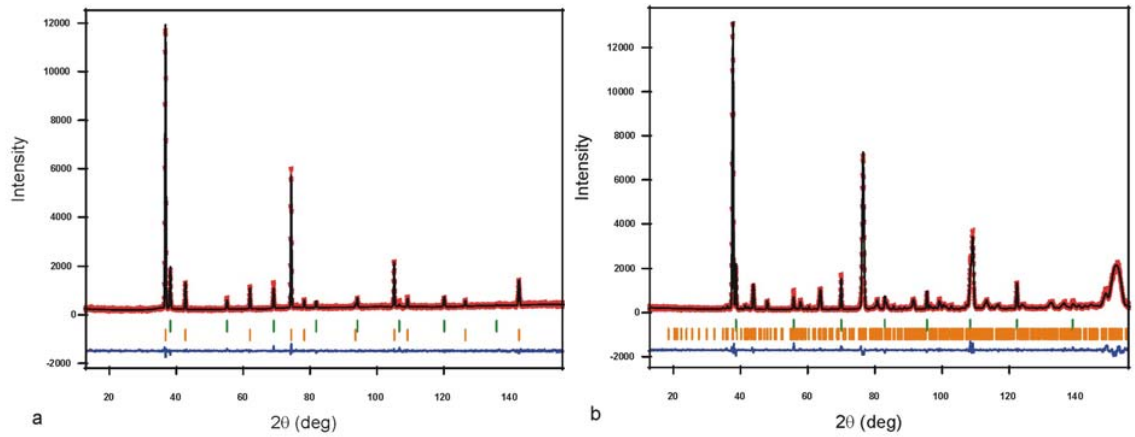

Fig. 2: Rietveld fits of Li_2TiO_3 a) at 1200 °C and b) at room temperature after cooling. Observed (red), calculated (solid black line), Bragg reflections of Li_2TiO_3 (orange) and of niobium (green).

Upon cooling, the monoclinic Li_2TiO_3 started to form below 1160 °C. At 1100 °C about 12% of the cubic phase was left, comparable to the amount of the cubic structure at the same temperature upon heating, and below 1100 °C, only the monoclinic Li_2TiO_3 modification was found (Fig. 2b).
It was shown, that the low temperature metastable α–phase is of space group Fm-3m and it is isostructural with the y-phase, which is the stable modification at high temperatures. The interlinked data points of the cubic unit cell volume at low temperatures and above 1100 °C indicate a constant thermal expansion (Fig. 3). Accordingly, by hydrothermal reaction, disordered cubic Li_2TiO_3 can be produced at temperatures far below its stability field.
During the first heating, the monoclinic structure, which starts to form above 300 °C, is disordered due to stacking faults. Between 300 and 900 °C, not all reflections have the theoretical intensity expected for space group C2/c, so that some reflections are missing, or are too broad, and some are too sharp. Another deviation from the known monoclinic Li_2TiO_3 of space group C2/c is the monoclinic beta angle upon the first heating. Below 1000 °C, the beta angles shows a lower value than above 1000 °C and it keeps a constant high value also upon cooling to room temperature. Therefore it seems that the fully ordered monoclinic Li_2TiO_3 can only be produced by heating to temperatures > 1000 °C.

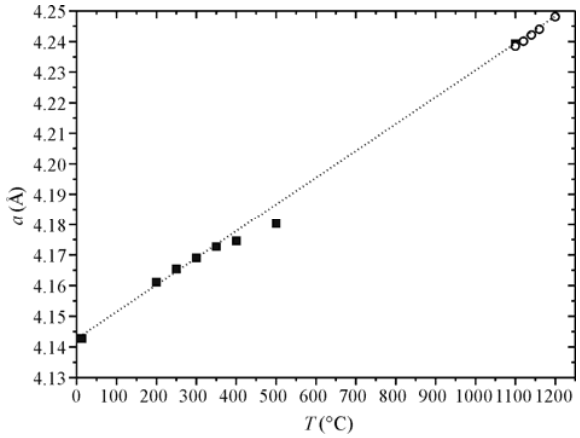

Fig. 3: Lattice constants of cubic Li_2TiO_3. The dashed line illustrates the connectivity between the low and the high temperature values upon heating (squares) and cooling (circles). The deviations from the linear trend at 400 and 500 °C may be explained by a preferred exsolution of the more mobile Li into the initial monoclinic structure.

Appendix C

Third publication

In-situ synchrotron X-ray diffraction study of the formation of cubic Li_2TiO_3 under hydrothermal conditions

European Journal of Inorganic Chemistry **14** 2221-2226 (2011)

Andreas Laumann,[a] Kirsten Marie Ørnsbjerg Jensen,[b] Christoffer Tyrsted,[b] Martin Bremholm,[c] Karl Thomas Fehr,[a] Michael Holzapfel,[d] Bo Brummerstedt Iversen[b]

[a] Ludwig-Maximilians-Universität München, Department of Earth and Environmental Sciences, Section for Mineralogy, Petrology and Geochemistry, Munich, Germany
[b] Aarhus University, Department of Chemistry and iNANO, Aarhus C, Denmark
[c] Department of Chemistry, Princeton University, Princeton, NJ 08544, USA
[d] Süd-Chemie AG, Battery Materials, Moosburg, Germany

DOI: 10.1002/ejic.201001133

In-situ Synchrotron X-ray Diffraction Study of the Formation of Cubic Li_2TiO_3 Under Hydrothermal Conditions

Andreas Laumann,[a] Kirsten Marie Ørnsbjerg Jensen,[b] Christoffer Tyrsted,[b] Martin Bremholm,[c] Karl Thomas Fehr,[a] Michael Holzapfel,[d] and Bo Brummerstedt Iversen*[b]

Keywords: Kinetics / Reaction mechanisms / Hydrothermal synthesis / Titanium / Lithium / Synchrotron diffraction

Synchrotron powder X-ray diffraction (PXRD) has been used to study in-situ the hydrothermal intercalation of lithium ions in titania powder following the reaction $TiO_2 + 2\ LiOH \rightarrow Li_2TiO_3 + H_2O$. Syntheses were performed in a sapphire capillary at temperatures between 133 and 230 °C. By sequential Rietveld refinement of the PXRD data, the particle growth of the metastable cubic α-Li_2TiO_3 compound was determined as a function of the reaction time, as well as the transformation of the cubic α-phase to its stable monoclinic β-modifications at a temperature above the critical point of water. The reactions were presumed to be controlled by nucleation and crystal growth, and therefore the Avrami-Erofe′ef equation was applied to model the reaction mechanisms of this intercalation process and an activation energy of 66(7) kJ/mol was determined.

Introduction

The compound Li_2TiO_3 exists in two structural modifications,[1] a cubic form of space group $Fm\bar{3}m$,[1–11] and a monoclinic structure of space group $C2/c$.[1,8–11] At low temperatures, the monoclinic form is stable, but it transforms to the cubic modification above ca. 1155 °C[1,8–12] before melting at ca. 1540 °C.[8–11] However, a metastable cubic modification can be produced at low temperatures by hydrothermal syntheses.[1–5] This metastable cubic modification is also known as α-Li_2TiO_3[1,10,11] and between 300 and 600 °C it transforms irreversibly to a monoclinic structure (β-Li_2TiO_3) e.g. in air[8–11] or in high vacuum.[1] Especially during the cubic-monoclinic transformation, β-Li_2TiO_3 is disordered due to stacking faults, which is indicated in the X-ray powder pattern by excessively sharp reflections of high intensity and missing, or very broad, reflections of low intensity, as well as by a reduced monoclinic β angle.[1] The final transformation to the well known ordered monoclinic β-Li_2TiO_3 of space group $C2/c$ occurs above 1000 °C.[1] The ordered structure is maintained upon cooling to room temperature.[1]

The crystal structure of the cubic Li_2TiO_3 phase is of the NaCl structure type, with a statistical distribution of lithium and titanium on one site, and oxygen on the other site.[1] The monoclinic structure in space group $C2/c$ can be derived from the parent cubic NaCl structure by the transformation

$$\begin{pmatrix} 1/2 & 1 & 1/2 \\ 3/2 & 0 & -3/2 \\ -3/2 & 1 & -3/2 \end{pmatrix}$$

from which the ideal monoclinic lattice constants $a_m = \sqrt{3/2}a_c$, $b_m = \sqrt{9/2}a_c$, $c_m = \sqrt{11/2}a_c$, and $\cos\beta_m = -1/\sqrt{33} \rightarrow \beta_m = 100.025°$ can be calculated. Ordering of the cations leads to a layered structure comprising three layers. The first layer only consists of lithium ions on 8*f* (Li1) and 4*d* (Li2) positions. The second layer is occupied by oxygen and the third layer has alternate titanium and lithium (Ti1, Ti2 and Li3) on 4*e* positions.

The compound α-Li_2TiO_3 can be produced by the hydrothermal reaction of anatase or rutile with lithium hydroxide for $LiOH/TiO_2 \geq 2$, and synthesis has been reported from a 2:1 ratio[1] up to a 50:1 ratio.[3] So far no other lithium titanium compounds than Li_2TiO_3 have been observed as products from the hydrothermal reaction of anatase or rutile in lithium hydroxide solution. Even when using a highly over-stoichiometric amount of lithium,[3] the surplus of lithium hydroxide remains unreacted and dissolved. Kinetic experiments of the hydrothermal formation of α-Li_2TiO_3 have

[a] Department of Earth and Environmental Sciences, Section for Mineralogy, Petrology und Geochemistry, Ludwig-Maximilians-Universität München,
Theresienstr. 41, 80333 Munich, Germany
[b] Centre for Materials Crystallography, Department of Chemistry and iNANO, Aarhus University,
Langelandsgade 140, 8000 Aarhus C, Denmark
Fax: +45-8619-6199
E-mail: bo@chem.au.dk
[c] Department of Chemistry, Princeton University,
Princeton, NJ 08544, USA
[d] Battery Materials, Süd-Chemie AG,
Ostenriederstr. 15, 85368 Moosburg, Germany
Supporting information for this article is available on the WWW under http://dx.doi.org/10.1002/ejic.201001133.

not been reported so far, whereas kinetic studies with divalent cations instead of lithium were performed in the system $ATiO_3$, where A = Ba, Ca, and Pb.[13–18]

Here, we report a time-resolved in-situ synchrotron powder X-ray diffraction (PXRD) study of the hydrothermal reaction of lithium hydroxide with titania. The kinetics of the formation of crystalline titania to α-Li_2TiO_3 were modelled for temperatures between 154 and 230 °C to determine the reaction mechanism.

Results

In all performed in-situ experiments, the hydrothermal reaction of titania in a lithium hydroxide solution to α-Li_2TiO_3 was recorded. The reaction can be expressed as

$$TiO_2(s) + 2\ LiOH(aq) \rightarrow Li_2TiO_3(s) + H_2O \quad (1)$$

At 133 °C, the lowest temperature of all performed experiments (EXP1), partial formation of Li_2TiO_3 was observed, but the kinetics were too slow for the complete formation of α-Li_2TiO_3 in a suitable time due to the restricted beam-time. The experiment was aborted after 26 min as the α-Li_2TiO_3 fraction was only ca. 20% and a high proportion of anatase and a minor proportion of rutile were still present. Higher temperatures lead to the complete formation of α-Li_2TiO_3 in less than 30 min (Table 1 and Figure 1).

Table 1. Temperature for each experiment, the times for the half-fraction, and the calculated values for the rate constant k (see kinetics section).

Run	T [°C]	$t_{1/2}$ [s]	k [s^{-1}][c]
EXP1[a]	133	–	–
EXP2	154	328.7	2.1×10^{-3}
EXP3[b]	168	156.1	4.4×10^{-3}
EXP4	169	121.5	5.7×10^{-3}
EXP5	195	38.9	1.8×10^{-2}
EXP6	215	22.7	3.1×10^{-2}
EXP7	230	21.1	3.3×10^{-2}

[a] Half-fraction was not reached within 30 min. [b] Experiment was heated to 420 °C after 22.5 min. holding time at 168 °C. [c] See kinetics section.

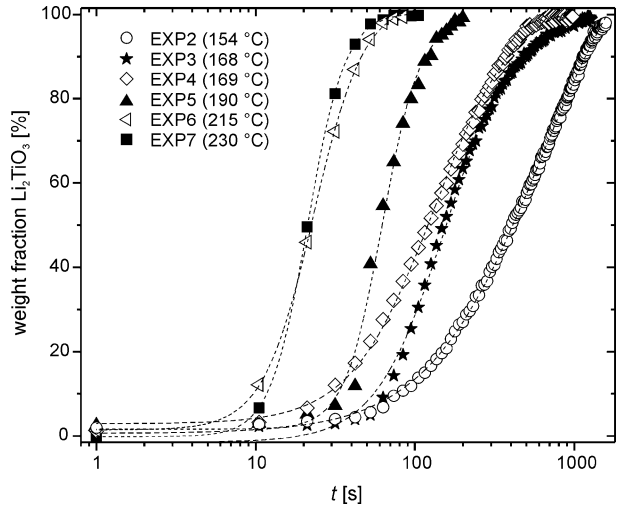

Figure 1. Data points and sigmoidal fits for the fractional progressions of EXP2–EXP7 vs. time.

The progress of all reactions could be fitted with a sigmoidal model. The fractional progress of α-Li_2TiO_3 and titania vs. time of EXP6 is plotted in detail in Figure 2, which shows an increasing fraction of the lithium titanate with a corresponding simultaneous decrease in the titania fraction. The temperature dependence of the half-fractions (α = 0.5) of Li_2TiO_3 displays an exponential decay, Figure 3.

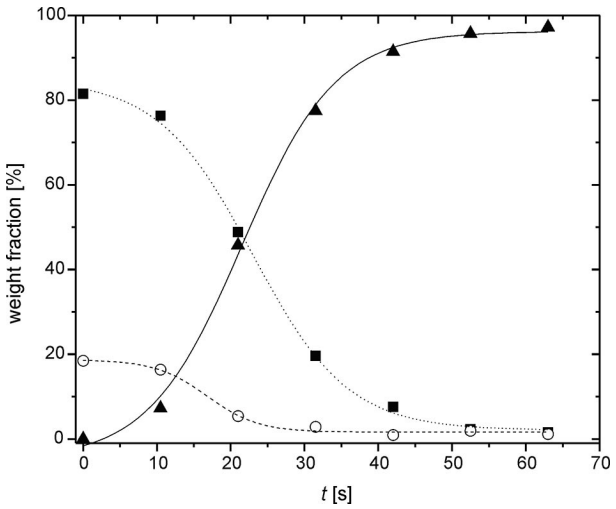

Figure 2. Fractional progression of anatase (squares) and rutile (circles) to α-Li_2TiO_3 (triangles) vs. time at 215 °C (EXP6) and sigmoidal fits of the formation of α-Li_2TiO_3 (solid) with the decay of anatase (dotted) and rutile (dashed).

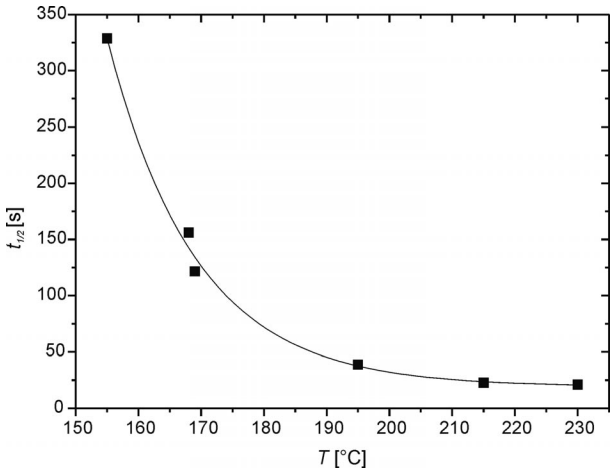

Figure 3. Half-fraction times, $t_{1/2}$, of the transformation to α-Li_2TiO_3 at different temperatures.

For EXP3, which was heated to 420 °C after 22.5 min, the progression of the reaction is shown in Figure 4. First, the formation of Li_2TiO_3 was observed with increasing intensity of the lithium titanate reflections and the diminishing reflections of titania, so that after about 18 min only reflections of lithium titanate were detected. The broad hump around 2Θ = 20° is caused by the aqueous lithium hydroxide solution in the sapphire capillary. Then, after 22.5 min, the temperature was set to 420 °C and the critical temperature of water (T_C = 374 °C) was crossed within a single detector exposure. The broad feature observed at a

temperature of 168 °C flattens as the fluid turns supercritical (Figure 4). At 420 °C, the reflections of the α-Li_2TiO_3 shift slightly to smaller 2Θ angles due to the thermal expansion of α-Li_2TiO_3. Moreover, new and broad reflections appear, whereof the reflection of the highest intensity at 2Θ ≈ 11.8° can clearly be ascribed to the (002) reflection of the monoclinic β-Li_2TiO_3 phase. Especially in the beginning of the cubic to monoclinic transformation, the monoclinic Li_2TiO_3 is disordered due to stacking faults[1] and it was not possible to refine the FWHM parameters (see discussion).

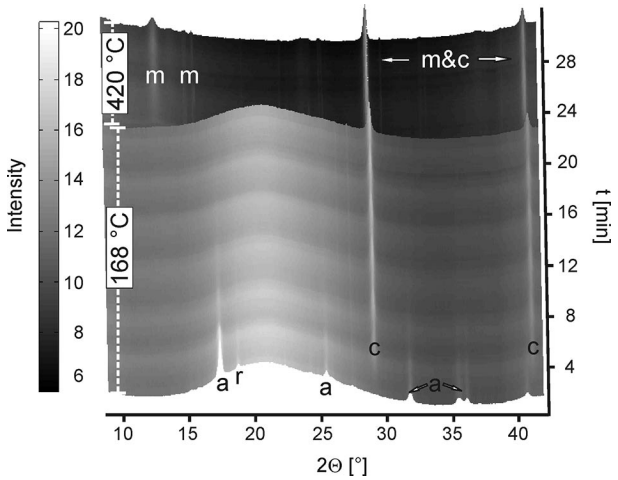

Figure 4. Three dimensional plot of diffraction data showing the transformation from anatase (a) and rutile (r) to the cubic α-Li_2TiO_3 (c) at 168 °C (EXP3). Heating to 420 °C after 23 min results in the beginning of the transformation from α-Li_2TiO_3 to the monoclinic β-Li_2TiO_3 (m). The broad hump around 2θ = 20° is caused by the lithium hydroxide solution.

Modelling of Anatase and α-Li_2TiO_3 Particles

The refined nanocrystal size of P25 yielded a value of ca. 20 nm, which is in good agreement with the specification of Evonik (21 nm). P25 comprises anatase and rutile in a ratio of 4:1, thus a reasonable refinement of the particle size of rutile was only possible at the very beginning of each experiment. Therefore, sequential refinement of the size of the anatase particles produced better results, especially for reactions at lower temperatures, where anatase was detectable over a longer period.

Anatase can be described in the tetragonal space group $I4_1/amd$ with unit cell parameters a = 3.785(1) Å and c = 9.482(3) Å.[19] The structure has various empty octahedral sites, where lithium possibly can be accommodated.[20–23] The unit cell parameters of anatase at the onset of all experiments show some minor variations compared with the theoretical values. These small changes are probably caused by a small displacement of the capillary due to the heating. With ongoing reaction time, the unit cell parameters changed and the values of the unit cell parameter a increased slightly and the values of the unit cell parameter c decreased, stronger with longer reaction time and particularly before the full cell formation of α-Li_2TiO_3 was accomplished (Figure 5). The particle size of anatase remained fairly constant until the lithium intercalation was completed (Figure 6).

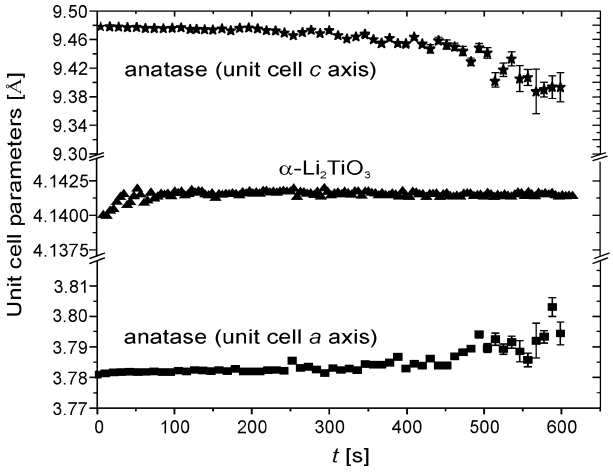

Figure 5. Progression of unit cell a axis (squares) and unit cell c axis (stars) of anatase and the constant unit cell of α-Li_2TiO_3 (triangles) with time and ongoing formation of α-Li_2TiO_3 (EXP2, 154 °C).

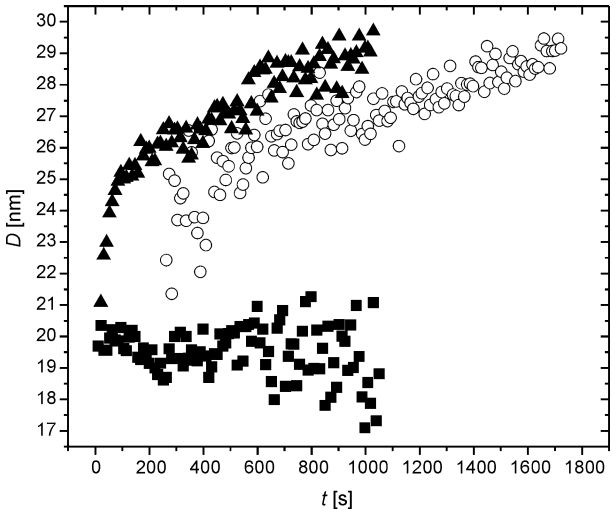

Figure 6. Particle growth of α-Li_2TiO_3 in EXP2 (circles) and in EXP6 (triangles), and the size of the anatase particles in EXP2 (squares) vs. reaction time (error approx. 1 nm). Due to the low fraction of α-Li_2TiO_3 in EXP2 before 250 s the FWHM parameters could not be refined. The same problem occurred for anatase particles after 1000 s. Both are indicated by the wider scattering of the data points of α-Li_2TiO_3 at the beginning of the formation and for anatase, when only a low fraction is left.

The unit cell parameter of the α-Li_2TiO_3 particles seem to increase slightly at the very beginning of each experiment, which also could be caused by errors in the refinement due to low fraction of the titanate. Then, during the formation to α-Li_2TiO_3 and until the experiments were aborted, the unit cell parameter stayed constant around 4.14 Å (Figure 5). The first detectable α-Li_2TiO_3 particles showed approximately the same size as the crystalline tita-

nia reactant P25 (Figure 6). With ongoing reaction time, the lithium titanate particles grew, slightly faster at higher temperatures. The two experiments with the highest synthesis temperature showed a similar fast particle growth, and in EXP6 the particle growth is ca. 8 nm within 1000 s (Figure 6).

Kinetics

As mentioned before, the increase of the fractions of the lithium titanate, as well as the decrease of the fractions of the titania powders, show a sigmoidal reaction progress, suggesting that nucleation and crystal growth control the reaction.[15] In solid state chemistry, the Avrami-Erofe'ef equation[24–27] is broadly applied to model phase transformations, nucleation and crystal growth. It relates the fraction of a reaction, α, at each temperature by using the relationship

$$\alpha = 1 - \exp[-k(t - t_0)^n] \quad (2)$$

where n is the Avrami exponent, t_0 the induction time, and k the rate constant. The exponent n gives details about the rate of nucleation and the mechanism of nuclei growth. The expression is most valid in the fractional range from $0.15 < \alpha < 0.5$. Reactions of the present study were fast, so that for EXP5, EXP6 and EXP7 only one or two data points would be found in the $0.15 < \alpha < 0.5$ range, and therefore these experiments are not included in the following considerations. The value of n can be determined by applying a Sharp–Hancock plot,[28] which is a plot of $\ln[-\ln(1 - \alpha)]$ vs. $\ln(t)$. This gives a straight line with a slope of n. Changes in the reaction mechanism can be identified as a change in the slope. At low fractions, the experiments EXP2, EXP3 and EXP4 show a slope of ca. 2. The reaction mechanism seems to change at about $\alpha = 0.35$, as is especially evident for EXP2. Thus, the range of $0.15 < \alpha < 0.85$ was applied for EXP2, EXP3 and EXP4 (Figure 7). At fractions $\alpha \approx 0.45$, the slope is less steep in all of the three experiments and an average value of $n \approx 1.2$ is obtained.

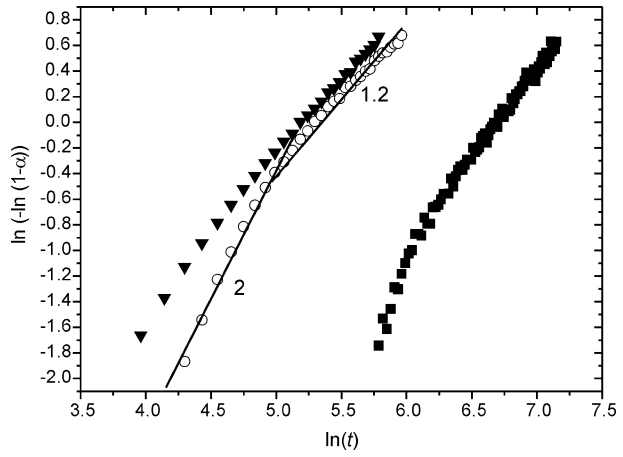

Figure 7. Sharp–Hancock plot for the transformation of P25 titania powder in lithium hydroxide solution to α-Li_2TiO_3 at 154 °C (squares), 168 °C (circles) and 169 °C (triangles).

In order to calculate the activation energy for the crystallization of α-Li_2TiO_3, $\ln(k)$ against $1/T(\mathrm{K}) \times 1000$ is plotted, displaying the logarithmic form of the Arrhenius equation

$$k = A \cdot \exp(-E_A/RT) \quad (3)$$

where A is the pre-exponential factor, E_A the effective activation energy, R the gas constant, and T the absolute temperature. The calculated values are listed in Table 1 and the Arrhenius plot in Figure 8 displays $\ln(k)$ vs. $1/T \times 1000$. E_A can be calculated from the slope of the plot, which gives a value of 66(7) kJ/mol.

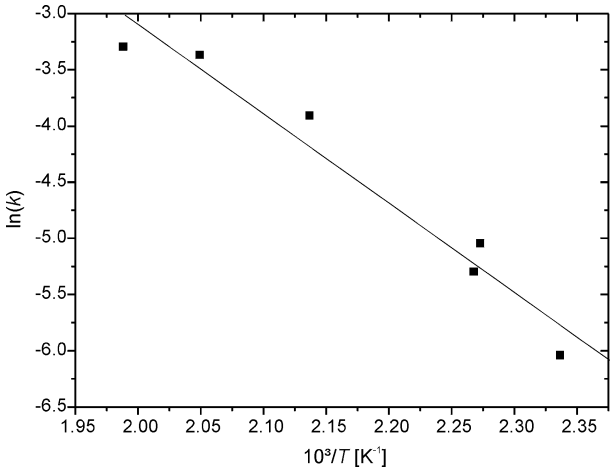

Figure 8. Arrhenius plot used to determine the activation energy of the intercalation of lithium in titania.

Discussion

Lithium Intercalation in Titania Powder

The unit cell parameters of anatase change during the formation of α-Li_2TiO_3, as shown in Figure 5. This observation might be explained by lithium ions inserting the anatase structure, without yet transforming to α-Li_2TiO_3. The simultaneous decrease of the titania fraction and the growth of the lithium titanate (Figure 2) proves that lithium intercalates the titania particles, i.e. a direct reaction to α-Li_2TiO_3 takes place without a prior formation of e.g. a $Ti(OH)_4$ phase, which has been proposed for the hydrothermal synthesis of $BaTiO_3$.[15] The comparable particle sizes of reactant and the first formed products (Figure 6) also suggests that lithium ions are intercalated in the titania structure without dissolving of the titania particles. Hypothesizing that the reaction mechanism is controlled by dissolution and recrystallization, one would expect a decrease in the average particle size of the titanium oxide precursors prior to and during the crystallization of the Li_2TiO_3. The constant size of the anatase indicates that a dissolution-recrystallization mechanism can be excluded and suggests a topotactic transformation mechanism.

Most studies on the intercalation of lithium ions in titania were performed by electrochemical intercalation of lithium e.g. in anatase.[20–23] By electrochemical intercalation,

Ti^{4+} is partially reduced to Ti^{3+}, and compositions of $Li_x(Ti^{3+}{}_xTi^{4+}{}_{1-x})O_2$ are obtained. For $x < 0.25$ the tetragonal anatase structure is maintained. The unit cell parameter a increases with lithium insertion, while c decreases,[21,22] as also observed in the present study (Figure 5). However, the reaction taking place here is hardly comparable with the electrochemical intercalation of lithium in anatase, as titanium is unlikely to be reduced under the present conditions. Nevertheless, before the anatase phase finally transforms to α-Li_2TiO_3, lithium ions might fill empty sites of the anatase structure and cause the minor change of the unit cell parameters. This will occur at the end of each reaction, when most of the anatase is already transformed to α-Li_2TiO_3 and in the remaining anatase some lithium ions will already have intercalated.

Cubic-Monoclinic Transformation of Li_2TiO_3

The transformation of the metastable α-Li_2TiO_3 to the monoclinic Li_2TiO_3 above 300 °C was so far only described in air or vacuum[1,5,8–11] and it takes place over a wide temperature range. The complete transformation to the β-phase occurs above 500 °C[1] and at 420 °C a two-phase system comprising the cubic and the monoclinic structure is expected. Lithium has a low X-ray scattering power and all reflections of the cubic phase are superimposed on the reflections of the monoclinic phase. Thus, the FWHM parameters had to be fixed, and the refined fraction of 47(1)% of the cubic phase at 420 °C must be considered as a first estimate only, which however compares well with fractions of the cubic phase [60(2)%] at 400 °C and at 500 °C [11.5(7)%] reported by Laumann et al.[1] This leads to the assumption, that the cubic to monoclinic transformation occurs at a similar temperature, irrespective of whether a dry powder is heated in high vacuum or in aqueous lithium hydroxide solution above the critical point of water.

Reaction Mechanism

The slope n which is obtained from Equation (3) can give information about the mechanisms of the reactions. According to Sharp and Hancock,[28] for n = 0.54–0.62 a diffusion-limited rate is inferred, where the rate of diffusion of the reactive species to the nucleation sites is the rate-determining step. For n = 1.0–1.24, a zero-order, first-order, or a phase boundary mechanism between the product and the reagent mixture is rate determining, and for n = 2.0–3.0, the formation of nucleation sites is the process that controls the rate. In the present study, the slope n = 2 in the beginning of the reactions (Figure 7) suggests that the nucleation of Li_2TiO_3 sites is the rate-determining step. As no sign of dissolution of the titania particles was observed, the formation of Li_2TiO_3 does not occur from solution, but rather formation of Li_2TiO_3 domains occur from within the titania particles. Then, the slope becomes less steep at higher fractions and $n \approx 1.2$ suggests that once enough Li_2TiO_3 nuclei are formed, the reaction mechanism changes, and then the reaction at the phase boundary is the rate determining mechanism at higher fractions. The rather high activation energy of 66(7) kJ/mol also suggests a phase boundary or nucleation controlled mechanism. $E_A < 32$ kJ/mol would be an indicator for diffusion controlled process.[29]

The present study focused on the reaction of the titania powder P25 with a 0.5 M lithium hydroxide solution. It is expected, that by using other titania reactants, or a higher or less concentrated lithium hydroxide solution, the kinetics, and even the reaction mechanisms might change. For the formation e.g. of $BaTiO_3$, the activation energies were found to depend mainly on the titania reactant,[16] thus for $BaTiO_3$ various activation energies between 21 kJ/mol[30] and 105.5 kJ/mol have been reported.[31] For the hydrothermal formation of the lithium titanate it was reported that coarser particles (ca. 100 nm) cause problems to fulfil a complete reaction at 160 °C,[5] whereas by using a 5 nm anatase, lithium intercalation can be performed in a 2.5 M lithium hydroxide solution at 60 °C.[32] Obviously, a faster reaction at the same temperature can be expected for a higher concentration of the lithium hydroxide solution. Here, especially at low temperatures, e.g. in EXP2 (154 °C) the reaction is slowed down before getting to the end of the complete formation of α-Li_2TiO_3, indicating that low concentrations of remaining lithium ions in the solution decelerate the kinetics (see Figure 1).

Conclusions

For the first time, in-situ synchrotron radiation has been used to study the interaction of titania powder in a lithium hydroxide solution under hydrothermal conditions. Lithium ions were found to intercalate in the titania structure without a prior dissolution of the titania compounds and the particle growth of the formed metastable cubic α-Li_2TiO_3 was recorded. Upon heating the suspension of α-Li_2TiO_3 particles in a lithium hydroxide solution above the critical point of water, α-Li_2TiO_3 was found to transform to the monoclinic β-Li_2TiO_3 in a similar way as observed for dry α-Li_2TiO_3 powder heated in air or in high vacuum. By applying the Avrami-Erofe'ef equation, the rate controlling mechanism could be determined for the reactions at lower temperatures. The process was found to be non-isokinetic due to a change from a nucleation controlled to a phase boundary controlled reaction, which may depend on the used titania reactant and the concentration of the lithium hydroxide solution. The calculated activation energy of 66(7) kJ/mol also will be sensitive to variations of the reaction conditions.

Experimental Section

Synthesis: All experiments were performed using an aqueous suspension of titania powder (Evonik, formerly Degussa, AEROXIDE TiO_2 P25) and dissolved lithium hydroxide (SQM, Chile). P25 comprises anatase and rutile in a ratio of about 4:1. Before the synchrotron experiments were started, 0.4 g of P25 and 0.58 g of $LiOH·H_2O$ were stirred in 25 mL of de-ionized water for 1 h in air. In total, kinetic data of 7 experiments, denoted EXP1 to EXP7

with increasing number for higher syntheses temperatures, were conducted. The adjusted temperatures were 133, 154, 168, 169, 195, 215 and 230 °C at a pressure of 230 bar. In addition EXP3 was subsequently heated to the maximal possible temperature of 420 °C after a holding time of 22.5 min at 168 °C.

Setup: The in-situ synchrotron data was recorded at beamline I711 at MAX-lab in Lund, Sweden.[33] The syntheses were performed in a custom build reactor[34–36] using a sapphire capillary with an inner diameter of 0.7 mm. For all experiments, the suspension was injected into the capillary with a syringe. The capillary was aligned in the X-ray beam, pressurized to 230 bar, and then heated to the desired temperature in a hot air flow. The temperature in the capillary was measured with a thermocouple right next to the beam. The reactor design has been described in detail elsewhere.[34,36]

Data Analysis: The wavelength was adjusted to 0.997 Å and the detector had a time resolution of 10.5 s per frame. The 2D diffraction data were integrated in the program Fit2D,[37] and subsequently, the time resolved PXRD data sets were analyzed by sequential Rietveld refinement using the program FullProf.[38] The peaks were fitted with the Thompson–Cox–Hastings pseudo-Voigt axial divergence asymmetry peak shape,[39] and the Gaussian and Lorentzian full width at half maximum (FWHM) is calculated from

$$FWHM_G^2 = (U + e^2)\tan^2\Theta + V\tan\Theta + W \quad (3)$$

$$FWHM_L^2 = (Y + \lambda/L)/\cos\Theta \quad (4)$$

where U, V, W and Y are the instrumental resolution parameters (obtained from a LaB_6 standard sample), λ is the wavelength, and $e = \Delta d/d$ and L are the "apparent" strain and size parameters, respectively. The atomic coordinates of anatase,[19] rutile,[40] the cubic Li_2TiO_3[1] and the monoclinic Li_2TiO_3[1] were fixed at the values from the literature. The isotropic thermal parameters (B_{iso}) were fixed to 1, a reasonable value higher than the room temperature data of Kataoka et al.[12] Test refinements with both lower and higher B_{iso} values showed negligible influence on the particle size and no influence on the observed trends.

The background was linearly interpolated between a set of background points with refinable intensity. In the Supporting Information specific examples of Rietveld refinements are shown together with relevant crystallographic details.

Supporting Information (see footnote on the first page of this article): Two dimensional PXRD data for all experiments and selected examples of Rietveld refinements of data sets from EXP6 and EXP3 with corresponding crystallographic information.

Acknowledgments

We would like to thank Mogens Christensen, Nina Lock, Jacob Becker-Christensen and Yngve Cerenius for help during measurements at the MAX-II synchrotron in Lund. Funding of this project was provided by the Danish Strategic Research Council (CEM), The Danish National Research Foundation (CMC), the Danish Research Council for Nature and Universe (Danscatt) and Süd-Chemie AG, Germany.

[1] A. Laumann, K. T. Fehr, H. Boysen, M. Hoelzel, M. Holzapfel, *Z. Kristallogr.* **2011**, *226*, 53.
[2] H. Song, H. Jiang, T. Liu, X. Liu, G. Meng, *Mater. Res. Bull.* **2007**, *42*, 334.
[3] M. Tomiha, N. Masaki, S. Uchida, T. Sato, *J. Mater. Sci.* **2002**, *37*, 2341.
[4] M. Tabuchi, A. Nakashima, H. Shigemura, K. Ado, H. Kobayashi, H. Sakaebe, K. Tasumi, *J. Mater. Chem.* **2003**, *13*, 1747.
[5] A. Laumann, K. T. Fehr, M. Holzapfel, M. Wachsmann, B. B. Iversen, *Solid State Ionics* **2010**, *181*, 1525.
[6] E. Kordes, *Fortschr. Mineral. Kristallogr. Petrogr.* **1933**, *17–18*, 27.
[7] E. Kordes, *Z. Kristallogr.* **1935**, *92*, 139.
[8] C. Gicquel, M. M. Mayer, R. Bouaziz, *C. R. Acad. Sci. Paris Série C* **1972**, *275*, 1427.
[9] J. C. Mikkelsen, *J. Am. Ceram. Soc.* **1980**, *63*, 331.
[10] H. Kleykamp, *J. Nucl. Mater.* **2001**, *295*, 244.
[11] H. Kleykamp, *Fusion Eng. Des.* **2002**, *61–62*, 361.
[12] K. Kataoka, Y. Takahashi, N. Kijima, H. Nagai, J. Akimoto, Y. Idemoto, K. Ohshima, *Mater. Res. Bull.* **2009**, *44*, 168.
[13] J. O. Eckert Jr., C. C. Hung-Houtson, B. L. Gersten, M. M. Lencka, R. E. Riman, *J. Am. Ceram. Soc.* **1996**, *79*, 2929.
[14] J. Moon, E. Suvaci, A. Morrone, S. A. Costantino, J. H. Adair, *J. Eur. Ceram. Soc.* **2003**, *23*, 2153.
[15] A. Testino, V. Buscaglia, M. T. Buscaglia, M. Viviani, P. Nanni, *Chem. Mater.* **2005**, *17*, 5346.
[16] R. I. Walton, F. Millange, R. I. Smith, T. C. Hansen, D. O'Hare, *J. Am. Chem. Soc.* **2001**, *123*, 12547.
[17] D. Croker, M. Loan, B. K. Hodnett, *Cryst. Growth Des.* **2009**, *9*, 2207.
[18] G. A. Rosetti Jr., D. J. Watson, R. E. Newnham, J. H. Adair, *J. Cryst. Growth* **1992**, *116*, 251.
[19] I. Djerdj, A. M. Tonejc, *J. Alloys Compd.* **2006**, *413*, 159.
[20] M. V. Koudriachova, S. W. de Leeuw, *Phys. Rev. B* **2004**, *69*, 0541016–1.
[21] F. Tielens, M. Calatyud, A. Beltrán, C. Minot, J. Andrés, *J. Electroanal. Chem.* **2005**, *581*, 216.
[22] M. Wagemaker, G. J. Kearley, A. A. van Well, H. Mutka, F. M. Mulder, *J. Am. Chem. Soc.* **2003**, *125*, 840.
[23] M. Wagemaker, A. A. van Well, G. J. Kearley, F. M. Mulder, *Solid State Ionics* **2004**, *175*, 191.
[24] M. J. Avrami, *J. Chem. Phys.* **1939**, *7*, 1103.
[25] M. J. Avrami, *J. Chem. Phys.* **1940**, *8*, 212.
[26] M. J. Avrami, *J. Chem. Phys.* **1941**, *9*, 177.
[27] B. V. C. Erofe'ev, *R. Dokl. Acad. Sci. SSSR* **1946**, *52*, 511.
[28] J. D. Hancock, J. H. Sharp, *J. Am. Ceram. Soc.* **1972**, *55*, 74.
[29] A. C. Lasagna, *Kinetic Theory in the Earth Sciences*, Princeton University Press, **1998**.
[30] N. A. Ovramenko, L. I. Shevts, F. D. Ovcharenko, B. Y. Komilovich, *Izv. Akad. Nauk SSSR, Neorg. Mater.* **1979**, *248*, 889.
[31] W. J. Hertl, *J. Am. Ceram. Soc.* **1988**, *71*, 879.
[32] C. Jiang, E. Hosono, M. Ichihara, I. Honma, H. Zhou, *J. Electrochem. Soc.* **2008**, *155*, A553.
[33] Y. Cerenius, K. Ståhl, L. A. Svensson, T. Ursby, Å. Oskarsson, J. Albertsson, A. Liljas, *J. Synchrotron Radiat.* **2000**, *7*, 203.
[34] M. Bremholm, H. Jensen, S. B. Iversen, B. B. Iversen, *J. Supercrit. Fluids* **2008**, *22*, 385.
[35] C. Tyrsted, J. Becker, P. Hald, M. Bremholm, J. S. Pedersen, J. Chevallier, Y. Cerenius, S. B. Iversen, B. B. Iversen, *Chem. Mater.* **2010**, *22*, 1814.
[36] J. Becker, M. Bremholm, C. Tyrsted, B. Pauw, K. M. Ørnsbjerg Jensen, J. Eltzholt, M. Christensen, B. B. Iversen, *J. Appl. Crystallogr.* **2010**, *43*, 729.
[37] A. P. Hammersley, S. O. Svensson, M. Hanfland, A. N. Fitch, D. Häusermann, *Adv. High Pressure Res.* **1996**, *14*, 235.
[38] J. Rodriguez-Carvajal, *Physica B* **1993**, *192*, 55.
[39] P. Thompson, D. E. Cox, J. B. Hastings, *J. Appl. Crystallogr.* **1987**, *20*, 79.
[40] X. Bokhimi, A. Morales, F. Pedraza, *J. Solid State Chem.* **2002**, *169*, 176.

Received: October 23, 2010
Published Online: March 30, 2011

Supporting Information

Two dimensional PXRD data

Figure S1a: EXP1 done at 133 °C. The (200) reflection of α-Li_2TiO_3 at 2Θ = 27.8° becomes visible after about 10 minutes. EXP1 can be seen in more detail in Figure S1b (starting after 7 minutes and in a smaller 2Θ range).

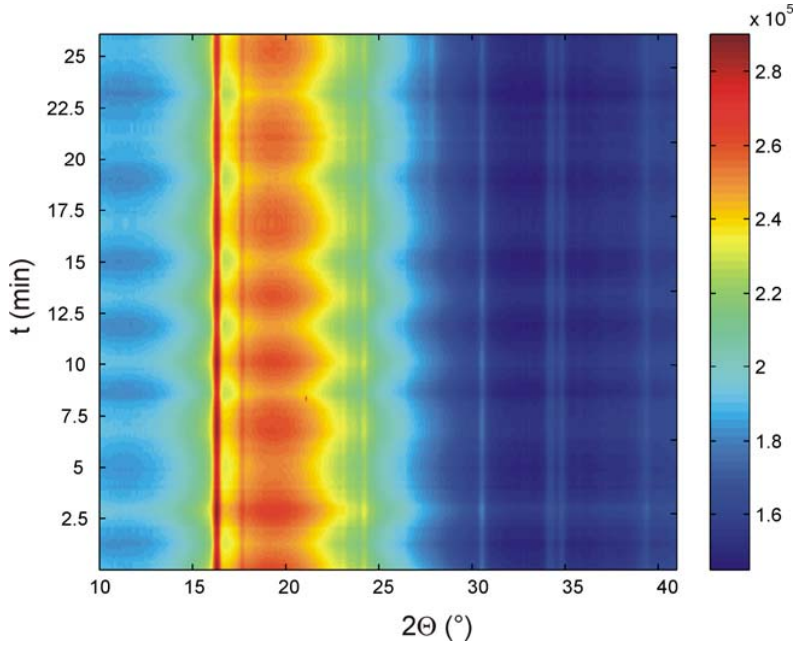

Figure S1b: Detailed view of EXP1 done at 133 °C. After about 20 minutes, besides the (200) reflection (see above), also the weaker [220] reflection of α-Li_2TiO_3 at 2Θ = 39.8° can be seen. The α-Li_2TiO_3 fraction did not increase above 20% within 26 minutes, and therefore the experiment was aborted.

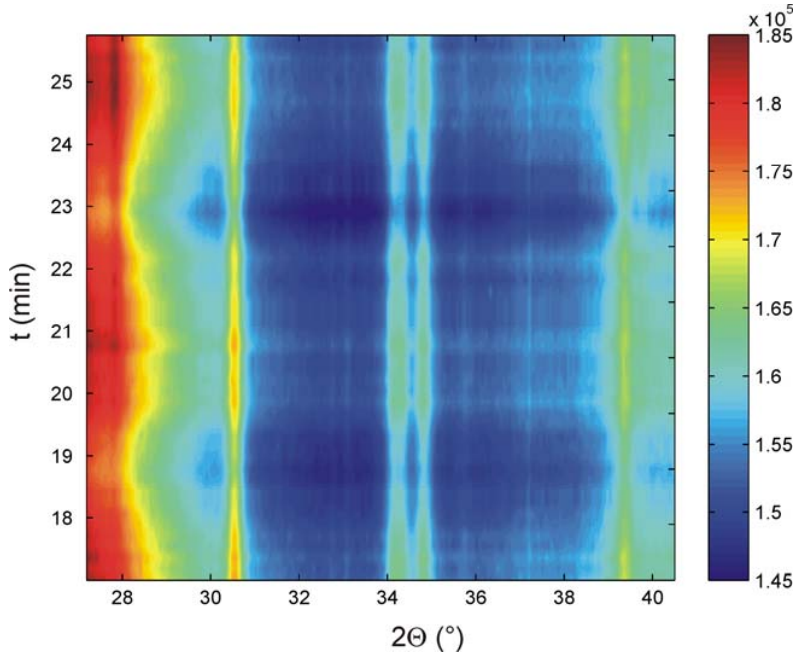

Figure S2: EXP2 done at 155 °C. The full formation of α-Li_2TiO_3 starting from anatase and rutile can be seen. The peak at 2Θ = 20.3° is not a Bragg Peak that can be associated with anatase, rutile or α-Li_2TiO_3. It does not change its relative intensity and it is probably caused by the sapphire capillary.

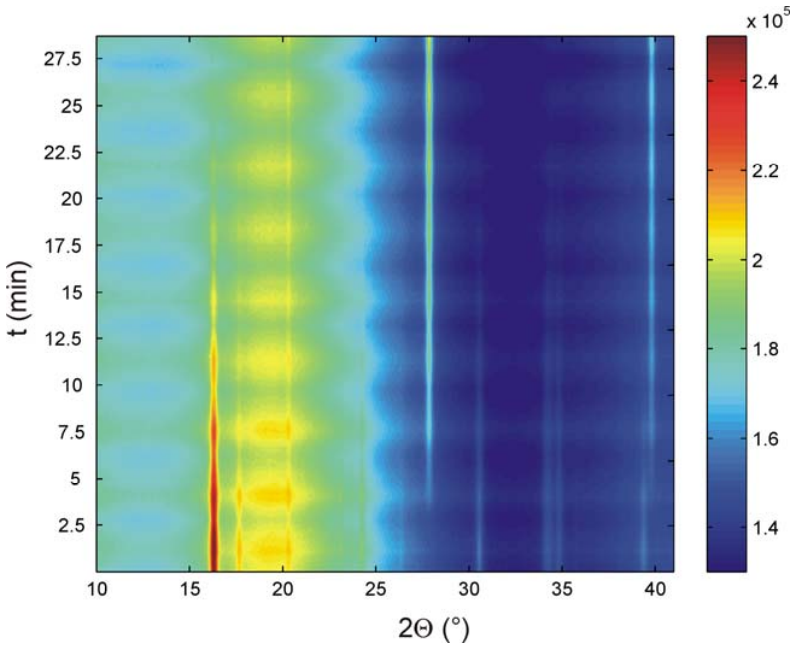

Figure S3a: EXP3 done at 168 °C and heated to 420 °C after ca. 22.5 minutes. Before heating up, the full formation of α-Li_2TiO_3 was observed and then at high temperatures, the expected transformation to β-Li_2TiO_3 started. The broad hump around 20° 2Θ is caused by the fluid phase in the capillary. Once the fluid turned supercritical, the XRPD pattern flattened. A detailed view of the temperature change is shown in Figure S3b.

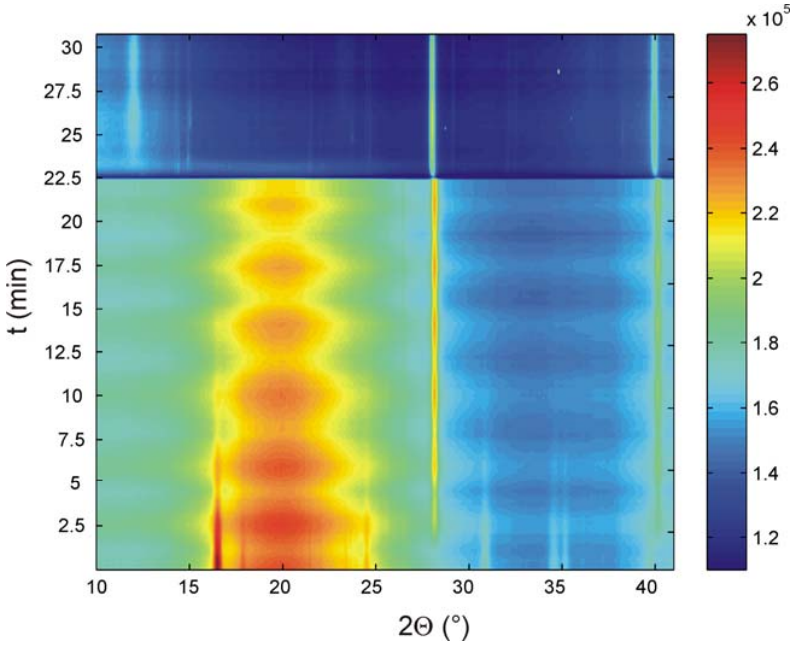

Figure S3b: Detailed view of EXP3 done at 168 °C and heated to 420 °C after about 22.5 minutes. The (002) reflection of the monoclinic β-Li_2TiO_3 is clearly visible at 11.8° 2Θ. The (-133) reflection around 2Θ = 28° which is the reflection of the second highest intensity of β-Li_2TiO_3, is superposed by the (200) reflection of α-Li_2TiO_3 (see Figure S9c).

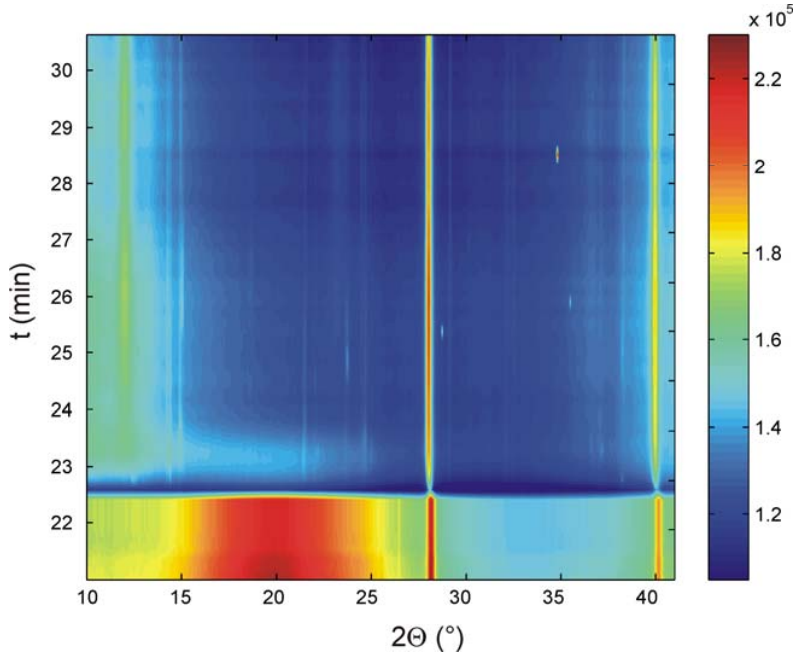

Figure S4: EXP4 done at 169 °C.

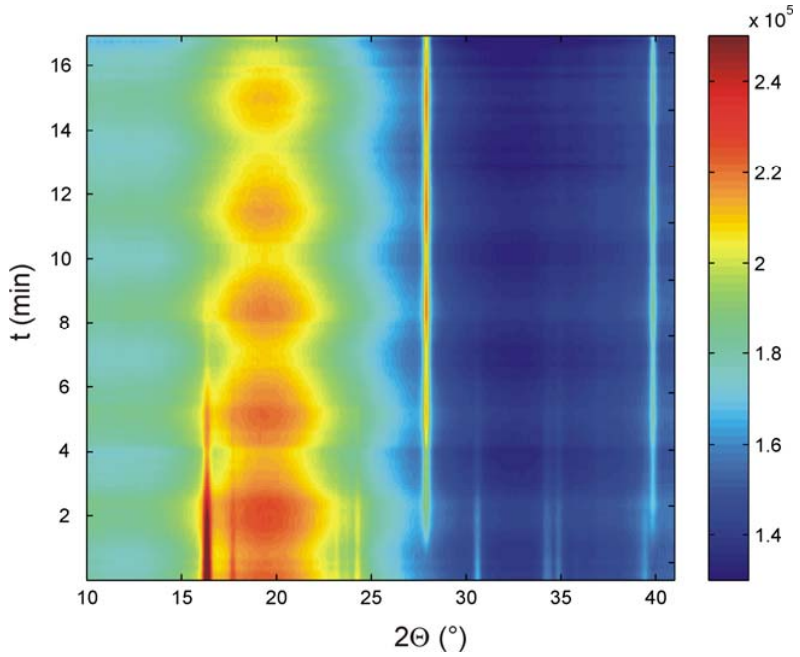

Figure S5: EXP5 done at 195 °C.

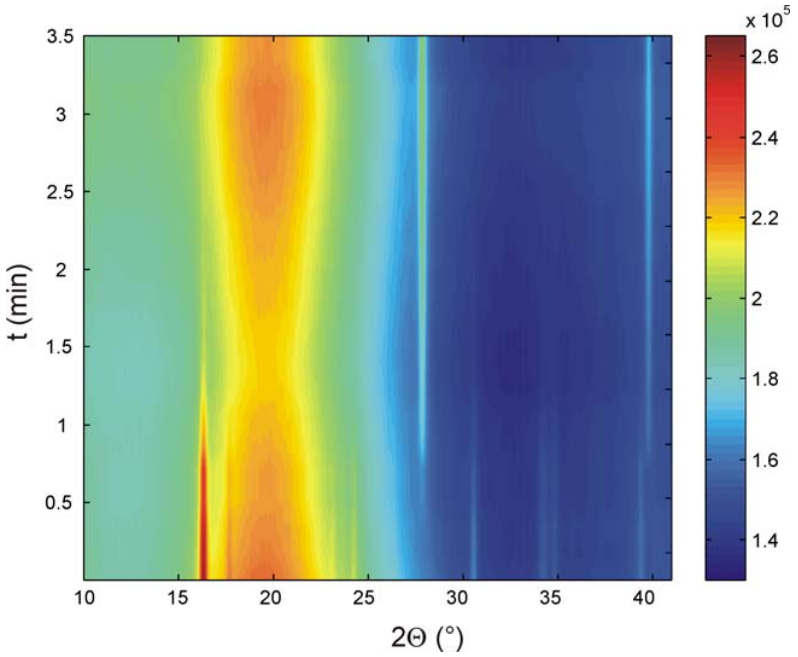

Figure S6: EXP6 done at 215 °C.

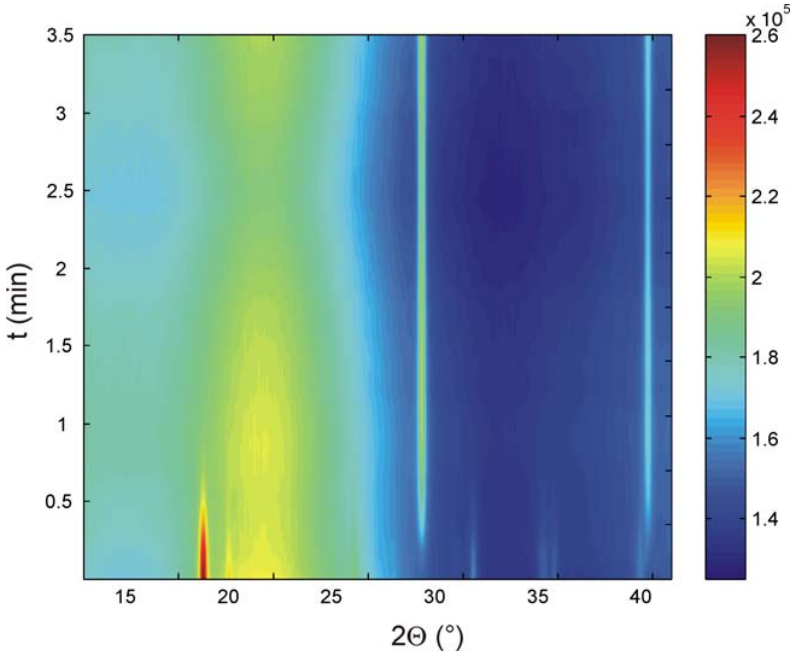

Figure S7: EXP7 done at 230 °C.

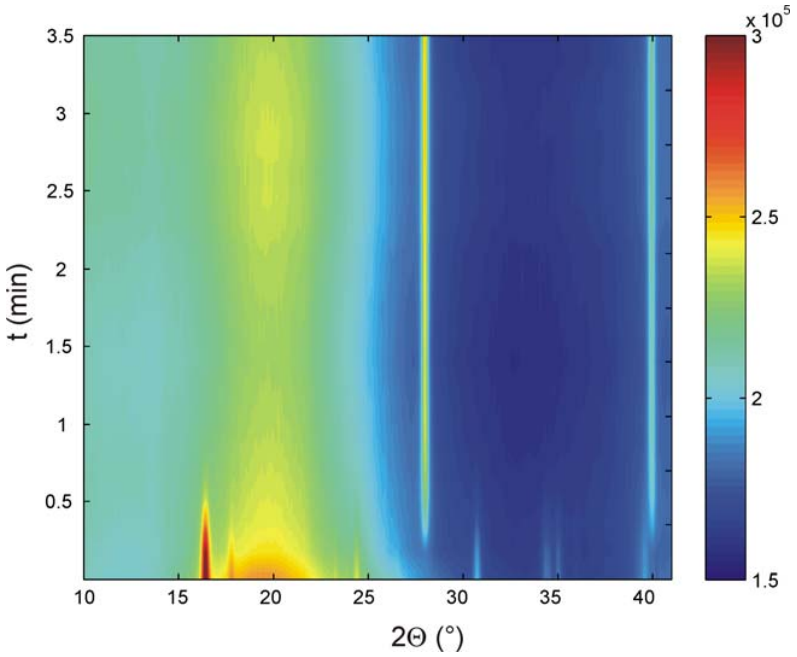

Selected examples of Rietveld refinements of EXP6 and EXP3

Figure S8a. Rietveld refinement of EXP6 done at 215 °C. The frame was recorded before the reaction started. Only reflections of anatase (green) and rutile (yellow) are visible. The red Bragg peaks index the positions where the reflections of α-Li_2TiO_3 would be expected.

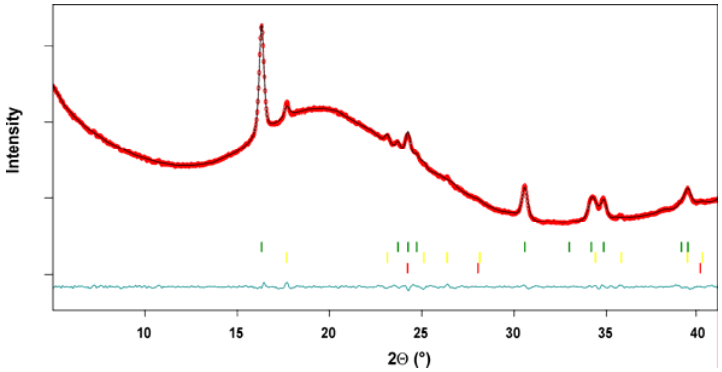

Parameters	anatase	rutile	α-Li_2TiO_3
Number of Bragg peaks	10	9	---
R_F (%)	0.697	3.49	---
a (Å)	3.78234(9)	4.5890(9)	---
c (Å)	9.4958(6)	2.9598(7)	---
Volume (Å³)	135.85(1)	62.33(2)	---
Weight fraction (%)	87(2)	13(1)	---
Number of data points: 1456; Number of refined background parameters: 50; Total number of refined parameters: 61, chi²: 1.94			

Figure S8b. Rietveld refinement of EXP6 done at 215 °C. The frame was recorded 21 seconds after the experiment started. Reflections of anatase (green), rutile (yellow) and of α-Li_2TiO_3 (red) are visible.

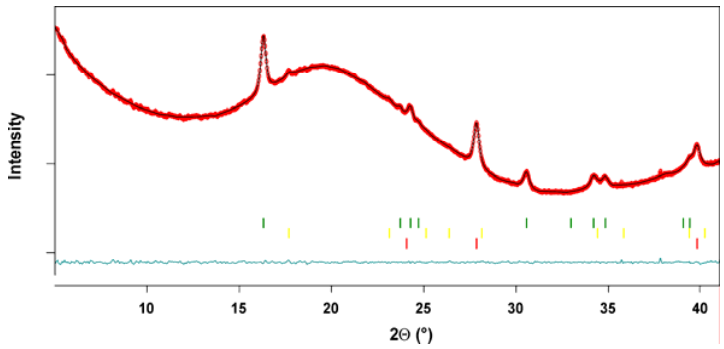

Parameters	anatase	rutile	α-Li_2TiO_3
Number of Bragg peaks	10	9	3
R_F (%)	0.301	2.73	0.528
a (Å)	3.7848(2)	4.587(2)	4.1444(1)
c (Å)	9.489(1)	2.961(2)	---
Volume (Å³)	135.92(2)	62.29(7)	71.185(3)
Weight fraction (%)	50(2)	5(1)	45(1)
Number of data points: 1456; Number of refined background parameters: 50; Total number of refined parameters: 62, chi²: 1.84			

Figure S8c. Rietveld refinement of EXP6 done at 215 °C. The frame was recorded 31.5 seconds after the experiment started. Reflections of anatase (green), rutile (yellow) and of α-Li_2TiO_3 (red) are visible. When comparing Figures S8b and S8c, the fast formation of α-Li_2TiO_3 becomes obvious, as the peak intensities of the anatase and the α-Li_2TiO_3 reflections change clearly within 10.5 seconds. The weight fraction of α-Li_2TiO_3 increases in that time from 45(1) to 70(1) % (see tables under Figures S8b and S8c).

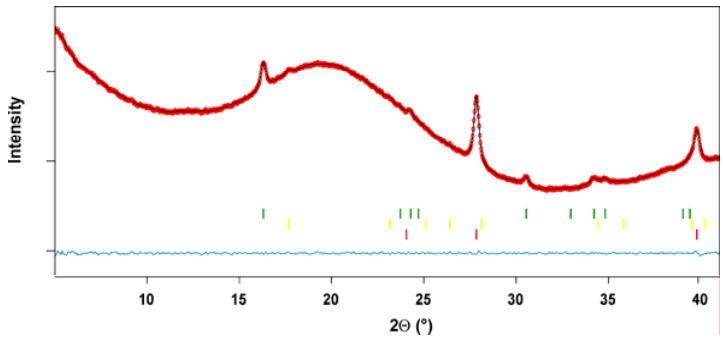

Parameters	anatase	rutile	α-Li_2TiO_3
Number of Bragg peaks	10	9	3
R_F (%)	0.418	2.26	0.169
a (Å)	3.7848(2)	4.587(2)	4.1444(1)
c (Å)	9.489(1)	2.961(2)	---
Volume (Å³)	135.90(3)	62.11(8)	71.231(2)
Weight fraction (%)	27(1)	3(1)	70(1)
Number of data points: 1456; Number of refined background parameters: 50; Total number of refined parameters: 62, chi²: 0.729			

Figure S8d. Rietveld refinement of EXP6 done at 215 °C. The frame was recorded 63 seconds after the experiment started. Only reflections of α-Li_2TiO_3 (red) are visible. The green and yellow Bragg peaks index the positions where the reflections of anatase and rutile would be expected.

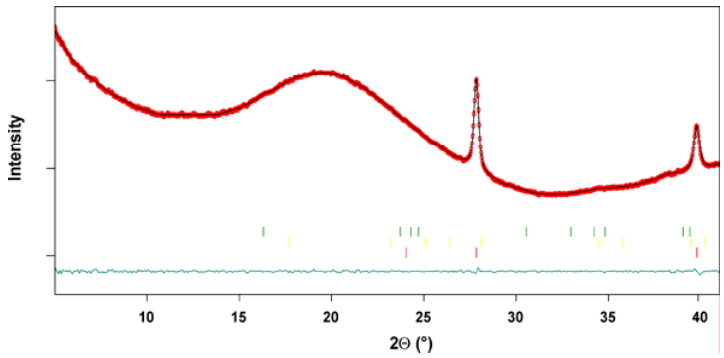

Parameters	anatase	rutile	α-Li_2TiO_3
Number of Bragg peaks	--	--	3
R_F (%)	--	--	0.117
a (Å)	--	--	4.14598(4)
c (Å)	--	--	---
Volume (Å³)	--	--	71.266(1)
Weight fraction (%)	--	--	100
Number of data points: 1456; Number of refined background parameters: 50; Total number of refined parameters: 54, chi²: 0.729			

Figure S9a. Rietveld refinement of EXP3 done at 168 °C. The frame was recorded before the reaction started. Only reflections of anatase (green) and rutile (yellow) are visible.

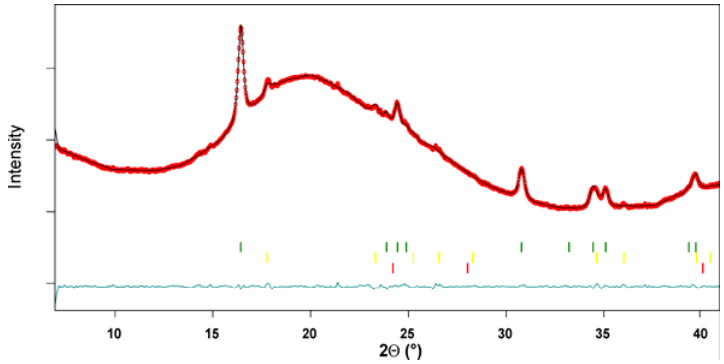

Parameters	anatase	rutile	α-Li_2TiO_3
Number of Bragg peaks	10	9	--
R_F (%)	0.758	3.16	--
a (Å)	3.7566(3)	4.562(1)	--
c (Å)	9.4225(8)	2.934(1)	--
Volume (Å³)	135.97(2)	61.08(3)	--
Weight fraction (%)	82(1)	18(1)	--
Number of data points: 1456; Number of refined background parameters: 38; Total number of refined parameters: 47, chi²: 0.729			

Figure S9b. Rietveld refinement of EXP3 done at 168 °C. The frame was recorded 13.5 minutes after the experiment started. Minor reflections of anatase (green) are still visible. The intensity of the rutile peaks (yellow) is at the detection limit. The main fraction is α-Li_2TiO_3 (red).

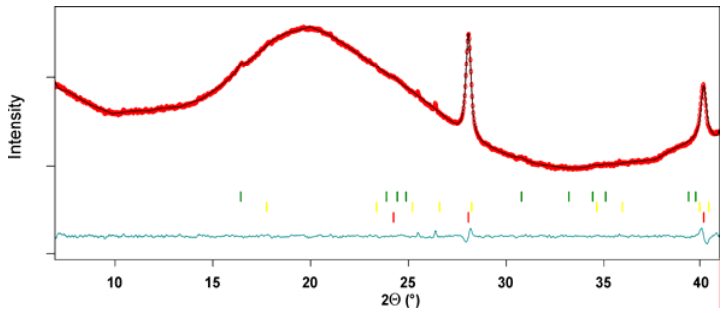

Parameters	anatase	rutile	α-Li_2TiO_3
Number of Bragg peaks	10	9	3
R_F (%)	4.36	17.0	0.168
a (Å)	3.75*	4.57*	4.11323(6)
c (Å)	9.43*	2.92*	---
Volume (Å³)	133.08	61.09	69.591(2)
Weight fraction (%)	4(1)	1(1)	95(2)
Number of data points: 1456; Number of refined background parameters: 50; Total number of refined parameters: 62, chi²: 0.729 * Structural parameters of anatase and rutile had to be fixed due to their low fraction. Especially the R_F factor of rutile shows that these values are not very reliable.			

Figure S9c. Rietveld refinement of EXP3 done at 420 °C (after prior heating to 168 °C). The frame was recorded after ca. 30 minutes. The broad main reflection at 2Θ = 11.8° and reflections of low intensity of β-Li_2TiO_3 (blue) are visible besides the peaks of α-Li_2TiO_3 (red).

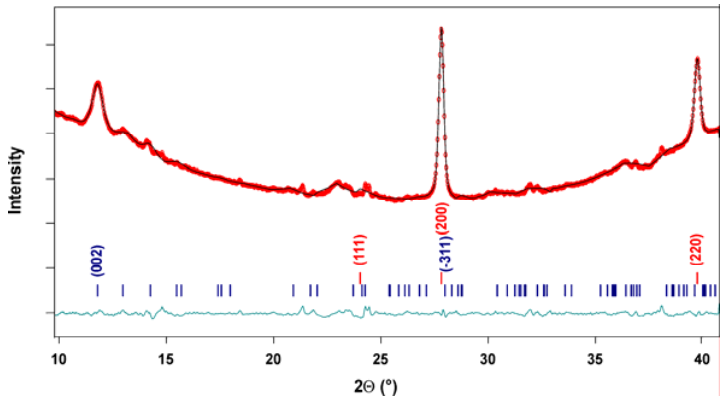

Parameters	α-Li_2TiO_3	β-Li_2TiO_3
Number of Bragg peaks	10	9
R_F (%)	0.798	1.27
a (Å)	4.1490(3)	4.140(3)
b (Å)	--	8.828(4)
c (Å)	--	9.853(5)
Angle β		99.78*
Volume (Å³)	71.423(8)	354.9(4)
Weight fraction (%)	47(1)	53(2)
Number of data points: 1456; Number of refined background parameters: 35; Total number of refined parameters: 44, chi²: 4.94 * Refinement of the β angle was not possible.		

Additional comment

Minor displacements of the sapphire capillary caused variations of the unit cell parameters within an error of 1%, e.g. the unit cell parameter of a = 4.11323(6) Å in EXP 3 and of a = 4.14598(4) Å in EXP6. The higher unit cell parameter of a = 4.1490(3) Å at 420 °C in EXP3 is due to the expected thermal expansion of the material at higher temperatures.

Supplementary material 2

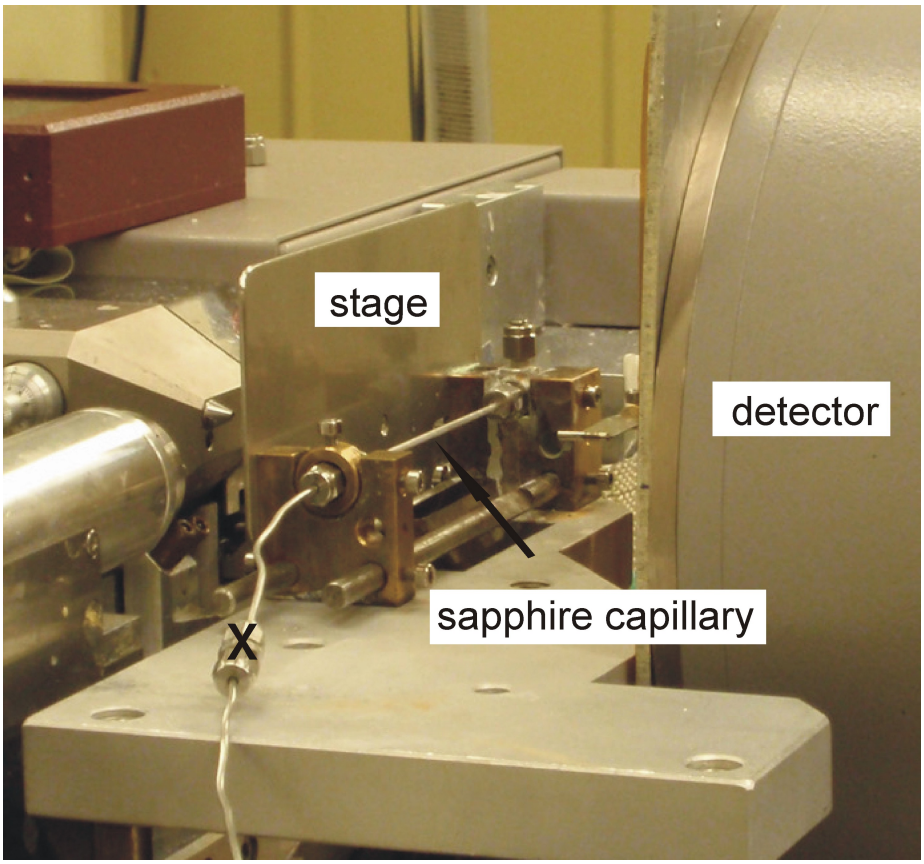

Figure C.1: Setup for the *in-situ* experiments at the synchrotron Lund. The reaction happens in the sapphire capillary, which the synchrotron beam has to pass through before it reaches the detector. At the mark (X) the suspension comprising P25 and the lithium hydroxide solution is injected. Then the system is closed, pressurized to 250 *bar* and heated to the desired temperature.

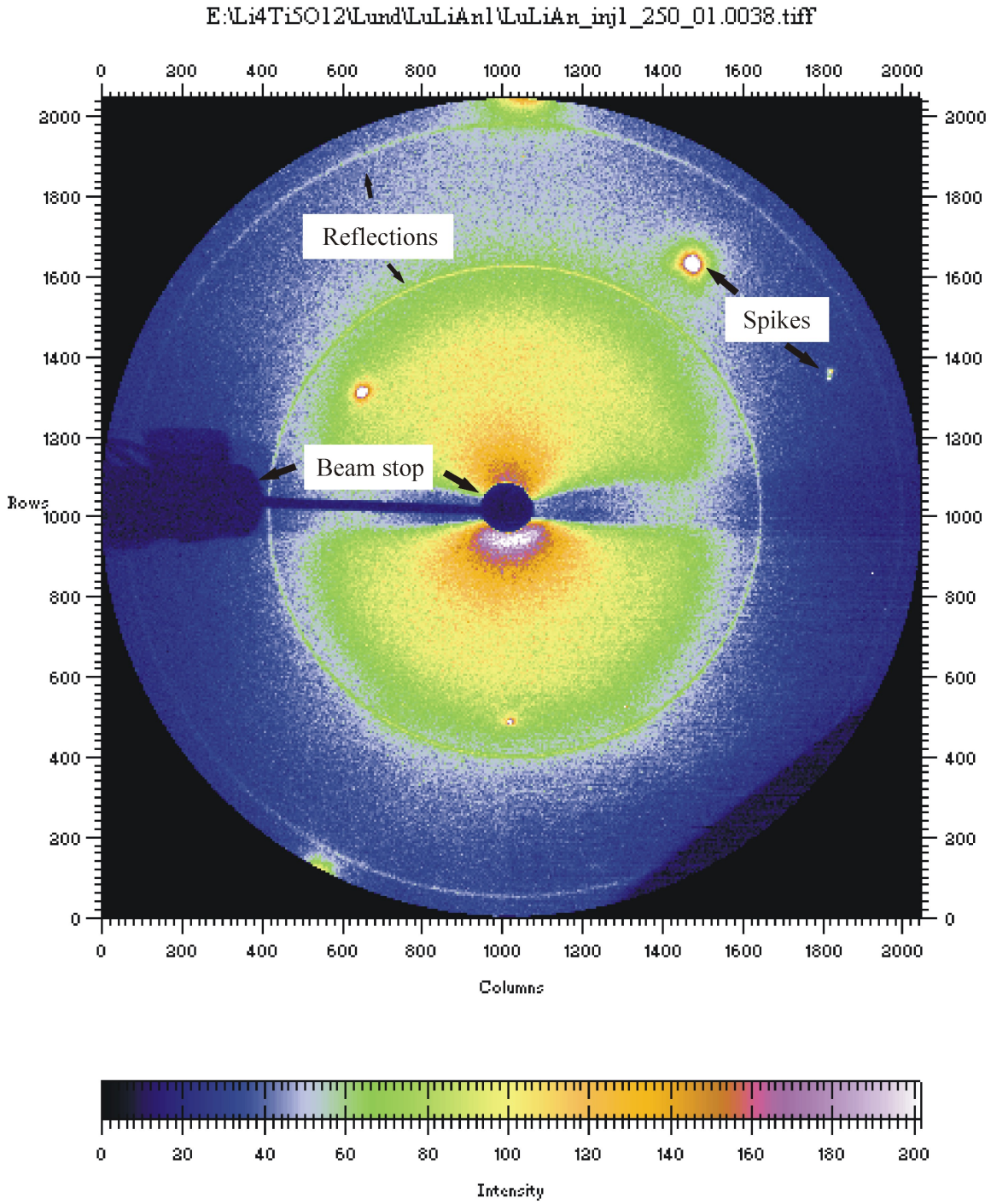

Figure C.2: 2D exposure of a single synchrotron X-ray pattern. Before a useful application of the data is possible, the exposures had to be masked carefully to subtract troublesome noise like the area of the beam-stop or spikes caused by the sapphire capillary.

Appendix D

Patent

Process for producing lithium titanium spinel and use thereof

WO 2009/146904 A1

Michael Holzapfel, Andreas Laumann, Gerhard Nuspl, Karl Thomas Fehr, Florian Kiefer

(12) NACH DEM VERTRAG ÜBER DIE INTERNATIONALE ZUSAMMENARBEIT AUF DEM GEBIET DES PATENTWESENS (PCT) VERÖFFENTLICHTE INTERNATIONALE ANMELDUNG

(19) Weltorganisation für geistiges Eigentum
Internationales Büro

(43) Internationales Veröffentlichungsdatum
10. Dezember 2009 (10.12.2009)

PCT

(10) Internationale Veröffentlichungsnummer
WO 2009/146904 A1

(51) Internationale Patentklassifikation:
C01G 23/00 (2006.01) *H01M 4/02* (2006.01)

(21) Internationales Aktenzeichen: PCT/EP2009/003972

(22) Internationales Anmeldedatum:
3. Juni 2009 (03.06.2009)

(25) Einreichungssprache: Deutsch

(26) Veröffentlichungssprache: Deutsch

(30) Angaben zur Priorität:
10 2008 026 580.2 3. Juni 2008 (03.06.2008) DE

(71) Anmelder *(für alle Bestimmungsstaaten mit Ausnahme von US)*: **SÜD-CHEMIE AG** [DE/DE]; Lenbachplatz 6, 80333 München (DE).

(72) Erfinder; und

(75) Erfinder/Anmelder *(nur für US)*: **HOLZAPFEL, Michael** [DE/DE]; Seydlitzstrasse 25, 80992 München (DE). **LAUMANN, Andreas** [DE/DE]; Guido-Schneble-Str. 63, 80689 München (DE). **NUSPL, Gerhard** [DE/DE]; Kolumbusstr. 6, 81543 München (DE). **FEHR, Karl** [DE/DE]; Valleystr. 44, 81371 München (DE). **KIEFER, Florian** [DE/DE]; Kurfürstenstr. 26, 80801 München (DE).

(74) Anwälte: **STOLMÁR, Matthias** et al.; Stolmár Scheele & Partner, Blumenstrasse 17, 80331 München (DE).

(81) Bestimmungsstaaten *(soweit nicht anders angegeben, für jede verfügbare nationale Schutzrechtsart)*: AE, AG, AL, AM, AO, AT, AU, AZ, BA, BB, BG, BH, BR, BW, BY, BZ, CA, CH, CL, CN, CO, CR, CU, CZ, DE, DK, DM, DO, DZ, EC, EE, EG, ES, FI, GB, GD, GE, GH, GM, GT, HN, HR, HU, ID, IL, IN, IS, JP, KE, KG, KM, KN, KP, KR, KZ, LA, LC, LK, LR, LS, LT, LU, LY, MA, MD, ME, MG, MK, MN, MW, MX, MY, MZ, NA, NG, NI, NO, NZ, OM, PG, PH, PL, PT, RO, RS, RU, SC, SD, SE, SG, SK, SL, SM, ST, SV, SY, TJ, TM, TN, TR, TT, TZ, UA, UG, US, UZ, VC, VN, ZA, ZM, ZW.

(84) Bestimmungsstaaten *(soweit nicht anders angegeben, für jede verfügbare regionale Schutzrechtsart)*: ARIPO (BW, GH, GM, KE, LS, MW, MZ, NA, SD, SL, SZ, TZ, UG, ZM, ZW), eurasisches (AM, AZ, BY, KG, KZ, MD, RU, TJ, TM), europäisches (AT, BE, BG, CH, CY, CZ, DE, DK, EE, ES, FI, FR, GB, GR, HR, HU, IE, IS, IT, LT, LU, LV, MC, MK, MT, NL, NO, PL, PT, RO, SE, SI, SK, TR), OAPI (BF, BJ, CF, CG, CI, CM, GA, GN, GQ, GW, ML, MR, NE, SN, TD, TG).

Veröffentlicht:

— *mit internationalem Recherchenbericht (Artikel 21 Absatz 3)*

(54) Title: PROCESS FOR PRODUCING LITHIUM TITANIUM SPINEL AND USE THEREOF

(54) Bezeichnung: VERFAHREN ZUR HERSTELLUNG VON LITHIUMTITAN-SPINELL UND DESSEN VERWENDUNG

Figur 1

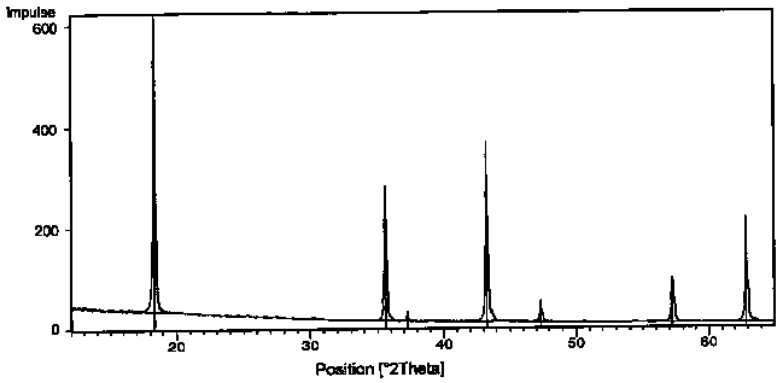

(57) Abstract: The present invention relates to undoped and doped lithium titanate $Li_4Ti_5O_{12}$ which is obtainable by the thermal reaction of a stoichiometric composite oxide containing Li_2TiO_3 and TiO_2, to the production of the stoichiometric composite oxide, and also to a process for producing lithium titanate $Li_4Ti_5O_{12}$ and use thereof as anode material in rechargeable lithium-ion batteries.

(57) Zusammenfassung: Die vorliegende Erfindung betrifft nicht-dotiertes und dotiertes Lithiumtitanat $Li_4Ti_5O_{12}$ erhältlich durch die thermische Umsetzung eines stöchiometrischen Kompositoxides enthaltend Li_2TiO_3 und TiO_2, die Herstellung des stöchiometrischen Kompositoxides sowie ein Verfahren zur Herstellung von Lithiumtitanat $Li_4Ti_5O_{12}$ und dessen Verwendung als Anodenmaterial in wiederauf ladbaren Lithium-Ionen-Batterien.

WO 2009/146904 A1

Appendix E

Fourth publication

DC and AC conductivity of $Li_{4/3}Ti_{5/3}O_4$ spinel

Solid State Ionics **181** 1111–1118 (2010)

Karl Thomas Fehr,[a] **Michael Holzapfel,**[b] **Andreas Laumann,**[a] **Elmar Schmidbauer**[c]

[a] Ludwig-Maximilians-Universität München, Department of Earth and Environmental Sciences, Section for Mineralogy, Petrology and Geochemistry, Munich, Germany
[b] Süd-Chemie AG, Battery Materials, Moosburg, Germany
[c] Ludwig-Maximilians-Universität München, Department of Earth and Environmental Sciences, Section for Geophysics, Munich, Germany

Solid State Ionics 181 (2010) 1111–1118

Contents lists available at ScienceDirect

Solid State Ionics

journal homepage: www.elsevier.com/locate/ssi

DC and AC conductivity of $Li_{4/3}Ti_{5/3}O_4$ spinel

K.T. Fehr [a], M. Holzapfel [b], A. Laumann [a], E. Schmidbauer [c,*]

[a] Department für Geo- und Umweltwissenschaften, Mineralogie, Petrologie und Geochemie, Universität München, Theresienstr 41, 80333 München, Germany
[b] Süd-Chemie AG, Ostenriederstr. 15, 85268 Moosburg, Germany
[c] Department für Geo- und Umweltwissenschaften, Geophysik, Universität München, Theresienstr 41, 80333 München, Germany

ARTICLE INFO

Article history:
Received 18 November 2009
Received in revised form 21 May 2010
Accepted 24 May 2010

Keywords:
Impedance specctroscopy
Ionic Li^+ conduction
$Li_{4/3}Ti_{5/3}O_4$ spinel

ABSTRACT

The electrical conductivity of polycrystalline $Li_{4/3}Ti_{5/3}O_4$ is reported between ~300 K and ~1000 K. Sintered and commercial pressed pellets were used for measurements. Impedance spectroscopy was applied (20 Hz–1 MHz) to determine the DC conductivity σ_{DC} and AC conductivity σ_{AC}. Anomalies of σ_{DC} were observed at higher temperatures as a consequence of presumed order–disorder phase transitions, coupled to diffusion of Li^+ between various spinel sites, as concluded in earlier work. There was a broad transitional region of σ_{DC} in this temperature range characterized by varying differential activation energies E_A. For sintered pellets, consisting of ~0.8–1.5 μm grains, after run 1 up to ~960 K, E_A values were E_A ~0.80 eV above ~740 K and E_A ~0.57 eV below ~500 K for effective σ_{DC} deduced from the sum of bulk and grain boundary resistivities, while in the transitional temperature range the values were lower with the data taken under flowing N_2. Typically, $\sigma_{DC}(500\ K) \sim 10^{-4}$–$10^{-6}\ \Omega^{-1}\ cm^{-1}$ and $\sigma_{DC}(300\ K) \sim 3 \times 10^{-10}\ \Omega^{-1}\ cm^{-1}$; predominant conduction is due to ionic Li^+ charge transport. For commercial ~0.1–0.3 μm grain pellets, after run 1 up, the respective values were E_A ~0.87 eV above ~800 K and E_A ~0.61 eV between 495 K and 380 K. Below ~620 K, for both materials bulk σ_{DC} could be determined, which is a factor of 3–10 above the effective σ_{DC}. For the frequency dependence of σ_{AC} of commercial $Li_{4/3}Ti_{5/3}O_4$, a power law behaviour was established between 349 and 443 K. Applying DC voltage measurements, for sintered $Li_{4/3}Ti_{5/3}O_4$ the electronic fraction of σ_{DC} was estimated to be <~1% of the ionic fraction between 465 and 830 K.

1. Introduction

In recent times interest has focussed on $Li_{4/3}Ti_{5/3}O_4$ as anode material for rechargeable Li-batteries [1–11]. It is a zero-strain Li^+ insertion host, which enables long cycle life during charge–discharge cycles. For high battery performance, apart of Li^+ ionic conduction, sufficient electronic conduction is required. One disadvantage of $Li_{4/3}Ti_{5/3}O_4$ is its low electronic conductivity. In order to improve the anode quality, the microstructural morphology of $Li_{4/3}Ti_{5/3}O_4$ grains is being optimized including thin films, and, apart from adding electronically conductive material, doping of $Li_{4/3}Ti_{5/3}O_4$ is attempted to enhance electronic conduction [8,9,11,12]. Electrical conductivity above ambient temperature is not of direct interest for Li-battery applications; only a few papers have been published and no satisfying analysis appears to have been made. DC and AC conductivity properties in that temperature range are the objective of this study.

The ionic Li^+ conduction is controlled by the lattice structure. The cation distribution in the cubic spinel $Li_{4/3}Ti_{5/3}O_4$ (space group Fd3m) is $(Li)[Li_{1/3}Ti_{5/3}]O_4$ with the Li in round brackets on tetrahedral (8a) sites and cations in square brackets on octahedral (16d) sites of the lattice [13,14]. In $Li_{4/3}Ti_{5/3}O_4$ at room temperature, one-eighth of the (8a) and one-half of the (16d) positions are occupied by cations, while at higher temperatures Li^+ reside temporarily in part on the interstitional octahedral (16c) and the tetrahedral (48f) sites, normally not occupied by cations. The unit cell parameter of $Li_{4/3}Ti_{5/3}O_4$ was found to be between $a_0 = 0.83538$ and 0.837 nm [1,4,13–16]. $Li_{4/3}Ti_{5/3}O_4$ is presumed to undergo two successive order–disorder phase transitions at higher temperatures, as a consequence of different distributions of Li^+ and cation vacancies (□), (1) to an ordered NaCl-type defect structure (Fd3m) and (2) to a disordered one at still higher temperatures (Fm3m), of the kind $(Li)_{8a}[Li_{1/3}Ti_{5/3}]_{16d}O_4 \rightarrow [Li□]_{16c}[Li_{1/3}Ti_{5/3}]_{16d}O_4 \rightarrow [Li_{4/3}□_{2/3}]_{16c}[Ti_{5/3}□_{1/3}]_{16d}O_4$, inferred from DTA, Raman spectra and electrical conductivity data [16]. $[Li□]_{16c}$ indicates full order of Li and □ on (16c) sites, while $[Li_{4/3}□_{2/3}]_{16c}$ means total disorder. These transitions are in analogy to Li^+ order–disorder processes at high temperatures in spinels of composition Li_2MCl_4 (M = Mg, Mn, Co) [17–20]. The diffusion of Li^+ in $Li_{4/3}Ti_{5/3}O_4$ at lower temperatures is thought to proceed either via the mechanism $Li^+_{8a} \rightarrow □_{16c} \rightarrow □_{8a}$ or $Li^+_{16c} \rightarrow □_{8a} \rightarrow □_{16c}$ in the intermediate phase. In the high-temperature phase, Li^+ also may migrate via $Li^+_{16c} \rightarrow □_{48f} \rightarrow □_{16c}$ [16]; further, a path $Li^+_{8a} \rightarrow □_{16c} \rightarrow □_{48f} \rightarrow □_{16d}$ was presumed [21]. Analysis of $Li_{4/3}Ti_{5/3}O_4$ IR spectra showed the Li^+_{8a} to migrate increasingly to (16c) positions up to

* Corresponding author. Tel.: +49 8921804212; fax: +49 8921804205.
E-mail address: schmidba@geophysik.uni-muenchen.de (E. Schmidbauer).

0167-2738/$ – see front matter © 2010 Elsevier B.V. All rights reserved.
doi:10.1016/j.ssi.2010.05.026

483 K [22]; the same process was inferred from Raman spectra at higher temperatures [16].

In the literature, for DC conductivity σ_{DC} of $Li_{4/3}Ti_{5/3}O_4$ in a large temperature range, varying results were reported as well as breaks in the log σ_{DC}–1/T curve. Similar results were observed earlier for spinels Li_2MCl_4 (M = Mg,Mn,Fe,Co,Cd,Ti,Zn) [23–27]. For $Li_{4/3}Ti_{5/3}O_4$, at higher temperatures a variation of conductivities were observed by several authors. Some results are presented in Table 1, where for log σ_{DC}–1/T curves activation energies E_A in different temperature ranges are given, breaks or no breaks and σ_{DC} at room temperature. As visible from Table 1, values of the ionic fraction of σ_{DC} at room temperature range from 2.5×10^{-7} to $\sim10^{-9}\ \Omega^{-1}\ cm^{-1}$. For pressed pellets of commercial $Li_{4/3}Ti_{5/3}O_4$ powder (Titan Kogyo, Japan) (grain size ~0.5 μm), the AC conductivity σ_{AC} as function of frequency could be fitted using a power law [21]. For the electronic fraction of σ_{DC} at room temperature it was reported $\sim8\times10^{-10}\ \Omega^{-1}\ cm^{-1}$ from DC measurements [11] and $<10^{-13}\ \Omega^{-1}\ cm^{-1}$ [31], and for $Li_{1.32}Ti_{1.67}O_{3.99}$ it was $3.9\times10^{-9}\ \Omega^{-1}\ cm^{-1}$ [9]. From the above data, certain discrepancies between electrical properties are obvious among the cited authors, which appear to depend on $Li_{4/3}Ti_{5/3}O_4$ preparation conditions and impurities, leading evidently to a variation in particle size and microstructure and, in addition, the results are likely to depend to some degree on the experimental setup.

It is therefore the aim of this study to determine electrical conduction in $Li_{4/3}Ti_{5/3}O_4$ pellets in a large temperature range by applying impedance spectroscopy. A combination of DC and AC conductivity data is expected to supply information on bulk and surface charge transport processes, also of interest for room temperature properties, and to elucidate certain inconsistencies of literature results.

2. Experimental and measurement methods

Two kinds of $Li_{4/3}Ti_{5/3}O_4$ samples were used for electrical measurements, one prepared by a ceramic processing technique (sample A) and pressed commercial powder (sample B). For preparation of sample A, powders of Li_2CO_3 (suprapure, Johnson-Matthey) and TiO_2 (99.99%, Aldrich) in proper portions were mixed in a ball mill in acetone. After drying, the mixture was pelletized and precalcined at 873 K for 10 h under air. The product was reground, pelletized (1.5 kbar) and heated twice at 1073 K for 24 h under air followed by slow cooling. X-ray analysis showed a pure spinel structure. Sample B was a commercial $Li_{4/3}Ti_{5/3}O_4$ EXM1979 powder from Süd-Chemie AG (Moosburg, Germany). Powder characteristics, as provided by the company, were: BET surface area 10 m^2/g, primary grain size 0.1–0.3 μm, impurity Fe (<200 mg/kg). For sintered $Li_{4/3}Ti_{5/3}O_4$ (sample A) primary grain size of 0.8–1.5 μm was observed.

X-ray powder diffraction patterns were recorded on a Stoe diffractometer (CuK_α-radiation, Ge monochromator). Fig. 1 displays the X-ray powder diffractogram of sample A, from which the unit cell parameter $a_0 = 0.83614$ nm was derived; this value is halfway between the above mentioned two extremes of literature data. For the commercial sample B, a diffractogram as that of Fig. 1 was provided by Süd-Chemie AG. Any impurity phases present to <~2% such as TiO_2 (anatase or rutile) are below detection by this technique. In order to test possible phase transitions at higher temperatures, differential scanning calorimetry DSC was applied on a Pegasus DSC 404C (Netzsch) calorimeter with the sample heated in Ar from ambient temperature to 1070 K up and down at a rate of 3 K/min; no λ-shaped transitions were observed indicating the absence of first-order phase transitions. AC impedance measurements were performed with the help of a Hewlett-Packard LCR-meter (4284A) which operated in the frequency range of 20 Hz–1 MHz; 1 V and 60 mV r.m.s. were applied to the electrodes. In addition, DC voltage measurements were performed at higher temperatures in order to gain some data points of the electronic fraction of σ_{DC}. The sample cell was inserted in a tube furnace for high-temperature measurements. For impedance studies above ambient temperature, after each temperature advance (20 K) 30 min were allowed for sample temperature equilibration. For electrical measurements, sintered samples were present as pellets, while commercial powder had to be pelletized (1.5 kbar). Both kinds of samples were disks 4 or 6 mm in diameter and 1 to 4 mm in thickness. Electrical contacts were made with Pt-powder and/or Ag-paint. Measurements were performed under flowing N_2 in order to avoid the possible influence of humidity at low temperatures. However, some high-temperature data also were taken under Ar and air.

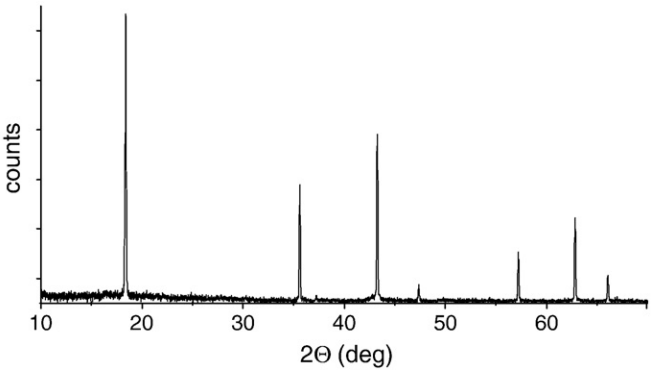

Fig. 1. X-ray powder diffractogram of sintered $Li_{4/3}Ti_{5/3}O_4$ (sample A).

Table 1
DC conductivity σ_{DC} at room temperature, activation energies E_A at various temperatures and number of breaks in the log σ_{DC}–1/T curve for $Li_{4/3}Ti_{5/3}O_4$, as derived by several authors.

E_A (eV)	T-range (K)	Break	σ_{DC} ($\Omega^{-1}\ cm^{-1}$)	Authors
0.51	<625	One	$\sim6.8\times10^{-8}$	[28]
0.73	~600–830	No	–	[29]
0.47	~360–500	No	–	[6]
0.51	~385–870	No	–	[7]
0.48	359–504	Two breaks	3×10^{-8}	[30]
0.42	504–736			[30]
0.80	736–975			[30]
~0.3–1.4	~590–870	Two breaks	$\sim10^{-9}$	[16]
0.94	~590–870	No	1.3×10^{-7} (433 K)	[21]
–	–	–	2.5×10^{-7}	[9]
–	–	–	$\sim3\times10^{-8}$	[11]
0.84	~320–~620	No	–	[47]

3. Electrical properties

Fig. 2 displays complex plane impedance plots for sintered $Li_{4/3}Ti_{5/3}O_4$ (sample A) on heating and cooling during run 1, under flowing N_2, up to a maximum of 530 K (Pt-powder contacts), well below the presumed transition temperature to the NaCl-structure with ordered $\square_{16c}$ (Fd3m), suggested to take place at ~800 K [16]. In that low-T range, bulk ionic Li^+ diffusion occurs primarily via $Li^+_{8a} \rightarrow \square_{16c} \rightarrow \square_{8a}$ as found from Raman and IR analysis [6,14]. At 391 K, a broad depressed high-frequency semicircular arc is observed and there is obviously a superposed smaller low-frequency arc; at 431 K, both arcs are clearly separated. The high-frequency arc next to the coordinate origin reflects bulk conduction. A rough evaluation for that arc gives a capacitance of $C_p \sim 3$ pF/cm related to the charge transport mechanism, associated with the arc; such a low capacitance is typical of bulk conduction. For the low-frequency arc it follows $C_p \sim 200$ pF/cm; this arc is obviously due to grain boundary processes, because interfacial contact layer/electrode effects are as a rule associated with a capacitance of $\sim10^5$–10^6 pF/cm [32]. Up to 491 K both arcs remain, while at the lowest frequencies a so called spike develops (Warburg response), characteristic of ionic conduction when blocking metallic electrodes are used. At high temperatures, the available frequency window was too small to allow measurements to be done to the coordinate origin. In principle, the electronic fraction of conduction

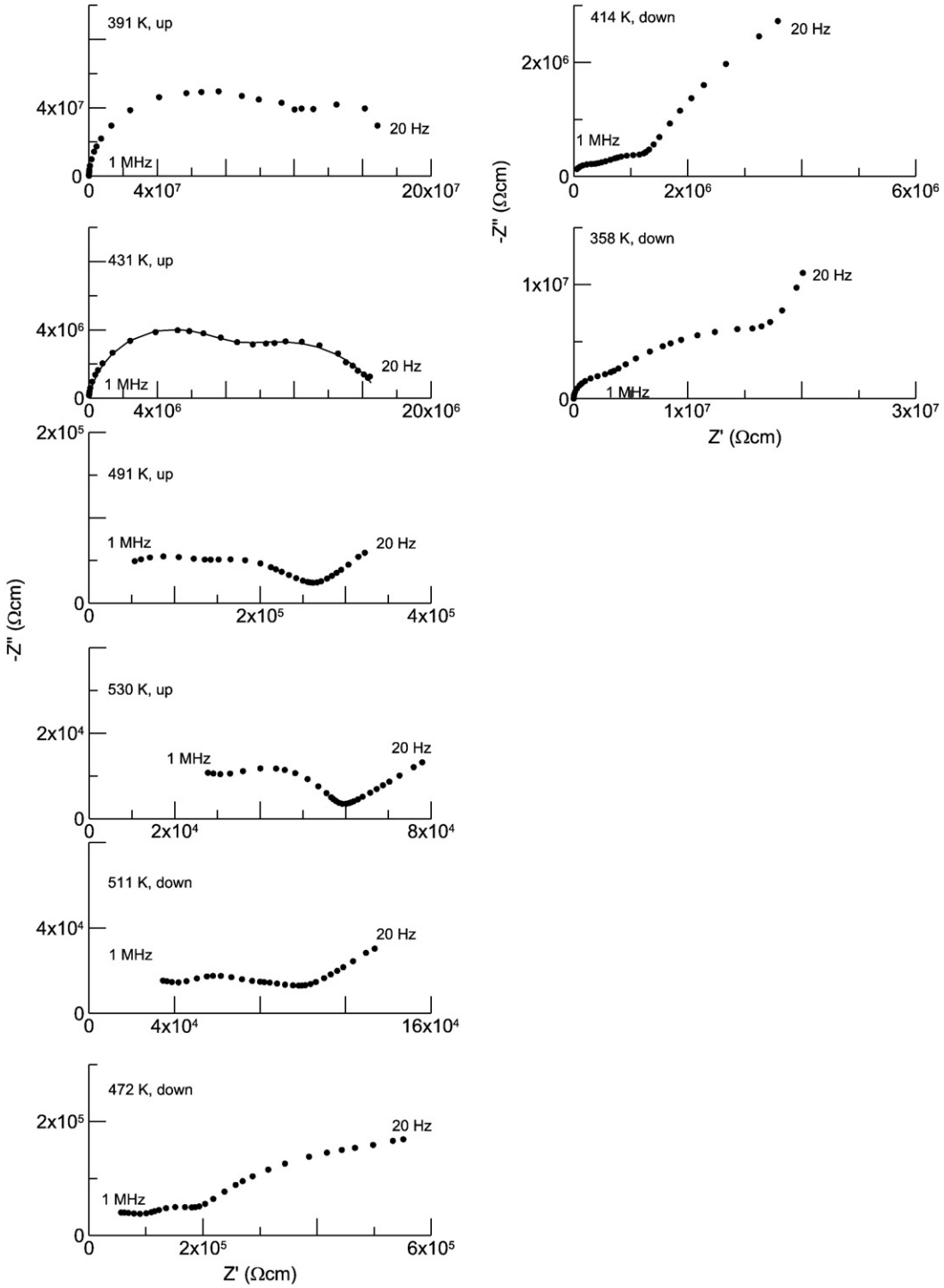

Fig. 2. Complex plane impedance plots for sample A; heating and cooling during run 1, under N_2, up to a maximum of 530 K.

can be involved in the shape of the impedance spectra at higher temperatures. Judging from the small room temperature electronic fraction of σ_{DC} according to literature data, we presume the same at high temperatures; this is substantiated by data shown below. From an arc, the DC resistivity can be determined by extrapolating to zero frequency and reading off the intersection with the Z′ axis. The fact that both arcs are weakly separated is indicative of similar relaxation times related to the charge transport mechanisms.

As no clear separation between high- and low-frequency arcs can be made at higher temperatures, only the sum of both resistivities can be determined, resulting in effective σ_{DC}. In order to check at moderate temperatures the individual fraction of bulk and grain boundary σ_{DC}, derived from the high- and low-frequency arcs, respectively, fits were made to a series of impedance spectra. An equivalent circuit was used consisting for each arc of a resistance in parallel to a constant phase CPE element (ZARC) and both are acting in series; the complex non-linear least squares fitting routine LEVMW was applied [33]. For the spectrum taken at 431 K during run 1 up to ~530 K, the solid line gives the result of fitting. On heating up to 960 K and subsequent cooling during run 2, spectra appear as depicted in Fig. 3. No essential differences at lower temperatures are seen relative to Fig. 2, at higher temperatures only effective values of σ_{DC} can be gained from the sum of resistivities of high-

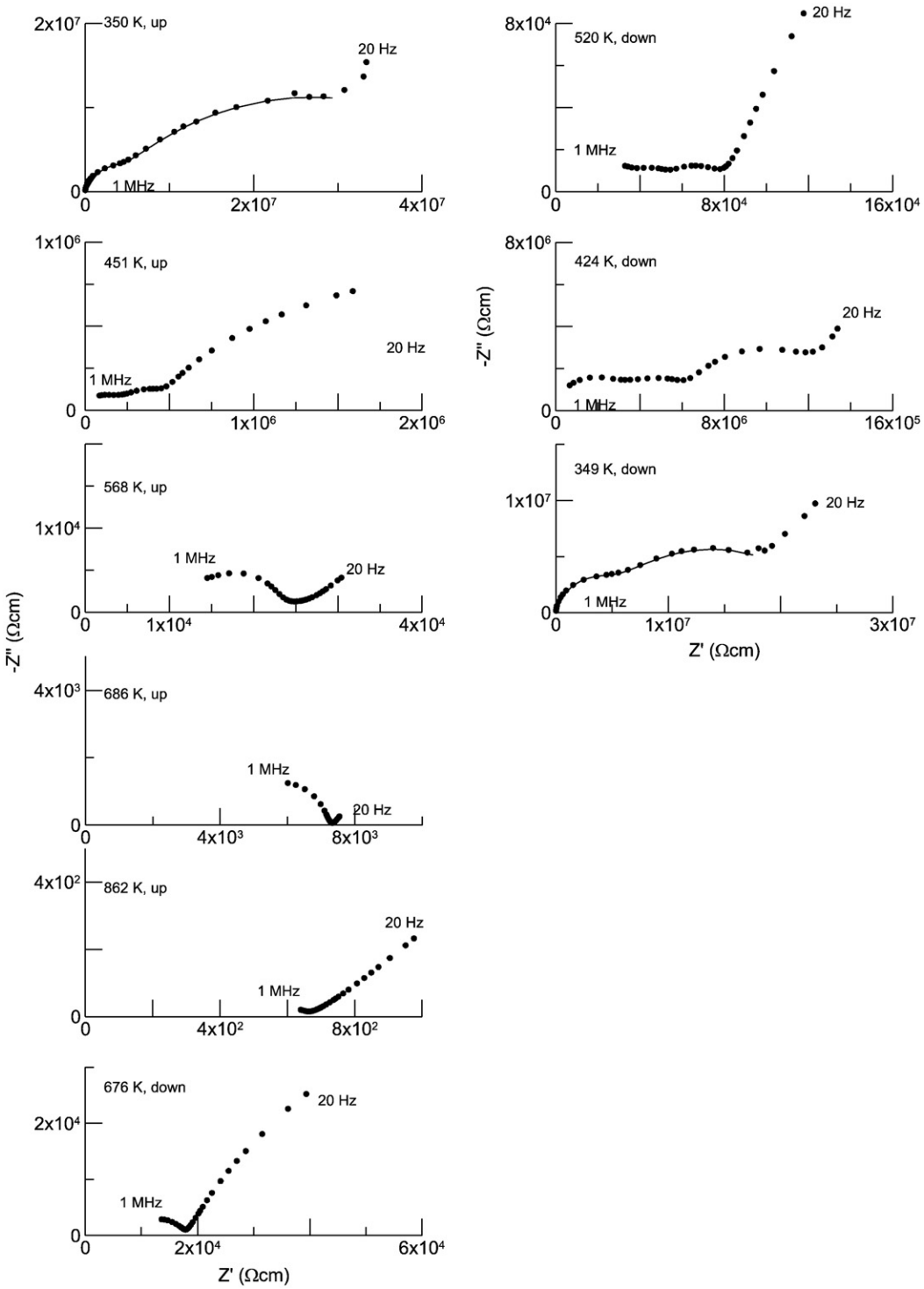

Fig. 3. Complex plane impedance plots for sample A; heating and cooling during run 2, under N_2, up to a maximum of 960 K.

and low-frequency arcs; for example, solid lines mark the result of fitting for low-temperature spectra. At no temperature there was a difference in semicircles (Figs. 2 and 3), when 1 V or 60 mV r.m.s. was applied to the Pt- electrodes.

Fig. 4 shows impedance plots for pelletized EXM1979 powder (sample B) on heating and cooling during run 1, under flowing N_2, up to a maximum of 530 K (Pt-powder contacts). There is some difference to the plots for sample A of Fig. 2. On heating, in Fig. 4 one broad asymmetric depressed semicircular arc is seen at 470 K, as also visible from Fig. 2 for sample A. A rough evaluation gives a capacitance of $C_p \sim 5$ pF/cm for the high-frequency arc and ~50 pF for the low-frequency arc. We assign the high-frequency arc to bulk conduction, while the large low-frequency arc arises from grain boundary processes, as found for data on sample A described above. The same kind of arcs are observed at the maximum temperature of 529 K. On cooling down, a small high-frequency arc evolves, which is clearly visible at 452 K; hence, a superposition of two semicircular arcs is observed. Evidently, on heating followed by cooling, some kind of baking of surface layers occurs, taking into account the measurement process at the highest temperatures to last several

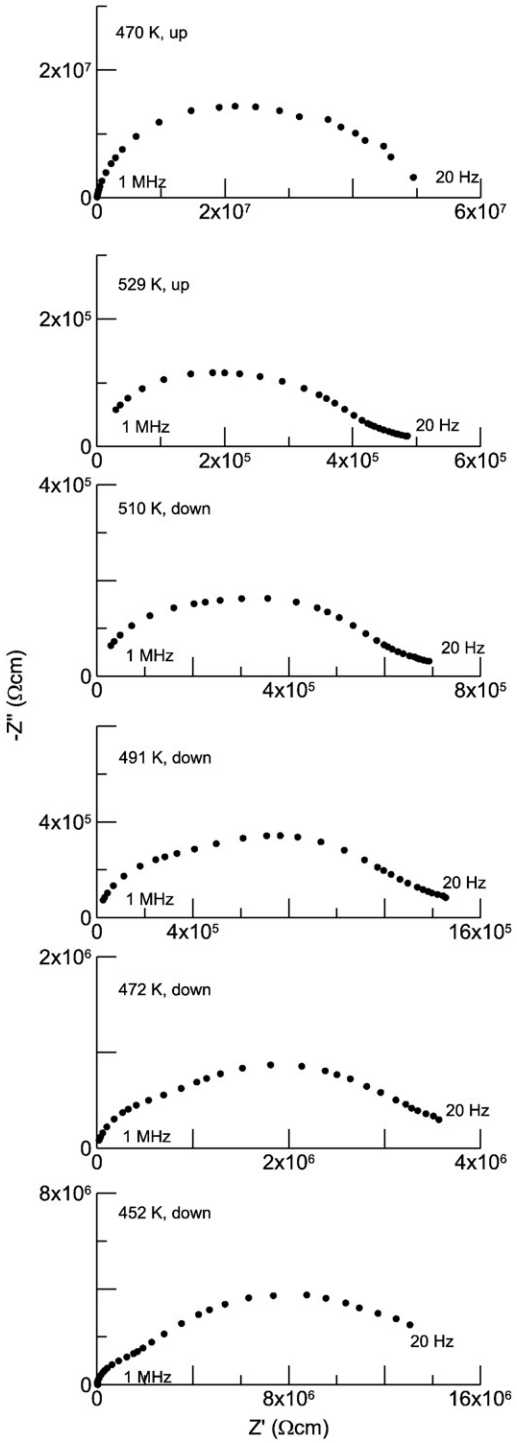

Fig. 4. Complex plane impedance plots for $Li_{4/3}Ti_{5/3}O_4$ EXM1979 (sample B); heating and cooling during run 1 under N_2 up to a maximum of 529 K.

hours. A subsequent run 2 under flowing N_2 up to a maximum of 964 K followed by cooling, resulted in impedance plots, as depicted in Fig. 5. At 430 K, the small high-frequency arc is clearly visible and the big low-frequency one exceeds the limit of measurement. With rising temperatures, only a part of the arcs can be determined, as visible from the 549 K graph. On cooling, at 570 K part of the low-frequency arc is visible and at the lowest frequencies the spike is present. On further cooling, for instance at 462 K, both arcs are seen, with the bulk high-frequency arc the dominating one and, at lower frequencies, a superposed small arc which we attribute to grain boundary processes. The plots during run 2 of sample B differ from those of sample A (Fig. 3). Results of fits are shown by solid lines.

Fig. 6 presents the variation with temperature of σ_{DC} for sample A. The curves taken on heating during run 1 up to 530 K followed by cooling, both representing bulk σ_{DC} data, differ considerably in the lower temperature ranges. On heating, Arrhenius behaviour is seen with activation energy of $E_A = 1.14$ eV; on cooling the same is noted, however with $E_A = 0.52$ eV. A variation of bulk conduction processes is likely to be responsible for the changed results. There is the question, how far a certain grain surface region must be considered to be part of the bulk; it could be part of a space-charge layer that forms when excess charge concentration is present [34].

On heating during run 2 up to ~960 K, only effective σ_{DC} data could be derived (Fig. 3). At lower temperatures Arrhenius behaviour of σ_{DC} is observed, followed by a moderate change in slope at ~625 K, a transitional region and a further clear change in slope at ~770 K and Arrhenius behaviour at still higher temperatures with $E_A = 0.96$ eV up to the maximum temperature of ~960 K. On cooling, a somewhat less steep slope occurs in that temperature range, characterized by $E_A \sim 0.80$ eV, followed by a change in slope at ~715 K and towards lower temperatures a weakly developed transitional region compared to heating; finally, in the low-T region $E_A = 0.57$ eV is derived. As for sample A, no difference of spectra could be detected when 1 V or 60 mV r.m.s. was applied to the electrodes.

In the literature, breaks were noted at ~870 K [16], well above the temperature of a break at 625 K [28] in agreement with our value. There is a transitional region for our sample which appears to correspond to the temperature range, where Li^+ order–disorder phenomena are presumed to occur. For a closer examination high-temperature X-ray and/or neutron diffraction analysis is required, which is outside the scope of this study. The observed anomaly parallels that for Li order–disorder processes at high temperatures in spinels of composition Li_2MCl_4 (M = Mg, Mn, Co), as noted above, which are accompanied by breaks in the σ_{DC} curves as well [19,20]; for example, for Li_2CoCl_4 the reported Li^+ ionic conductivity of $\sigma_{DC}(673\ K) \sim 5.0 \times 10^{-2}\ \Omega^{-1}\ cm^{-1}$ is much higher than $\sigma_{DC}(673\ K) \sim 1.5 \times 10^{-4}\ \Omega^{-1}\ cm^{-1}$ derived for sample A from the graph in Fig. 6. It contains also data of bulk σ_{DC} at not too high temperatures, taken during run 2 up and down; they are a factor of 3–10 above the effective σ_{DC}. Run 3 up and down led to the same results as run 2 down. It follows that up to ~500 K our $E_A = 0.57$ eV agrees with 0.6 eV observed earlier [16], it is somewhat above 0.47–0.51 eV of other workers [6,28,30] and well below 0.94 eV [21] and 0.84 [47]. The discrepancy to the latter values is too large to be interpreted in terms of measurement errors. We conclude that the microstructure of the measured $Li_{4/3}Ti_{5/3}O_4$ differs in some respect from material used in the literature with regard to the core of grains and the contact area grain–grain.

A further check with literature data is the magnitude of the extrapolated effective σ_{DC} at room temperature. From Fig. 6 it follows extrapolated $\sigma_{DC}(295\ K) \sim 3 \times 10^{-10}\ \Omega^{-1}\ cm^{-1}$, derived from data of run 2 down, which is of the same order of magnitude as literature data cited above. On cooling, the difference of our smooth curve in Fig. 6 in the high-T range, to one given in the literature [16] could in part be related to different measurement times, when variable stages of equilibrium for diffusing Li^+ were attained. A further mechanism leading possibly to differing results is the effect of impurities. Taking into account the relation $\sigma_{DC} = e\ n\ \langle v \rangle$, with e the positive charge, n the concentration of charge carriers and $\langle v \rangle$ the mobility, theoretically the temperature dependence of σ_{DC} is presumed to be caused by the variation in $\langle v \rangle$ but it could involve to some extent a variation with temperature of the concentration of n too, as a consequence of an increasing fraction of $\square_{8a}$ because of rising occupation of (16c) sites by Li^+.

We made an attempt to measure the electronic fraction of σ_{DC}, applying DC voltage to the ionically blocking Pt-electrodes at various temperatures according to a method utilized earlier [35–37]. On application of 100 mV to a sample under N_2 after run 3 of sample A,

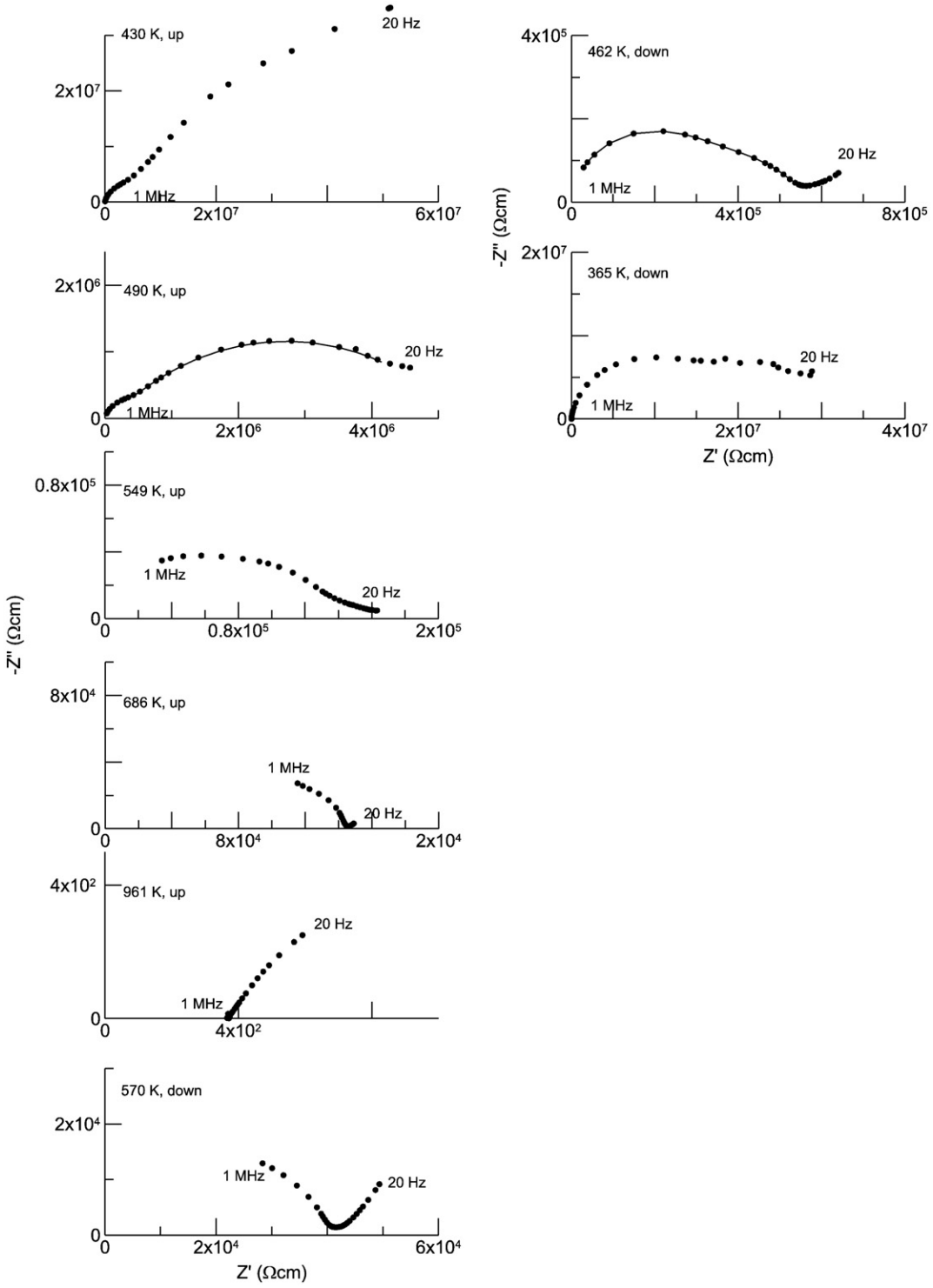

Fig. 5. Complex plane impedance plots for sample B; heating and cooling during run 2 under N_2 up to a maximum of 964 K.

after a short time a decrease in current with time sets in, until the polarization due to pile up of Li^+ charges at one electrode has come to a steady state, with the rate constant determined by the diffusion constant of Li^+; the remaining DC current is due to electronic conduction. The DC current, measured via a reference resistor, was read off after a waiting time of up to ~24 h at the lowest temperatures. The obtained results are seen from Fig. 6. The Arrhenius behaviour is noted at higher temperatures with activation energy of $E_A = 0.31$ eV. There appears to be a break at ~580 K; it is tempting to correlate it with the change in slope of σ_{DC}, implying an interdependence of electronic and ionic conduction, however, this reasoning is rather speculative. We believe that the data in the low-temperature region does not reflect steady state conditions. For this reason any extrapolation to room temperature appears to be inadequate. The results show that at higher temperatures the electronic fraction of σ_{DC} is of the order of <~1% of the ionic fraction as also observed at room temperature.

Fig. 7 reveals for sample B the temperature dependence of σ_{DC}. During run 1 up to 529 K, measurable σ_{DC} values could only be determined above ~450 K, while below this value σ_{DC} was too small

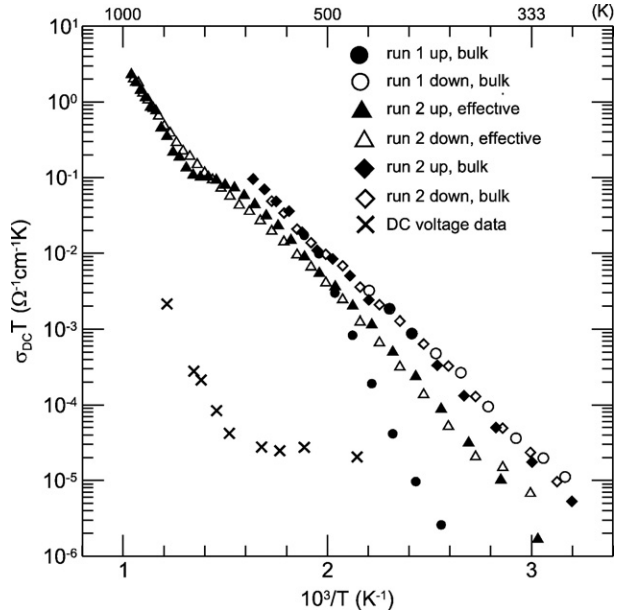

Fig. 6. DC conductivity σ_{DC} as a function of 1/T for sample A during run 1 (up to 530 K) and run 2 (up to 960 K) under N_2; in addition, the electronic fraction of σ_{DC} is shown, using DC voltage measurements.

to be measured. There is hardly a difference between data on heating and cooling, unlike those for sintered material. During run 2 up to 964 K, in fact three sections can be distinguished, characterized by $E_A = 1.35$ eV between ~475 and 605 K, $E_A = 0.54$ eV between ~605 and 715 K and $E_A = 0.98$ eV above 715 K and two changes in slope, at ~580 and 690 K. On cooling, a smooth curve is detected, showing no such clear separation into three segments, with $E_A = 0.87$ eV above ~800 K, and $E_A = 0.61$ eV between ~495 and 380 K. Judging from the impedance plots below ~500 K, the cooling curve represents in fact bulk σ_{DC}, because the grain boundary arc in Fig. 4 is rather reduced. Data taken during run 3 up and down were in fact identical with those recorded during run 2 down. Measurements at higher temperatures also were conducted in air; there were only small differences to the curves of Fig. 7. In order to use a true neutral atmosphere we repeated all measurements under flowing Ar. As compared to N_2, we observed during run 2 down an enhanced contribution of the surface conductivity to σ_{DC}. Thus, the effective σ_{DC} is below the curve presented in Fig. 7, about a factor of five at lower temperatures, which is associated with slightly lower E_A. However there is in fact no difference to the bulk σ_{DC}; the same is valid for run 3. The extrapolated effective $\sigma_{DC}(295\ \mathrm{K}) \sim 10^{-10}\ \Omega^{-1}\ \mathrm{cm}^{-1}$, derived from data of run 2 down, is very similar to sample A.

In order to analyse the dynamics of mobile Li^+ ions, we measured the frequency dependence of σ_{AC}. Fig. 8 presents for sample B the frequency variation of σ_{AC} during run 2 down under N_2. An approximate power law is obeyed, as observed for many ionic charge transport processes in glassy and crystalline oxides. Thereafter, $\sigma_{AC} = \sigma_{DC} + A_0\omega^s$ with A_0 and s temperature dependent constants, which is Jonscher's universal dynamic response law [38]. In our case of ionic Li^+ conduction, $\sigma_{DC} = \lim_{\omega \to 0} \sigma_{AC}$, fits were made to the data points at various temperatures, using σ_{DC}, A_0 and the exponent s as free variables. Results are marked by solid lines. From 349 to 443 K, the exponent s is varying between 0.29 and 0.34, i.e. there is hardly a temperature dependence. It is noteworthy that bulk and grain boundary conduction cannot be distinguished from Fig. 8. In general, at low frequencies data points related to grain boundary and/or interfacial sample/electrode arcs in impedance plots lead to a downward trend of curves. The dispersion of σ_{AC} between 20 Hz and 1 MHz in this temperature range is about half that observed earlier for commercial $Li_{4/3}Ti_{5/3}O_4$ [21]. In the literature on semiconducting glassy and disordered crystalline solids, it is as a rule observed s = 0.5–1.0 [39], including results at low temperatures, i.e. above our values. Both kinds of commercial $Li_{4/3}Ti_{5/3}O_4$ powders show evidently differences either with respect to lattice defects such as cation vacancies or to incorporated impurities. For hopping conduction at higher temperatures, all log σ_{AC}–1/T curves merge into that for σ_{DC} and no information can be gained from σ_{AC} about the dynamics of hopping processes.

4. Discussion

For σ_{DC} at lower temperatures, bulk E_A is evidently controlled by the diffusion path $Li^+_{8a} \rightarrow \square_{16c} \rightarrow \square_{8a}$ as follows from Raman and IR

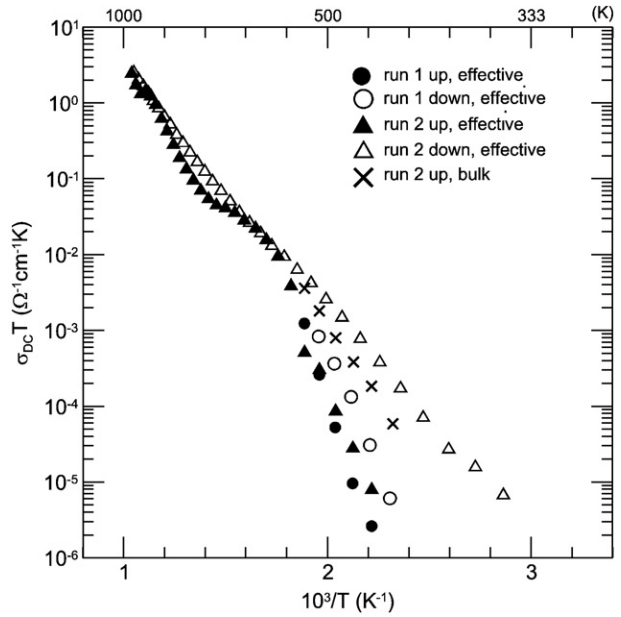

Fig. 7. DC conductivity σ_{DC} as a function of 1/T for sample B on heating and cooling during run 1 (up to 529 K) and run 2 (up to 964 K) under N_2.

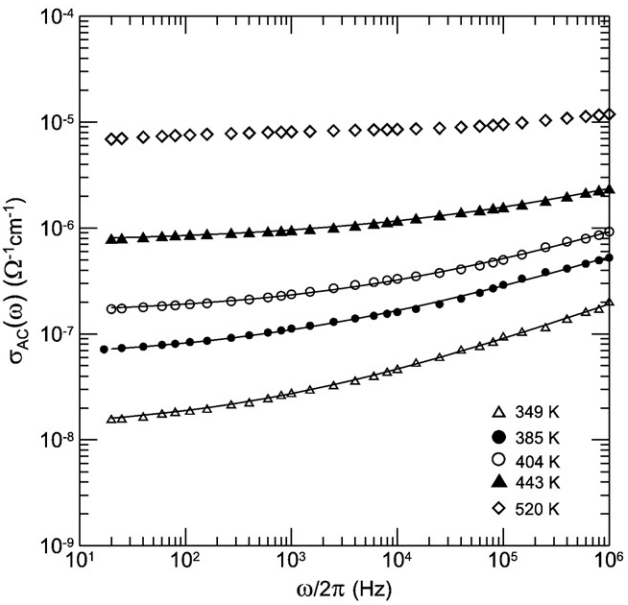

Fig. 8. Frequency dependence of the AC conductivity σ_{AC} for sample B, during run 2 down under N_2.

analysis. The magnitude of E_A is correlated with the bottleneck size of the diffusion path, which is given by the fact that (16c) sites are located between two (8a) sites. On the other hand, quite different E_A values of 0.47–0.94 eV were reported in this temperature range [16,21,28–31]. An essential part may be played by non-stoichiometry and/or impurities, giving rise to a certain variation of ionic Li^+ conduction paths, which are three-dimensional in the spinel lattice. The fact that for our data the derived E_A values at the highest applied temperatures are above those inferred <~530 K, is indicative of the dominance of a diffusion path including most probably occupation of tetrahedral (48f) sites, as proposed previously. In the literature, very rarely mention is made of the heating and cooling rates during electrical measurements. When the rates are enhanced, no equilibrium states are expected during approach to any transitions, thus, differences in the variation with temperature of σ_{DC} can occur and breaks may be more or less well developed. An additional point is that in the literature hardly bulk and surface processes were distinguished. Analysis of grain boundary and surface area processes can be made from impedance spectra when adequate equivalent circuits are used [40]. One of our problems is to interpret data of bulk σ_{DC} for sample A acquired during run 1 up to 530 K and down which show enormous differences in σ_{DC} and E_A values; by contrast, there is a rather small difference for sample B (Fig. 7). For sintered material, there appear to be inhomogeneous disordered grain regions that impede Li^+ conduction on heating while some kind of alteration took place at the maximum applied temperature, resulting in enhanced σ_{DC}. There are several models describing ionic conduction in solids. Apart from the picture of independent hopping ions, coupling of hopping ions with their environment by Coulomb interaction was presumed [41]. In this model the power law exponent s in Jonscher's universal dynamic response law for σ_{AC} is a coupling parameter being a measure of interaction; our low s values point to weak interaction. In a further model, considering interaction as well, correlated forward–backward hops are considered to be responsible for the AC conductivity [42].

The low electronic fraction of σ_{DC} is due to lattice defects. The electronic structure of $Li_{4/3}Ti_{5/3}O_4$ is characterized by an empty conduction Ti_{3d} (t_{2g}) band, a full O_{2p} valence band and a gap of 2–3 eV [13,43–46], hence it represents an insulator in view of the large gap. Electronic conduction is, thus, due to localized levels in the gap as a consequence of lattice defects.

5. Conclusion

The variation with temperature of the conductivity of sintered and commercial $Li_{4/3}Ti_{5/3}O_4$ shows that there are marked differences which are suggested to be a consequence of differences in the microstructure of grains and in a variation of grain boundary processes. Both phenomena also are of interest for room temperature properties. The points in question are an inhomogeneous core of grains by lattice defects of variable kind and probably inhomogeneous grain surface layers, both eventually affected by the presence of impurities. The same kind of defects evidently has led to varying results in the literature as activation energies and high-temperature transitional regions are concerned. For a more precise interpretation of electrical processes, detailed microstructural analyses are required applying advanced techniques.

Acknowledgements

Thanks are due Mrs. D. Richard for conducting DSC measurements. We also thank Dr. H. Boysen, Department für Geo- und Umweltwissenschaften, Kristallographie, Universität München, for valuable discussions.

References

[1] K.M. Colbow, J.R. Dahn, R.R. Haering, J. Power Sources 26 (1989) 397.
[2] E. Ferg, R.J. Grummow, A. de Kock, M.M. Thackeray, J. Electrochem. Soc. 141 (1994) L147.
[3] T. Ohzuku, A. Ueda, N. Yamamoto, Y. Iwakoshi, J. Power Sources 54 (1995) 99.
[4] T. Ohzuku, A. Ueda, N. Yamamoto, J. Electrochem. Soc. 142 (1995) 1431.
[5] S. Scharner, W. Weppner, P. Schmid-Beurmann, J. Electrochem. Soc. 146 (1999) 857.
[6] M. Nakayama, Y. Ishida, H. Ikuta, M. Wakihara, Solid State Ionics 117 (1999) 265.
[7] P.P. Prosini, R. Mancini, L. Petrucci, V. Contini, P. Villano, Solid State Ionics 144 (2001) 185.
[8] S. Huang, Z. Wen, X. Zhu, Z. Gu, Electrochem. Commun. 6 (2004) 1093.
[9] S. Huang, Z. Wen, X. Zhu, Z. Lin, J. Power Sources 165 (2007) 408.
[10] J. Wolfenstine, U. Lee, J.L. Allen, J. Power Sources 154 (2006) 287.
[11] J. Wolfenstine, J.L. Allen, J. Power Sources 180 (2008) 582.
[12] Y. Zhao, G. Liu, L. Liu, Z. Jiang, J. Solid State Electrochem. 13 (2009) 705.
[13] M.R. Harrison, P.P. Edwards, J.B. Goodenough, J. Solid State Chem. 54 (1984) 136.
[14] S. Scharner, W. Weppner, P. Schmid-Beurmann, J. Solid State Chem. 134 (1997) 170.
[15] D.W. Murphy, R.J. Cava, S.M. Zahurak, A. Santoro, Solid State Ionics 9&10 (1983) 413.
[16] I.A. Leonidov, O.N. Leonidova, L.A. Perelyaeva, R.F. Samigullina, S.A. Kovyazina, M.V. Patrakeev, Phys. Solid State 45 (2003) 2183.
[17] H.D. Lutz, W. Schmidt, H. Haeuseler, Z. anorg. allg. Chem. 453 (1979) 121.
[18] J.L. Soubeyroux, C. Cros, W. Gang, R. Kanno, M. Pouchard, Solid State Ionics 15 (1985) 293.
[19] R. Kanno, Y. Takeda, O. Yamamoto, C. Cros, W. Gang, G. Hagenmuller, Solid State Ionics 20 (1986) 99.
[20] R. Kanno, Y. Takeda, A. Takahashi, O. Yamamoto, R. Suyama, S. Kume, J. Solid State Chem. 71 (1987) 196.
[21] M. Wilkening, R. Amade, W. Iwaniak, P. Heitjans, Phys. Chem. Chem. Phys. 9 (2007) 1239.
[22] C. Pecharroman, J.M. Amarilla, Phys. Rev. B 62 (2000) 12062.
[23] H.D. Lutz, W. Schmidt, H. Haeusler, J. Phys. Chem. Solids 42 (1981) 287.
[24] C. Cros, L. Hanebali, L. Latie, G. Villeneuve, W. Gang, Solid State Ionics 9&10 (1983) 139.
[25] R. Kanno, Y. Takeda, K. Takada, O. Yamamoto, Solid State Ionics 9&10 (1983) 153.
[26] R. Kanno, Y. Takeda, O. Yamamoto, Solid State Ionics 28–30 (1988) 1276.
[27] R. Kanno, Y. Takeda, M. Mori, O. Yamamoto, Chem. Letters (Japan) 18 (1989) 223.
[28] S. Hayashi, H. Hatano, J. Ceram. Soc. Japan 102 (1994) 378.
[29] D. Tsubone, T. Hashimoto, K. Igarashi, T. Shimizu, J. Ceram. Soc. Japan 102 (1994) 180.
[30] G. Vitins, G. Kizane, A. Lusis, J. Tiliks, J. Solid State Electrochem. 6 (2002) 311.
[31] C.H. Chen, J.T. Vaughey, A.N. Jansen, D.V. Dees, A.J. Kahaian, T. Goacher, M.M. Thackeray, J. Electrochem. Soc. 148 (2001) A102.
[32] J.R. Macdonald, Impedance spectroscopy, Whiley Sons, New York, 1987.
[33] J.R. Macdonald, Solid State Ionics 176 (2005) 1961.
[34] J. Maier, Prog. Solid State Chem. 23 (1995) 171.
[35] R.W. Fest, N.M. Tallan, J. Appl. Phys. 36 (1965) 543.
[36] C. Simonnet, A. Grandjean, M. Malki, Solid State Ionics 175 (2004) 695.
[37] R. Amin, P. Balaya, J. Maier, Electrochem. Solid-State Lett. 10 (2007) A13.
[38] A.K. Jonscher, Dielectric Relaxation in Solids, Chelsea Dielectric, London, 1983.
[39] J.C. Dyre, T.B. Schroeder, Rev. Mod. Phys. 72 (2000) 873.
[40] J. Fleig, P. Pham, P. Sztulzaft, J. Maier, Solid State Ionics 113–115 (1998) 739.
[41] K.L. Ngai, J.N. Mundy, H. Jain, O. Kanert, G. Balzer-Jollenbeck, Phys. Rev. B39 (1989) 6169.
[42] K. Funke, Prog. Solid State Chem. 22 (1993) 111.
[43] P.P. Edwards, R.G. Egdell, I. Fragala, J.B. Goodenough, M.R. Harrison, A.F. Orchard, E.G. Scott, J. Solid State Chem. 54 (1984) 127.
[44] P.-E. Lippens, M. Womes, P. Kubiak, J.-C. Jumas, J. Olivier-Fourcade, Solid State Sciences 6 (2004) 161.
[45] D. Liu, C. Ouyang, J. Shu, J. Jiang, Z. Wang, L. Chen, Phys. Stat. Sol. (b) 243 (2006) 1835.
[46] C.Y. Ouyang, Z.Y. Zhong, M.S. Lei, Electrochem. Commun. 9 (2007) 1107.
[47] W. Iwaniak, J. Fritsche, M. Zukalova, R. Winter, M. Wilkening, P. Heitjans, Defect Diffus. Forum 289–292 (2009) 565.

Appendix F

Fifth publication

Lithium migration at high temperatures in $Li_4Ti_5O_{12}$ studied by neutron diffraction

Chemistry of Materials **23** 2753 (2011)

Andreas Laumann,[a] **Hans Boysen,**[b] **Martin Bremholm,**[c] **Karl Thomas Fehr,**[a] **Markus Hoelzel,**[d,e] **Michael Holzapfel**[f]

[a] Ludwig-Maximilians-Universität München, Department of Earth and Environmental Sciences, Section for Mineralogy, Petrology and Geochemistry, Munich, Germany
[b] LMU München, Department für Geo- und Umweltwissenschaften, Sektion Mineralogie
[c] Department of Chemistry, Princeton University, Princeton, NJ 08544, USA
[d] Fachbereich Material- und Geowissenschaften, Fachgebiet Strukturforschung, Technische Universität Darmstadt, 63762 Darmstadt, Germany
[e] Forschungsneutronenquelle FRM II, 85747 Garching, Germany
[f] Süd-Chemie AG, Battery Materials, Moosburg, Germany

CHEMISTRY OF MATERIALS

ARTICLE

pubs.acs.org/cm

Lithium Migration at High Temperatures in $Li_4Ti_5O_{12}$ Studied by Neutron Diffraction

Andreas Laumann,[*,†] Hans Boysen,[‡] Martin Bremholm,[§] K. Thomas Fehr,[†] Markus Hoelzel,[⊥,¶] and Michael Holzapfel[∥]

[†]Department für Geo- und Umweltwissenschaften, Sektion für Mineralogie, Petrologie und Geochemie, LMU München, Theresienstrasse 41, 80333 München, Germany

[‡]Department für Geo- und Umweltwissenschaften, Sektion Kristallographie, LMU München, Am Coulombwall 6, 85748 Garching, Germany

[§]Department of Chemistry, Princeton University, Washington Road, Princeton, New Jersey 08544, United States

[⊥]Fachbereich Material- und Geowissenschaften, Fachgebiet Strukturforschung, Technische Universität Darmstadt, Petersenstrasse 23, 63762 Darmstadt, Germany

[¶]Forschungsneutronenquelle FRM II, Technische Universität München, Lichtenbergstrasse 1, 85747 Garching, Germany

[∥]Battery Materials, Süd-Chemie AG, Ostenrieder Strasse 15, 85368 Moosburg, Germany

Supporting Information

ABSTRACT: The structure of $Li_4Ti_5O_{12}$ was investigated by neutron powder diffraction, and the study revealed unprecedented details about lithium migration at high temperatures. A commercial sample of the battery anode material $Li_4Ti_5O_{12}$ (spinel-type) was measured from room temperature to 1100 °C. Up to 500 °C, linearly increasing values for the unit cell parameter, the isotropic atomic displacement parameters, and the oxygen position are observed. At 700 °C, a change of slope occurs, which is assigned to the beginning migration of lithium. Previous investigations identified the octahedral 16c site in the spinel structure as the migration position of lithium upon heating to high temperatures, and because of that, several phase transitions of $Li_4Ti_5O_{12}$ at high temperatures have been proposed. Here, we unambiguously identify that the lithium atoms occupy split sites around the 16c positions and order−disorder phase transitions of $Li_4Ti_5O_{12}$ were not observed. One-particle potential shows that the occupancy of 16c is an unstable configuration and that the split-site structure leads to a more favorable migration position. Occupation of the lithium sites (32e) results in the same long-range diffusion path in all ⟨110⟩ directions. The onset of lithium migration can explain the change of the ionic conductivity of $Li_4Ti_5O_{12}$ at high temperatures, which has been observed by impedance spectroscopic studies. Further heating to 1000 °C resulted in a partial decomposition of $Li_4Ti_5O_{12}$ into the ramsdellite-type $Li_2Ti_3O_7$ and the cubic γ-Li_2TiO_3, and at 1100 °C, the $Li_4Ti_5O_{12}$ spinel was fully decomposed.

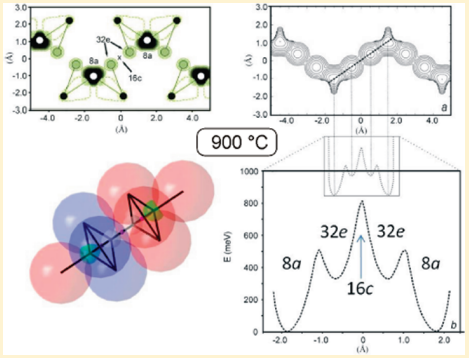

KEYWORDS: $Li_4Ti_5O_{12}$, lithium-ion batteries, neutron diffraction, lithium migration, decomposition

INTRODUCTION

In the current efforts to develop and produce active materials for long-life lithium-ion batteries, e.g., for electronic vehicles or stationary power plants, the anode material $Li_4Ti_5O_{12}$ is a very promising candidate because of its long-term stability at high capacity and its inherent safety.[1−6] Its spinel structure of space group $Fd\bar{3}m$ was determined by Deschanvres et al.[7] and recently reinvestigated by single-crystal X-ray diffraction.[8] Its unit cell contains eight formula units of $(Li)^{8a}[Li_{1/3}Ti_{5/3}]^{16d}O_4^{32e}$, in which lithium fully occupies the tetrahedral 8a sites. The octahedral 16d sites are occupied randomly by lithium atoms ($^1/_6$) and titanium atoms ($^5/_6$),[8,9] and the oxygen atoms are on the 32e sites.[2,8] With a theoretical specific capacity of 175 mAh/g, three Li^+ ions can be intercalated electrochemically in $Li_4Ti_5O_{12}$ at a flat potential of 1.55 V. During lithiation, lithium shifts from tetrahedral 8a sites toward the octahedral 16c sites $[(Li)_{1-x}^{8a}[Li]_{2x}^{16c}[Li_{1/3}Ti_{5/3}]^{16d}O_4^{32e}]$, causing only minor structural strain ("zero strain material"), which is ascribed to enable the excellent cyclability of $Li_4Ti_5O_{12}$.[2,3,10−12]

Upon heating of the $Li_4Ti_5O_{12}$ samples, variations of its activation energy were determined by impedance spectroscopy,[13−16] which have been assigned to structural changes of the order−disorder type.[13−15] Similar conclusions were reported based on data obtained by IR spectroscopy,[17] Raman spectroscopy,[14] and NMR spectroscopy.[18] Following the impedance data, $Li_4Ti_5O_{12}$ is presumed to undergo two order−disorder phase transitions

Received: November 20, 2010
Revised: April 5, 2011

   dx.doi.org/10.1021/cm103332y | *Chem. Mater.* XXXX, XXX, 000–000

upon heating. The first transition is due to migration of lithium from 8a to 16c sites and the transition to an ordered NaCl type structure with $Fd\bar{3}m$ structure ($[Li]^{16c}[Li_{1/3}Ti_{5/3}]^{16d}O_4{}^{32e}$), and the second transition is due to migration of lithium from 16d to 16c sites, transforming it into a disordered NaCl structure with $Fm\bar{3}m$ ($[Li_{4/3}]^{16c}[Ti_{5/3}]^{16d}O_4{}^{32e}$).[13,14] All proposed structural transformations are well below the decomposition temperature of $Li_4Ti_5O_{12}$ into the ramsdellite-type $Li_2Ti_3O_7$ and the cubic Li_2TiO_3 at approximately 1000 °C.[19−21] However, inconsistencies about the lithium distribution in $Li_4Ti_5O_{12}$ are also reported at room temperature. Contrary to the most common opinion in the literature, a partial occupation of 16c octahedral positions due to migration of tetrahedrally bound lithium to interstitial sites has been proposed[13,14] and shown by NMR spectroscopy[18] and an IR spectroscopy study[17] at room temperature.

A lithium diffusion path of $Li_4Ti_5O_{12}$ at room temperature, 8a → 16c → 8a or 8a → 16c → 48f → 16d, and direct lithium hopping between 16c and 16d or 8a and 48f have been proposed,[22] whereas in the recent publication of Wagemaker et al.,[23] the 16c octahedral position was identified as the saddle point of the energy barrier between two tetrahedral 8a sites. The latter results in a negligible occupation time of lithium on 16c when hopping from one 8a to another 8a.

Neutron powder diffraction has so far mainly been applied to study the lithium intercalation process in $Li_4Ti_5O_{12}$.[10−12,24] The aim of the present study was to elucidate the structural changes and diffusion properties during stepwise heating up to 1100 °C. An increase in the lithium-ion mobility was found starting at approximately 700 °C and analyzed in detail at 900 °C. Phase transitions of the order−disorder type were not observed. Decomposition of $Li_4Ti_5O_{12}$ to $Li_2Ti_3O_7$ and cubic γ-Li_2TiO_3 started at 1000 °C, leading to complete decomposition at 1100 °C.

EXPERIMENTAL SECTION

The $Li_4Ti_5O_{12}$ powder used was a commercial compound provided by Süd-Chemie AG, Moosburg, Germany. Preliminary laboratory powder X-ray diffraction (PXRD) characterization [STOE STADI P, Cu Kα_1 radiation, λ = 1.544 056 Å, curved Ge(111) monochromator] showed a pure phase.

Neutron powder diffraction measurements were carried out on a high-resolution SPODI diffractometer[25] at FRM II (Garching, Germany). The wavelength, λ, was determined from the measurement of a silicon standard (NIST SRM 640c) to be 1.5483 Å. For multitemperature measurements, a niobium container was filled with 2 g of the commercial $Li_4Ti_5O_{12}$ powder and placed in a high-temperature vacuum furnace. The reflections from niobium were included in all refinements. Diffraction patterns were collected at room temperature, 300, 500, 700, 900, 1000, and 1100 °C. Additional patterns were recorded after cooling to 700 °C and further to room temperature. Each data set was collected for 2 h after a holding time of 15 min for temperature equilibration. The neutron powder patterns were recorded from 0.95° to 160° 2θ with a step size of 0.05°. Rietveld refinement was performed using the program *FullProf*.[26] The pseudo-Voigt function in the formulation of Thompson−Cox−Hastings[27] was used to model the line shape. The background was linearly interpolated between a set of background points with refinable intensities. Additional refinements, including anharmonic terms in the Debye−Waller factor, were performed using the program *JANA*.[28]

RESULTS

The structure refinement of $Li_4Ti_5O_{12}$ was performed following the convention of most of the previous literature on this compound (e.g., refs 8,12, and 22), i.e., using the second setting of the space group $Fd\bar{3}m$ in the International Tables of Crystallography[29] with the symmetry center at the origin and Li1 on 8a ($^1/_8\ ^1/_8\ ^1/_8$), Ti/Li2 on 16d ($^1/_2\ ^1/_2\ ^1/_2$), and O on 32e ($x\ x\ x$) sites. Here x is close to $^1/_4$ and is often written as $x = {}^1/_4 + u$. The small value of u determines the relative size of the tetrahedra and octahedra; a positive value increases the tetrahedral volume. The bond lengths Li1−O and Ti/Li2−O are equal at $u = {}^1/_{80}$. For standard refinements, lithium was fixed to full occupancy on 8a sites and to $^1/_6$ occupancy on 16d sites and titanium to $^5/_6$ on 16d sites, as reported before.[8,12,24]

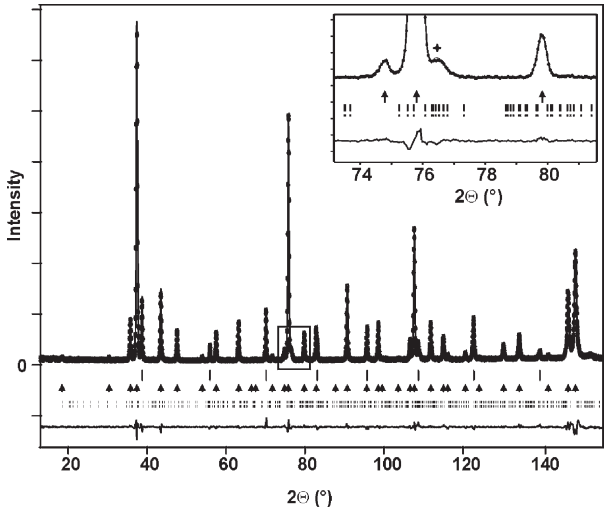

Figure 1. Rietveld fit of $Li_4Ti_5O_{12}$ at room temperature. Observed (circles) and calculated (solid line) patterns, Bragg reflections of niobium (solid ticks), $Li_4Ti_5O_{12}$ (arrows), β-Li_2TiO_3 (dashed ticks), and the difference curve (below) are shown. The asterisk in the inset marks the only obvious group of reflections of β-Li_2TiO_3 that are not superposed by $Li_4Ti_5O_{12}$ peaks.

The spinel $Li_4Ti_5O_{12}$ was refined in space group $Fd\bar{3}m$ with a unit cell parameter of a = 8.35952(4) Å at 15 °C, showing good agreement with reported values, e.g., a = 8.352(4) Å[8] and a = 8.35950 Å[3] (Figure 1). A minor impurity phase of monoclinic Li_2TiO_3 (β-Li_2TiO_3) was found to be present <3 wt %, but could not be detected by PXRD. The structure of β-Li_2TiO_3 is described as pseudocubic, leading to similar neutron powder and PXRD patterns of β-Li_2TiO_3 and $Li_4Ti_5O_{12}$, and as such, nearly all reflections of β-Li_2TiO_3 with higher intensity are superimposed by reflections of the major phase $Li_4Ti_5O_{12}$. Only one group of reflections at approximately 77° 2θ clearly indicates the presence of β-Li_2TiO_3 (see the inset of Figure 1). All other β-Li_2TiO_3 reflections either are too low in intensity or only cause peak broadening or weak shoulders on $Li_4Ti_5O_{12}$ reflections. The low content does not allow a structural refinement of β-Li_2TiO_3, and therefore the structural values of Kataoka et al.[30] were used. The impurity of β-Li_2TiO_3 was within uncertainties constant up to 700 °C. At 900 °C, no clear reflection of β-Li_2TiO_3 could be detected.

Neutron Diffraction Measurements upon Heating and Cooling of the $Li_4Ti_5O_{12}$ Sample. Up to 700 °C, the unit cell parameter (Figure 2a), the u parameter of oxygen (Figure 2b), the Li1−O (tetrahedra) and Li2/Ti−O (octahedra) bond distances (Figure 2c), and all isotropic thermal displacement parameters B_{iso} (Figure 2d) increased in a near-linear manner (Table 1). At higher temperatures and as is clearly seen at 900 °C,

dx.doi.org/10.1021/cm103332y |*Chem. Mater.* XXXX, XXX, 000–000

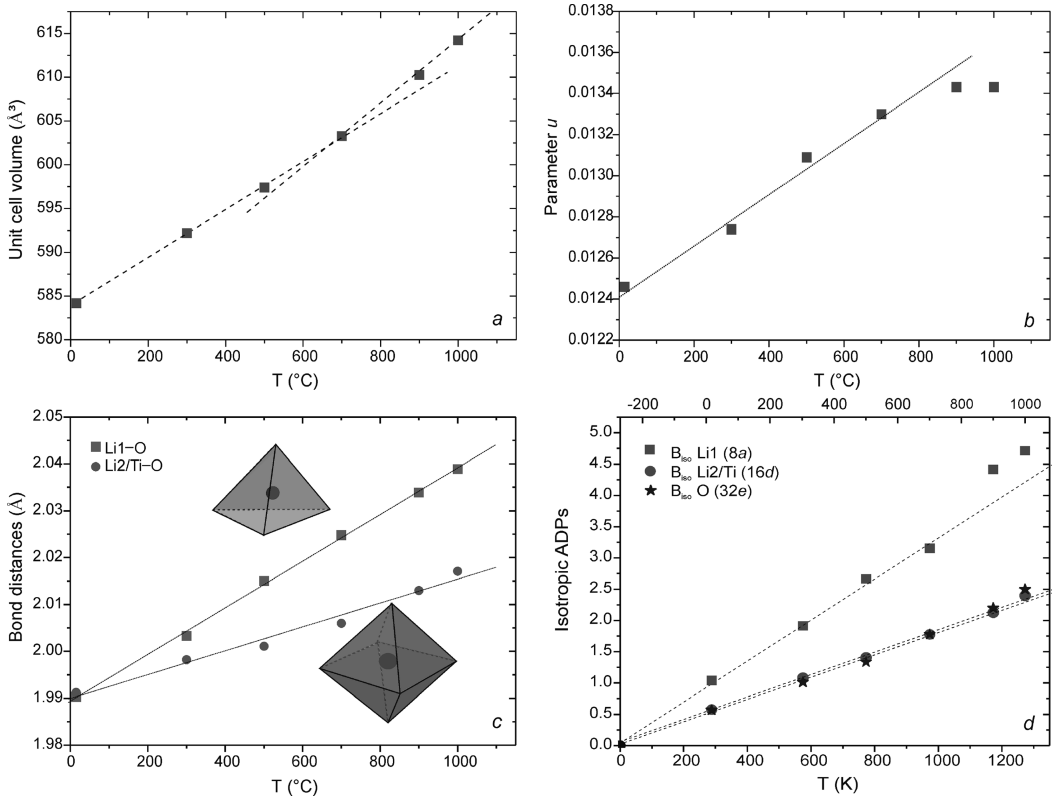

Figure 2. Structural evolution of $Li_4Ti_5O_{12}$ upon heating: (a) the unit cell volume with linear fits for T < 700 °C and > 700 °C, (b) the parameter u, (c) selected bond distances, and (d) the isotropic ADPs (the straight lines are fitted to the values below 900 °C passing through 0 K).

Table 1. Structural Parameters of $Li_4Ti_5O_{12}$ at Varying Temperatures[a]

	temp (°C)					
	15	300	500	700	900	1000
a (Å)	8.35956(3)	8.39766(5)	8.42219(5)	8.44977(6)	8.48218(5)	8.50051(6)
V (Å^3)	584.186(4)	592.208(6)	597.413(6)	603.301(5)	610.270(7)	614.236(7)
u	0.01246(3)	0.01273(4)	0.01313(4)	0.01335(3)	0.01344(4)	0.01348(5)
B_{iso} Li (8a)	1.02(7)	1.90(11)	2.66(13)	3.11(11)	4.44(17)	4.76(19)
B_{iso} Li/Ti (16d)	0.62(2)	1.21(3)	1.38(3)	1.74(3)	2.12(3)	2.36(4)
B_{iso} O (32e)	0.59(1)	1.07(2)	1.34(2)	1.75(1)	2.22(2)	2.50(2)
R_p	4.70	5.48	4.94	3.68	4.13	3.83
R_{wp}	5.63	6.59	6.10	4.67	5.27	4.96
χ^2	2.74	1.91	1.63	1.91	2.52	1.82

[a] Number of data points: 3138. Number of refined background parameters: 52 (46 at 1000 °C). Total number of refined parameters: 78 (73 at 1000 °C).

these parameters, except the bond distances, show deviations from linearity, which will be discussed in detail below.

At 1000 °C, $Li_4Ti_5O_{12}$ started to decompose into the ramsdellite-type phase $Li_2Ti_3O_7$ and the cubic Li_2TiO_3 (γ-Li_2TiO_3), with fractions, excluding niobium, of 3.18(4) and 1.29(7) wt %, respectively. Monoclinic β-Li_2TiO_3 undergoes an order−disorder transformation at high temperatures to the cubic γ-Li_2TiO_3: for compositions Li/Ti ∼ 2, the transformation temperature is approximately 1150 °C.[20,30] Lower Li/Ti ratios are reported to reduce the transformation temperature.[19−21]

At 1100 °C, $Li_4Ti_5O_{12}$ had fully decomposed into $Li_2Ti_3O_7$ and γ-Li_2TiO_3 in a fractional ratio of 2.61(2):1 wt % (Table 2 and Figure 3). At 1100 °C, γ-Li_2TiO_3 has a unit cell parameter of a = 4.24394(4) Å, which is close to a previously reported value at the same temperature, a = 4.23929(10) Å.[31]

Upon cooling to 700 °C, the γ-Li_2TiO_3 phase did undergo the expected transformation to the stable β-Li_2TiO_3. To conserve the ramsdellite-type structure of $Li_2Ti_3O_7$, the compound must be quenched rapidly to room temperature.[32] Slow cooling of $Li_2Ti_3O_7$ will result in its decomposition to $Li_4Ti_5O_{12}$ and TiO_2. At 700 °C and at room temperature, besides $Li_2Ti_3O_7$ and the β-Li_2TiO_3, $Li_4Ti_5O_{12}$ reappeared with a fraction of ∼15 wt %, and a minor fraction of rutile (<1 wt %) was detected at room temperature. The temperature-dependent progression upon heating of the $Li_4Ti_5O_{12}$ sample to its decomposition starting at 1000 °C is presented in Figure 4.

dx.doi.org/10.1021/cm103332y |Chem. Mater. XXXX, XXX, 000–000

Table 2. Structural Parameters of γ-Li_2TiO_3 and $Li_2Ti_3O_7$ at 1100 °C[a]

compound	γ-Li_2TiO_3	$Li_2Ti_3O_7$
a (Å)	4.24394(4)	5.09801(6)
b (Å)		9.7095(1)
c (Å)		2.98604(3)
V (Å^3)	76.438(1)	147.805(3)
composition (%)[b]	27.74(2)	72.25(3)
R_F (%)	3.5	6.64

[a] Number of data points: 3138. Number of refined background parameters: 46. Total number of refined parameters: 72. R_p: 3.68. R_{wp}: 4.63. χ^2: 1.78. [b] Niobium content excluded.

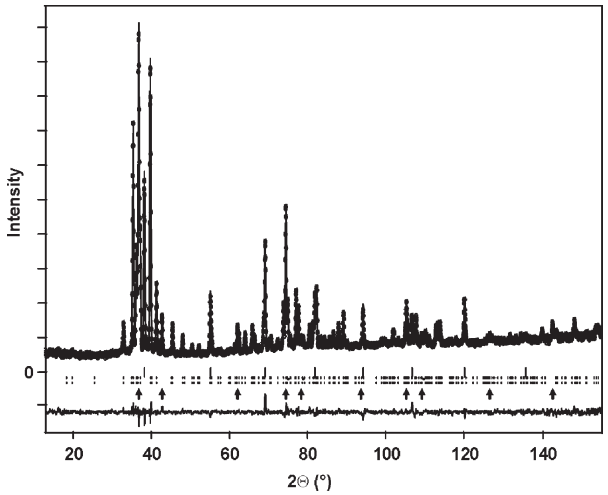

Figure 3. Rietveld fit of the decomposition products $Li_2Ti_3O_7$ and γ-Li_2TiO_3 at 1100 °C. Observed (circles) and calculated (solid line) pattern intensities, Bragg reflections of niobium (solid ticks), $Li_2Ti_3O_7$ (dashed ticks), cubic γ-Li_2TiO_3 (arrows), and the difference curve (below) are shown.

Lithium Migration at High Temperatures. As mentioned above, the unit cell volume, the oxygen position (parameter u), and the isotropic thermal displacement parameter B_{iso} of Li1 on 8a deviated significantly from a linear trend at high temperatures. Therefore, test refinements following the proposal of Leonidov et al.[13,14] were performed, with lithium either partially or fully on 16c instead of 8a or with all lithium on 16c ($[Li_{4/3}]^{16c}[Ti_{5/3}]^{16d}O_4^{32e}$) either in space group $Fd\bar{3}m$ or in space group $Fm\bar{3}m$. All of these attempts were unsuccessful and, especially, $^4/_3$ of lithium on 16c can be completely ruled out.

On the contrary, remaining in space group $Fd\bar{3}m$, refinements of the lithium occupancy on 8a at higher temperatures enabled stable fits and showed increasing lithium deficits with increasing temperature. Confirming full occupancy at low temperatures, at 700 °C, the refinement revealed a small deficit, slightly larger than the error margin [0.97(2)], suggesting almost full occupancy, but at 900 °C, a striking decrease of ~14% toward 0.86(2) was revealed. This apparent lithium deficit is not due to evaporation of lithium (see the later discussion) but can be assigned to anharmonic motions and/or migration to other sites in the structure. This could be shown by additional refinements using the program *JANA*,[28] which allows the inclusion of anharmonic terms in the Debye–Waller factor. Note that the

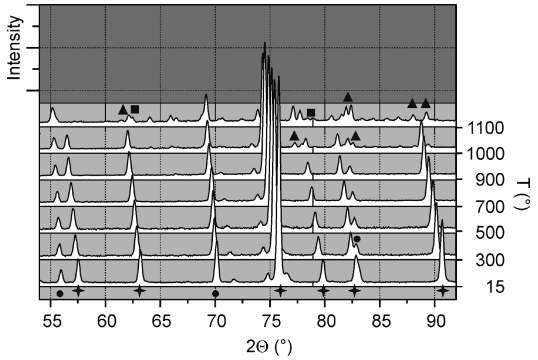

Figure 4. Diffraction patterns (2θ range, 54–92°) as a function of the temperature, with the marked main reflections of $Li_4Ti_5O_{12}$ (asterisks), $Li_2Ti_3O_7$ (triangles), γ-Li_2TiO_3 (squares), and niobium (circles). The partial decomposition of $Li_4Ti_5O_{12}$ into $Li_2Ti_3O_7$ and γ-Li_2TiO_3 can be seen at 1000 °C, and at 1100 °C, $Li_4Ti_5O_{12}$ is fully decomposed.

local symmetry of $\bar{4}3m$ only allows one isotropic harmonic displacement parameter (ADP). There are one third-order term, c^{123}, and two fourth-order terms, d^{1111} and d^{1122}. While c^{123} turned out to be highly significant, the other two were less reliable and produced some artifacts, and thus only c^{123} was used in the following refinements. During these refinements, the lithium occupancy on 16d was kept constant. A subsequent difference Fourier analysis revealed weak but significant negative residual densities within the 16c octahedron (note that the scattering length of lithium is negative). This was found as two peaks along the *xxx* direction displaced from the central 16c position. Therefore, a new atom Li* was introduced on a 32e site. A free refinement of both the occupancy and an isotropic ADP (U_{iso} of Li*) was unsuccessful because of the usually strong correlation between these two parameters, in particular for the very low occupancy. Therefore, U_{iso} was constrained to that of Li1. Free refinement of the occupancies of Li1 and Li* gave values such that the overall sum was conserved within the rather large standard uncertainties, and so, in the final refinement, the overall occupancy was fixed. The results are given in Table 3 and selected bond lengths in Table 4. It should be added that similar refinements at lower temperatures were unsuccessful because of the lower occupancy of the Li* site, and at higher temperatures, the results might be influenced by the gradual onset of the $Li_4Ti_5O_{12}$ decomposition (see above).

Although these results should not be taken too literally because of the necessary constraints, the general distribution of lithium can be deduced with confidence. The corresponding probability density function (PDF) as derived from the ADPs is shown in Figure 5. Assuming Boltzmann statistics for single particle motion, a one-particle potential (OPP) can be deduced. In such OPP maps, the saddle points may be interpreted as activation energies of ion diffusion (for details, see, e.g., ref 33). Figure 6a shows the two-dimensional potential landscape, and Figure 6b shows a one-dimensional section along [111].

DISCUSSION

Composition and Phase Relations of $Li_4Ti_5O_{12}$. Refinements from room temperature up to 700 °C showed a constant ratio of $Li_4Ti_5O_{12}$ and β-Li_2TiO_3. At room temperature, these two phases are immiscible and mixtures of both are common when having lithium in excess; see, e.g., refs 2 and 34. At 900 °C, a

dx.doi.org/10.1021/cm103332y |*Chem. Mater.* XXXX, XXX, 000–000

Table 3. Structural Parameters for $Li_4Ti_5O_{12}$ at 900 °C with a Li* 32e Site Included: Fractional Atomic Coordinates and Isotropic or Equivalent Isotropic Displacement Parameters (Å^2), as Well as the Anisotropic and Anharmonic ADPs of Li1 and O

	x	y	z	U_{iso}*/U_{eq}	occupacy
Li1 (8a)	0.125	0.125	0.125	0.037(1)*	0.86(2)
Li2 (16d)	0.5	0.5	0.5	0.0271(5)*	0.1667
Ti (16d)	0.5	0.5	0.5	0.0271(5)*	0.8333
O (32e)	0.26299(5)	0.26299(5)	0.26299(5)	0.02787(13)	1
Li* (32e)	0.043(8)	0.043(8)	0.043(8)	0.037(1)*	0.034(6)
Anisotropic and Anharmonic ADPs					
Li1				$c^{123} = -0.007(2)$	
O				$U_{11} = U_{22} = U_{33} = 0.0279(2)$ Å^2, $U_{12} = U_{13} = U_{23} = -0.0044(2)$ Å^2	

Table 4. Selected Bond Lengths (Å) of $Li_4Ti_5O_{12}$ at 900 °C

Li1−O (4×)	2.0272(5)	Li*−O1 (3×)	1.98(7)
Li1−Li* (4×)	1.20(7)	Li*−O1 (3×)	2.62(7)
Li1−Li* (4×)	2.47(7)	Li*−Li* (1×)	1.28(10)
Ti/Li2−O (6×)	2.0164(5)	Li*−Li* (3×)	1.96(10)

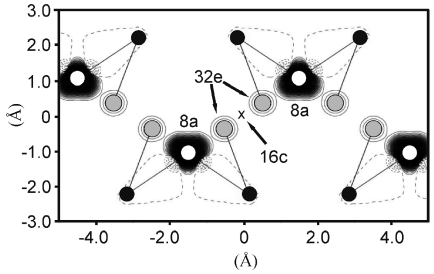

Figure 5. PDF of lithium at 900 °C in the *xxz* plane through 8a and 16c sites. The shortest bond distances between lithium [Li on 8a (white), Li* on 32e (gray), and O on 32e (black)] are indicated. Long dashed lines indicate zero densities and short dashed lines negative densities.

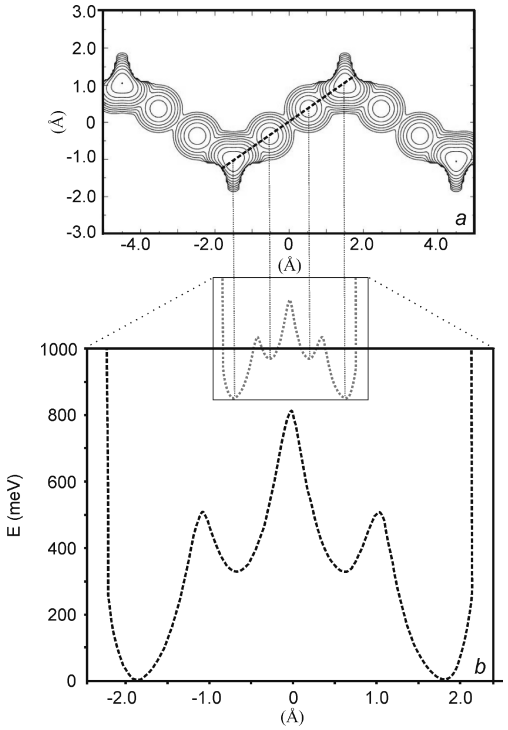

Figure 6. (a) OPP of lithium at 900 °C in the *xxz* plane through 8a, 32e, and 16c sites (the same section as that in Figure 5). Contour lines are in steps of 100 meV. The dotted line shows the linear section along the [111] direction depicted in part b.

rather homogeneous phase was found to be present and the β-Li_2TiO_3 impurities were <0.5 wt %. Vtiņš et al. mentioned that mixtures of $Li_4Ti_5O_{12}$ and β-Li_2TiO_3 form solid solutions of $Li_{2-x}Ti_{1+x}O_3$ above 900 °C.[15] For our sample, either the annealing for 2 h at 900 °C was too short or the temperature was too low to obtain a complete solid solution and therefore still a minor fraction of β-Li_2TiO_3 was detected.

Decomposition of the $Li_4Ti_5O_{12}$ sample started at 1000 °C, which is within the reported range.[19,20] At 1100 °C, the spinel had fully decomposed into the ramsdellite-type $Li_2Ti_3O_7$ and γ-Li_2TiO_3. The ratio of $Li_2Ti_3O_7$ to γ-Li_2TiO_3 of 2.61(2):1 at 1100 °C equals a Li/Ti ratio of 0.82(1):1, which is ∼2% higher than the Li/Ti ratio in $Li_4Ti_5O_{12}$. Considering the minor β-Li_2TiO_3 fraction at low temperature, the Li/Ti ratio is rather stable during the whole experiment and no sign of lithium evaporation was noticeable. Therefore, e.g., the usage of 8% lithium in excess for the syntheses of $Li_4Ti_5O_{12}$ to compensate for the lithium loss at high temperatures[1] and similar assumptions in refs 35 and 36 should be considered with care. A plausible explanation for using lithium in excess might be the similarity of the diffraction patterns of $Li_4Ti_5O_{12}$ and β-Li_2TiO_3. Minor impurities of β-Li_2TiO_3 are hard to detect by standard PXRD, whereas only a slight lithium deficiency in $Li_4Ti_5O_{12}$ causes clear reflections of titania.

Structure Evolution with Temperature. As seen from the behavior of the *u* parameter in Figure 2, the 8a tetrahedral volume increases strongly with the temperature. The volume increase of the 16d octahedron is less, which is due to the stronger Ti−O bond in the octahedron compared with the Li−O bond in the tetrahedron, and thus the Li1−O distance is already becoming larger than the Li2/Ti−O distance (u > 0.0125) below 100 °C (Figure 2c). Extrapolation of the isotropic ADPs to 0 K shows that all pass through B_{iso} = 0 at 0 K (Figure 2d). This means that no appreciable disorder is present in this compound. Only B_{iso} of Li1 on the 8a site starts to deviate above 700 °C, indicating the onset of anharmonic motion. For this reason, anharmonic refinements have been performed at 900 °C.

Lithium Migration. Regarding, e.g., the recent study by Vijayakumar et al.[18] on a $Li_4Ti_5O_{12}$ sample, one can propose that the lithium occupancy in $Li_4Ti_5O_{12}$ depends on the

dx.doi.org/10.1021/cm103332y |*Chem. Mater.* XXXX, XXX, 000–000

synthesis technique and/or the synthesis temperature. In ref 18, NMR was used to determine that lithium partly occupies the 16c position at room temperature, in contrast to the observations of the present study. Other studies show that the crystallinity of the $Li_4Ti_5O_{12}$ samples strongly depends on the annealing temperature[37] and that the electrochemical intercalation of more than three Li^+ ions in nanoparticulate $Li_4Ti_5O_{12}$ samples is possible.[11] This suggests that the particle size as well as the synthesis conditions influences the crystal structure, and probably also the ionic conductivity and lithium migration in $Li_4Ti_5O_{12}$. In the present study, below 700 °C, the lithium occupancy on crystallographic sites other than 8a and 16d could not be proven. Higher lithium mobility was determined at 700 °C, and lithium migration of approximately 14(2)% from tetrahedral 8a sites to the split sites around 16c is determined at 900 °C. The PDF of lithium on 8a at 900 °C (Figure 5) shows bulges in the directions of the tetrahedral faces, typical for anharmonic vibrations in tetrahedral symmetry. The negative areas in Figure 5 are artifacts due to series termination effects, which usually appear for very large gradients of the PDF. Here they simply demonstrate the repulsion toward the nearest oxygen atom. It has to be noted that the distance between Li* and the nearest oxygen is similar to that between Li1 and oxygen (cf. Table 4), meaning that a transient bond between Li* and oxygen is established (indicated by the connecting lines in Figure 5). Note that Li* exactly on 16c would lead to an unacceptable long distance of about 2.24 Å. Therewith, a plausible diffusion path may be presented. Stimulated by the anharmonic vibration, lithium passes from 8a through the face of the surrounding oxygen tetrahedron to the neighboring Li* site (step 1), switches to the adjacent Li* site (step 2), where it is bonded transiently to another oxygen, and jumps into the next tetrahedron (step 1′). In this way, only rather short jump distances are involved: 1.20, 1.28, and 1.20 Å (cf. Table 4). This process is facilitated by the increase of the tetrahedral volume (see Figure 2c), meaning an enlargement of the opening of the oxygen triangle formed by the tetrahedral face. From Figure 6a,b, the activation energies for steps 1 and 2 are about 500 and 800 meV, respectively. The ADP of Li* being isotropic and constrained to that of Li1 is certainly an oversimplification imposed by the refinement requirements, such that the true activation energies are expected to be somewhat lower. Therewith, they are in good agreement with the experimental value of 640 meV[14] at the same temperature. It should be emphasized that the PDF, as determined by diffraction methods, is a time and space average and is thus comparable to macroscopic measurements. It does not represent an actual single-hopping process, which is triggered by phonon-assisted opening of the "windows". Wagemaker et al.[23] proposed that the 16c position is unoccupied and that there is a saddle point of the energy barrier between the two 8a positions. Although their NMR measurements were done at room temperature and on partially intercalated samples, they can be compared with our findings at high temperatures because the potential landscape imposed by the surrounding framework is still similar. Hence, the results of the present study at 900 °C match nicely with the lithium diffusion path at low temperatures, refining it further by observation on the 32e sites. Similarly, one could propose that the possible lithium occupancy, other than on 8a or 16d, will be on split sites 32e rather than exactly on 16c. Because in using NMR no direct average structure information can be revealed, it might be possible that Vijayakumar et al.[18] observed the signal of the chemical shift of lithium on 32e instead of lithium on 16c.

Theories about the order−disorder phase transformations of $Li_4Ti_5O_{12}$ at high temperatures are based on changes of the conductivity measured by impedance spectroscopy.[13,14] Whether the method to synthesize $Li_4Ti_5O_{12}$ or the measurement conditions for high-temperature experiments influence the results has to be verified. High-temperature measurements were performed either in air or in vacuum, operated with different heating rates, and the constitution of the sample varies by using either pressed pellets[13−16] or a loose powder, as in the present study. Here, neutron powder diffraction was applied to study $Li_4Ti_5O_{12}$ at high temperatures, and no order−disorder phase transition could be observed, except partial lithium migration to split sites around the 16c positions at 900 °C and higher lithium mobility starting at 700 °C.

CONCLUSIONS

The inferred order−disorder phase transitions upon heating of $Li_4Ti_5O_{12}$ cannot be confirmed by the present study. Because of higher lithium mobility above 700 °C, lithium ions start to migrate from the tetrahedral 8a positions but do not reside on 16c sites, as was assumed before. Lithium ions are displaced from the 16c sites into metastable positions determined by a potential minimum imposed by the surrounding oxygen geometry. It has already been shown before using NMR measurements at low temperatures that the 16c sites are unfavorable positions for lithium diffusion, which compares well with our findings for the lithium occupancy and lithium diffusion in $Li_4Ti_5O_{12}$ at high temperatures. The activation energy determined in the present study at 900 °C is in good agreement with the literature. Moreover, neutron powder diffraction is able to reveal the actual details of the long-range three-dimensional zigzag diffusion path in all ⟨110⟩ directions.

ASSOCIATED CONTENT

Supporting Information. Seven CIF files recorded at room temperature (15 °C), 300, 500, 700, 900, 1000, and 1100 °C, created using the program *FULLPROF*,[26] and a CIF file of the 900 °C measurement, created by the program *JANA*.[28] This material is available free of charge via the Internet at http://pubs.acs.org.

AUTHOR INFORMATION

Corresponding Author

*E-mail: laumann@min.uni-muenchen.de.

ACKNOWLEDGMENT

E. Schmidbauer is thanked for fruitful discussions. M.B. thanks the Villum Kann Rasmussen Foundation for funding, and A.L. thanks Süd-Chemie AG for funding.

REFERENCES

(1) Ferg, E.; Gummow, R. J.; De Kock, A.; Thackeray, M. M. *J. Electrochem. Soc.* **1994**, *141*, L147.

(2) Ohzuku, T.; Ueda, A.; Yamamoto, N. *J. Electrochem. Soc.* **1995**, *142*, 1431.

(3) Scharner, S.; Weppner, W.; Schmid-Beurmann, R. *J. Electrochem. Soc.* **1999**, *146*, 857.

(4) Matsui, E.; Abe, Y.; Senna, M.; Guerfi, A.; Zaghib, K. *J. Am. Ceram. Soc.* **2008**, *91*, 1522.

(5) Colbow, K. M.; Dahn, J. R.; Haering, R. R. *J. Power Sources* **1989**, *26*, 397.
(6) Zaghib, K.; Simoneau, M.; Armand, M.; Gauthier, M. *J. Power Sources* **1999**, *81*−*82*, 300.
(7) Deschanvres, A.; Raveau, B.; Sekkal, Z. *Mater. Res. Bull.* **1971**, *6*, 699.
(8) Kataoka, K.; Takahashi, Y.; Kijima, N.; Akimoto, J.; Oshima, K. *J. Phys. Chem. Solids* **2008**, *69*, 1454.
(9) Julien, C. M.; Zaghib, K. *Electrochim. Acta* **2004**, *50*, 411.
(10) Wagemaker, M.; Simon, D. R.; Kelder, E. M.; Schoonman, J.; Ringpfeil, C.; Haake, U.; Lützenkirchen-Hecht, D.; Frahm, R.; Mulder, F. M. *Adv. Mater.* **2006**, *18*, 3169.
(11) Borghols, W. J. H.; Wagemaker, M.; Lafont, U.; Kelder, E. M.; Mulder, F. M. *J. Am. Chem. Soc.* **2010**, *131*, 17786.
(12) Colin, J.-F.; Godbole, V.; Novák, P. *Electrochem. Commun.* **2010**, *12*, 804.
(13) Leonidov, I. A.; Leonidova, O. N.; Perelyaeva, L. A.; Samigullina, R. F.; Kovyazina, S. A.; Patrakeev, M. V. *Phys. Solid State* **2003**, *45*, 2079.
(14) Leonidov, I. A.; Leonidova, O. N.; Samigullina, R. F.; Partrakeev, M. V. *J. Struct. Chem.* **2004**, *45*, 262.
(15) Vitiņš, Ģ.; Ķizāne, G.; Lūsis, A.; Tiliks, J. *J. Solid State Electrochem.* **2002**, *6*, 311.
(16) Fehr, K. T.; Holzapfel, M.; Laumann, A.; Schmidbauer, E. *Solid State Ionics* **2010**, *181*, 1111.
(17) Pecharromán, C.; Amarilla, J. M. *Phys. Rev. B* **2000**, *62*, 12063.
(18) Vijayakumar, M.; Kerisit, S.; Rosso, K. M.; Burton, S. D.; Sears, J. A.; Yang, Z.; Graff, G. L.; Liu, J.; Hu, J. *J. Power Sources* **2011**, *196*, 2211.
(19) Gicquel, C.; Mayer, M. M.; Bouaziz, R. *C. R. Acad. Sci. Paris, Sér. C* **1972**, *275*, 1427.
(20) Izquierdo, G.; West, A. *Mater. Res. Bull.* **1980**, *15*, 1655.
(21) Kleykamp, H. *Fusion Eng. Des.* **2002**, *61*−*62*, 361.
(22) Wilkening, M.; Amade, R.; Iwaniak, W.; Heitjans, P. *Phys. Chem. Chem. Phys.* **2007**, *9*, 1239.
(23) Wagemaker, M.; van Eck, E. R. H.; Kentgens, A. P. M.; Mulder, F. M. *J. Phys. Chem. B* **2009**, *113*, 224.
(24) Aldon, L.; Kubiak, P.; Womes, M.; Jumas, J. C.; Olivier-Fourcade, J.; Tirado, J. L.; Corredor, J. I.; Vicente, C. P. *Chem. Mater.* **2004**, *16*, 5721.
(25) Hoelzel, M.; Senyshyn, A.; Gilles, R.; Boysen, H.; Fuess, H. *Neutron News* **2007**, *18*, 23.
(26) Rodríguez-Carvajal, J. *Physica B* **1993**, *192*, 55.
(27) Thompson, P.; Cox, D. E.; Hastings, J. B. *J. Appl. Crystallogr.* **1987**, *20*, 79.
(28) Petricek, V.; Dušek, M. *The Crystallographic Computing System JANA2000*; Institute of Physics: Praha, Czech Republic, 2000.
(29) Han, T. *International Tables for Crystallography*; Reidel: Dordecht, The Netherlands, 1983; Vol. A.
(30) Kataoka, K.; Takahashi, Y. Y.; Kijima, N.; Nagai, H. *Mater. Res. Bull.* **2009**, *44*, 168.
(31) Laumann, A.; Fehr, K. T.; Boysen, H.; Hoelzel, M.; Holzapfel, M. *Z. Kristallogr.* **2011**, *226*, 53.
(32) Mikkelsen, J. C. *J. Am. Ceram. Soc.* **1980**, *63*, 331.
(33) Boysen, H. *Z. Kristallogr.* **2003**, *218*, 123.
(34) Laumann, A.; Fehr, K. T.; Holzapfel, M.; Wachsmann, M.; Iversen, B. B. *Solid State Ionics* **2010**, *181*, 1525.
(35) Huang, S.; Wen, Z.; Zhu, X.; Gu, Z. *Electrochem. Commun.* **2004**, *6*, 1093.
(36) Yu, Y.; Shui, J. L.; Chen, C. H. *Solid State Commun.* **2005**, *135*, 485.
(37) Qiu, Z.; Yang, L.; Tang, Y.; Fang, S.; Huang, J. *Chin. J. Chem.* **2010**, *28*, 911.

Appendix G

Sixth publication

Continuous flow hydrothermal synthesis of $Li_4Ti_5O_{12}$ – investigation of structural disorder during annealing in air and its effects on the electrochemical performance

Under preparation

Andreas Laumann,[a] **Martin Bremholm,**[b] **Peter Hald,**[c] **Karl Thomas Fehr,**[a] **Michael Holzapfel,**[d] **Bo Brummerstedt Iversen**[c]

[a] Ludwig-Maximilians-Universität München, Department of Earth and Environmental Sciences, Section for Mineralogy, Petrology and Geochemistry, Munich, Germany
[b] Department of Chemistry, Princeton University, Princeton, NJ 08544, USA
[c] Aarhus University, Department of Chemistry and iNANO, Aarhus C, Denmark
[d] Süd-Chemie AG, Battery Materials, Moosburg, Germany

Continuous flow hydrothermal synthesis of $Li_4Ti_5O_{12}$ - investigation of structural disorder during annealing in air and its effect on the electrochemical performance

Andreas Laumann,[1] Martin Bremholm,[2] Peter Hald,[3] Michael Holzapfel,[4] Karl Thomas Fehr,[1] and Bo Brummerstedt Iversen[3,*]

[1] Department für Geo- und Umweltwissenschaften, Sektion Mineralogie, Petrologie und Geochemie, Universität München, Theresienstr. 41, 80333 München, Germany
[2] Department of Chemistry, Princeton University, Princeton, NJ 08544, USA
[3] Centre for Materials Crystallography, Department of Chemistry and iNANO, Aarhus University, Langelandsgade 140, DK-8000 Aarhus C, Denmark
[4] Battery Materials, Süd-Chemie AG, Ostenrieder Str. 15, 85368 Moosburg, Germany

* Corresponding author: bo@chem.au.dk

Keywords: $Li_4Ti_5O_{12}$, hydrothermal synthesis, powder X-ray diffraction, microstructure analysis, electrochemical performance.

Abstract

The anode material $Li_4Ti_5O_{12}$ was for the first time crystallized directly by a novel hydrothermal method using lithium ethoxide and titanium isopropoxide as reactants. Crystalline particles are obtained in a single step and in less than one minute by mixing the reactants with superheated water in a continuous flow reactor at near- and supercritical conditions (T = 350 °C, P = 250 bar). The average crystallite size is 4.6 nm with a specific surface area of 230 m^2/g, and the anatase impurity level <1 wt%. *In-situ* synchrotron X-ray powder diffraction upon annealing of the hydrothermally produced nanocrystalline $Li_4Ti_5O_{12}$ was performed in order to investigate the structural and microstructural changes from ambient temperature to 727 °C. Although crystalline, the as prepared nanocrystals show severe crystallographic strain but upon annealing at temperatures above ~500 °C the strain is found to relax drastically concurrent with the onset of crystal growth. Comparison of

electrochemical tests of $Li_4Ti_5O_{12}$ as prepared and after annealing at 600 °C shows that the annealing results in a significant improvement of the performance. The origin of the crystallographic strain is discussed and further optimization of the synthetic approach is suggested.

Introduction

$Li_4Ti_5O_{12}$ is known as an inherently safe anode material for rechargeable lithium-ion batteries with high potential as an alternative to the currently most used graphite. Its safety [1, 2], its excellent lithium ion mobility [3], its long cycle life [4, 5], and the low volume change [2, 4, 6] which $Li_4Ti_5O_{12}$ undergoes during the charge and discharge process are the main advantages of $Li_4Ti_5O_{12}$ compared with graphite, especially for large–scale applications like electric vehicles (EV) and batteries for stationary power plants. Due to the subtle structural changes during the electrochemical lithium insertion process of $Li_4Ti_5O_{12}$ and its lithiated form $Li_7Ti_5O_{12}$, the material is also called "zero-strain material" [2,3,6]. $Li_4Ti_5O_{12}$ possesses a flat potential of about 1.55 V (vs. Li^+/Li) with a theoretical capacity of 175 mAh/g. But also higher capacities of nanoparticulate $Li_4Ti_5O_{12}$ have been reported [7 - 10], which recently were attributed to a higher lithium insertion probability in $Li_4Ti_5O_{12}$ due to the reduced particle size [10]. However, apart from one sample of the study of Borghols *et al.* [10], the initial high capacities of more than 200 mAh/g decrease rapidly to expected values below 200 mAh/g. The fast decrease in capacity of nanoparticulate $Li_4Ti_5O_{12}$ is ascribed to the low crystallinity [8]. For a $Li_4Ti_5O_{12}$ compound synthesized via a sol-gel process, the highest crystallinity was obtained at 900 °C [9]. Aggregation of nanoparticles can lead to fast decreasing of the capacity, or a general lower capacity [11, 12]. Surfactants [11] or gelating agents for the sol-gel process [12] improve the dispersion of the particles and can increase the capacity and the cyclability.

The crystal structure of $Li_4Ti_5O_{12}$ was determined by Deschanvres *et al.* [13] to be of the spinel-type (space group *Fd-3m*) and was confirmed by single crystal X-ray diffraction

[14]. The unit cell contains eight formula units of $Li^{8a}[Li_{1/3}Ti_{5/3}]^{16d}O_4^{32e}$, in which lithium fully occupies the tetrahedral 8*a* sites. The octahedral 16*d* sites are randomly occupied by 1/6 of lithium and 5/6 of titanium and oxygen occupies the 32*e* tetrahedral sites [14,15].

Recently a neutron diffraction study of $Li_4Ti_5O_{12}$ at elevated temperatures showed increased mobility and delocalization of lithium above 700 °C [16], which earlier by spectroscopic methods has been ascribed to order-disorder phase transitions upon heating of $Li_4Ti_5O_{12}$ by spectroscopic methods [17-20].

Various methods to synthesize $Li_4Ti_5O_{12}$ are described, whereof the most common are solid-state reactions, sol-gel, and spray drying or spray pyrolysis techniques [1 - 22]. These methods either use high synthesis temperatures or require post-annealing at temperatures of approximate 800 °C. $Li_4Ti_5O_{12}$ can not be obtained by hydrothermal reactions of crystalline titania in lithium hydroxide solution [23, 24]. In contrary to results of previous studies [25, 26], the product of this reaction is α-Li_2TiO_3, a metastable compound, in which lithium is bond weakly and can be removed e.g. with deionized water. Thus α-Li_2TiO_3 can theoretically be driven to a Li/Ti ratio of about 4/5, and may be optimized to produce phase-pure $Li_4Ti_5O_{12}$ after heat-treatment [23].

For the first time, this study shows that $Li_4Ti_5O_{12}$ can be produced in sub- and supercritical fluids at $T > 350$ °C and a pressure of 250 bar in a one-step synthesis. The lithium titanium spinel produced has a very high specific surface area of ~230 m²/g and a primary particle size of about 5 nm, in general an indicator for an excellent power capability. However, the material shows an amorphous fraction of approximately 11%, which leads to a capacity fade when cycled in electrochemical tests. Annealing at only 600 °C improved the electrochemical performance which is due to the strain relaxation and the overall higher crystalline fraction, demonstrated by *in-situ* synchrotron powder X-ray (PXRD) diffraction upon heating to 727 °C.

Experimental

Setup

The syntheses were performed in a continuous flow hydrothermal reactor, which is designed for high pressures and temperatures. An outline of the reactor design is shown in Fig. 1. When the desired temperature and pressure are maintained, a prepared solution or suspension of reactants, and a solvent to react with, are pumped separately in the reactor. The solvents were heated close to, or above their critical point in the first heating block, so that the cold reactants hit the hot solvent and start to react immediately. The product remains, depending on the flow rate of reactant and solvent, up to 1 minute in the hot zone of the second heating block before it exits the outlet valve. Experiments were performed for set temperatures of the heaters between 350 and 425 °C at a constant pressure of 250 bar. A product which was found to be phase-pure by standard powder X-ray diffraction (referred to as LTO in the following), the reaction conditions were: both heaters were set to 425 °C, the pressure was 250 bar and the flow rates were 3 ml/min and 6 ml/min for the reactants and the preheated water, respectively. For the current configuration of the flow reactor, these conditions practically correspond to the maximum heat input. The injection of the cold reactants into the reactor results in a temperature at the mixing point of 350 °C and a maximum of 360 °C in the final section. The residence time in heated part of the reactor can be estimated from the reactor volume, the overall flow rate and average fluid density to ~30 s.

Reactants

The reactants were prepared using lithium and titanium reactants in a ratio of 4:5 with 5% lithium in excess. The lithium component was lithium metal dissolved in absolute ethanol, and titanium (IV) isopropoxide (TTIP) (Sigma-Aldrich, 97%) was used as titanium precursor. For sample LTO, 0.745 g of lithium metal was dissolved in 100 ml of absolute ethanol, and then, 300 ml of isopropyl alcohol (IPA) and 37 ml of TTIP were added under stirring. After

dissolving higher amounts of lithium metal in absolute ethanol, the solution appeared saturated, *i.e.* the mixture did not totally turn clear. After adding TTIP (50 ml) the mixture turned clear. To prevent clogging of the continuous flow reactor, IPA was used to dilute the solutions. After syntheses, the products were separated from the solvent using a centrifuge and washing with IPA. For the syntheses in the flow reactor, deionized water was used as the preheated solvent.

Electrochemistry

Sample LTO, produced by hydrothermal synthesis, and a fraction of the same batch annealed at 600 °C for 12 hours (LTO-HT) were used as active materials for half-cells to test the electrochemical performance of the material. Electrodes were prepared of 85% active material (loading 2.3 mg/cm²), 10% carbon black and 5% poly(vinylidene difluoride) PVdF binder on Al foil. The electrolyte was a mixture of ethylene carbonate (EC) and dimethyl carbonate (DMC) (1:1 molar ratio), 1 M $LiPF_6$. Lithium metal was used as counter electrode and glass fibre as separator. The cells were dried at 105 °C under vacuum, assembled in an argon-filled glove box, cycled between 1.0-2.0 V vs. Li/Li^+ and held at 1.0 V until the current reached *C*/50, *D*/50 for the discharge at 2.0 V, respectively.

Characterization

Synchrotron powder X-ray (PXRD) measurements were performed on LTO (Table 1) at beamline Bl02B2, SPring8, Japan. PXRD patterns were recorded in temperature increments of 100 °C in a temperature range from 27 °C to 727 °C. Measuring time for each temperature step was 2.5 minutes. Structural Rietveld refinements were performed by using the program FullProf [28] and the peaks were fitted with the Thompson-Cox-Hastings pseudo-Voigt Axial divergence asymmetry peak shape [29]. The Gaussian and Lorentzian full width at half maximum (FWHM) is calculated from

$$FWHM_G^2 = (U + e^2)\tan^2\Theta + V\tan\Theta + W \quad (1)$$

$$FWHM_L = (Y + \lambda / L)/\cos\Theta \quad (2)$$

where *U*, *V*, *W* and *Y* are the instrumental resolution parameters (obtained from a LaB_6 standard sample), λ is the wavelength, and $e=\Delta d/d$ and *L* are the "apparent" strain and size parameters, respectively. The wavelength (λ = 0.4332 Å) and the instrumental broadening were determined with a CeO_2 standard. The *in situ* measurements were performed in a 0.5 mm quartz capillary. BET measurements were performed with a Micromeritics Gemini VII.

Results

Products in general were of white colour, only when a slow flow rate of the solvent was used, some products had a blue tint. Thus, partial reduction of tetravalent to trivalent titanium can be expected when the reaction conditions are slightly reducing. In the following we focus on the sample prepared by the optimized conditions

The $Li_4Ti_5O_{12}$ particles form flake-like aggregates (Fig. 2a) with a very high specific surface area (BET), e.g. LTO of ~230 m²/g, indicating a open structure of the aggregates. After heating to 600 °C (LTO-HT), the flake-like aggregates had transformed to isotropic shape (Fig. 2b).

PXRD

Preliminary PXRD measurements with standard X-ray powder diffraction revealed that syntheses in the continuous flow reactor brought out $Li_4Ti_5O_{12}$ samples of which some showed minor impurities of anatase. LTO was found to be phase-pure, and was therefore studied in detail by synchrotron PXRD upon heating from room temperature to 727 °C. It could clearly be identified as $Li_4Ti_5O_{12}$ and was refined in space group *Fd-3m*. Due to the low X-ray scattering factor for light elements, such as Li, the atomic occupancies of $Li_4Ti_5O_{12}$ were fixed to the stoichiometric values. The unit cell parameter of *a* = 8.3526(5) Å of LTO at

room temperature is slightly lower than values reported before: Kataoka *et al.* a = 8.352(4) Å [14], Laumann *et al.* a = 8.35952(4) Å [30]. The increase of the unit cell upon heating is depicted in Fig. 4a and Table 1.

At room temperature, an impurity of ~0.5 wt% anatase was found (Fig. 3), which could not be detected by standard PXRD. Upon heating of LTO to 527 °C, this impurity was constant at about 0.5 wt%. At 627 °C, higher impurities of anatase were found and at 727 °C an impurity of ~5 wt%, comprising anatase and rutile, was present. It was observed, that lithium from LTO started to react with the quartz capillary at 627 °C, and at 727 °C distinct reflections of high-quartz (PDF No.: 870703) were detected. The reaction of lithium with the quartz capillary is likely the cause for the increase of anatase and rutile impurities.

Strain *and size*

From room temperature up to 527 °C, LTO showed extremely high strain. Strong correlation of the strain parameter U with B_{iso} was found and results in unphysical B_{iso} values. By constraining the B_{iso}'s of all atoms to a global B_{iso} enabled refinement with reliable values. At 627 °C, the strain decreased remarkably (Table 1 and Fig. 4b). In order to present data which was refined uniformly, data at 627 and 727 °C was treated the same way, although B_{iso} returned to reliable values when the sample was comparatively strain-free.

The particle size of $Li_4Ti_5O_{12}$ at room temperature was refined to be 4.6(3) nm (Table 1 and Fig. 4d). Upon heating to 427 °C, the particle sizes were constant within error range. Then, after having a size of 6.4(3) nm at 527 °C, at 627 °C the particle size reached 14.5(8) nm, and the measurement at 727 °C depicted particles of 62(1) nm in size. The sharpening of the $Li_4Ti_5O_{12}$ peaks with increasing particle size is shown in Fig. 4e.

Crystallinity

The refined scale factor of LTO can be regarded as a measure of the crystallinity of the sample. Considering LTO to be fully crystalline at 727 °C, the observed scale factor for the synthesized LTO corresponds to a crystallinity of 88.9(5) % (Table 1 and Fig. 4c). Similar to the particle size and the strain, the scale factor shows no significant change between room temperature and 527 °C. Striking changes were observed at 627 °C and especially at 727 °C.

Table 1: Crystallographic data. Unit cell dimension, volume, the oxygen position (parameter *u*), the particles size and strain, the normalized scale factor (sf) and the reliability factors of LTO between 27 and 727 °C.

Temp. (°C)	27	127	227	327	427	527	627	727
a (Å)	8.3526(5)	8.3598(5)	8.3768(5)	8.3863(5)	8.4035(5)	8.4174(4)	8.4323(2)	8.4567(1)
V (Å³)	582.73(6)	584.23(6)	5.8781(6)	589.81(6)	593.45(6)	596.403	599.56(3)	603.92(1)
Parameter (*u*)	0.2611(1)	0.2615(1)	0.2615(1)	0.2612(1)	0.2616(1)	0.2622(1)	0.2627(1)	0.26329(9)
Size (nm)	4.6(3)	4.6(4)	4.6(3)	4.6(3)	5.0(4)	6.4(3)	14.5(8)	62(1)
Strain (%)	3.9(2)	4.3(2)	4.7(1)	4.9(1)	4.8(1)	4.9(1)	0.4(1)	0.7(1)
Normalized sf.	0.889(5)	0.883(5)	0.864(5)	0.885(5)	0.903(4)	0.910(4)	0.972(3)	1.000(6)
*R*p	2.51	2.40	2.52	2.38	2.36	2.22	2.95	3.61
*R*wp	3.13	3.00	3.16	2.95	2.94	2.82	3.91	5.10
χ^2	1.89	2.44	2.62	2.29	2.34	2.23	4.67	8.17[1]

[1] High error caused by the transformation of anatase to rutil and the quartz reaction with Li forming Li_2SiO_3

Number of data points: 3175 (3138); Number of refined background parameters: 52 (46)²; Total number of refined parameters: 77 (73)

Electrochemistry

Electrochemical tests were performed on various samples without heat treatment and in particular on LTO (Fig. 5a and 5c), and the annealed sample LTO-HT (Fig 6b and d). Although the synthesis conditions varied, electrochemical measurements of $Li_4Ti_5O_{12}$ samples without heat treatment showed only minor aberrations from each other. The first charging cycle at *C*/10 shows a very high specific capacity (> 200 mAh/g). By charging and discharging at higher rates (up to 20*C*/20*D*), the specific capacity degreases to about 80 mAh/g for charging and to 100 mAh/g for discharging, respectively (Fig. 5a). In the following cycles the specific capacity at 1*C*/1*D* drops to ~140 mAh/g and degreases to a value of ~ 100 mAh/g after 85 cycles (Fig. 5c).

LTO-HT showed a much better electrochemical performance than LTO, in terms of the specific capacity, the capacity at high rates (Fig. 5b), and the long term cyclability (Fig. 5d). The characteristic plateau at 1.55 V of LTO-HT is flatter and longer than the one of LTO, which indicates the particle growth due to annealing. In the first cycle the specific capacity is ~160 mAh/g and decreases only by ~5 mAh/g after 50 cycles (Fig. 5d).

Discussion

In a short reaction time of ~30 s and the low reaction temperature of the continuous flow synthesis, crystalline (~89%) $Li_4Ti_5O_{12}$ was produced in a single step are but with a high degree of crystal strain. Above 527 °C the crystalline fraction is observed to increase to 100% concurrent with relaxation of the crystal strain and growth of the nanoparticles. The origin of the strain broadening is defects in the crystal structure and could be due to disordered lithium. Refinement at higher temperatures revealed as well higher fractions of titania, most likely due to the reaction of lithium with the glass capillary and is specific to the *in situ* measurement. The general lower capacity of LTO (Fig. 5a), compared with LTO-HT (Fig. 5b), matches well

with the 89% crystallinity of LTO, thus the increase of the crystalline fraction due to annealing might result in the higher overall capacity.

At fist glance, the amorphous fraction might also be the reason for the extreme high specific capacity in the first charging cycle of LTO (Fig. 5a). Lithium ions seem to be inserted in a compound which does not release Li^+ in the following discharge cycle. But considering the recent publication of Borghols *et al.* [10], nanoparticulate $Li_4Ti_5O_{12}$ samples were thought to increase the capacity in the first cycles. The authors used $Li_4Ti_5O_{12}$ samples of 12 and of 31 nm and measured very high capacities especially in the first cycles, which they ascribed to a higher lithium intercalation than 3 Li^+, and thus compounds like $Li_8Ti_5O_{12}$ were described. Although the sample of smaller particle size had initially a higher capacity, its capacity dropped quickly below the one with 31 nm. The decreasing capacity of the 12 nm $Li_4Ti_5O_{12}$ within the first 50 cycles could not fully be explained, but was partly ascribed to the possible formation of a solid electrolyte interface (SEI) around the particles due to the high particles surface, which forms areas where reversible intercalation is hindered. Therefore the high capacity of LTO in the first cycle could be ascribed to both, its small particle size and to the amorphous fraction of titania and $Li_4Ti_5O_{12}$.

However, the relatively fast capacity decrease of samples without heat treatment, and of LTO (Fig. 5c), we refer to their low crystallinity. Low crystallinity in battery materials [33] and also in $Li_4Ti_5O_{12}$ [32] was attributed to cause a poor cycling performance, and heat treatment improved the cyclability of the active materials in correspondence with the observations of this study.

It can be proposed that a higher hydrothermal synthesis temperature, longer synthesis time and a higher concentration of the reactants could be implemented to obtain a product of higher crystallinity and of less strain, which would improve the electrochemical performance of $Li_4Ti_5O_{12}$ synthesized by continuous flow reactions. Considering the flake like form of the $Li_4Ti_5O_{12}$ particles after hydrothermal reactions, a better dispersion of the nanoparticles by

adding e.g. surfactants might improve the rate capability as well. When comparing the electrochemical performance of the heat treated sample which other presented and commercial $Li_4Ti_5O_{12}$ samples, its cyclability and its capacity at high rates are competitive.

Conclusions

The present study is the first method so far describing the synthesis $Li_4Ti_5O_{12}$ in a direct way via sub- or supercritical synthesis (T > 350°C) by using a lithium ethoxide solution and TTIP as reactants. However, the short reaction time and the relative low temperature of about 350 °C resulted in only partly crystalline samples. Annealing at 600 °C formed a $Li_4Ti_5O_{12}$ compound which is competitive with other $Li_4Ti_5O_{12}$ active materials, which all have been produced at higher temperatures. The annealing to 600 °C only causes minor particle growth as demonstrated by synchrotron PXRD and thus $Li_4Ti_5O_{12}$ nanoparticles with an excellent cyclability and rate performance can be produced.

Acknowledgments

We want to thank Stefanie Busl and Genofeva Wendrich from Süd-Chemie AG Moosburg for their great help with taking the electrochemical measurements. M.B. thanks the Villum Kann Rasmussen foundation for funding and A.L thanks Süd-Chemie AG for the funding.

References

[1] Ferg, E.; Gummow, R. J.; De Kock, A.; J. Electrochem. Soc. **141** (1994) L147.

[2] Zaghib, K.; Armand, M.; Gauthier, M.; J. Electrochem. Soc. **145** (1998) 3135.

[3] Colbow, K.M.; Dahn, J.R.; Haering, R.R.: J. Power Sources **26** (1989) 397.

[4] Ohzuku, T.; Ueda, A.; Yamamoto, N.: J. Electrochem. Soc. **142** (1995) 1431.

[5] Zaghib, K.; Simoneau, M.; Armand, M.; Gauthier, M.: J. Power Sources **81-82** (1999) 300.

[6] Scharner, S.; Weppner, W.; Schmid-Beurmann, R.; J. Electrochem. Soc. **146** (1999) 857.

[7] Shen, C.; Zhang, X.; Zhou, Y.; Li, Hu.: Mater. Chem. and Phys. **78** (200) 437.

[8] Kim, D. H.; Ahn, Y. S.; Kim, J.: Electrochem. Commun. **7** (2005) 1340.

[9] Du Pasquier, A.; Huang, C. C.; Spitler, T.; J. Power Sources **186** (2009) 508.

[10] Borghols, W. J. H.; Wagemaker, M.; Lafont, U.; Kelder, E. M. Mulder, F. M.; J. Am. Chem. Soc. **131** (2010) 17786.

[11] Jiang, C.; Ichihara, M.; Honma, I.; Zhou, H.; Electrochim. Acta **52** (2007) 6470.

[12] Hao, Y. J.; Lai, Q. Y.; Lu, J. Z.; Liu, D. Q.; Ji, X. Y.: J. Alloys Compd. **439** (2007) 330.

[13] Deschanvres A.; Raveau, B.; Sekkal, Z.: Mater. Res. Bull. **6** (1971) 699.

[14] Kataoka, K.; Takahashi, Y.; Kijima, N.; Akimoto, J.; Oshima, K.: J. Phys. Chem. Solids, **69** (2008) 1454.

[15] Julien, C. M.; Zaghib, K.; Electrochim. Acta **50** (2004) 411.

[16] Laumann, A.; Boysen, H.; Bremholm, M.; Fehr, K. T.; Hoelzel, M.; Holzapfel, M.: *Submitted to to Chem. Mater.*

[17] Leonidov, I. A.; Leonidova, O. N.; Perelyaeva, L. A.; Samigullina, R. F.; Kovyazina, S. A. and Patrakeev, M. V.; Phys. Solid State **45** (2003) 2079.

[18] Leonidov , I. A.; Leonidova, O. N.; Samigullina, R. F.; Partrakeev, M. V.; J. Struct. Chem. **45** (2004) 262.

[19] Pecharromán, C.; Amarilla, J. M. Phys. Rev. B **62** (2000) 12063

[20] Vijayakumar, M.; Kerisit, S.; Rosso, K. M.; Burton, S. D.; Sears, J. A.; Yang, Z.; Graff, G. L. Liu, J.; Hu, J.: J. Power Sources, (2010), doi:10.1016/j.jpowsour.2010.09.060, *in press*.

[21] Rho, Y. H.; Kanamura, K.; Fujisaki, M.; Hamagami, J.; Suda, S.; Umegaki, T.; Solid State Ionics **151** (2002) 151.

[22] Ju, S. H.; Kang, Y. C.; J. Power Sources **189** (2009) 185.

[23] Laumann, A.; Fehr, K.T. Holzapfel, M.; Wachsmann, M.; Iversen, B.B.: Solid State Ionics, 181 (2010) 1525.

[24] Laumann, A.; Ørnsbjerg Jensen, K. M.; Tyrsted, C.; Bremholm, M.; Fehr, K. T.; Holzapfel, M., Iversen, B. B.: *Submitted to Eur. J. Inorg. Chem.*

[25] Zhang, D. R.; Liu, H. L.; Jiun, R. H. ; Zhang, N. Z.; Liu, Y. X.; Kang, Y. S.: J. Ind. Eng. Chem. **13** (2007) 92.

[26] Jiang, C.; Hosono, E.; Ichihara, M.; Honma, I.; Zhou, H.: J. Electrochem. Soc. **155** (2008) A553.

[27] Hald, P.; Becker, J.; Bremholm, M.; Pedersen, J. S.; Chevallier, J. Iversen, S. B.; Iversen, B. B.; J. Solid State Chem. **179** (2006) 2674.

[28] Rodriguez-Carvajal, J.: FULLPROF: A program for Rietveld refinement and pattern matching analysis. Abstracts of the satellite meeting on powder diffraction of the XV congress of the International Union of Crystallography, Toulouse, France (1990) 127.

[29] Thompson, P.; Cox, D.E.; Hastings, J.B.: J. Appl. Crystallogr. **20** (1987) 79-83.

[30] Laumann, A.; Fehr, K. T.; Boysen, H.; Hoelzel, M.; Holzapfel, M.: Z. Kristallogr. (2010), doi: 10.1524/zkri.2010.1286, in press.

[31] Sugita: Sugita, M.; Tsuji, M.; and Abe, M.: Bull. Chem. Soc. Jpn. **63** (1990) 1978.

[32] Qiu, Z.; Yang, Li.; Tang, Y.; Fang, S.; Huang, J.: Chin. J. Chem. **28** (2010) 911.

[33] Qi, J.; Xu, P.; Lv, Z.; Liu, X.; Wen, A.: J. Alloys Compd. **462** (2008) 164.

Figures

Figure 1: Outline of the continuous flow hydrothermal reactor used to synthesize $Li_4TiO_5O_{12}$ nanoparticles.

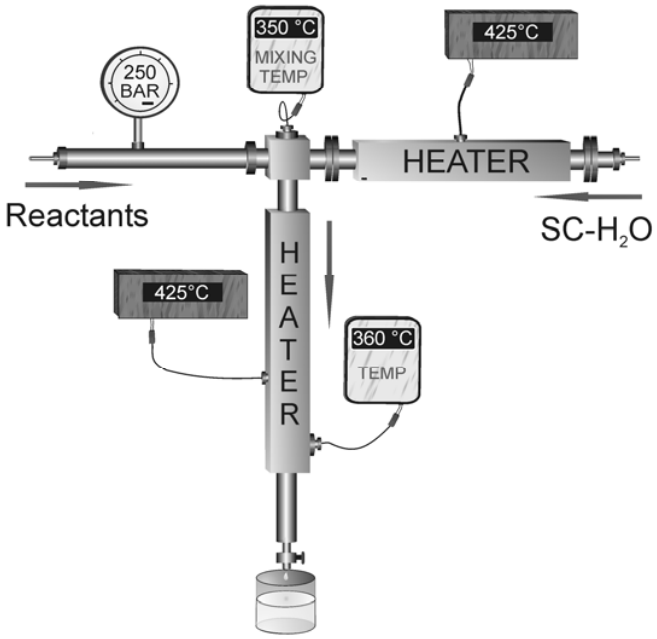

Figure 2: SEM pictures of a) flake-like $Li_4Ti_5O_{12}$ particles after hydrothermal synthesis (LTO) and b) $Li_4Ti_5O_{12}$ particles after annealing at 600 °C (LTO-HT).

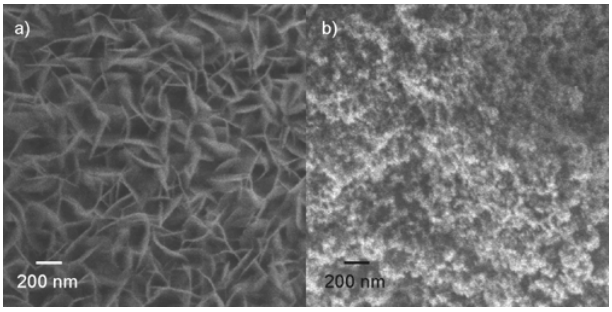

Fig. 3: Structure and Rietveld fit of $Li_4Ti_5O_{12}$ LTO at 27 °C. The inset shows the unit cell of $Li_4Ti_5O_{12}$.

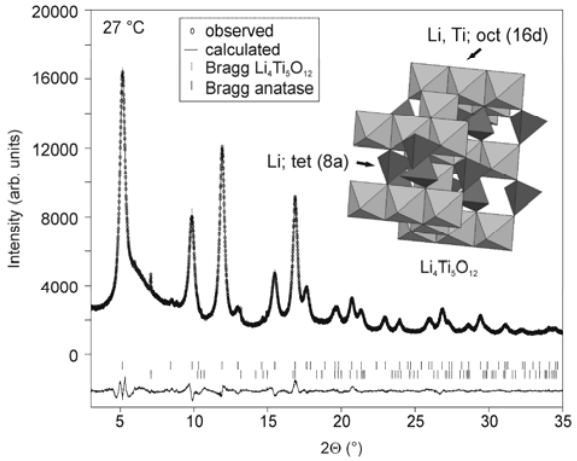

Fig. 4: a) unit cell parameter, b) strain and Global B_{iso}, c) scale factor, d) particle size and e) multi-temperature plot upon annealing of LTO to 727 °C, with detailed view of the (440) reflection given in the inset.

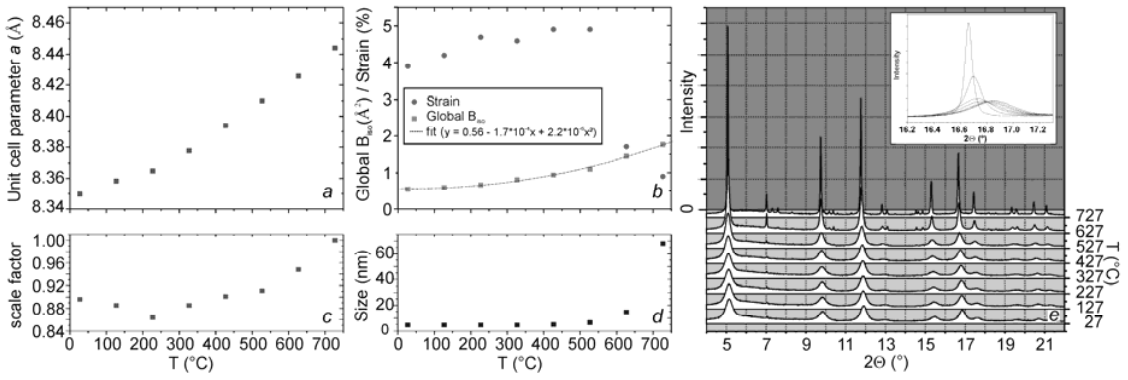

Fig. 5a-d: a) Charge-discharge plateaus of sample 1 without heat treatment for currents from C/10 to 20C, D/10 to 20D, respectively; b) charge-discharge plateaus of the heat-treated sample for currents from C/10 to 20C, D/10 to 20D, respectively; c) cyclability of sample 1 and d) cyclability of the heat-treated sample.

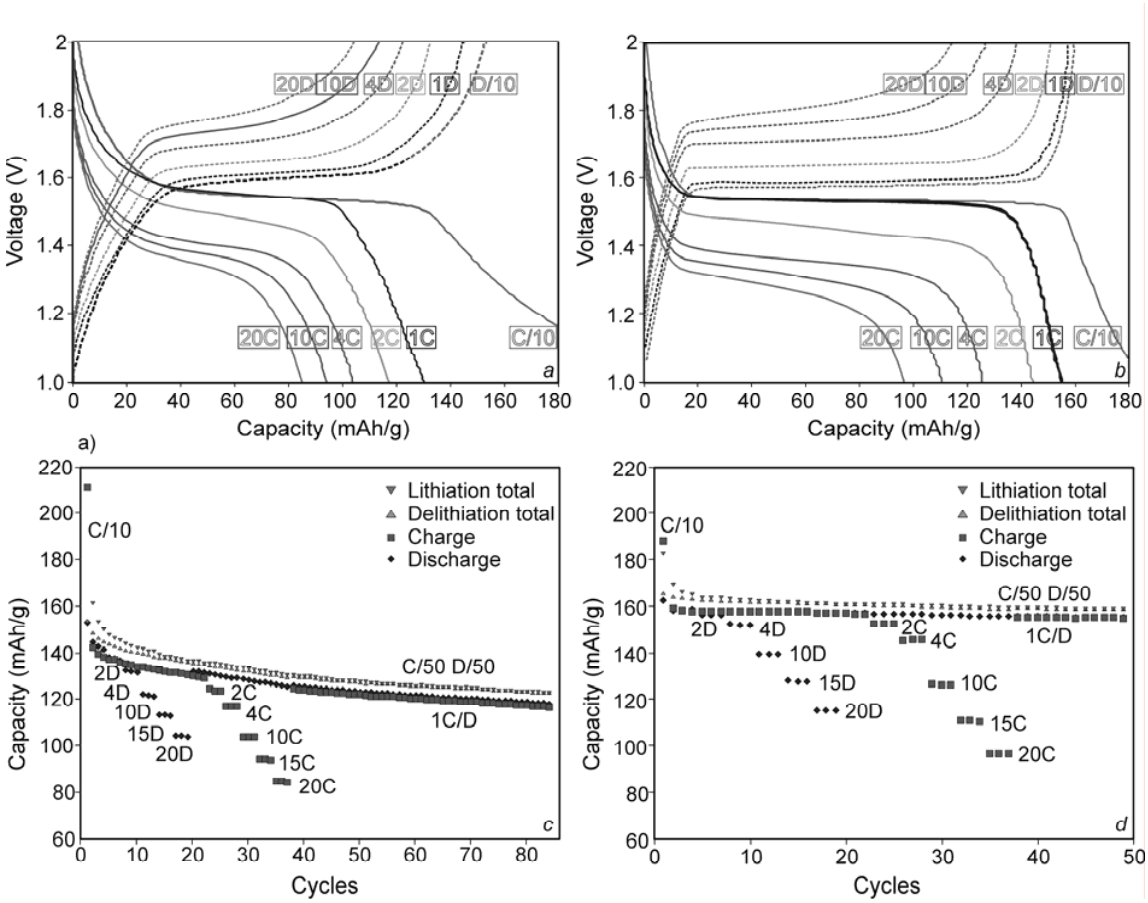

Bibliography

L. Aldon, P. Kubiak, M. Womes, J. C. Jumas, J. Olivier-Fourcade, J. L. Tirado, J. I. Corredor, and C. P. Vicente. Chemical and electrochemical Li-insertion into the $Li_4Ti_5O_{12}$ spinel. *Chem. Mater.*, 16:5721–5725, 2004.

N. W. Ashcroft and N. D. Mermin. *Solid State Physic*. Holt, Rinehart, and Winston, New York, 1976.

M. J. Avrami. Kinetics of phase change. I General theory. *J. Chem. Phys.*, 7:1103–1112, 1939.

M. J. Avrami. Kinetics of phase change. II Transformation-time relations for random distribution of nuclei. *J. Chem. Phys.*, 8:212–223, 1940.

M. J. Avrami. Kinetics of phase change. III Granulation, phase change an microstructures. *J. Chem. Phys.*, 9:177–184, 1941.

P. G. Balakrishnan, R. Ramesh, and T. P. Kumar. Safety mechanisms in lithium-ion batteries. *J. Power Sources*, 155:401–414, 2006.

F. Barblan, E. Brandenberger, and P. Niggli. Geregelte und ungeregelte Strukturen von Titanaten und Ferriten und geregelte Umwandlungen der TiO_2 Modifikationen. *Helv. Chim. Acta*, 27:88–96, 1958.

L. Baños, M. E. Villafuerte-Castrejón, R. Valenzuela, and A. R. West. Kinetics and mechanism of the cation-ordering transformation in Li_2TiO_3-Li_3NbO_4 solid solutions. *J. Chem. Soc. Farady. Trans.*, 86:2979–2983, 1990.

J. Becker, M. Bremholm, C. Tyrsted, B. Pauw, K. M. Ørnsbjerg Jensen, J. Eltzholt, M. Christensen, and B. B. Iversen. Experimental setup for *in situ* X-ray SAXS/WAXS/PDF studies of the formation and growth of nanoparticles in near- and supercritical fluids. *J. Appl. Cryst.*, 43:729–736, 2010.

I. Belharouak, W. Lu, and K. Amine. Safety characteristics of the $Li_4Ti_5O_{12}/LiMn_2O_4$ Li-ion battery. *Mater. Res. Soc. Symp. Proc.*, 972:0972–AA13–04, 2007.

X. Bokhimi, A. Morales, and F. Pedraza. Crystallography and crystallite morphology of rutile synthesized at low temperature. *J. Solid State Chem.*, 169:176–181, 2002.

W. J. H. Borghols, M. Wagemaker, U. Lafont, E. M. Kelder, and F. M. Mulder. Size effects in the $Li_{4+x}Ti_5O_{12}$ spinel. *J. Am. Chem. Soc.*, 131:17786–17792, 2010.

M. Bremholm, H. Jensen, S. B. Iversen, and B. B. Iversen. Reactor design for *in situ* X-ray scattering studies of nanoparticle formation in supercritical water syntheses. *J. Supercrit. Fluids*, 22:385–390, 2008.

K. Byrappa and T. Adschiri. Hydrothermal technology for nanotechnology. *Progress in Crystal Growth and Characterization of Materials*, 53:117–166, 2007.

M. Castellanos and A. R. West. Order-disorder phenomena in oxides with rock salt structures: the system Li_2TiO_3-MgO. *J. Mater. Sci.*, 14:450–454, 1979.

Y. Cerenius, K. Stahl, L. A. Svensson, T. Ursby, A. Oskarsson, J. Albertsson, and A. Liljas. The crystallography beamline I711 at MAX II. *J. Synchrotron Rad.*, 7:203–208, 2000.

K. M. Colbow, J. R. Dahn, and R. R. Haering. Structure and electrochemistry of the spinel oxides $LiTi_2O_4$ and $Li_{4/3}Ti_{5/3}O_4$. *J. Power Sources*, 26:397–402, 1989.

J. F. Colin, V. Godbole, and P. Novak. *In situ* neutron diffraction study of Li insertion in $Li_4Ti_5O_{12}$. *Electrochem. Commun.*, 12:804–807, 2010.

D. Croker, M. Loan, and B. K. Hodnett. Kinetics and mechanisms of the hydrothermal crystallization of calcium titanate species. *Cryst. Growth Des.*, 9:2207–2213, 2009.

A. Deschanvres, B. Raveau, and Z. Sekkal. Mise en evidence et etude cristallographique d'une nouvelle solution solide de type spinelle $Li_{1+x}Ti_{2-x}O_4$ $0 \leq x \leq 0.333$. *Mater. Res. Bull.*, 6:699–704, 1971.

I. Djerdj and A. M. Tonejc. Structural investigations of nanocrystalline TiO_2 samples. *J. Alloys Compd.*, 413:159–174, 2006.

M. M. Doeff, J. D. Wilcox, R. Kostecki, and G. Lau. Optimization of carbon coating on $LiFePO_4$. *J. Power Sources*, 163:180–184, 2006.

K. Dokko, S. Koizumi, and K. Sharaishi. Electrochemical properties of $LiFePO_4$ prepared via hydrothermal route. *J. Power Sources*, 165:656–659, 2007.

B. V. C. Erofeev. Generalized equations of chemical kinetics and its applications in reactions involving solids. *R. Dokl. Acad. Sci. URSS*, 52:511–514, 1946.

D. Fattakhova and P. Krtil. Electrochemical activity of hydrothermally synthesized Li-Ti-O cubic oxides toward Li insertion syntheses. *J. Electrochem. Soc.*, 149:A1224–A1229, 2002a.

D. Fattakhova and P. Krtil. Solvothermal synthesis of electrochemically active nanocrystalline Li-Ti-O spinel. *Mat. Res. Soc. Symp. Proc.*, 703:165–169, 2002b.

D. Fattakhova, V. Petrykin, J. Brus, T. Kostlanova·, J. Dedecek, and P. Krtil. Solvothermal synthesis and electrochemical behaviour of nanocrystalline cubic Li-Ti-O oxides with cationic disorder. *Solid State Ionics*, 176:1877–1885, 2005.

K. T. Fehr, R. Hochleitner, A. Laumann, E. Schmidbauer, and J. Schneider. Mineralogy, Mössbauer spectroscopy and electrical conductivity of heterosite $(Fe^{3+},Mn^{3+})PO_4$. *Phys. Chem. Minerals.*, 37:179–189, 2010a.

K. T. Fehr, M. Holzapfel, A. Laumann, and E. Schmidbauer. DC and AC conductivity of $Li_{4/3}Ti_{5/3}O_4$ spinel. *Solid State Ionics*, 181:1111–1118, 2010b.

C. Gicquel, M. M. Michel Mayer, and R. Bouaziz. Sur quelques composés oxygénés du titane et des alcalins (Li, Na); Étude des binaries M_2O-TiO_2 dans les zones riches en oxide alcalin. *C. R. Acad. Sc. Paris Série C*, 275:1427–1430, 1972.

J. B. Goddenough and Y. Kim. Challenges for rechargeable Li batteries. *Chemistry of Materials*, 22:587–603, 2010.

T. Hahn. *International Tables for Crystallography, Vol. A*. Reidel, Dordecht/Boston, 1983.

A. P. Hammersley, S. O. Svensson, M. Hanfland, A. N. Fitch, and D. Hausermann. Two-dimensional detector software: From real detector to idealised image or two-theta scan. *Adv. High Pressure Res.*, 14:235–248, 1996.

J. D. Hancock and J. H. Sharp. Method of comparing solid-state kinetic data and its applications to the decomposition of kaolinite, brucite and $BaCO_3$. *J. Am. Ceram. Soc.*, 55:74–77, 1972.

W. J. Hertl. Kinetics of barium titanate synthesis. *J. Am. Ceram. Soc.*, 71:879–883, 1988.

M. Hoelzel, A. Senyshyn, R. Gilles, H. Boysen, and H. Fuess. Scientific review: The structure powder diffractometer SPODI. *Neutron News*, 18:23–26, 2007.

R. A. Huggins. *Advanced Batteries - Materials Science Aspects*. Springer, Stanford, 2009.

L. Irbe. *Master thesis* - P*hasenbeziehungen von* Li_2TiO_3 *im* S*ystem* Li-Ti-O-H. Ludwig-Maximilians Universität, Munich, 2010.

W. Iwaniak, J. Fritzsche, M. Zukalov·, M. Wilkening R. Winter, and P. Heitjans. Li conductivity of nanocrystalline $Li_4Ti_5O_{12}$ prepared by a sol-gel method and high-energy ball milling. *Defect and Diffusion Forum*, 298-292:565–570, 2009.

G. Izquierdo and A. West. Phase equilibria in the system Li_2O-TiO_2. *Mater. Res. Bull.*, 15:1655–1660, 1980.

C. Jiang, E. Hosono, M. Ichihara, I. Honma, and H. Zhou. Synthesis of nanocrystalline $Li_4Ti_5O_{12}$ by chemical lithiation of anatase nanocrystals and postannealing. *J. Electrochem. Soc.*, 155:A553–A556, 2008.

G. A. Rosetti Jr., D. J. Watson, R. E. Newnham, and J. H. Adair. Kinetics of the hydrothermal crystallization of the perovskite lead titanate. *J. Cryst. Growth*, 116:251, 1992.

J. O. Eckert Jr., C. C. Hung-Houtson, B. L. Gersten, M. M. Lencka, and R. E. Riman. Kinetics and mechanisms of hydrothermal synthesis of barium titanate. *J. A. Ceram. Soc.*, 79:2929–2939, 1996.

C. M. Julien and K. Zaghib. Electrochemistry and local structure of nano-sized $Li_{4/3}Me_{5/3}O_4$ (Me = Mn, Ti) spinels. *Electrochim. Acta*, 50:411–416, 2004.

K. Kataoka, Y. Takahashi, N. Kijima, J. Akimoto, and K. Oshima. Single crystal growth and structure refinement of $Li_4Ti_5O_{12}$. *J. Phys. Chem. Solids*, 69:1454–1456, 2008.

H. Kleykamp. Enthalpy, heat capacity and enthalpy of transformation of Li_2TiO_3. *J. Nucl. Mater.*, 295:244–248, 2001.

H. Kleykamp. Phase equilibria in the Li-Ti-O system and physical properties of Li_2TiO_3. *Fusion Eng. Des.*, 61-62:361–366, 2002.

E. Kordes. Über die Steinsalzstruktur der Verbindung Li_2TiO_3 und ihre Mischbarkeit mit MgO. *Fortschr. Mineral. Krist.*, 17-18:27–33, 1933.

E. Kordes. Die Steinsalzstruktur der Verbindung Li_2TiO_3 und ihre Mischbarkeit mit MgO und $Li_2Fe_2O_4$. *Z. Kristallogr.*, 92:139, 1935.

M. V. Koudriachova and S. W. de Leeuw. Orthorhombic distortion on Li intercalation in anatase. *Phys. Rev. B*, 69:54106, 2004.

A. C. Lasaga. *Kinetic Theory in the Earth Sciences*. Princeton University Press, Princeton, 1998.

A. Laumann, K. T. Fehr, M. Holzapfel, M. Wachsmann, and B. B. Iversen. Metastable formation of low temperature cubic Li_2TiO_3 under hydrothermal conditions — its stability and structural properties. *Solid State Ionics*, 181:1525–1529, 2010.

A. Laumann, H. Boysen, M. Bremholm, K. T. Fehrand M. Hoelzel, and M. Holzapfel. The lithium migration path at high temperatures in $Li_4Ti_5O_{12}$ studied by *in-situ* neutron diffraction. *Chem. Mater.*, 23:2753–2759, 2011a.

A. Laumann, K. T. Fehr, H. Boysen, M. Hoelzel, and M. Holzapfel. Temperature-dependent structural transformations of hydrothermally synthesized cubic Li_2TiO_3 studied by *in-situ* neutron diffraction. *Z. Kristallogr.*, 226:53–61, 2011b.

A. Laumann, K. M. Ørnsbjerg Jensen, C. Tyrsted, M. Bremholm, K. T. Fehr, M. Holzapfel, and B. B. Iversen. In-situ synchrotron radiation study of the formation of cubic Li_2TiO_3 under hydrothermal conditions. *Europ. J. Inorg. Chem.*, 14:2221–2226, 2011c.

I. A. Leonidov, O. N. Leonidova, L. A. Perelyaeva, R. F. Samigullina, S. A. Kovyazina, and M. V. Patrakeev. Structure, ionic conduction, and phase transformations in lithium titanate $Li_4Ti_5O_{12}$. *Phys. Solid State*, 45:2183–2188, 2003.

I. A. Leonidov, O. N. Leonidova, R. F. Samigullina, and M. V. Partrakeev. Structural aspects of lithium transfer in solid electrolytes $Li_{2x}Zn_{2-3x}Ti_{1+x}O_4$ ($0.33 \leq x \leq 0.67$). *J. Struct. Chem.*, 45:262–268, 2004.

E. Lester, P. Blood, J. Denyer, D. Giddings, B. Azzopardi, and M. Poliakoff. Reaction engineering: The supercritical water hydrothermal synthesis of nanoparticles. *J. of Supercritical Fluids*, 37:209–214, 2006.

C. Liu, F. Li, L. Ma, and H. Cheng. Advanced materials for energy storage. *Adv. Mater.*, 22:E28–E62, 2010.

J. C. Mikkelsen. Pseudobinary phase relations of Li_2TiO_3. *J. Am. Ceram. Soc.*, 63:331–335, 1980.

J. Moon, E. Suvaci, A. Morrone, S. A. Costantino, and J. H. Adair. Formation mechanisms and morphological changes during the hydrothermal synthesis of $BaTiO_3$ particles from a chemically modified, amorphous titanium (hydrous) oxide precursor. *J. Eur. Ceram. Soc.*, 23:2153–2161, 2003.

J. Morales, R. Trócoli, S. Franger, and J. Santos-Peña. Cycling-induced stress in lithium ion negative electrodes: $LiAl/LiFePO_4$ and $Li_{4/3}Ti_{2/3}O_2/LiFePO_4$ cells. *Electrochim. Acta*, 55:3075–3082, 2010.

T. Ohzuko, A. Ueda, and N. Yamamoto. Zero-strain insertion material of $Li[Li_{1/3}Ti_{5/3}]O_4$ for rechargeable lithium cells. *J. Electrochem. Soc.*, 142:1431–1435, 1995.

N. A. Ovramenko, L. I. Shevts, F. D. Ovcharenko, and B. Y. Komilovich. Hydrothermal synthesis of certain alkaline earth metal titanates. *IzV. Akad. Nauk SSSR, Neorg. Mater.*, 3:242–245, 1978.

A. K. Padhi, K. S. Nanjundaswamy, and J. B. Goodenough. Phospho-olivines as positive-electrode materials for rechargeable lithium batteries. *J. Electrochem Soc.*, 144:1188–11192, 1997.

C. Pecharroman and J. M. Amarilla. Thermal evolution of infrared vibrational properties of $Li_{4/3}Ti_{5/3}O_4$ measured by specular reflectance. *Phys. Rev. B*, 62:12063–12068, 2000.

X. R. Pei, S. L. Zhang, J. W. Zhang, J. J. Yang, and Z. S. Jin. Preparation and characterization of rock salt-type $LiTiO_2$. *Chinese J. Inorg. Chem.*, 22:84–88, 2007.

V. Petricek and M. Dusek. *The Crystallographic Computing System* JANA*2000*. Institute of Physics, Praha, Czech Republic, 2000.

J. Qi, P. Xu, Z. Lv, X. Liu, and A. Wen. Effect of crystallinity on the electrochemical performance of nanometer Al-stabilized α-nickel hydroxide. *J. Alloys Compd.*, 462:164–169, 2008.

Z. Qiu, L. Yang, Y. Tang, S. Fang, and J. Huang. $Li_4Ti_5O_{12}$ nanoparticles prepared with gel-hydrothermal process as a high performance anode material for Li-ion batteries. *Chin. J. Chem.*, 28:911–915, 2010.

J. Rodríguez-Carvajal. Recent advances in magnetic structure determination by neutron powder diffraction. *Physica B*, 192:55–69, 1993.

S. Scharner, W. Weppner, and R. Schmid-Beurmann. Evidence of two-phase formation upon lithium insertion into the $Li_{1.33}Ti_{1.67}O_4$ spinel. *J. Electrochem. Soc.*, 146:857–861, 1999.

B. Scrosati and J. Garche. Materials for next-generation lithium batteries. *J. Power Sources*, 195:2419–2430, 2010.

J. Shu. Li-Ti-O compounds and carbon-coated Li-Ti-O compounds as anode materials for lithium ion batteries. *Electrochim. Acta*, 54:2869–2876, 2009.

A. K. Shukla and T. P. Kumar. Materials for next-generation lithium batteries. *Current Science*, 94:314–331, 2008.

L. M. Sikhwivhilu, S. R. Suprakas, and N. J. Coville. Influence of bases on hydrothermal synthesis of titanate nanostructures. *Appl. Phys. A*, 94:963–973, 2009.

D. R. Simon. *Dissertation - Characterization of* $Li_4Ti_5O_{12}$ *and* $LiMn_2O_4$ *spinel materials treated with aqueous solutions.* University of Cincinnaty, 2007.

H. Song, H. Jiang, T. Liu, X. Liu, and G. Meng. Preparation and photocatalytic activity of alkali titanate nano materials $A_2Ti_nO_{2n+1}$ (A = Li, Na and K). *Mater. Res. Bull.*, 42: 334–344, 2007.

M. Sugita, M. Tsuji, and M. Abe. Synthetic inorganic ion-exchange materials. LVIII. hydrothermal synthesis of a new layered lithium titanate and its alkali ion exchange. *Bull. Chem. Soc. Jpn.*, 63:1978–1984, 1990.

M. Tabuchi, A. Nakashima, H. Shigemura, K. Ado, H. Kobayashi, H. Sakaebe, and K. Tasumi. Fine $Li_{(4-x)/3}Ti_{(2-2x)/3}Fe_xO_2$ ($0.18 \leq x \leq 0.67$) powder with cubic rock-salt structure as a positive electrode material for rechargeable lithium batteries. *J. Mater. Chem.*, 13:1747–1757, 2003.

A. Testino, V. Buscaglia, M. T. Buscaglia, M. Viviani, and P. Nanni. Kinetic modeling of aqueous and hydrothermal synthesis of barium titanate ($BaTiO_3$). *Chem. Mater.*, 17: 5346–5356, 2005.

P. Thompson, D. E. Cox, and J. B. Hastings. Rietveld refinement of Debye-Scherrer synchrotron X-ray data from Al_2O_3. *J. Appl. Crystallogr.*, 2:79–83, 1987.

F. Tielens, M. Calatayud, A. Beltrán, C. Minot, and J. Andrés. Lithium insertion and mobility in the TiO_2-anatase/titanate structure: A periodic DFT study. *J. Electroanal. Chem.*, 581:216–223, 2005.

M. Tomiha, N. Masaki, S. Uchida, and T. Sato. Hydrothermal synthesis of alkali titanates from nano size titania powder. *J. Mater. Sci.*, 37:2341–2344, 2002.

K. Tsuchiya, C. Alvani, H. Kawamura, H. Yamada, S. Casadio, and V. Contini. Effect of TiO_2 on the reduction of lithium titanate induced by H_2 in the sweep gas. *Fusion Eng. Des.*, 69:443–447, 2003.

C. Tyrsted, P. Hald J. Becker, M. Bremholm, J. S. Pedersen, J. Chevallier, Y. Cerenius, S. B. Iversen, and B. B. Iversen. *In-situ* synchrotron radiation study of formation and growth of crystalline $Ce_xZr_{1-x}O_2$ nanoparticles synthesized in supercritical water. *Chem. Mater.*, 22:1814–1820, 2010.

M. Vijayakumar, S. Kerisit, Z. Yang, G. L. Graff, J. Liu, J. A. Sears, S. D. Burton, K. M. Rosso, and J. Hu. Combined ^{6,7}Li NMR and molecular dynamics study ofLi diffusion in Li_2TiO_3. *J. Phys. Chem. C*, 113:20108–20116, 2009.

M. Vijayakumar, S. Kerisit, K. M. Rosso, S. D. Burton, J. A. Sears, Z. Yang, G. L. Graff, J. Liu, and J. Hu. Lithium diffusion in $Li_4Ti_5O_{12}$ at high temperatures. *J. Power Sources*, doi:10.1016/j.jpowsour.2010.09.060, 2010.

G. Vītņiš, G. Ķizāne, A. Lūsis, and J. Tīliks. Electrical conductivity studies in the system Li_2TiO_3-$Li_{1.33}Ti_{1.67}O_4$. *Solid State Electrochem.*, 6:311–319, 2002.

M. Wagemaker, G. J. Kearley, A. A. van Well, H. Mutka, and F. M. Mulder. Multiple Li positions inside oxygen octahedra in lithiated TiO_2 anatase. *J. Am. Chem. Soc.*, 125: 840–848, 2003.

M. Wagemaker, A. A. van Well, G. J. Kearley, and F. M. Mulder. The life and times of lithium in anatase TiO_2. *Solid State Ionics*, 175:191–193, 2004.

M. Wagemaker, D. R. Simon, E. M. Kelder, J. Schoonman, C. Ringpfeil, U. Haake, D. Lützenkirchen-Hecht, R. Frahm, and F. M. Mulder. A kinetic two-phase and equilibrium solid solution in spinel $Li_{4+x}Ti_5O_{12}$. *Adv. Mater.*, 18:3169–3173, 2006.

R. I. Walton, F. Millange, R. I. Smith, T. C. Hansen, and D. O'Hare. Real time observation of the hydrothermal crystallization of barium titanate using in situ neutron powder diffraction. *J. Am. Chem. Soc.*, 123:12547–12555, 2001.

T. Xu, W. Wang, M. L. Gordin, D. Wang, and D. Choi. Lithium-ion batteries for stationary energy storage. *Energy Storage Technologies*, 62:24–30, 2010.

M. Yoshimura and K. Byrappa. Hydrothermal processing of materials: past, present and future. *J. Mater. Sci.*, 43:2085–2090, 2008.

K. Zaghib, M. Armand, and K. Gauthier. Electrochemistry of anodes in solid-state Li-ion polymer batteries. *J. Electrochem. Soc.*, 145:3135–3140, 1998.

K. Zaghib, M. Simoneau, M. Armand, and M. Gauthier. Electrochemical study of $Li_4Ti_5O_{12}$ as negative electrode for Li-ion polymer rechargeable batteries. *J. Power Sources*, 81-82:300–305, 1999.

V. M. Zainullina, V. P. Zhukov, T. A. Denisova, and L.G. Maksimova. Electronic structure and chemical bonding in monoclinic and cubic $Li_{2-x}H_xTiO_3$ ($0 \leq x \leq 2$). *J. Struct. Chem.*, 44:180–186, 2003.

D. R. Zhang, H. L. Liu, R. H. Jiun, N. Z. Zhang, Y. X. Liu, and Y. S. Kang. Synthesis and characterization of nanocrystalline $LiTiO_2$ using a one-step hydrothermal method. *J. Ind. Eng. Chem.*, 13:92–96, 2007.

Acknowledgements

First of all I would like to thank Karl Thomas Fehr for supervising this dissertation and for giving me the opportunity to work in this interesting field. This would not have been possible without the support of Norbert Schall, who made the collaboration with the Süd-Chemie AG happen.

Many thanks to Michael Holzapfel for his invaluable advice. I would also like to deeply thank Hans Boysen, who always made time for me and helped me with the treatment of the neutron data.

The Department of Chemistry and iNano in Aarhus takes a very special place here, and foremost Bo Brummerstedt Iversen. You gave me the opportunity to expand my horizon, and to work in excellent conditions in your group as well as at the beam-lines in Lund and Grenoble. Special thanks to Kirsten for our data-treatment time, to Peter for the introduction in the aquarium, and to Christopher, Mogens, Nina, Jacob and Charlotte for their support at the synchrotrons and the University.

Takk takk takk to Martin Bremholm, who made it possible from the very beginning for me to come to Aarhus. It was a pity that you left to the US when I arrived in Aarhus, but from you I learned a lot. Looking forward to seeing you in the Big Apple!

Thank you to Steffi, Vefi and Lucy for helping me with LiAn, AmLi and CriLit, to everyone in the Battery Materials group who helped me with my syntheses, and Christoph, the walking encyclopedia, for deepening my knowledge.

Thanks to Elmar Schmidbauer for the impedance measurements, to Martin for AAS, to Kai for DSC and the good wine, to Linda for filling the bombs, and to Sandra and Margot for being always a great help.

Jonathan, my bohemian friend, thanks for the discussions and everything. Same same for Yan, you know. A special mention deserve my officemates Saskia, Yaping, Christoph and Felix, for their company, discussions, travels, discoveries and lots of coffee together — and stopping me whenever I had too much of the coffee, though after noticing I was becoming unbearable. A big thank you also to all in our department, with whom I had

a great time at and outside work, Oryaëlle, Stefan, Mike, Benoit, Rosanna, Rosie, Jackie, Alex, Werner, Teresa and everyone else I might have forgotten.

María, la reina del tysetting, muchísimas gracias por eso y mucho más, estoy muy feliz de que ahora los dos tengamos tiempo otra vez! Vielen Dank an meine Familie für alles was sie für mich gemacht hat und vor allem dir Mumpfi, dass du immer zugehört hast wenn ich gerade nicht weiter wusste und ich danach sicher war dass alles klappt - und es hat, und deshalb jetzt erst mal ab an den Strand!